PARTICLE COLLISIONS AND COALESCENCE IN FLUIDS

by
Iraklis Anestis Valioulis

W. M. Keck Laboratory of Hydraulics and Water Resources
Division of Engineering and Applied Science
CALIFORNIA INSTITUTE OF TECHNOLOGY
Pasadena, California

Report No. KH-R-44

March 1983

PARTICLE COLLISIONS AND COALESCENCE IN FLUIDS

by

Iraklis Anestis Valioulis

Project Supervisor:

E. John List
Professor of Environmental Engineering Science

Supported by

National Oceanic and Atmospheric Administration
Grant Numbers:
NOAA/Sea Grant NA80AA-D-00120,
NOAA NA80RA-D0-0084

Grants from the Andrew W. Mellon Foundation
to the Environmental Quality Laboratory at Caltech

W. M. Keck Laboratory of Hydraulics and Water Resources
Division of Engineering and Applied Science
CALIFORNIA INSTITUTE OF TECHNOLOGY
Pasadena, California

Report No. KH-R-44

March 1983

to Louise

ACKNOWLEDGMENTS

To Professor E. John List for his guidance and friendship. Working with him made me the envy of my colleagues at Caltech.

To Dr. Henry J. Pearson who taught me that methodology and patience are the keys to successful research.

To Dr. R. C. Y. Koh whose computer expertise facilitated the completion of this work.

To Professors N. H. Brooks and R. C. Flagan whose comments were often a source of inspiration for me.

To Melinda Hendrix-Werts and Joan Mathews who have been instrumental in the editing of this Thesis.

Financial support for this work was provided by NOAA/Sea Grant NA80AA-D-00120, NOAA grant NA80RA-DO-0084 and a Mellon Foundation Grant to the Environmental Quality Laboratory at Caltech.

ABSTRACT

Coagulation, in the physical context, is looked upon here first from the fundamental perspective of collision and coalescence of individual particles. A Monte Carlo technique is used to investigate the particle size distribution in a suspension of coagulating particles when one or more collision mechanisms operate. The effect of interparticle forces - hydrodynamic, van der Waals' and electrostatic - on the collision probability of the particles is examined. The results obtained are used to evaluate the well-known dynamic equilibrium hypothesis according to which an equilibrium particle size distribution is assumed to exist under the action of a given collision mechanism. It is shown that dimensional analysis cannot, in general, be used to predict steady state particle size distributions, mainly because of the strong dependence of the interparticle forces on the sizes of the interacting particles.

The insight into particle kinetics thus gained from the Monte Carlo simulation of collision processes is used to develop a numerical simulation of a rectangular settling basin. The computer model follows the spatial and temporal development of the influent particle size distribution towards the outlet of the tank, accounting for all of the basic kinetics of particle collision and coalescence processes and including transport processes such as particle settling, advection, resuspension and turbulent mixing. The influence of the particle size-density relationship and floc deaggregation by turbulent shearing are also modeled. Of necessity, modeling of some of these processes has been somewhat empirical since the physical and biochemical nature of the

flocs are unique to a particular suspension and their determination requires experimental work. The results of the simulations performed indicate that the particle size-density relationship, the collision efficiencies between flocs and the influent particle size distribution are of major importance to the performance of the sedimentation basin. Clearly, further modifications, improvements and trials are needed in order to use the model for the design of new facilities. Nevertheless, the computer model may serve as a guide for selection of several design and operation variables for the successful treatment of a particular waste or the selective removal of pollutants whose concentration depends on the shape of the effluent particle size distribution.

TABLE OF CONTENTS

TABLE OF CONTENTS (continued)

LIST OF FIGURES

LIST OF FIGURES (continued)

LIST OF FIGURES (continued)

CHAPTER II

LIST OF FIGURES (continued)

LIST OF FIGURES (continued)

LIST OF TABLES

INTRODUCTION

Suspended particles are ubiquitous in most environmental or industrial flows. They affect both the bulk properties of the fluid and the surfaces with which the suspension is in contact. Information on the physical characteristics of the individual particles and the properties of the flow is required in order to predict the behavior of the suspension. The knowledge of the fluid-particle interactions, however, is not sufficient for successful modeling of flows in which particles interact with each other. Coagulation, the process of collision and coalescence of particles, modifies the distribution of suspended mass in the particle size space. Particle-particle interactions become thus important in quantifying the fate of suspended matter in flows in which coagulation occurs.

More specifically, the coagulation process in dispersive systems has applications in colloid chemistry (precipitation of colloidal particles from liquids), in atmospheric physics (coalescence of cloud particles in a vapour-air medium), in industrial processes (deposition of particles in heat-exchangers) and is of major importance in air and water pollution practice (fate of particulates discharged in water or air, mass-fluid separation processes). This work is primarily concerned with solid particles suspended in water, but the techniques used and the conclusions reached have general applications. In Chapter I a physical simulation is used to provide a better understanding of the mechanisms that cause collision and coalescence of particles in fluids. The dynamics of a population of coagulating particles are examined when one or more coagulation mechanisms operate. A review of the interparticle

forces is carried out, including a comprehensive evaluation of their effect on the collision probability of the particles. The information obtained is used in Chapter II to develop a numerical model simulating the operation of a rectangular sedimentation basin. The computer model is based on the fundamental mechanisms which govern particle motion and growth and includes transport processes such as particle advection, turbulent mixing and particle resuspension. The model follows the spatial and temporal development of the particle size distribution in the tank and, from the local development of the particle size spectrum, predicts the overall performance of the settling tank.

CHAPTER I: MONTE CARLO SIMULATION OF PARTICLE COLLISIONS

1. THE DYNAMIC EQUILIBRIUM HYPOTHESIS

Reasoning on dimensional grounds, Friedlander (1960a,b) and Hunt (1980) derived expressions for the dynamic steady state size distribution n(v) of coagulating particles. n(v) is defined by

$$dN = n(v)dv \tag{1.1}$$

where dN is the number of particles with volumes in the range v to v+dv per unit volume of fluid, so that n(v) is the number density of particles in v-space.

The underlying idea was inspired by Kolmogorov's (see Monin and Yaglom, 1975) equilibrium theory of turbulence. Friedlander assumed that a state of dynamic equilibrium would exist between production, coagulation and loss through sedimentation of particles in atmospheric aerosols. He hoped that the particle size distribution would reach a dynamic steady state (i.e. would remain invariant with time), sustained by a flux of particle volume through the size-space. If it is further assumed that there exist size ranges where only one of the coagulation mechanisms listed in Table 1 is important, then the size distribution in some subrange will depend only on the particle volume v, the constant particle volume flux E through the size distribution and a dimensional parameter (K_b , $K_{sh}=G$ or $K_{sh}=(\varepsilon/\nu)^{1/2}$ and K_{ds}) characterizing the dominant coagulation mechanism (Table 1). Hunt extended Friedlander's ideas to hydrosols, included a shearing and differential settling dominated

Table 1. Various mechanisms for particle collisions.

Mechanism	Collision Function β	Source	Dimensional Parameter
Brownian Motion	$\frac{2kT}{3\mu}\frac{(r_i+r_j)^2}{r_i r_j} = 4\pi\,(D_i+D_j)(r_i+r_j)$	Smoluchowski (1916)	$K_b = \frac{kT}{\mu}$
Laminar Shear	$1.33G\,(r_i+r_j)^3$	Smoluchowski (1917)	G
Pure Strain (extension)	$4.89\dot{\gamma}\,(r_i+r_j)^3$	Zeichner and Schowalter (1977)	$\dot{\gamma}$
Isotropic Turbulent Shear	$2.3^*(r_i+r_j)^3(\varepsilon/\nu)^{1/2}$	Saffman and Turner (1956)	$\left(\frac{\varepsilon}{\nu}\right)^{1/2}$
Turbulent Inertia	$\frac{1.27(\rho_p-\rho_f)}{\mu}\left(\frac{\varepsilon^3}{\nu}\right)^{1/4}(r_i+r_j)^2\lvert r_i^2-r_j^2\rvert$	Saffman and Turner (1956)	$\frac{(\rho_p-\rho_f)}{\mu}\left(\frac{\varepsilon^3}{\nu}\right)^{1/4}$
Differential Sedimentation	$\frac{0.7g(\rho_p-\rho_f)}{\mu}(r_i+r_j)^2\lvert r_i^2-r_j^2\rvert$	Findheisen (1939)	$K_{ds} = \frac{g(\rho_p-\rho_f)}{\mu}$

* corrected from original, see Pearson et al. (1983)

subrange and used dimensional analysis to derive the following expressions for n(v):

$$n(v) = A_b(E/K_b)^{1/2}\, v^{-3/2} \tag{1.2}$$

$$n(v) = A_{sh}(E/K_{sh})^{1/2}\, v^{-2} \tag{1.3}$$

$$n(v) = A_{ds}(E/K_{ds})^{1/2}\, v^{-13/6} \tag{1.4}$$

where A_b , A_{sh}, A_{ds} are dimensionless constants.

Jeffrey (1981) offered a new derivation of Hunt's results which clarifies the assumptions involved in the dimensional arguments. The change with time of the particle size distribution n(v) is given by the General Dynamic Equation (GDE)

$$\frac{\partial n(v)}{\partial t} = I(v) + \frac{1}{2}\int_0^v \beta(v', v-v')n(v')n(v-v')dv' - \int_0^\infty \beta(v,v')n(v)n(v')dv' + w(v)\frac{\partial n(v)}{\partial z} \tag{1.5}$$

where $\beta(v,v')$ is the collision function which represents the geometry and dynamics of the collision mechanism, I(v) is a source of particles (through condensation, for example) and $w(v)\frac{\partial n(v)}{\partial z}$ is a particle sink resulting from particles sedimenting in the z direction at their Stokes' settling velocity, w(v). For homogeneous particle systems and for size ranges where the source term is negligible the steady state form of Eq. 1.5 is

$$\frac{1}{2}\int_0^v \beta(v', v-v')n(v')n(v-v')dv' = \int_0^\infty \beta(v,v')n(v)n(v')dv \tag{1.6}$$

The integral on the l.h.s. of Eq. 1.6 represents the rate of gain of particles of volume v by coagulation of pairs of smaller particles,

conserving volume; the integral on the r.h.s. represents the flux of particles out of the size range (v,v+dv) due to their coagulation with particles of all sizes. Derivation of Hunt's expressions proceeds (Jeffrey, 1981) under the assumption that collisions between particles of similar size contribute mostly to the r.h.s. term of Eq. 1.6. Jeffrey approximates

$$\int_0^\infty \beta(v,v')n(v)n(v')dv' \cong \beta(v,v)n^2(v)v \qquad (1.7)$$

which, if multiplied by v^2 to convert from number density flux to volume flux is precisely the flux E of particle volume through the size-space. The general expression then follows

$$n(v) \sim \left(\frac{E}{\beta}\right)^{1/2} v^{-3/2} \qquad (1.8)$$

The collision function $\beta(v,v')$ is the probability that two particles of sizes v and v' will collide in unit time. This probability is equal to the common volume two particles sweep per unit time under the influence of one or more physical mechanisms in a unit volume of fluid. If non-interference of the different coagulation mechanisms is assumed, then subranges exist where a sole mechanism dominates and $\beta(v,v')$ is given by the expressions listed in Table 1; from Eq. 1.8 Hunt's expressions then follow.

It is clear that two assumptions are needed for the dynamic equilibrium hypothesis to be valid:

1. Collisions between particles of similar size are more important, or, equivalently, there is non-interference of particles of a size characteristic of one collision mechanism with those of another.

2. An equilibrium size distribution is established.

The latter assumption can be justified from the regularities observed in the size distributions of both atmospheric aerosols (Friedlander, 1960a,b) and hydrosols (Faisst, 1976).

2. VERIFICATION OF THE THEORY

Hunt (1980) studied the coagulation of solid particles (three types of small clay particles and finely divided crystalline silica) in artificial sea-water in the laminar shear generated between two rotating coaxial cylinders when the outer one was rotated. Some of his results support the predictions of the theory for Brownian motion and laminar shear induced coagulation, but none of the steady state size distributions attained in the experiments had size regimes exhibiting the power law behavior of both the coagulation mechanisms. Settling of particles caused Hunt's systems to be in a quasi-dynamic steady state; the size-distributions obtained were decreasing in magnitude while remaining similar in shape as the time progressed. Also, the dimensionless parameters A_b and A_{sh} appearing in Eqs. 1.2 and 1.3 were not the same for the different suspensions studied. Hunt attributed this variation to properties of the suspensions which modified the coagulation rate.

Pearson, Valioulis and List (1983) developed a method for Monte Carlo simulation of the evolution of a coagulating suspension. The logical sequence of their simulation is given in Figure 2.1. Spherical particles move in a cubical box or 'control' volume (shown in Figure 2.2) under the influence of Brownian motion and/or fluid shear.

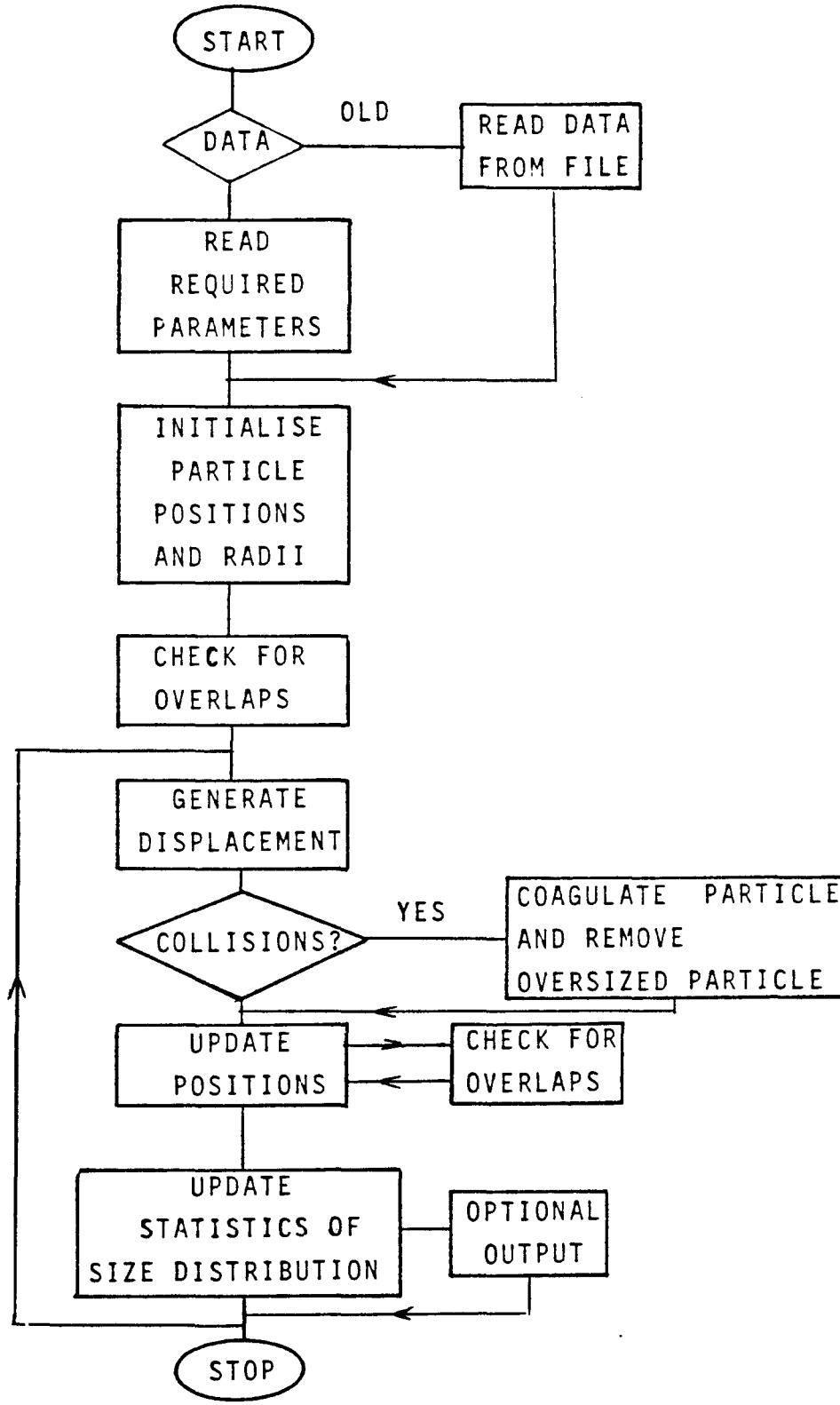

Fig. 2.1. Schematic representation of the logical sequence of the simulation.

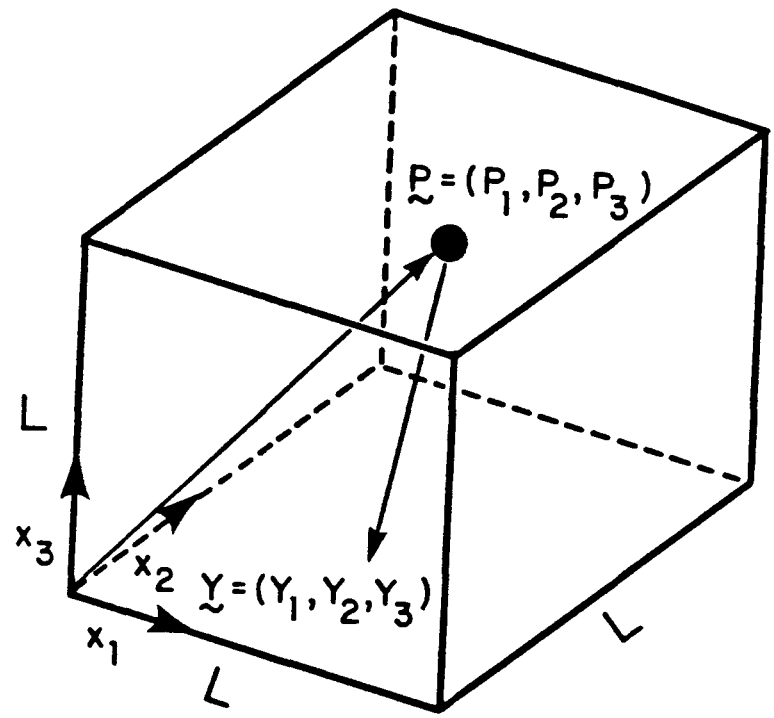

Fig. 2.2. Schematic representation of the 'control' volume and definition of the coordinate system used in the simulation.

Hydrodynamic and colloidal forces are ignored so that particles move on straight paths. Particles in suspension have unit volume, v_o , or integral multiples, $v_i = i \cdot v_o$ of the unit volume. Colliding particles coagulate to form a larger, still spherical particle, conserving volume. The model employs periodic boundary conditions which allow an infinite homogeneous system to be simulated approximately by a finite volume. A system in dynamic equilibrium is successfully modeled by using the following technique. A fixed number N_A of particles of unit volume are added to the population at random each time step, and any particles which have reached a preset maximum volume, v_{max} , are removed. The addition of small particles is a crude representation of the flux of particle volume into the size range from coagulation of particles smaller than v_o. The removal of particles larger than v_{max} represents the physical loss of large particles from the box by sedimentation or vertical concentration gradients. This procedure is consistent with the first hypothesis of the theory and is justified *a posteriori* by the success of the simulation in reproducing Hunt's (1980) dimensional results for Brownian motion, laminar shear and isotropic turbulent shear induced coagulation. Pearson, Valioulis and List (1983) concluded that the final steady state size distributions attained in their computer 'experiments' were insensitive to the size range covered by the simulation. However, as in Hunt's experiments, no one single simulation gave a size distribution having both Brownian motion and shear coagulation dominated regimes.

Their computer program, operating in a different mode, allows also the direct measurement of the collision function. On collision, particles are not coagulated but one of them simply repositioned so as

to avoid repeated collisions of the same particle pair. In this manner the analytic estimates for the collision function for Brownian motion, laminar shear and isotropic turbulent shear were verified.

The present study is a sequel to the work by Pearson, Valioulis and List (1983) and is an attempt to improve the realism of their results by accounting for the modifications to the coagulation rate caused by hydrodynamic, van der Waals' and electrostatic forces acting between the approaching particles. Differential sedimentation induced coagulation is also modeled and the validity of Hunt's (1980) dimensional arguments are reexamined in the light of the results of the simulations performed in this study.

3. BROWNIAN DIFFUSION

3.a. Hydrodynamic Interactions

Smoluchowski's (1916) classical model for Brownian motion induced coagulation applies to extremely dilute systems where only binary particle encounters are considered. The two particles are treated as rigid spheres describing Brownian motions independently of each other with a constant relative diffusion coefficient

$$D_{12} = D_1 + D_2 \qquad (3.1)$$

where the single particle diffusion coefficients

$$D_1 = kTb_1 \qquad D_2 = kTb_2 \tag{3.2}$$

are functions of the particle mobilities b_1 and b_2 which are determined by Stokes' law. For a particle of radius r the mobility is $b=1/(6\pi\mu r)$, where μ is the fluid dynamic viscosity. In Eqs. 3.2 k is Boltzmann's constant and T is the absolute temperature. However, this formulation ignores hydrodynamic forces which tend to correlate the particle motions as the particle separation decreases. The motion of one particle generates a velocity gradient of order s^{-2} at distance s in the surrounding fluid. This velocity gradient causes a particle located at that distance to act as a force dipole which induces a velocity of order s^{-4} at the location of the first particle (Batchelor, 1976). Thus, Eq. 3.1 becomes increasingly invalid as the particle separation decreases.

Spielman (1970) modified the relative diffusion coefficient to account for such particle interactions by extending Einstein's (1926) ingenious argument. In an unbounded system of particles a hypothetical dynamic equilibrium is assumed: at any point in space, the mean radial number density flux J_D of particles 2 relative to particle 1 due to Brownian diffusion is balanced by an advective flux J_F. The latter arises from the action of an arbitrary steady conservative force F derivable from a potential V and acting between the particles:

$$J_D + J_F = 0 \tag{3.3}$$

$$J_D = -D_{12}(dN/dr) \qquad J_F = N\,u \tag{3.4}$$

where N is the number density of particles 2 and u the relative radial velocity imparted to the particles by the conservative force F

$$u = bF \qquad F = -dV/dr \tag{3.5}$$

Here b is the relative particle mobility which is a function of separation.

Under equilibrium the number density of particles 2 must be Boltzmann distributed

$$N = N_{\infty} \exp(-V/(kT)) \tag{3.6}$$

where N_{∞} is the number density of particles 2 at infinite interparticle distance. Then the relative particle diffusion flux is

$$J_D = -D_{12}(dN/dr) = (D_{12}/(kT))(dV/dr)\ N \tag{3.7}$$

and the flux induced by the conservative force F

$$J_F = -N\ b(dV/dr) \tag{3.8}$$

The hypothetical equilibrium situation (Eq. 3.3) is invoked then to deduce from Eqs. 3.7 and 3.8 the relative particle diffusivity

$$D_{12} = bkT \tag{3.9}$$

which is a function of interparticle separation. Following Einstein

(1926) it is now assumed that Eq. 3.9 is valid even when the force F is removed. This is only justified if inertial effects are ignored so that the two fluxes become superposable (Batchelor, 1976). The relative mobility b can be computed from the exact solution of Stokes equations for two spheres moving along their line of centers obtained by Stimson and Jeffery (1926). Both the rotational motion, and the motion perpendicular to the line of centers of the particles, are irrelevant when spherical particles are considered, since all motions are then hydrodynamically uncoupled through Stokes' equations (Brenner,1964).

The hydrodynamic force between two approaching particles determined from the linearised equations of motion becomes singular at zero separation. This unphysical behavior is explained by the breakdown of continuum flow at distances of the order of the fluid molecular mean free path. Van der Waals' short range forces which diverge at particle contact can be considered to overcome this difficulty in the collision problem.

3.b Van der Waals' Forces

The attractive London-van der Waals' forces arise from the synchronized dipoles created by fluctuating charges in the electron clouds of the interacting bodies. Hamaker (1937) assumed additivity of the pairwise interactions of the constituent atoms and molecules and derived his well-known formula for the van der Waals' interaction energy V_A between spherical particles

$$\frac{V_A}{kT} = -\frac{A}{6kT}\left[\frac{2r_1r_2}{r^2-(r_1+r_2)^2} + \frac{2r_1r_2}{r^2-(r_1-r_2)^2} + \log\frac{r^2-(r_1+r_2)^2}{r^2-(r_1-r_2)^2}\right] \quad (3.10)$$

Here r is the distance between particle centers and A is the Hamaker constant. Schenkel and Kitchener (1960) incorporated retardation effects in Hamaker's formula and recommended the best-fit approximation to their numerical integrations

$$\frac{V_A}{kT} = -\frac{A}{6kT}\frac{r_2}{h(r_1+r_2)}\frac{1}{1+1.77p}, \qquad 0 < p < 0.57$$

$$\frac{V_A}{kT} = -\frac{2A}{kT}\frac{r_2}{h(r_1+r_2)}\left[-\frac{2.45}{60p} + \frac{2.17}{180p^2} - \frac{0.52}{420p^3}\right], \quad p \gtrsim 0.57 \quad (3.11)$$

where $p = 2\pi h/\alpha$ and $\alpha = \lambda/r_1$; h is the dimensionless minimum distance between the particles, $h=(r-r_2-r_1)/r_1$ and λ =100nm is the London wave length; λ introduces another length in the problem, so the collision efficiencies become a function of the absolute size of the particles.

Langbein (1971) used Lifshitz's continuum theory which considers the bulk electrodynamic response of particle 1 to all electrodynamic fluctuations in particle 2 (and vice versa) to obtain an expression for the van der Waals' potential which avoids all approximations inherent in Hamaker's expression. According to Lifshitz's theory the van der Waals' attractive energy A is separated to three frequency regimes: ultraviolet, infrared and microwave frequencies contribute to A, each one possessing a characteristic wavelenth (Parsegian and Nigham, 1970). Electromagnetic retardation occurs when the interparticle distance is larger than the characteristic wavelength and is due to the finite time

of propagation of electromagnetic waves which causes a phase difference between the fluctuating charges in the electron clouds of the interacting particles. Langbein's (1971) solution is in terms of a multiply infinite series and is difficult to evaluate. Smith et al. (1973) and Kiefer et al. (1978) compared Langbein's formulation with Hamaker's expression. They concluded that the latter represents well the ultraviolet and infrared contributions to the frequency spectrum; the microwave radiation is represented poorly when the dielectric permittivities of the particles and the medium are very different. This is the case of solid particles in water where only the microwave contribution is retarded (Smith et al., 1973). This suggests that Eq. 3.11, which accounts for the microwave retardation only, is a good appoximation to Langbein's (1971) exact formulation provided that the Hamaker constant is determined experimentally or calculated from Lifshitz's theory (Zeichner and Schowalter, 1979).

The generalized Smoluchowski equation for the diffusing particles under the action of interparticle conservative forces is given by Spielman (1970)

$$\frac{\partial N}{\partial t} = -\text{div } J_{12} = \frac{1}{r^2}\frac{\partial}{\partial r}\left[r^2\left(D_{12}\frac{\partial N}{\partial r} + Nb\frac{dV_A}{dr}\right)\right] \qquad (3.12)$$

with boundary conditions

$$\begin{aligned} N = 0 \text{ and } V_A = -\infty \quad &\text{when} \quad r = r_1 + r_2 \\ N = N_\infty \text{ and } V_A = 0 \quad &\text{when} \quad r = \infty \end{aligned} \qquad (3.13)$$

The steady state solution of this equation gives the diffusive flux J_{12} of particles 2 into a sphere of radius $r_1 + r_2$

$$-4\pi r^2 J_{12} = \frac{4\pi D_\infty N_\infty (r_1+r_2)}{\left(1+\frac{r_2}{r_1}\right)\int_{1+\frac{r_2}{r_1}}^{\infty}\left(\frac{D_\infty}{D_{12}}\right)\exp\left(\frac{V_A}{kT}\right)\frac{ds}{s^2}} \qquad (3.14)$$

where D_∞ is the relative particle diffusion coefficient in the absence of any interparticle forces and s the dimensionless separation $s=r/r_1$. The collision rate depends on the integral of the particle interactions over all separations. A collision efficiency can be defined

$$E_b^{-1}(r_1,r_2) = \left(1+\frac{r_2}{r_1}\right)\int_{1+\frac{r_2}{r_1}}^{\infty}\left(\frac{D_\infty}{D_{12}}\right)\exp\left(\frac{V_A}{kT}\right)\frac{ds}{s^2} \qquad (3.15)$$

as the enhancement of the collision rate over the collision rate in the absence of any interactions between the particles. $E_b(r_1,r_2)$ is the inverse of Fuchs' (1964) stability factor.

3.c. Collision Efficiencies for Brownian Diffusion Accounting for Hydrodynamic and van der Waals' Forces.

The relative diffusion coefficients, D_{12}, were determined as a function of particle separation by summing the series solution to Stokes' equations obtained by Stimson and Jeffery (1926) (as corrected by Spielman, 1970). A single convergence criterion c=0.0001 was used for each series, which were assumed to converge when the condition $|(S_{n+1}-S_n)/S_n| < c$ was fulfilled; S_n is the nth-partial sum of a series. All the numerical calculations were performed to a precision of thirteen significant figures. For dimensionless separations $s < 0.001$ the asymptotic formula

$$\frac{D_{12}}{D_\infty} = \left(\frac{r_1}{r_2}+1\right)h \qquad (3.16)$$

developed by Brenner (1966) was used; this speeds up the calculations since the series converges slowly at small separations. The results (first obtained by Spielman) are shown in Figure 3.1.

The integration in Eq. 3.15 was performed numerically using Simpson's formula. A successively decreasing integration step was used to account for the more rapid variation of the integrand with decreasing particle separation. The integration ranged over a dimensionless separation $10^{-6} < r/r_2 < 500$, where r_2 is the larger of the two particles; extending the integration range did not alter the results.

To assess the significance of retardation, both the retarded (Eq. 3.11) and the unretarded (Eq. 3.10) potential were used to compute collision efficiencies for particles of equal size and for various values of A/(kT). Figure 3.2 is a comparison between the unretarded and retarded potential for different values of the retardation parameter α. The curves collapse for dimensionless separations s less than about 0.001; for larger interparticle distances electromagnetic retardation reduces the attractive potential significantly. The curve for the retarded potential in Figure 3.2 approaches the curve for the unretarded potential as r_1 decreases (or as α increases); the limit $\alpha \to \infty$ corresponds to the unretarded case. (α =0.1 with λ =100nm corresponds to a particle radius r_1 =1μm).

In the calculations represented by the curves marked with W in Figure 3.3 hydrodynamic interactions are ignored; the curves marked with H represent collision efficiencies when both van der Waals' and hydrodynamic forces operate. Retardation assumes increasing importance as the van der Waals' energy of attraction increases. The hydrodynamic forces tend to dominate the collision process as the van der Waals'

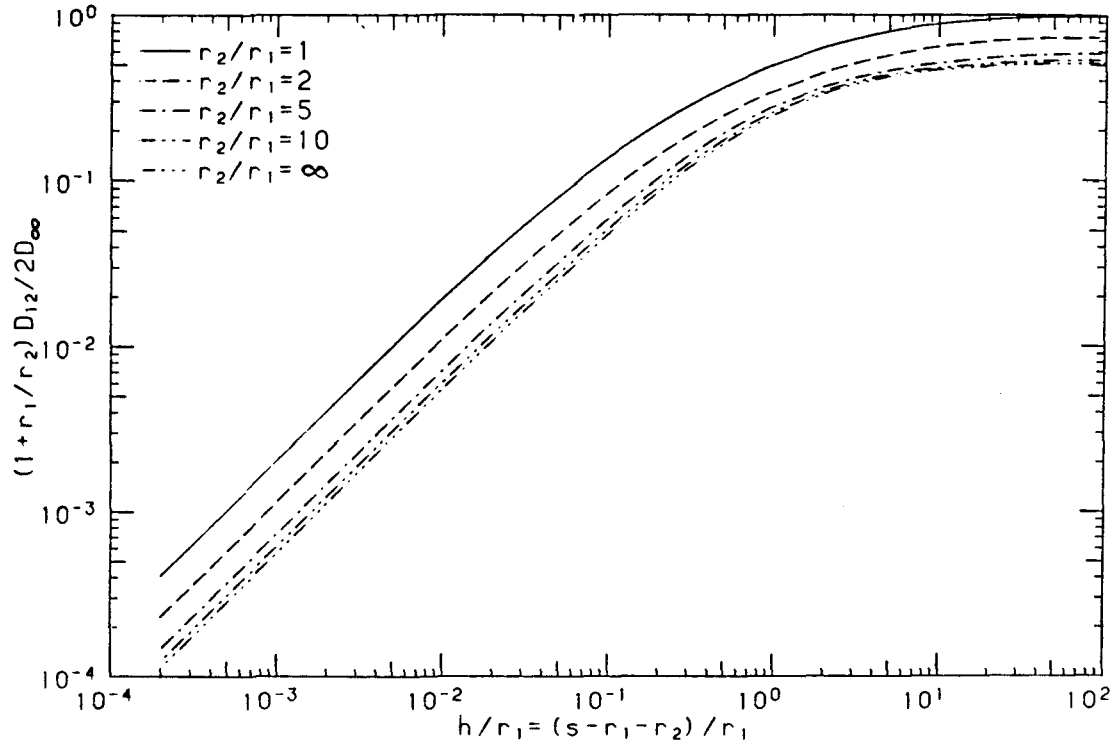

Fig. 3.1. Normalised particle diffusivity vs. dimensionless particle separation. D_{12} is the relative diffusion coefficient of particles with radii r_1 and r_2 in Stokes' flow; $D_\infty=D_1+D_2$, where D_1 and D_2 are the undisturbed particle diffusivities.

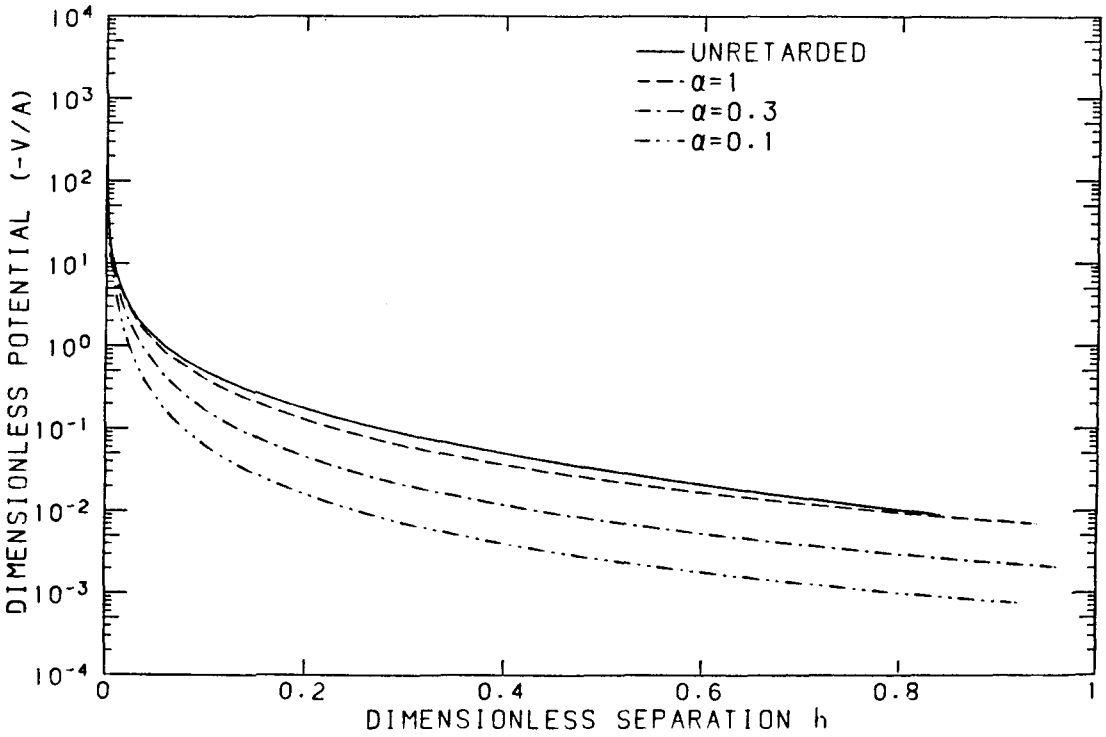

Fig. 3.2. Dimensionless van der Waals' potential vs. dimensionless particle separation for various values of the retardation parameter α.

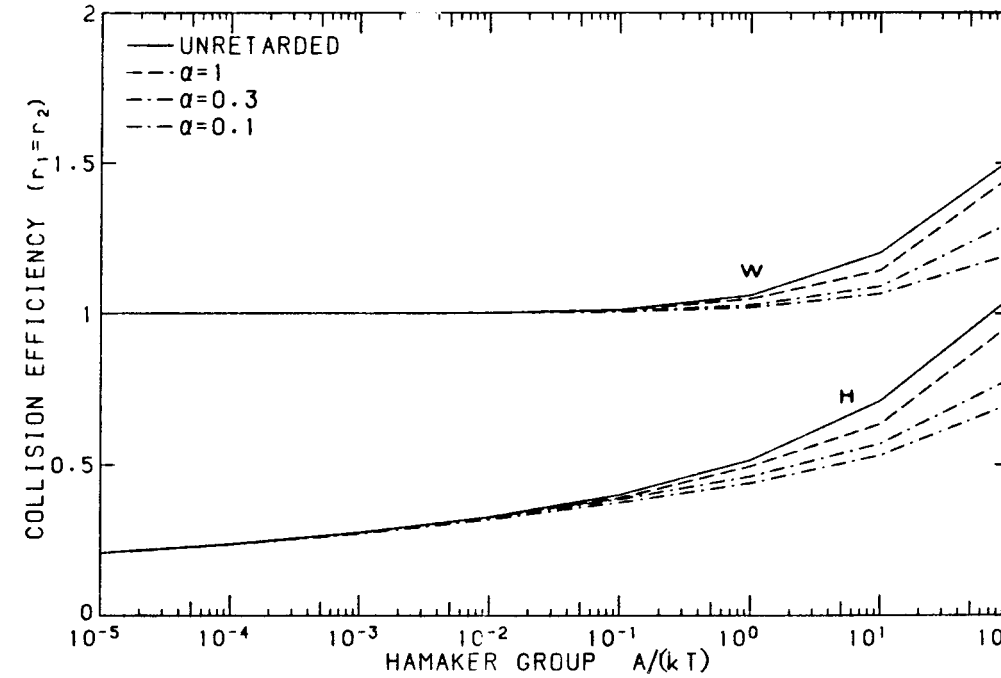

Fig. 3.3. Effect of retardation on the collision efficiency of equal size particles for various values of A/(kT).

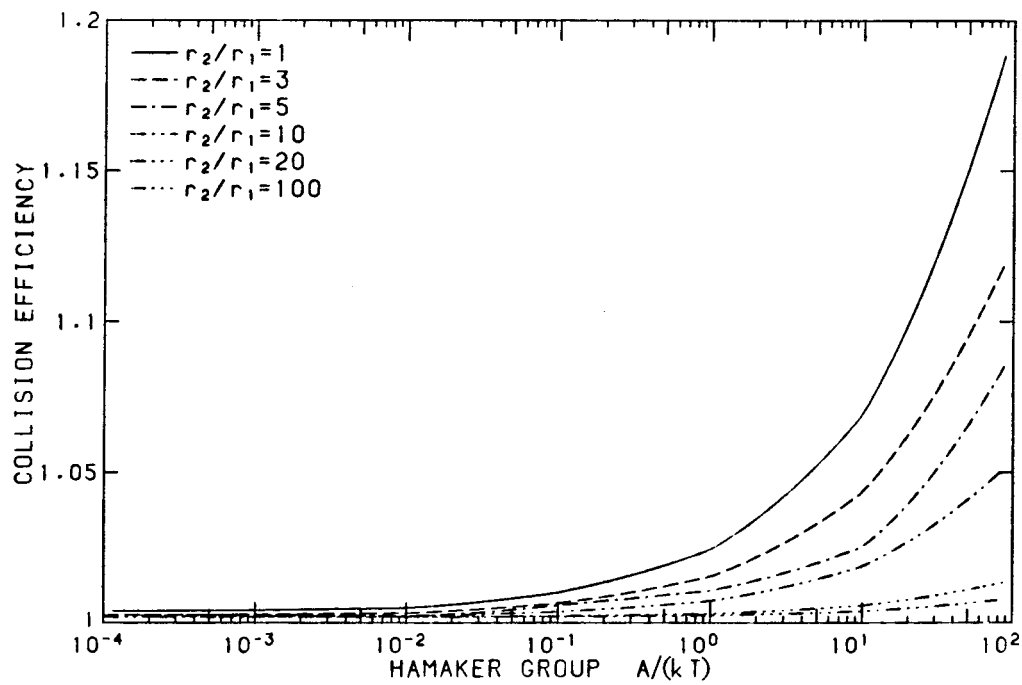

Fig. 3.4. Collision efficiences of particles with various relative sizes and for various values of A/(kT) when only van der Waals' forces operate.

forces become of shorter range.

The efficiencies computed with the unretarded potential for equal size particles agreed very well with Spielman's results; this provided a check for the validity of the calculations.

The effect of the relative size of the interacting particles on the collision efficiency when only van der Waals' forces are considered is shown in Figure 3.4. For these and all subsequently described calculations the retarded potential with α =0.1 is used. The enhancement of the collision rate decreases as the interacting particles become of increasingly different size. The computed efficiencies are lower than the ones calculated by Twomey (1977), who did not include retardation, and are in agreement with the results obtained by Schmidt-Ott and Burtscher (1982).

Hydrodynamic forces reduce the collision efficiency of interacting particles (Figures 3.5 and 3.6). The effect is more pronounced for particles of similar size and for small A/(kT). This is illustrated in Figure 3.6 where the reduction in the collision efficiency due to hydrodynamic forces for different particle pairs and at various A/(kT) is shown. E_H stands for the collision efficiency when both hydrodynamic and van der Waals' forces operate; E_W is the collision efficiency when only van der Waals' forces act. The curves shown approach zero as the interparticle attractive energy decreases. In the limit $A \to 0$ collisions are theoretically impossible since in Stokes' flow the hydrodynamic repulsive force between the particles grows without bound as the particle separation decreases.

Reported experimental collision efficiencies range from 0.35 to 0.7 for equal size particles (see Zeichner and Schowalter, 1979, for a

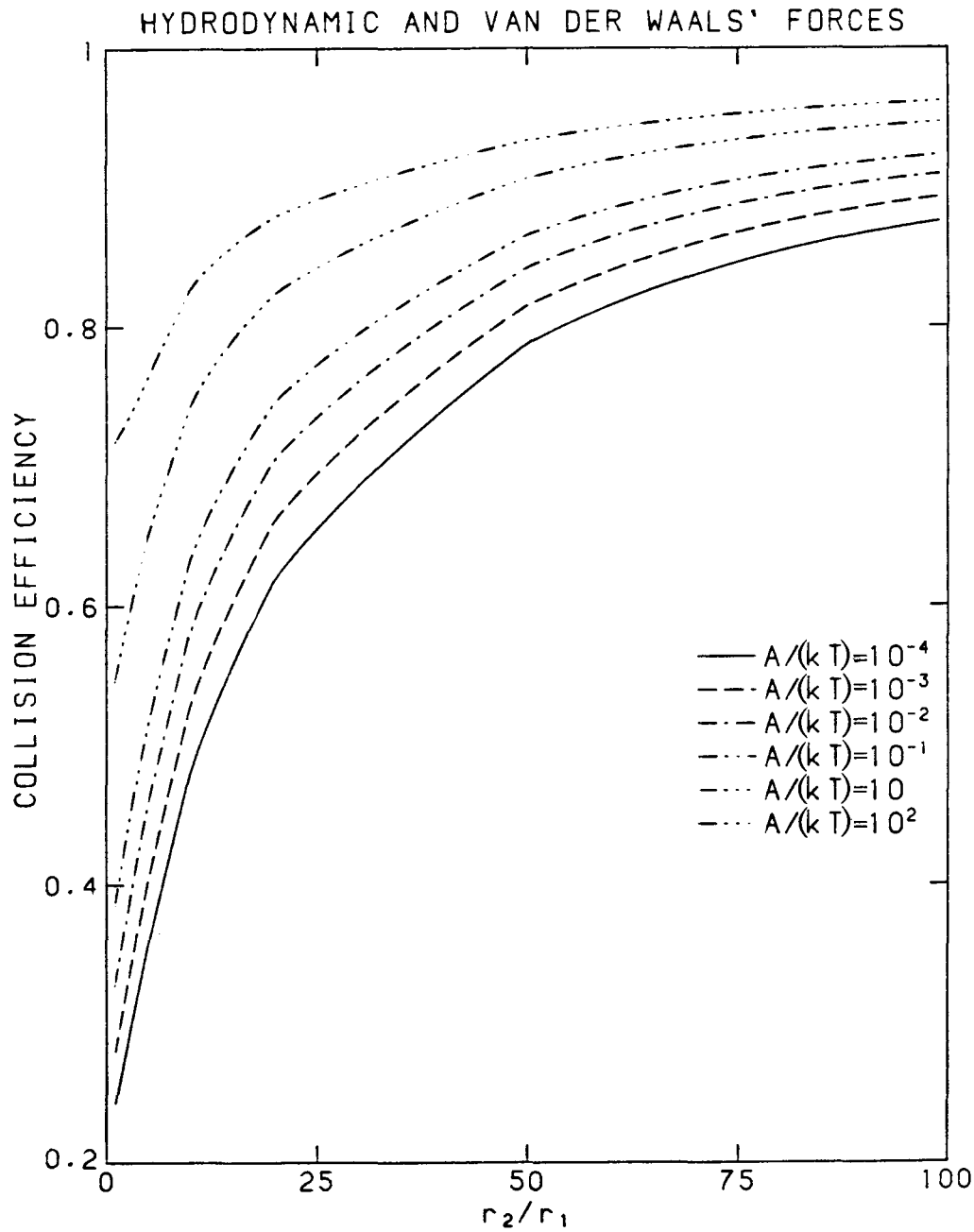

Fig. 3.5. Collision efficiences of particles with various relative sizes and for various values of A/(kT) when van der Waals' and hydrodynamic forces operate.

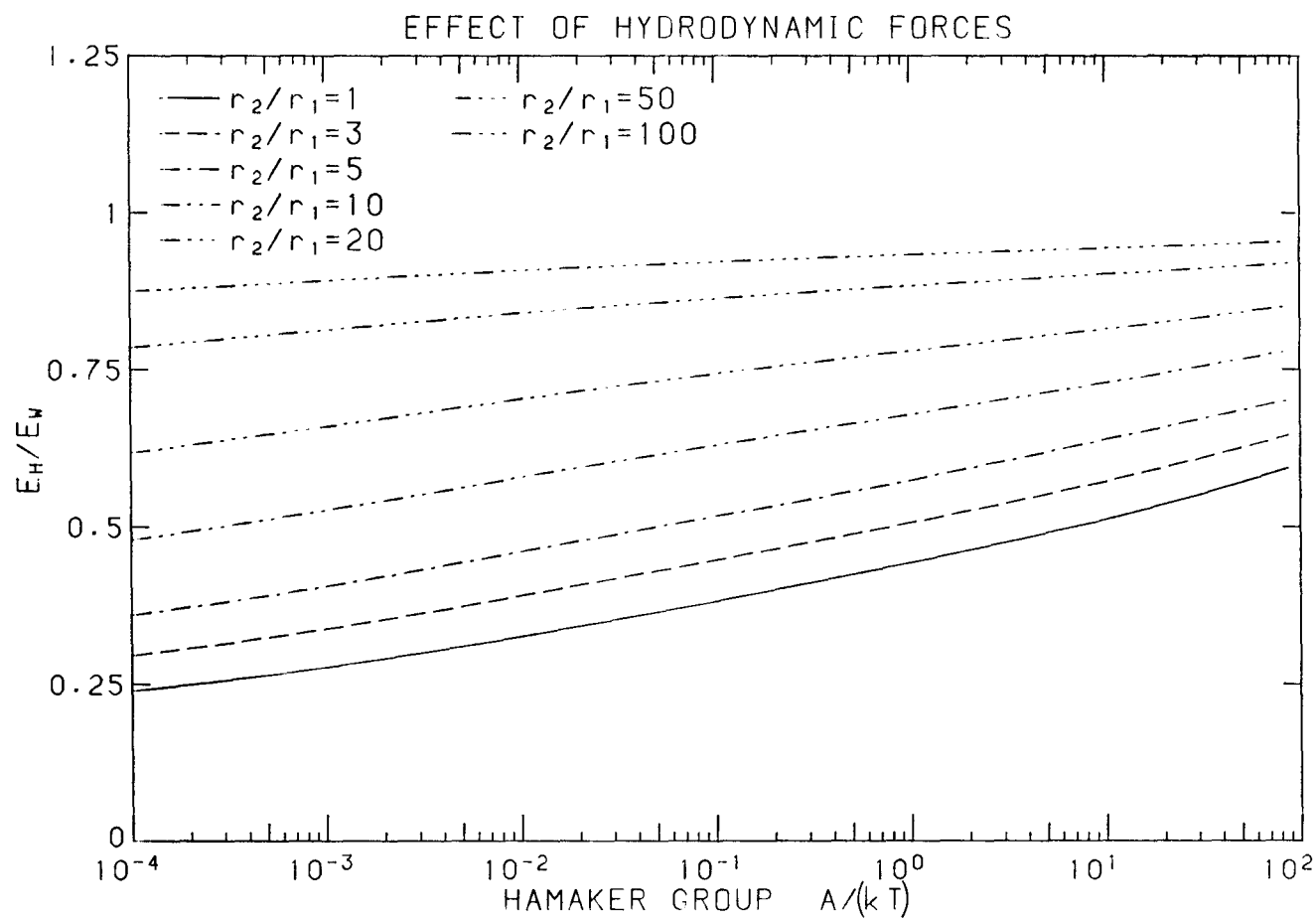

Fig. 3.6. Evaluation of the relative importance of hydrodynamic and van der Waals' forces in modifying the collision rate of two spherical particles.

recent survey a result which according to Figure 3.3 implies a maximum value for the Hamaker constant of about $2 \cdot 10^{-19}$ Joules (at 300°K) for the retarded potential. According to Lyklema (1968) the Hamaker constant of most hydrophobic colloids in water ranges from about 10^{-19} Joules to about $2 \cdot 10^{-22}$ Joules corresponding to Hamaker groups (at 300°K) of about 25 and 0.06 respectively (according to Stumm and Morgan (1981) A ranges from about 10^{-19} Joules to 10^{-21} Joules). According to Figure 3.3 these correspond to a collision efficiency of about 0.65 and 0.35 respectively (for the retarded potential), which are in the range of collision efficiencies determined experimentally.

Theoretical estimation of the van der Waals' attractive energy (Hamaker constant A) is carried out by Lifshitz's (1956) method. This requires knowledge of the frequency ω dependent dielectric permittivities $\varepsilon(\omega)$ of the particles and the dispersive medium. Apart from the difficulty of estimating $\varepsilon(\omega)$ (Smith et al., 1973), it has been shown (Parsegian and Nigham, 1970) that considerable dumping of the microwave radiation takes place in dispersions of high ionic strength. This complicates the theoretical determination of A and suggests that its experimental determination may be more promising for practical applications. Experimental determination of the collision efficiency and subsequent estimation of the Hamaker constant is carried out directly from optical data (Gregory, 1969) or indirectly in rapid coagulation experiments of monodisperse systems in which double layer forces are assumed to be negligible. In the latter case the coagulation rate is determined by means of the half-life of the dispersion assuming a monodisperse system of particles (Zeichner and Schowalter, 1979). Then numerical calculations (or Figure 3.3) give the value of the

Hamaker constant. Large scale modeling via the General Dynamic Equation can be accomplished then, since the collision efficiencies between particles of unlike sizes can be obtained readily from Figure 3.5.

3.d. Double Layer Forces

Dispersed particles in natural waters carry an electric charge. Since the dispersion is electrically neutral, the aqueous phase carries an equal charge of opposite sign. Close to the particle surface a compact layer of specifically adsorbed ions is formed (Stern layer). The outer (Gouy) layer consists of the excess of oppositely charged ions (counter ions) of the dispersing medium. According to the Gouy-Chapman model (Verwey and Overbeek, 1948) an equilibrium is established in the outer (diffuse) layer between electrostatic forces and forces due to the thermal motion of the ions. This causes the diffuse layer to extend outwards from the particle surface into the solution, the concentration of counter ions diminishing with distance.

This local distribution of charges in an electrically neutral solution induces double layer interaction forces between approaching particles. Significant simplifications are needed in order to describe quantitatively the interparticle double layer forces. A sufficiently dilute system of negatively charged spherical particles is assumed so that only binary particle encounters are considered. The particles can have different sizes but carry the same charge. The realistic assumption of thin double layers and small surface potentials is applicable to particles suspended in most natural waters (Lyklema,

1968). Then two types of particle encounters are subject to approximate analytical description: a) the particle surface potential remains constant during the interaction, and b) their surface charge density remains constant. According to the Gouy-Chapman model of the electrical double layer the electrostatic potential $\Psi(s)$ at any point around a spherical particle satisfies

$$\frac{d^2\Psi(s)}{ds^2} = \frac{8\pi cez}{\varepsilon} \sinh\left(\frac{ze\Psi}{2kT}\right) \tag{3.17}$$

where s is the distance from the surface of the particle, z is the valence of the ionic species in solution, $e=1.6\ 10^{-19}$ Cb, the charge of the electron, ε the dielectric constant of the suspending medium ($\varepsilon = 89 \cdot 10^{-12}$ Cb/(Vcm) for water), c the number of ion pairs (ions/cm^3), $k=1.38 \cdot 10^{-23}$ VCb/°K Boltzmanns' constant and T the absolute temperature. The double layer surface charge density σ is related to Ψ by

$$\sigma = -\frac{\varepsilon}{4\pi}\left(\frac{d\Psi}{ds}\right)_{s=0} \tag{3.18}$$

According to the Gouy-Chapman model Eq. 3.18 gives

$$\sigma = \left(\frac{2}{\pi}\ \varepsilon kTc\right)^{1/2} \sinh\left(\frac{ze\Psi_{s=0}}{kT}\right) \tag{3.19}$$

Traditionally the constant potential assumption has been used to evaluate the double layer forces. Then the Debye-Huckel linearized form of Eq. 3.17 (Verwey and Overbeek, 1948), applicable to small potentials, can be used. The constant potential assumption is equivalent to assuming equilibrium between the adsorbed ions and the bulk solution

during the time of the interparticle interaction. Frens and Overbeek (1971) and Bell and Peterson (1972) showed that the time scale of the Brownian interaction between particles (of the order of 10^{-7}sec) is too short for electrochemical equilibrium to be restored. Thus the surface charge density rather than the surface potential remains constant during the time scale of the Brownian interaction. The particle surface potential increases then infinitely (Bell and Peterson, 1972) as the interparticle distance decreases invalidating the convenient assumption of small potentials. This increase in the surface potential causes the repulsion at small distances to be stronger at constant charge density than at constant potential.

For thin double layers, symmetrical electrolytes (one electrolyte only with ions of charge number +z and -z) and for dimensionless interparticle separations κs greater than about 4 (where κ^{-1} is the Debye-Huckel length, a measure of the double layer thickness) the linear superposition approximation to the diffuse layer interaction between spheres obtained by Bell et al.(1970) can be used. It is assumed that the potential of one particle remains undisturbed due to the presence of the other. Then the interparticle force f is given by

$$f = \frac{\varepsilon(kT)^2}{e^2} Y_1 Y_2 (1+\kappa r) r_1 r_2 \exp(-\kappa s)/r^2 \qquad (3.20)$$

where r_1, r_2 are the radii of the particles and r the center-to-center distance between them. The 'effective' reduced potential Y is approximated by (Bell et al., 1970)

$$Y = 4\tanh(\Phi/4) \qquad (3.21)$$

valid for $\kappa r > 10$ and $\Phi < 8$. The reduced (dimensionless) potential Φ is given by

$$\Phi = ze\,\Psi_o/(kT) \tag{3.22}$$

where Ψ_o is the surface potential of a single particle alone in the fluid. Eq. 3.20 is equally valid for the constant surface potential and constant charge density case for large interparticle distances. The energy of interaction V_p of the two spherical particles at separation s is then

$$V_p = \int_s^\infty f(r)dr \tag{3.23}$$

At small separations Derjaguin's (1954) approximation can be used. It states that the double-layer force between a pair of spheres can be derived from the interaction energy of two flat double layers. Frens and Overbeek (1971) obtained the interaction energy V_F^σ at constant surface charge density of two approaching flat double layers in terms of the interaction energy V_F^Ψ at constant surface potential

$$V_F^\sigma = V_F^\Psi + \frac{8\varepsilon kT}{\kappa}\left[(\Phi_H - \Phi)\sinh\left(\frac{\Phi}{2}\right) - 2\left(\cosh\frac{\Phi_H}{2} - \cosh\frac{\Phi}{2}\right)\right] \tag{3.24}$$

Here Φ_H is the reduced electrostatic potential half-way between the flat double layers. Φ_H can be computed from the implicit relation (Verwey and Overbeek, 1948)

$$\kappa s = \exp\left(-\frac{\Phi_H}{2}\right)\left\{F\left(\exp(-\Phi_H), \frac{\pi}{2}\right) - \left(F\,\exp(-\Phi_H), \arcsin\exp\left[-(\Phi - \Phi_H)\right]\right)\right\} \tag{3.25}$$

where $F(a, \phi)$ is the elliptic integral of the first kind. Hogg et al.

(1965) used Derjaguin's approximation to obtain the potential energy V_F^{Ψ} of two approaching flat double layers at constant surface potential

$$V_F^{\Psi} = \frac{\varepsilon\kappa}{8\pi}\left[\left(\Psi_{o1}^2 + \Psi_{o2}^2\right)\left(1 - \coth(\kappa s)\right) + 2\Psi_{o1}\Psi_{o2}/\sinh(\kappa s)\right] \qquad (3.26)$$

valid for $\Psi_{oi} < 25$mv. Here Ψ_{o1} and Ψ_{o2} are the surface electrostatic potentials of the undisturbed flat double layers. Given the surface charge density σ of the particles, Φ (or Ψ_o) is computed from Eq. 3.19; Eqs. 3.25 and 3.26 give Φ_H and V_F^{Ψ} respectively, so V_F^{σ} can be computed from Eq. 3.24. The interaction energy V_R^{σ} between two spherical double layers at small separations is then given in terms of the potential energy V_F^{σ} of two flat double layers by

$$V_R^{\sigma} = \frac{2\pi r_1 r_2}{r_1 + r_2}\int_s^{\infty} V_F^{\sigma}(r)dr \qquad (3.27)$$

The electric potential drop Ψ_d across the diffuse part of the double layer (Gouy layer) is approximated customarily by the electrokinetic (zeta) potential Ψ_ζ obtained from the electrophoretic mobility of the particle. The corresponding electrokinetic charge σ_ζ is then approximately equal to the charge density σ_d in the diffuse layer. For thin double layers the latter is set equal to the particle surface charge density σ.

Natural waters and wastewater are the dispersions of concern here. Water of ionic strength (molarity) I is treated as a monovalent symmetrical electrolyte with the same ionic strength (Stumm and Morgan, 1981). The double layer thickness κ^{-1}(in cm) is associated to I

according to (Stumm and Morgan, 1981)

$$\kappa^{-1} \cong 2.8\ 10^{-8}\ I^{-0.5}$$

For natural waters and sea-water I is 0.01 and 0.65 respectively. κ^{-1} ranges typically from 5 to 20nm in fresh water and is about 0.4nm in sea-water (Stumm and Morgan, 1981). For simplicity the interacting particles are assumed here to carry the same negative charge. This is a first approximation to the wide spectrum of positively and negatively charged surfaces existing in natural waters.

3.e. Collision Efficiencies of Spherical Particles in Brownian Diffusion Accounting for Hydrodynamic, van der Waals' and Double Layer Forces.

The collision efficiency of spherical particles subject to Brownian diffusion and accounting for hydrodynamic, van der Waals' and double layer forces can be computed from Eq. 3.15. The interaction energy of two approaching particles is the sum of the attractive van der Waals potential V_A and the repulsive electrostatic potential V_R^{σ} at constant surface charge

$$V_P = V_A + V_R^{\sigma}$$

The salient features of the curve of the interaction energy V_P against separation are shown in Figure 3.7. At small and large particle separations the van der Waals energy outweighs the repulsion. At

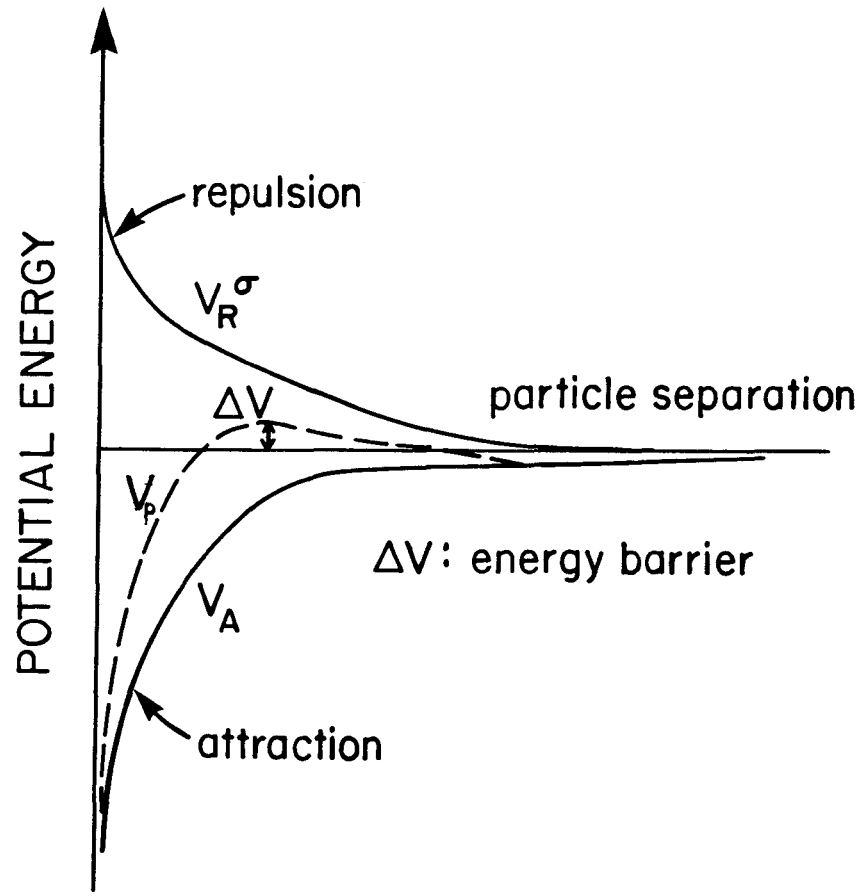

Fig. 3.7. Schematic illustration of the potential energy as a function of particle surface separation.

intermediate separations the electrostatic repulsion predominates creating a maximum in the potential energy curve (energy barrier). This energy barrier reduces the coagulation rate between two particles and can even prevent them from colliding. Since the collision efficiency (Eq. 3.15) involves V_P as an exponential factor the height of the energy barrier is the most significant factor governing the behaviour of the collision efficiency; the rest of the curve in Figure 3.7 is of little importance.

For large dimensionless interparticle distances κs, V_R^{σ} is determined from Eqs. 3.20 and 3.23. For small values of κs, Eq. 3.27 is used. The transition from Eq. 3.23 to 3.27 is such that the curve of V_R^{σ} vs. κs is as smooth as possible. The van der Waals' energy of attraction V_A is given by Eq. 3.10.

For the near-field computation the potential half-way between two approaching flat double layers is needed (see Eqs. 3.24 and 3.25). The elliptic integral in Eq. 3.25 was numerically evaluated using Simpson's formula. The half-way potential Φ_H is plotted in Figure 3.8 against the dimensionless double layer separation κs for five dimensionless undisturbed potentials in the range of interest. A second-order polynomial can be fitted to the numerical results obtained from the integration to an accuracy of better than 0.998; the resulting equation is used in all subsequent calculations.

Figure 3.9 shows the effect of the van der Waals' energy of attraction on the collision efficiency of the interacting pairs. The ionic strength I=0.05 and both particles have the same (negative) dimensionless undisturbed surface potential $\Phi = 0.5$. corresponding to a surface charge density $\sigma = 0.67\ 10^{-6}\ Cb/cm^2$. The sequence of Figures

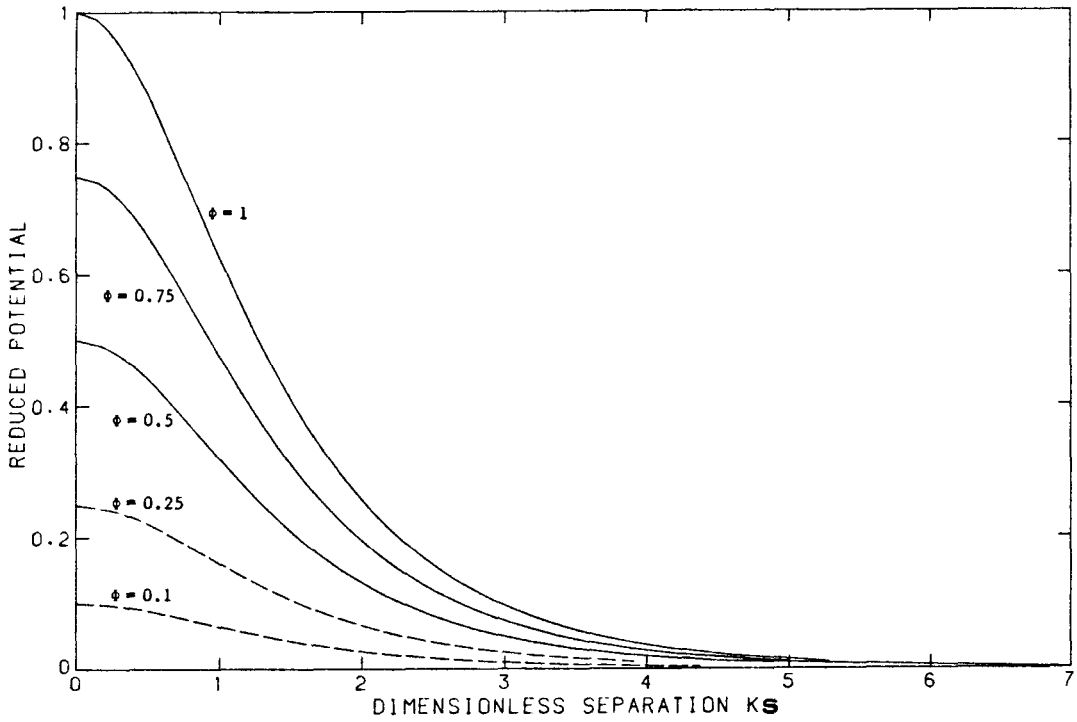

Fig. 3.8. Potential half-way between two flat double layers.

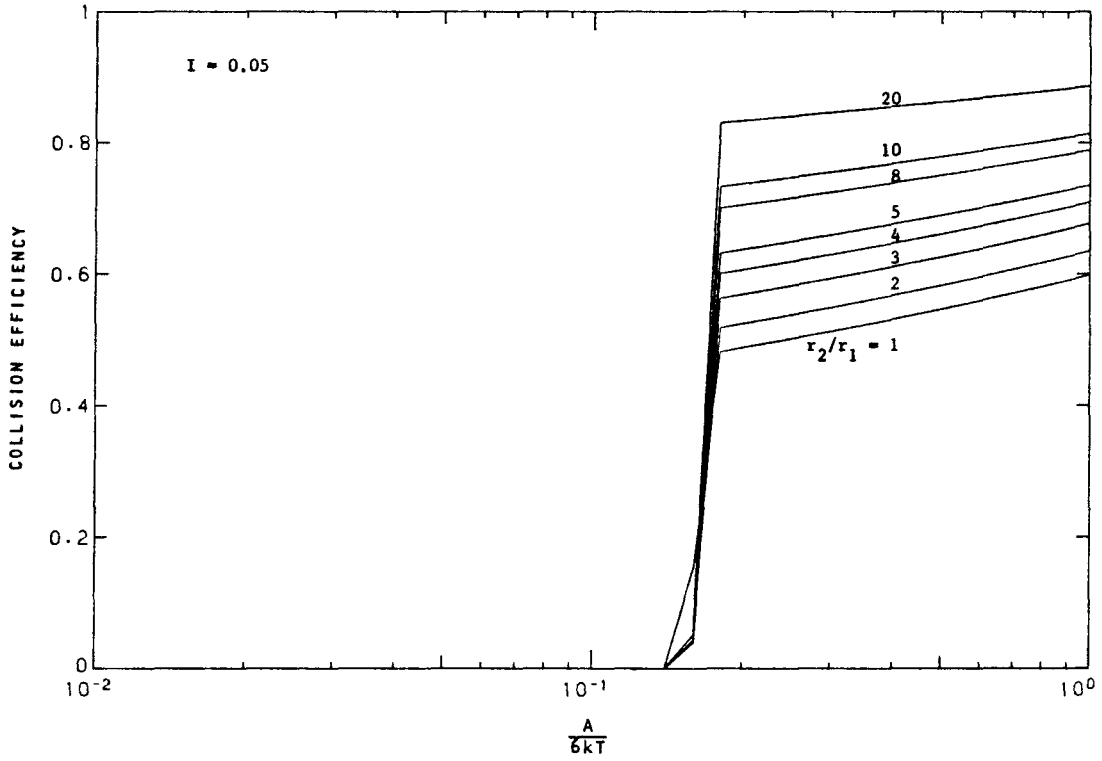

Fig. 3.9. Collision efficiences of particles in Brownian diffusion (I=0.05).

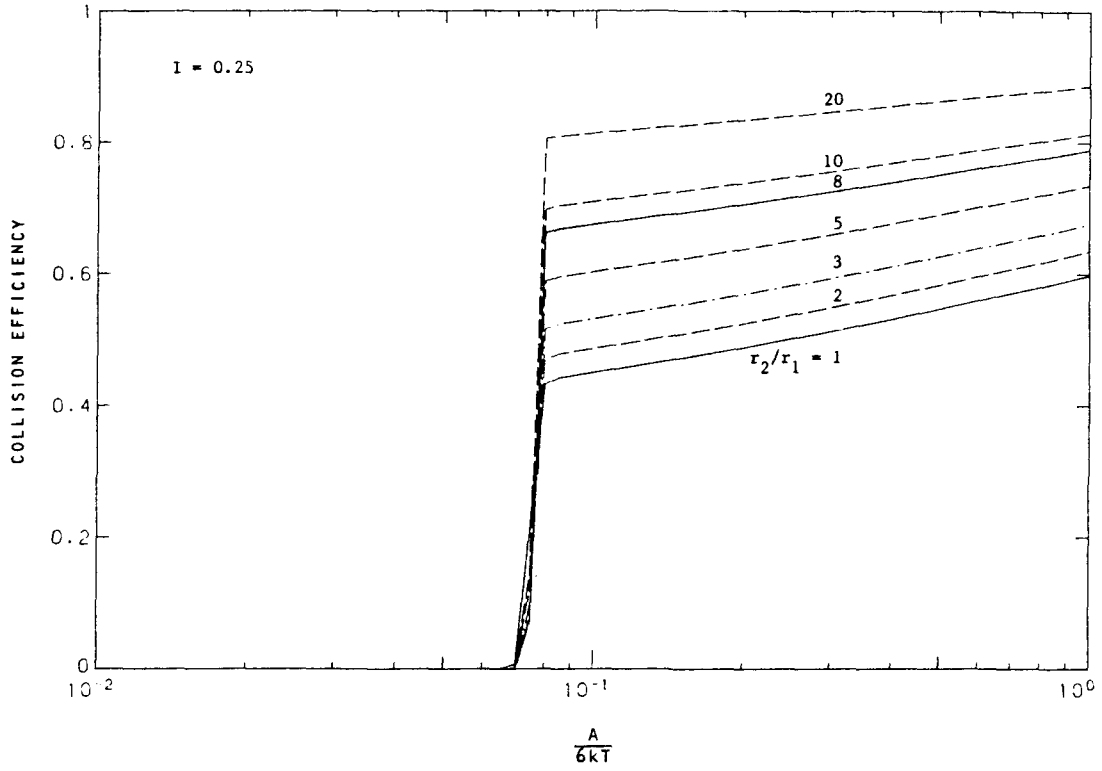

Fig. 3.10. Collision efficiences of particles in Brownian diffusion (I=0.25).

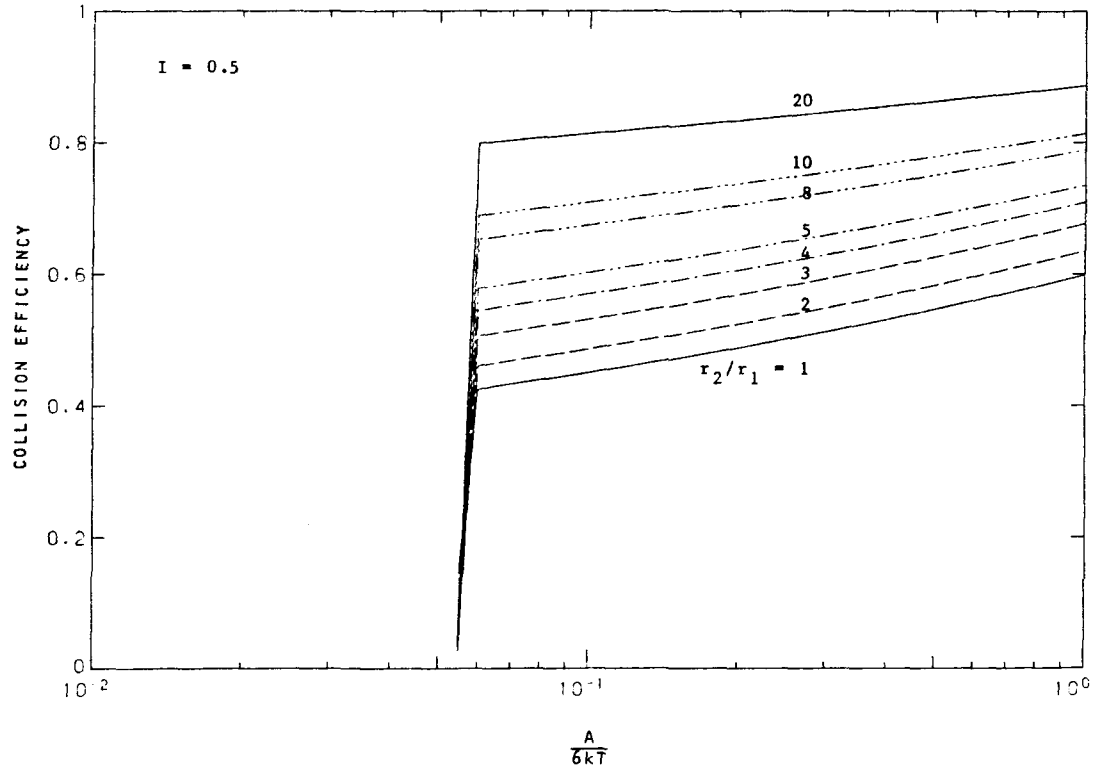

Fig. 3.11. Collision efficiences of particles in Brownian diffusion (I=0.5).

3.9, 3.10 and 3.11 illustrate the effect of the ionic strength on the collision efficiency. The horizontal parts of the curves shown are identical in the range of A/(6kT) they overlap. This is the regime of 'rapid' coagulation where the particle behavior is not influenced by electrostatic interactions. The transition from kinetically stable (no significant change in the number density of the particles during the observation time) to unstable state of the dispersion shifts to smaller A/(6kT) as the ionic strength of the solution increases. The transition is abrupt, so a quantitative criterion of coagulation (or stability) can exist.

The rapid variation of the collision efficiency with the van der Waals energy of attraction occurs in the 'slow' coagulation regime. According to Figures 3.9, 3.10 and 3.11 the transition from slow to rapid coagulation is independent of particle size. This is consistent with experimental results (Ottewill and Show, 1966) and theoretical calculations (Honig et al., 1971). Collision efficiencies are very small here, so the dispersion is stable for the time scales of most practical applications. The half-life time $t^S_{1/2}$ in which the number N of particles in an initially monodisperse system is reduced to one-half the original value by Brownian motion is (Smoluchowski, 1916)

$$t^S_{1/2} = \frac{3\mu}{4kTN} \tag{3.30}$$

Here any particle interactions are ignored (Eq. 3.30 is approximate since only collisions between primary particles of radius r are considered). The collision efficiency as defined in Eq. 3.15 is equivalent to

$$E_b(r_1,r_2) = t^S_{1/2} / t_{1/2} \tag{3.31}$$

where in $t_{1/2}$ hydrodynamic, van der Waals' and electrostatic interactions between the particles are considered. For water at ambient temperature Eq. 3.30 reduces to (Verwey and Overbeek, 1948)

$$t_{1/2} = E_b(r_1, r_2) \frac{2.10^{11}}{N} \tag{3.32}$$

where N is the number of particles per cm^3 and $t_{1/2}$ is in seconds.

The number density of particles in primary sewage sludge is, for example, of order 10^9 cm^{-3} (Faisst, 1976) corresponding to a half-life time of $t_{1/2}$=E•55 hrs. Natural waters have particle number densities of order 10^5 -10^7 cm^{-3} (O'Melia, 1980). A collision efficiency smaller than 0.001 implies a stable dispersion for all practical purposes. Consequently, only the transition from slow to rapid coagulation, given by the bend in the curves in Figures 3.9, 3.10 and 3.11 is of interest.

For the computations presented the unretarded potential (Eq. 3.10) is used. Practically there is no change in the transition from slow to rapid coagulation when the retarded potential (Eq. 3.11) is used. This is so because the energy barrier for coagulation is typically at a dimensionless particle separation of order 1 where retardation effects are not important.

Honig and Mull (1971) derived an expression for the critical electrolyte concentration at the onset of coagulation in a monodisperse system of particles with constant charge surfaces. The transition from slow to rapid coagulation is assumed to occur when the energy of interaction V_P and its derivative with respect to interparticle separation are both zero

$$\begin{aligned} V_P &= V_A + V_R^{\sigma} = 0 \\ dV_P/ds &= 0 \end{aligned} \tag{3.33}$$

For particles of different sizes the analysis by Honig and Mull (1971) is equally valid. At small separations s the van der Waals' energy of attraction between two spherical particles reduces to (Hamaker, 1937)

$$\frac{V_A}{kT} = -\frac{A}{6kT}\frac{r_1 r_2}{(r_1 + r_2)s} \tag{3.34}$$

The repulsive energy due to surface charge at small interparticle distances is obtained from Eq. 3.27. The conditions expressed by Eqs. 3.33 reduce then to

$$\frac{A}{6}\frac{1}{s} = 2\pi \int_s^{\infty} V_P(r)dr \tag{3.35}$$

and

$$\frac{A}{6}\frac{1}{s^2} = 2\pi\, V_R^{\sigma}(s) \tag{3.36}$$

and are independent of particle size. Honig and Mull (1971) solved Eqs. 3.35 and 3.36 numerically. For the small surface charges of interest here their criterion for the onset of coagulation becomes (in our notation)

$$I \gtrsim 2355 \quad \frac{kT}{e}\,\frac{\varepsilon^{1/3}}{eN_V}\,\frac{\sigma^{4/3}}{A^{2/3}} \tag{3.37}$$

valid for $A\sigma < 2\cdot 10^{-26}$. In Eq. 3.37 $N_V = 6.03\cdot 10^{23}\,\text{mole}^{-1}$ is Avogadro's number. For water at 20°C Eq. 3.37 reduces to

$$I \gtrsim 1.29\ 10^{-6}\,\frac{\sigma^{4/3}}{A^{2/3}} \tag{3.38}$$

valid for $A\sigma < 2 \cdot 10^{-26}$ (if this restriction is violated the plotted results of Honig and Mull (1971) can be used); here the ionic strength is in moles/liter (molarity), σ in Cb/cm^2 and A in Joules. Any combination of I, σ and A that do not satisfy Eq. 3.38 implies a stable dispersion for all practical purposes.

3.f. Summary

The aim of the work described in Sections 3.a through 3.e has been to improve the collision rate given by Smoluchowski's (1916) classical theory for Brownian diffusion. The computed collision efficiencies take into account hydrodynamic, van der Waals' and double layer interactions between two approaching particles.

The short-range van der Waals' potential and the long-range hydrodynamic forces tend to affect both the collision rate and the functional dependence of the collision rate on the relative sizes of the interacting particles. For practical applications only rapid coagulation is important. Double layer forces determine the onset of coagulation. Once collisions occur, the coagulation rate is determined solely from the relative mobility of the particles (modified to account for hydrodynamic forces) and the Hamaker constant.

The collision efficiencies obtained above will be used next to provide support or otherwise for Hunt's (1980) dimensional arguments. In the form presented here, however, the collision efficiencies can also be incorporated into the General Dynamic Equation (GDE) to obtain realistic results in large-scale modeling. Table 2, where several

Table 2: Collision efficiencies for Brownian diffusion
Retardation parameter $\alpha = 0.1$

Van der Waals' forces

$A/(kT)$ \ r_2/r_1	1	3	5	10	20	50	100
10^{-4}	1.0040	1.0027	1.0024	1.0022	1.0021	1.0021	1.0020
10^{-3}	1.0042	1.0028	1.0028	1.0023	1.0022	1.0021	1.0020
10^{-2}	1.0053	1.0035	1.0030	1.0025	1.0023	1.0021	1.0020
10^{-1}	1.0098	1.0064	1.0040	1.0037	1.0029	1.0024	1.0022
10^{0}	1.0248	1.0157	1.0116	1.0075	1.0049	1.0032	1.0026
10	1.0691	1.0435	1.0251	1.0189	1.0120	1.0059	1.0040
10^{2}	1.1983	1.1255	1.0905	1.0540	1.0300	1.0142	1.0082

Van der Waals' and hydrodynamic forces

$A/(kT)$ \ r_2/r_1	1	3	5	10	20	50	100
10^{-4}	0.2409	0.2971	0.3615	0.9810	0.6198	0.7875	0.8763
10^{-3}	0.2791	0.3401	0.4079	0.5287	0.6620	0.8154	0.8936
10^{-2}	0.3286	0.3931	0.4628	0.5824	0.7060	0.8425	0.9101
10^{-1}	0.3867	0.4512	0.5207	0.6338	0.7468	0.8659	0.9237
10^{0}	0.4546	0.5150	0.5806	0.6841	0.7838	0.8862	0.9354
10	0.5477	0.5981	0.6562	0.7430	0.8245	0.9070	0.9471
10^{2}	0.7194	0.7335	0.7700	0.8266	0.8796	0.9341	0.9620

Table 3. Approximations for collision efficiences in Brownian diffusion. Retardation parameter $\alpha = 0.1$. (valid for $1 \leq r_2/r_1 \leq 20$)

$$E_b(r_1,r_2) = a + bx + cx^2 , \qquad x = \frac{r_2}{r_1}$$

A/(kT)	a	b x 10^2	b x 10^4
10^{-4}	0.20476	3.4380	-6.8101
10^{-3}	0.24189	3.6450	-7.7214
10^{-2}	0.29092	3.7830	-8.5445
10^{-1}	0.35031	3.7367	-8.7799
10^{0}	0.42068	3.5065	-8.4639
10	0.51820	3.0145	-7.4242
10^{2}	0.69756	1.6075	-3.4718

computed collision efficiencies are listed, and Figure 3.5 serve this purpose. In the latter the collision efficiency is given as a function of the ratio of the radii of the interacting particles for various energies of attraction. The curves in Figure 3.5 are given in parametric form in Table 3. Interpolation can be used for intermediate values of the Hamaker constant. Experimental information on the Hamaker constant, the charge on the particles and the ionic strength of the dispersive medium are then needed to predict the time evolution of the particle size distribution in a coagulating dispersion.

3.g. Computer Simulation

For Brownian induced coagulation in the presence of van der Waals' forces and hydrodynamic interactions, the functional dependence of the collision efficiency on the relative size of the interacting particles (see Figure 3.5) suggests that the first assumption in the theory is invalid.

The computer simulation of Pearson et al. (1983) is used to investigate the dependence of the steady state size distribution on the externally imposed conditions, in particular the particle size range covered in any computer run. The collision function β depends only on the relative size of the interacting particles; the collision efficiency E_b depends both on the relative and the absolute size of the interacting particles. The collision rate of particles r_1 and r_2, per unit time and per volume V of fluid, under the influence of hydrodynamic and van der Waals' forces can be set equal to the collision rate of the

same number of non-interacting particles t_1 and t_2, per volume V_t of fluid and per unit time

$$\frac{2}{3}\left(\frac{kT}{\mu}\right)\frac{(r_1+r_2)^2}{r_1 r_2}\frac{E_b}{V} = \frac{2}{3}\left(\frac{kT}{\mu}\right)\frac{(t_1+t_2)^2}{t_1 t_2}\frac{1}{V_t} \tag{3.39}$$

Solving Eq. 3.39 for t_2/t_1 we obtain

$$\frac{t_2}{t_1} = -1 + \frac{1}{2}\frac{\left(1+\frac{r_2}{r_1}\right)^2}{\frac{r_2}{r_1}}\frac{E_b}{E_1} + \frac{1}{2}\left(1+\frac{r_2}{r_1}\right)\sqrt{\frac{E_b}{E_1}\frac{r_1}{r_2}\left[\frac{\left(1+\frac{r_2}{r_1}\right)^2}{\frac{r_2}{r_1}}\frac{E_b}{E_1} - 4\right]} \tag{3.40}$$

where we have put $V_t = E_1 \cdot V$; E_1 is the collision efficiency for $r_2/r_1 = 1$ and is introduced so that Eq. 3.39 has real roots. For $r_2/r_1 = 1$ Eq. 3.40 gives $t_2/t_1 = 1$. Thus, the collision rate in a monodisperse non-interacting system of particles, per volume V of fluid, is equal to the collision rate, per volume $(V \cdot E_1)$ of fluid, in a system of the same number of particles of equal size between which hydrodynamic and van der Waals' forces act (hereupon referred to as the realistic system). Eq. 3.40 maps the realistic system of particles of all sizes onto a non-interacting particle system; the latter is simulated in the model and the evolution of the size distribution of the realistic system is followed using Eq. 3.39. The method for generating the particle displacements at each step and updating their positions is described in detail in Pearson et al. (1983). The initial volume concentration of suspended particles used in the simulations ranges from 0.1% to 1%; such a high concentration is necessary in order to achieve results in reasonable computation times.

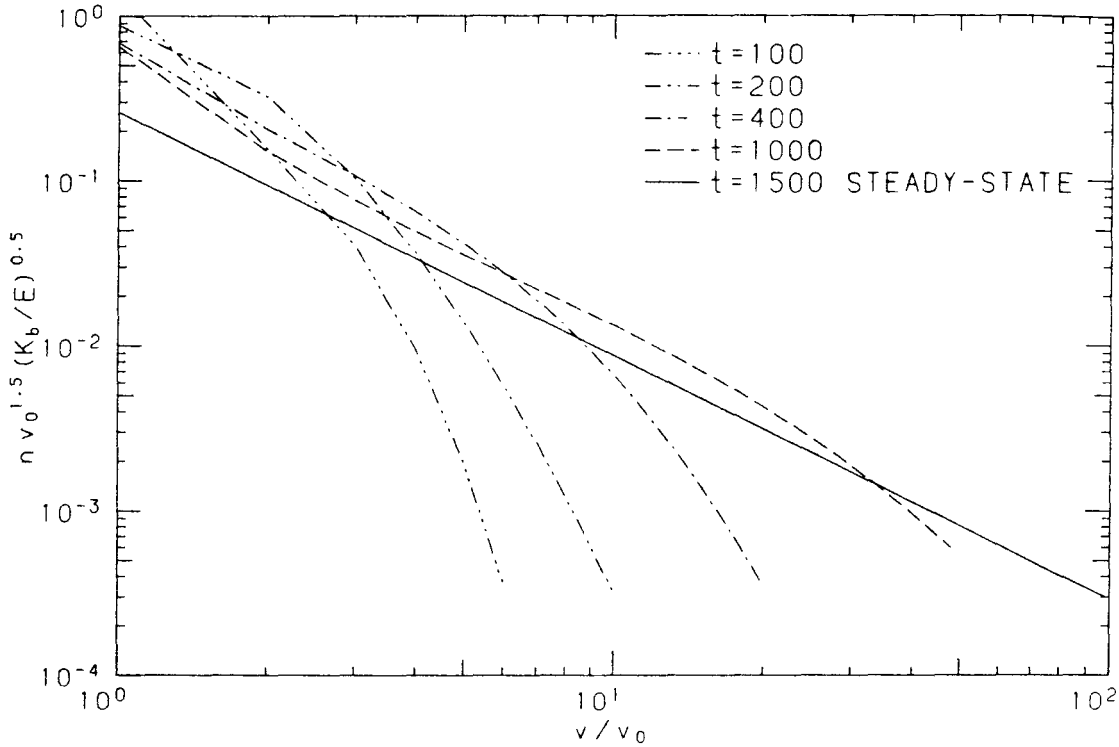

Fig. 3.12. Evolution of the normalised size distribution for Brownian motion. V=125, r_o=0.075, D_o=0.005, Δt=0.25, N_A=1, r_{max}=0.375.

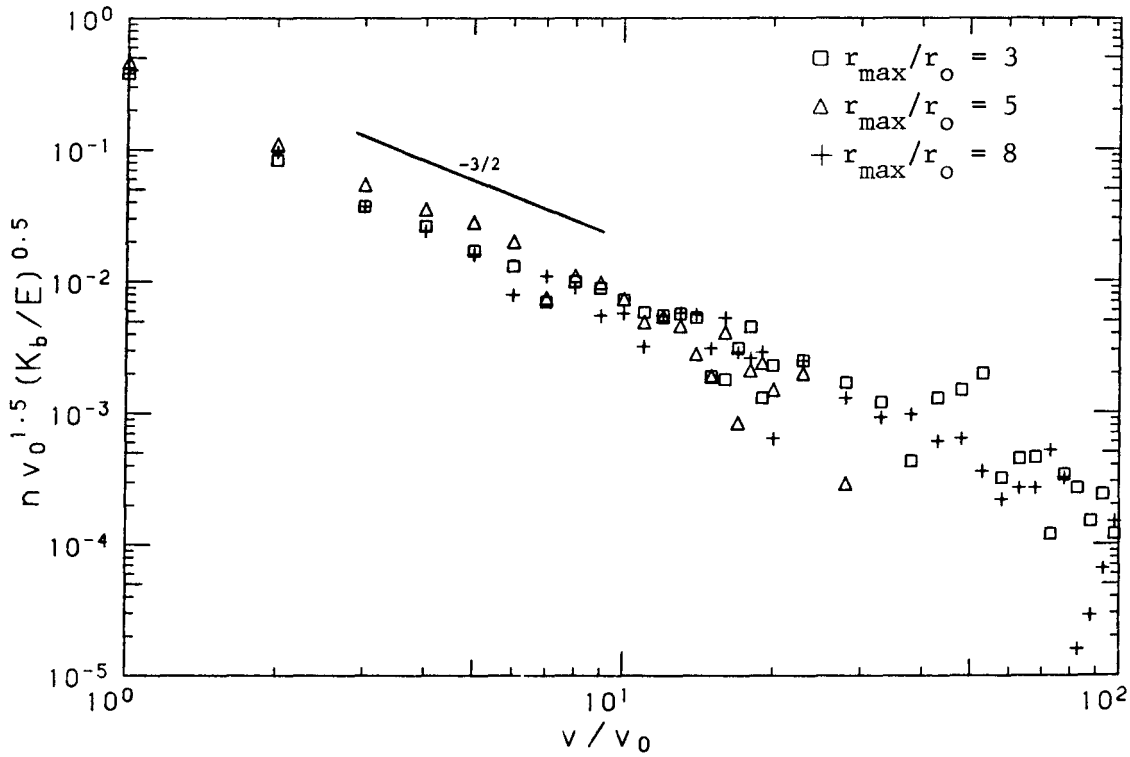

Fig. 3.13. Comparison of the steady state non-dimensional size distribution for Brownian motion for different r_{max}/r_o. Non-interacting system. V=125, r_o=0.075, D_o=0.005, Δt=0.25, N_A=1; Δ r_{max}=0.225; □ r_{max}=0.375; + r_{max}=0.6.

Figure 3.12 shows the time development of the normalised particle size distribution of a population of particles undergoing Brownian induced coagulation. The suspension is initially monodisperse and has a volume concentration of 0.57%. The curves shown are smoothed approximations to ensemble averages of actual data points from five simulation runs. The data in the small size range attain a slope of about -3/2 once particles ten-fold in volume are created. The level of the distribution declines then gradually until, after about 1200 time-steps, a dynamic equilibrium is reached; this occurs when the first large particle is physically removed from the 'control' volume.

All lengths in the computer model are non-dimensionalised with the radius of the unit particle and the time-scale used depends only on the magnitude of the diffusion coefficient of the unit particle. An aerosol particle of 1 μm radius has a diffusivity of about $13\ 10^{-8} cm^2$ /sec (Pruppacher and Klett, 1978). For a micron-size particle then, 1 sec of real time corresponds to about 15 time steps in the simulation. Similarly, for a particle of radius 0.1 μm, 1 sec of real time is equivalent to 264 time steps. Thus, for the volume concentrations used here the growth of the population of suspended particles examined is very rapid.

The series of simulation runs shown in Figures 3.13, 3.14 and 3.15 illustrate the effect that the ratio v_{max}/v_o (i.e. the size range covered by the simulation) has on the final steady state size distributions; v_o is the unit particle volume and v_{max} the volume of the largest particle allowed to remain in the system. All simulation runs were started with a monodisperse population of particles. In all figures three runs with v_{max}/v_o =27,125 and 512 are shown. The points

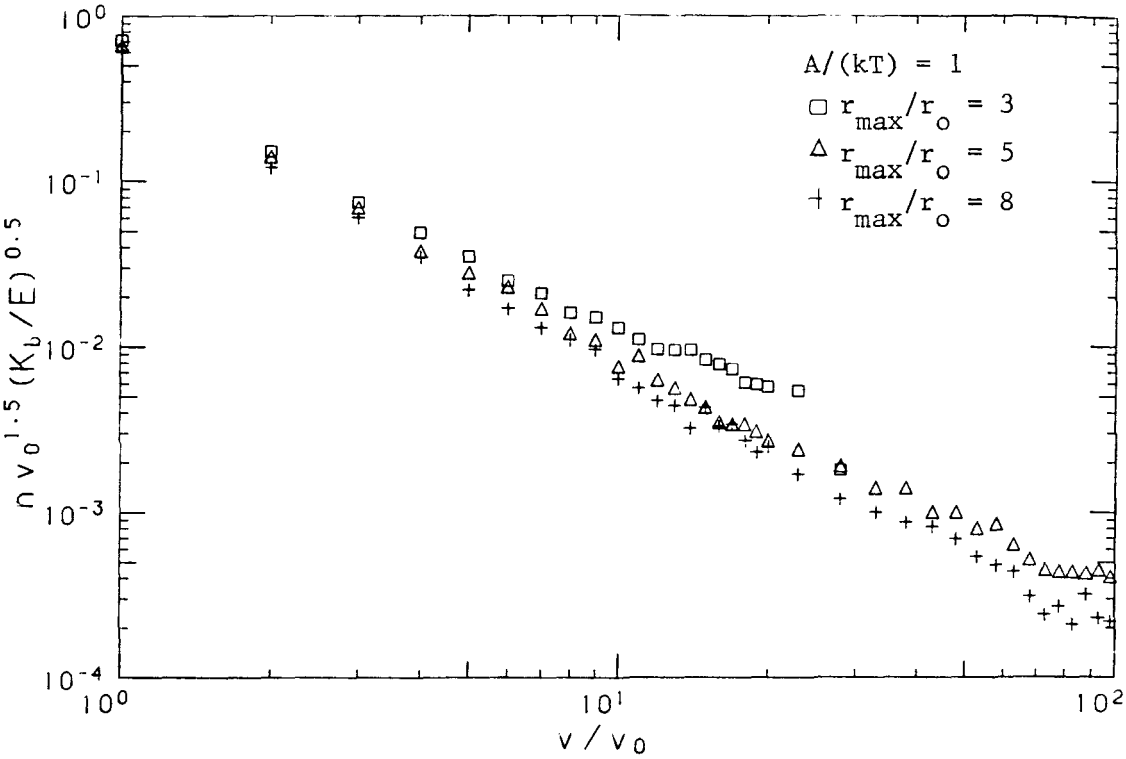

Fig. 3.14. Comparison of the steady state non-dimensional size distribution for Brownian motion for different r_{max}/r_o for A/(kT)=1. Realistic system. V=125, r_o=0.075, D_o=0.005, Δt=0.25, N_A=1; □ r_{max}=0.225; △ r_{max}=0.375; + r_{max}=0.6.

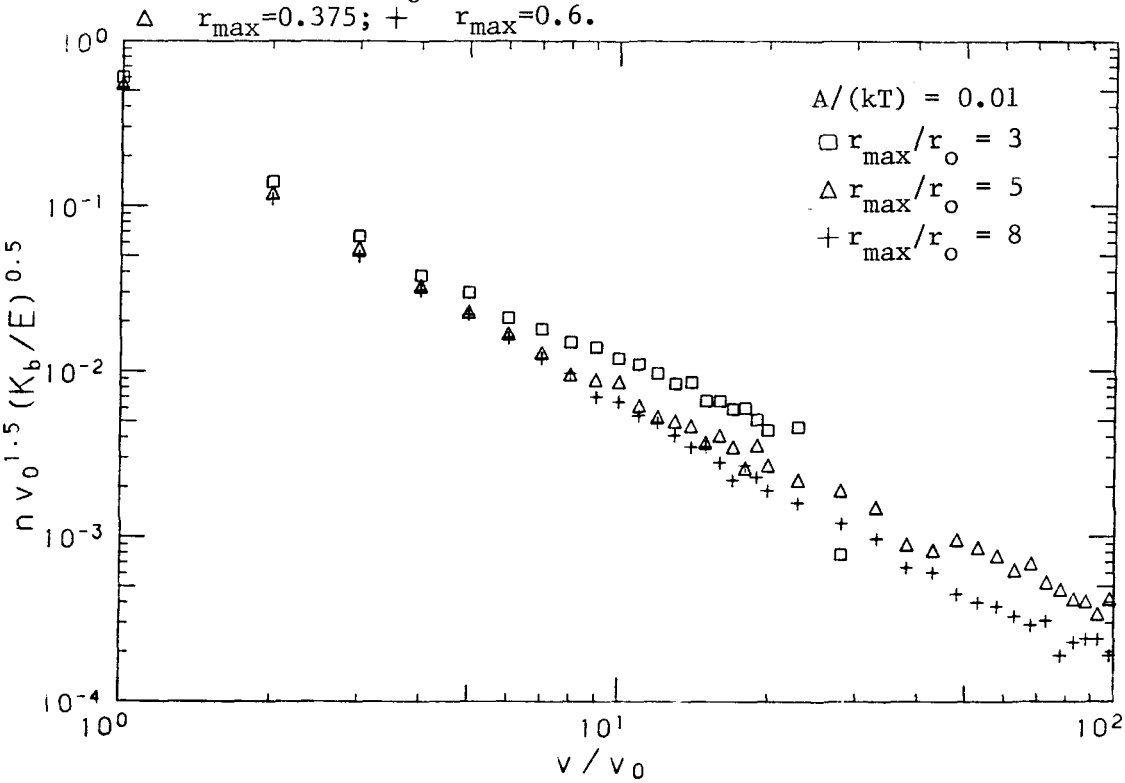

Fig. 3.15. Comparison of the steady state non-dimensional size distribution for Brownian motion for different r_{max}/r_o for A/(kT)=0.01. Realistic system. V=125, r_o=0.075, D_o=0.005, Δt=0.25, N_A=1; □ r_{max}=0.225; △ r_{max}=0.375; + r_{max}=0.6.

plotted in Figure 3.13 are numerical data obtained by Pearson et al. who did not account for interparticle forces. The data shown are averaged over 1000 time steps; this is necessary because of the small number of particles involved in the simulation (typically about 200 to 400 particles). The data points, when non-dimensionalised according to Eq. 1.2 and plotted logarithmically against particle volume (non-dimensionalised with the unit particle volume), collapse onto a slope of -3/2.

Pearson et al., based on the results shown in Figure 3.13, suggest that the final steady state distribution of a system of particles undergoing Brownian coagulation is insensitive to the size range covered by the simulation.

The next two figures show how the steady state size distribution is modified when hydrodynamic and van der Waals' forces between the particles are considered. For the simulations in Figure 3.14 the Hamaker group A/(kT) is 1 and for those in Figure 3.15 it is 0.01 (it thus covers the range of Hamaker constants found in natural waters). The data shown are averaged over 2000 time steps; because of the decreased coagulation rate the size distribution evolves slower, so a longer time average is required to obtain meaningful results. Again the data points when normalised according to Eq. 1.2 exhibit the -3/2 power law. The level of the distributions as determined by the intercept of the best fit line of slope -3/2 with the axis v/v_o is considerably above the simulation runs of Pearson et al. This is shown in Figure 3.16 where the results of two computer simulations at different A/(kT) are compared with the non-interacting system of Pearson et al., all other parameters being the same.

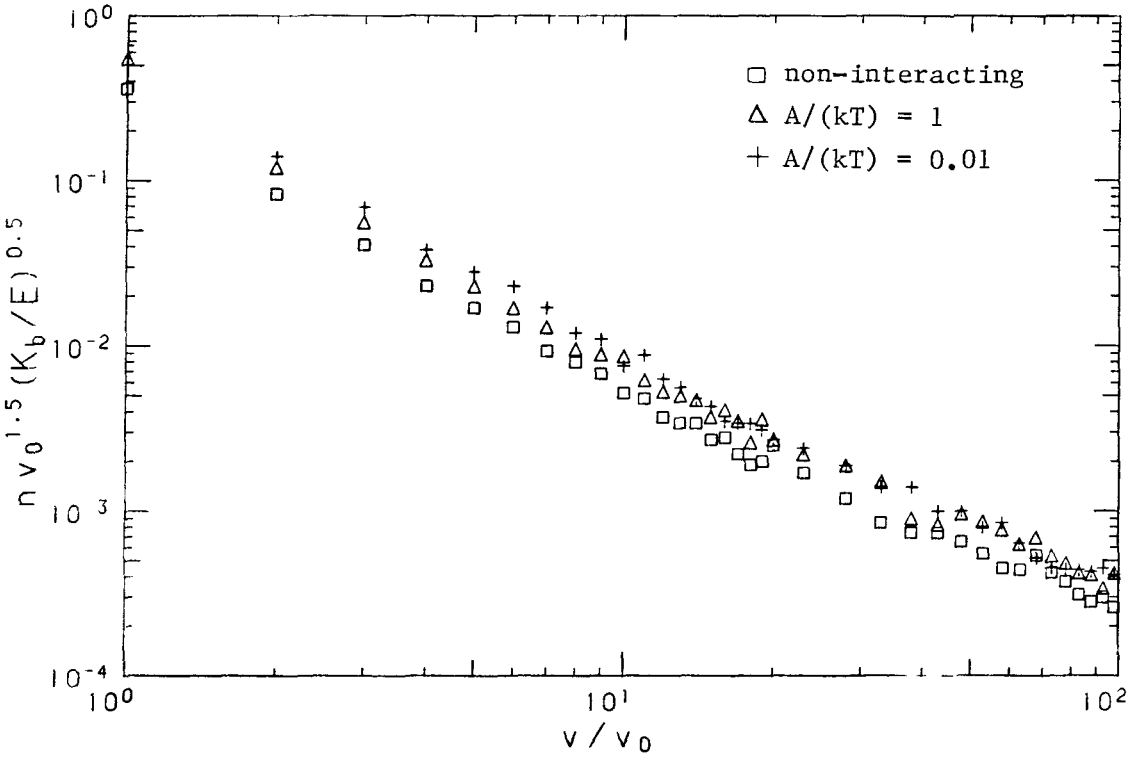

Fig. 3.16. Comparison of the steady state non-dimensional size distribution for a non-interacting system and for two realistic suspensions with different values of A/(kT). V=125, r_o=0.075, D_o=0.005, Δt=0.25, N_A=1, r_{max}=0.375; □ non-interacting system; Δ realistic system with AkT=1; + realistic system with A/kT=0.01.

At the upper end of the size range the results of all three simulation runs in both Figures 3.14 and 3.15 are statistically identical. It seems that the constant addition of unit particles, which clearly cannot represent properly the creation of unit particles by coagulation of smaller ones, covers the influence of v_{max} on the smallest particles of the simulation. For the largest part of the size range a consistent decline in level of the size distribution with increasing v_{max}/v_o occurs in both Figures 3.14 and 3.15. Contrary to the 'non-interacting' particle system of Pearson et al. the size range influences the final steady state size distribution.

4. LAMINAR SHEAR

Adler (1981) used the rigorous theory for the hydrodynamic interaction of two unequal spheres in simple shear flow (Batchelor and Green, 1972, Arp and Mason, 1976) to correct Smoluchowski's (1917) expression for the collision rate of spherical particles with radii r_1 and r_2 and number concentrations N_1 and N_2, per unit volume of fluid. Adler's (1981) formulation for the collision rate is

$$\text{collision rate} = 2/3\ N_1 N_2 (r_1+r_2)^3 G\ E_{sh}\ (r_1,r_2) \qquad (4.1)$$

where $E_{sh}(r_1,r_2)$ is Adler's (1981) correction factor (or collision efficiency) to Smoluchowski's (1917) expression for the collision rate, which considers only binary particle encounters and assumes that

particles move on straight paths (rectilinear approach). Geometrical exclusion determines the collision cross-section of the two particles. Hydrodynamic forces induce curvature in the particle trajectories which can be open or closed (Adler, 1981). Between the two kinds of trajectories a separation surface exists whose cross-section at infinite interparticle distance defines a 'curvilinear' collision cross-section (Adler, 1981). In the absence of other forces the cross-section of the separation surface tends to zero at large distances (Batchelor and Green, 1972), the singular behavior of the interparticle hydrodynamic force in Stokes' flow at particle contact. When, in addition, van der Waals' or other external forces act between the particles a non-zero curvilinear cross-section may exist (Adler, 1981).

The correction $E_{sh}(r_1,r_2)$ to the rectilinear collision rate is equivalent to defining a curvilinear collision cross-section a^2

$$a^2 = E_{sh}^{2/3}(r_1,r_2)(r_1 + r_2)^2 \qquad (4.2)$$

For two unequal spherical particles in simple shear flow in the presence of van der Waals' forces $E_{sh}(r_1,r_2)$ is a function of the relative size of the interacting particles and the dimensionless parameter

$$H = A/(144\,\pi\mu\, r_2^3\, G) \qquad (4.2)$$

where A is the van der Waals' energy of attraction, G the rate of strain and r_2 the radius of the large particle. H represents the relative strength of the shear and the attractive van der Waals' forces. The

collision efficiency $E_{sh}(r_1,r_2)$ is plotted in Figure 4.1 against the relative size of the interacting particles for various values of H. Adler (1981) reports corrections to the rectilinear collision rate for four different relative particle sizes r_2/r_1=1, 2, 5, 10 and for H ranging from 10^{-2} to 10^{-5}. Interpolation was used to obtain the collision rate corrections for intermediate values of r_2/r_1. Figure 4.1 indicates that homocoagulation (coagulation between particles of similar size) is favored over heterocoagulation. The first requirement for the existence of a quasi-stationary size distribution in a coagulating system of particles is, thus, fulfilled.

The computer simulation model of Pearson et al. is used to study the evolution of the size distribution of a coagulating population of particles subjected to laminar shear and accounting for van der Waals' forces. The correction to the curvilinear collision cross-section obtained from Eq. 4.2 is used in the simulation to check for particle collisions.

Figure 4.2 illustrates the evolution in time of an initially monodisperse suspension of particles with an initial volume concentration of 0.57% colliding under the influence of simple shear. The data of six simulation runs with identical initial conditions are averaged and normalised according to the dimensional arguments (see Eq. 1.3) to give the plotted curves. The temporal development of the size distribution follows a pattern similar to the Brownian system, that is, the upper portion of the size spectrum attains a slope of -2 once a range of about one decade in volume is reached. Notice that the size distribution approaches its steady state value long before a dynamic equilibrium is attained. If r_o represents an aerosol particle with

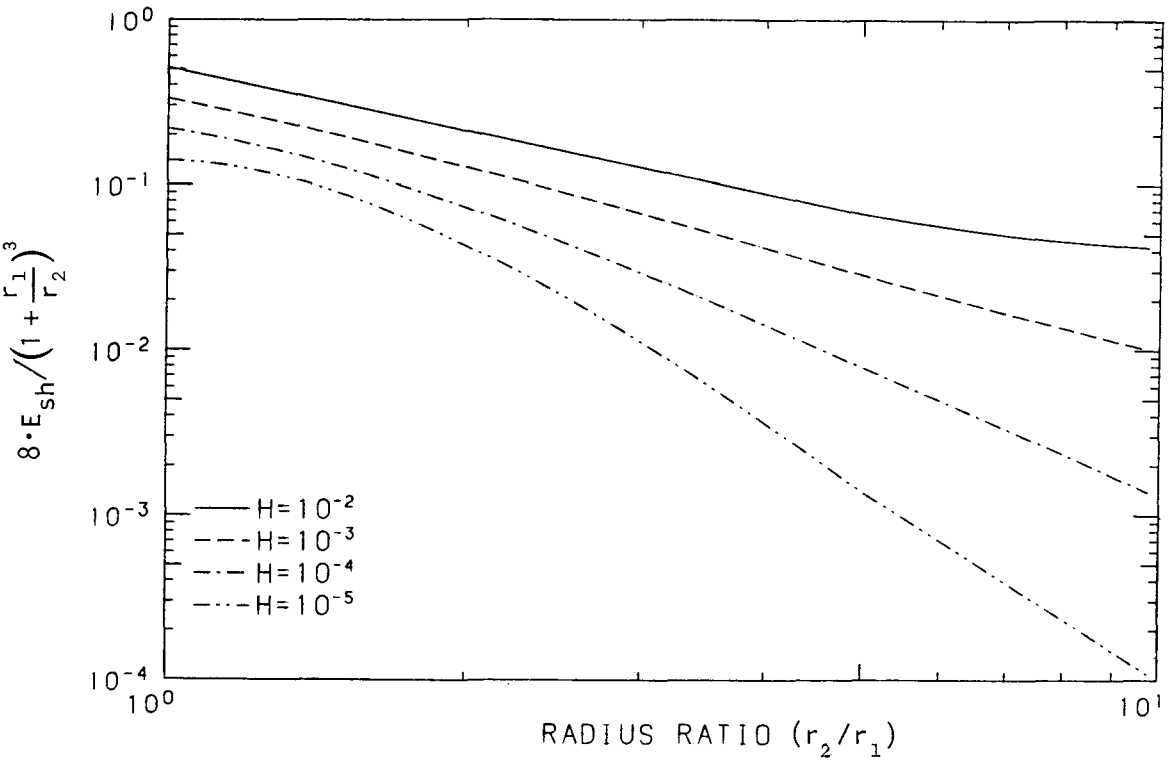

Fig. 4.1. Collision efficiencies of spherical particles in simple shear (Adler, 1981).

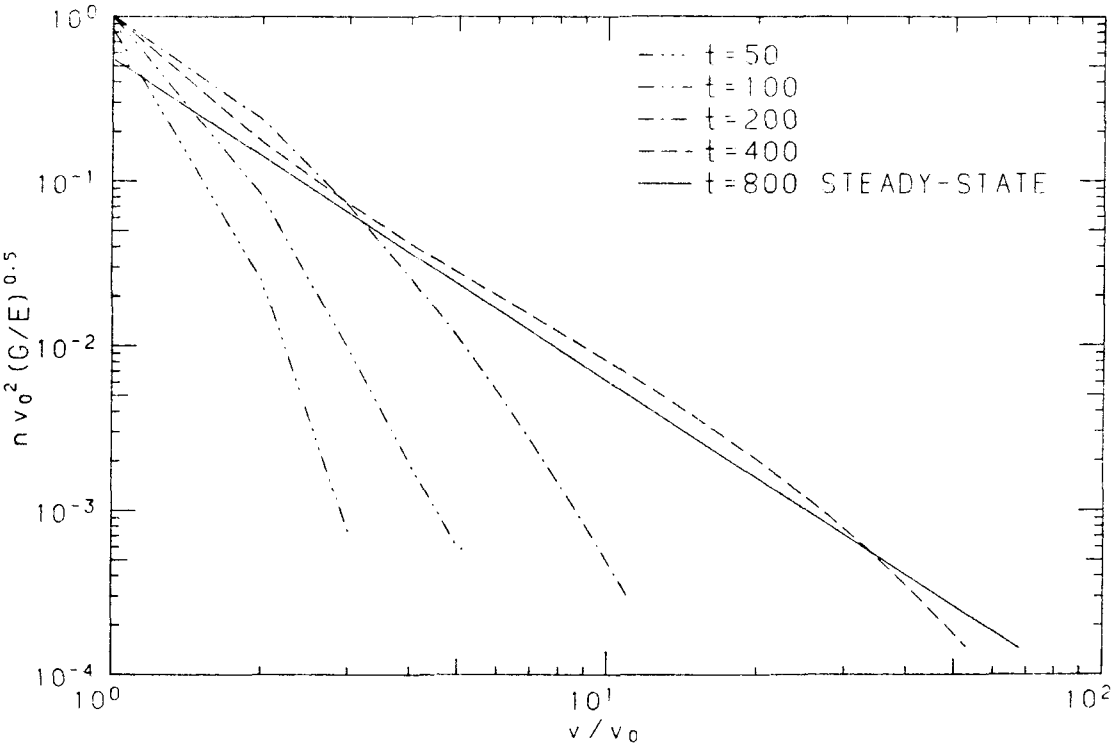

Fig. 4.2. Evolution of the normalised size distribution for laminar shear. $H=10^{-2}$, G=1, V=125, $r_o=0.075$, $\Delta t=1$, $N_{initial}=400$, $N_A=5$, $r_{max}=0.375$.

radius 1μm, then the strain rate used corresponds to $G=125sec^{-1}$ and the time step to 1/125 seconds; if r_0 is set equivalent to a micron-size hydrosol particle, $G=2sec^{-1}$ and the time step corresponds to 0.5 seconds.

Figure 4.3 is a comparison of the steady state size distribution of three coagulating populations of particles when the maximum size of particle, v_{max} , allowed to stay in the 'control' volume varies. For the three sets of data shown $H=10^{-2}$ and $v_{max}/v_o=27,125$ and 512. The numerical results, non-dimensionalised according to Eq. 1.3 and averaged over 2000 time steps collapse onto a slope of -2. The three populations of particles are statistically identical: the size range does not influence the final steady state size distribution.

The effect of the hydrodynamic interactions in decreasing the coagulation rate is illustrated in Figure 4.4. The final steady state size distribution of two populations of particles at $H=10^{-2}$ and 10^{-4} are compared with the non-interacting system of Pearson et al. The size distribution shifts upwards as the strength of the shear (i.e. rate of strain) decreases.

5. DIFFERENTIAL SEDIMENTATION

5.a. Hydrodynamic Interactions and Computer Simulation

In contrast to Brownian diffusion and fluid shearing, differential

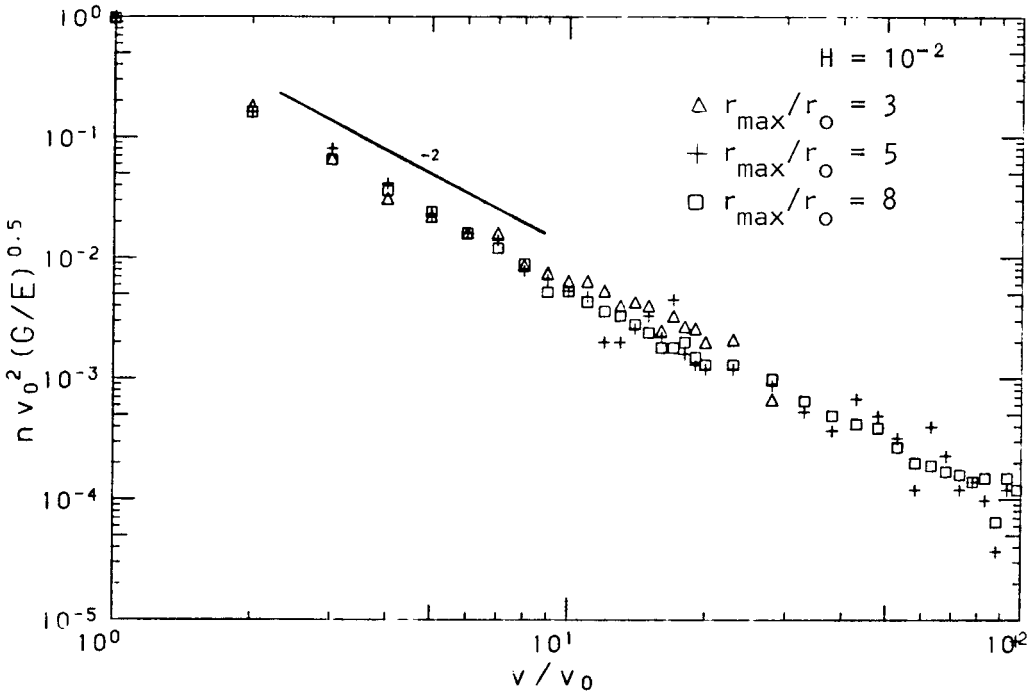

Fig. 4.3. Comparison of the steady state normalised size distribution for laminar shear for different values of r_{max}/r_o. $H=10^{-2}$, G=1, V=125, r_o=0.075, Δt=1, N_A=5; △ r_{max}=0.0225; + r_{max}=0.375; □ r_{max}=0.6.

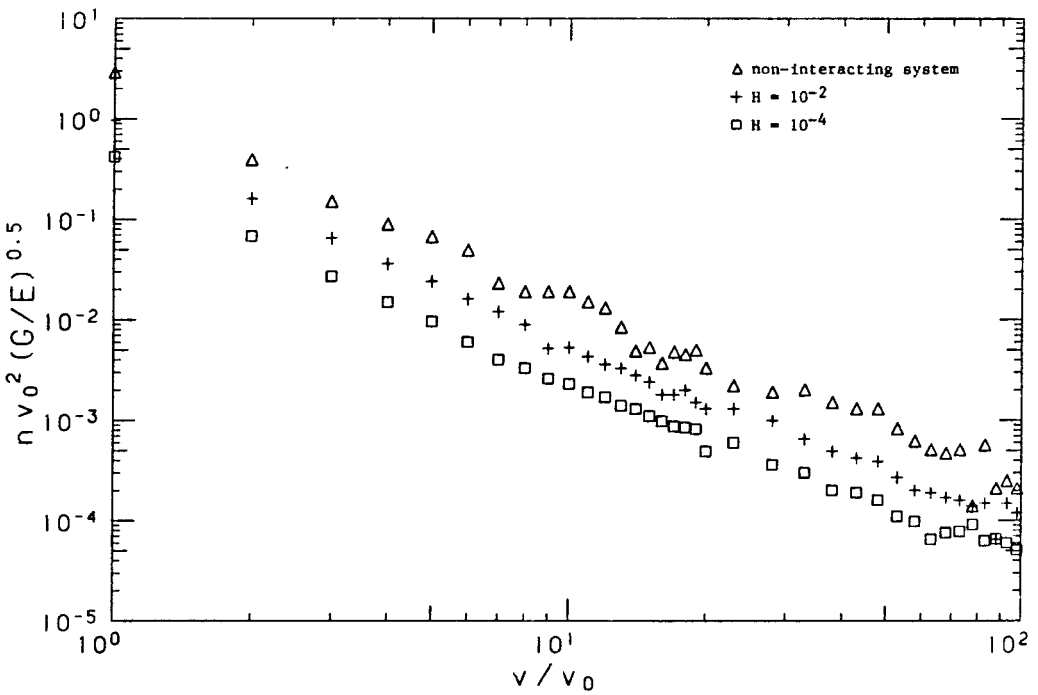

Fig. 4.4. Comparison of the steady state normalised size distribution for laminar shear for a non-interacting system and for two realistic systems with different values of $H=A/(144\ \pi\mu r^3 G)$. △ non-interacting system, G=1, V=1, r_o=0.03, Δt=1, N_A=10, r_{max}=0.15; + realistic system, $H=10^{-2}$, G=1, V=125, r_o=0.075, Δt=1, N_A=5, r_{max}=0.375; □ realistic system, $H=10^{-4}$, G=1, V=125, r_o=0.075, Δt=1, N_A=1, r_{max}=0.375.

sedimentation induced coagulation involves a physical property of the particles: their density excess ratio, $\frac{\rho_p - \rho_f}{\rho_f}$ over that of the fluid. Collisions and subsequent coagulation may occur when larger or heavier particles overtake smaller ones.

The presence of a particle moving with velocity u induces a velocity gradient of order ur/s^2 at a distance s in the surrounding fluid (Batchelor, 1976). This velocity gradient modifies the trajectory of an approaching particle as if a force dipole were located at the position of the particle. The collision rate, per unit volume of fluid and unit time, of particles with sizes r_1 and r_2 is given by the rectilinear collision function for differential settling (Table 1) multiplied by the number densities N_1 and N_2 of the particles and the collision efficiency $E_{ds}(r_1,r_2)$

$$\text{collision rate} = (2/9)\,\pi K_{ds}(r_1+r_2)^2 |(r_1^2 - r_2^2)| N_1 N_2 E_{ds}(r_1,r_2) \qquad (5.1)$$

Theoretical computations of the collision efficiency are based on several assumptions (see Pruppacher and Klett, 1978) and yield approximately the same values for E_{ds} as given by Eq. 5.2. Experimental difficulties have not allowed verification of the computed collision efficiencies in the laboratory, mainly because of the critical role which molecular or other short range forces play in coalescing two particles which are brought into contact by their relative motion (Tag, 1974). Neiburger et al. (1974) obtained an analytic expression for theoretical collision efficiencies, computed assuming Stokes flow (with the slip-flow correction) and modified to be consistent with

experimental results:

$$E_{ds} = E_o + E_1 + E_2 + E_3 + E_4$$

where
$$E_o = 0.95 - (0.7 - 0.005\, r_2)^4 \,(7.92 - 0.12\, r_2 + 0.001\, r_2^2)$$
$$E_1 = -\left(\frac{r_1}{r_2} - 0.5\right)^2$$
$$E_2 = -1.5 \exp\left[-(0.0015\, r_2^2 + 8)\frac{r_1}{r_2}\right] \qquad (5.2)$$
$$E_3 = -(1 - 0.007\, r_2) \exp\left[-0.651\, r_2 \left(1 - \frac{r_1}{r_2}\right)\right]$$
$$E_4 = \begin{cases} 0 & r_2 < 20\mu m \\ \exp\left[-30\left(1 - \frac{r_1}{r_2}\right)\right] & r_2 \geq 20\mu m \end{cases}$$

E_{ds} is plotted in Figure 5.2 as a function of the particle ratio $p=r_1/r_2 (r_2 > r_1)$ for different r_1. For fixed relative particle size the collision efficiency E_{ds} increases with increasing particle size since the deflecting hydrodynamic forces become less important as particle inertia increases. For the same reason E_{ds} decreases with p when $p << 1$, for fixed r_2. For p near unity 'wake' capture occurs when the two particles are large enough for inertial effects to become appreciable.

The coagulation process was simulated by imposing on each spherical particle its Stokes° terminal settling velocity w

$$w = \frac{2}{9} \frac{g(\rho_p - \rho_f)}{\mu} r^2 \qquad (5.3)$$

valid for time scales greater than the particle viscous relaxation time

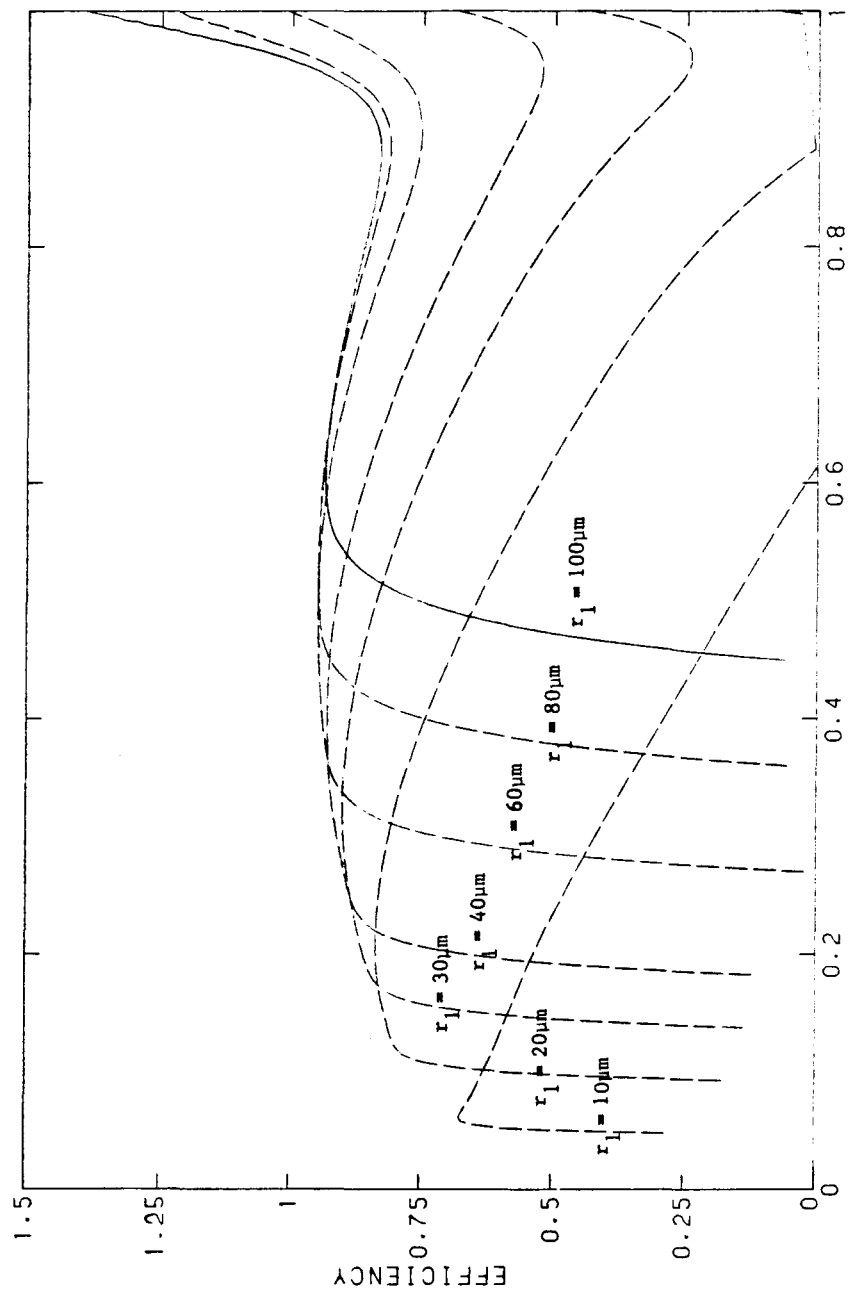

Fig. 5.1. Collision efficiences of sedimenting particles of various sizes (Neiburger et al., 1974).

$t = \frac{2}{9}\frac{r^2}{\nu}$. All particles have the same density and are moving in a 'control volume' of variable dimensions. Particles reaching the bottom are reintroduced at the top at a random cross-sectional position. This is necessary in order to prevent the simulation from becoming deterministic after a certain time: collisions would cease after each particle had swept out its own path through the control volume. Particles move in straight paths during the time step Δt. Eq. 5.1 suggests that hydrodynamic interactions can be incorporated in the simulation by using an effective collision cross-section

$$\text{effective collision cross-section} = E_{ds}(r_1,r_2)\ (r_1+r_2)^2 \qquad (5.5)$$

to check for particle collisions. Notice, however, that this formulation assumes that collisions between particles of equal size do not occur even when their collision efficiency is non-zero, ignoring thus wake capture.

The algorithm was verified using a non-coagulating version of the simulation with two particle sizes. The collision rates computed from the simulation were in agreement with the prediction of the theoretical model (see Figure 6.1 in Section 6).

An initially monodisperse system of spherical particles was subjected to gravity settling. Weak Brownian diffusion or weak fluid shearing operated at the same time to initiate the coagulation process. When uniform shearing motion $u = G \cdot x$ is imposed in the presence of settling, the particle crosses the streamlines perpendicular to the

direction of the shearing during the time step Δt. The particle displacement Y(i) in any time step is then

$$Y(i) = (Y_1(i),0,Y_3(i))$$
$$Y_1(i) = G\cdot(P_3(i)+0.5Y_3(i))\cdot\Delta t, \qquad Y_3(i) = (2/9)K_{ds}r^2\Delta t \tag{5.6}$$

where $P(i)=(P_1(i),P_2(i),P_3(i))$ is the position of the particle i at the beginning of the time step. It is necessary to take into account the 'average' vertical position of the particle during any time step Δt to predict correctly the collision rates.

5.b. Simulation Results

Figure 5.2 shows the steady state size distributions of two initially monodisperse systems subjected to weak Brownian motion and weak laminar shearing, respectively, and gravity settling. Hydrodynamic interactions such as discussed in Sections 3 and 4, are initially ignored but will be discussed later. The size distributions are collapsed when non-dimensionalised according to Eq. 1.4 and plotted against particle volume, non-dimensionalised with the unit particle volume. A constant -13/6 slope line is drawn for comparison. The data shown in Figure 5.2 are results of the simulation averaged over 1600 time steps. A long-time average is needed to reduce the scattering of the data at the long tail of the distribution caused by the high collision probability of the large particles.

The next figure illustrates how weak Brownian motion modifies the

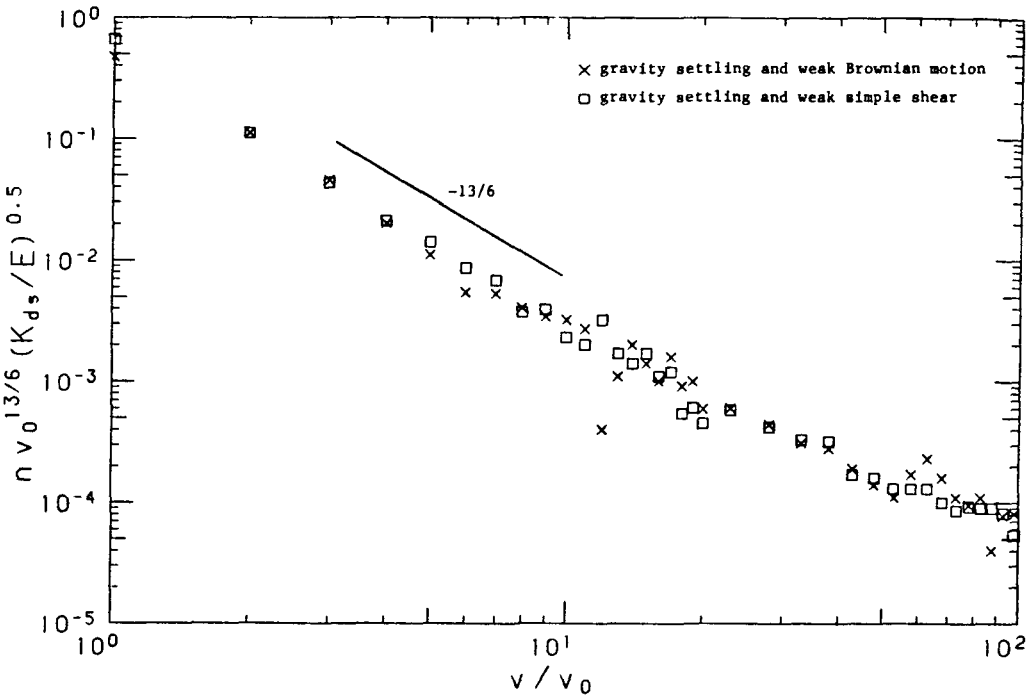

Fig. 5.2. Non-dimensional steady state particle size distributions for differential sedimentation and weak Brownian motion or weak laminar shear. Non-interacting suspensions. □ K_{ds}=50, G=2, V=125, r_o=0.075, Δt=0.25, N_A=1, r_{max}=0.375; × K_{ds}=50, D_o=0.005, V=128, r_o=0.075, Δt=0.25, N_A=1, r_{max}=0.375.

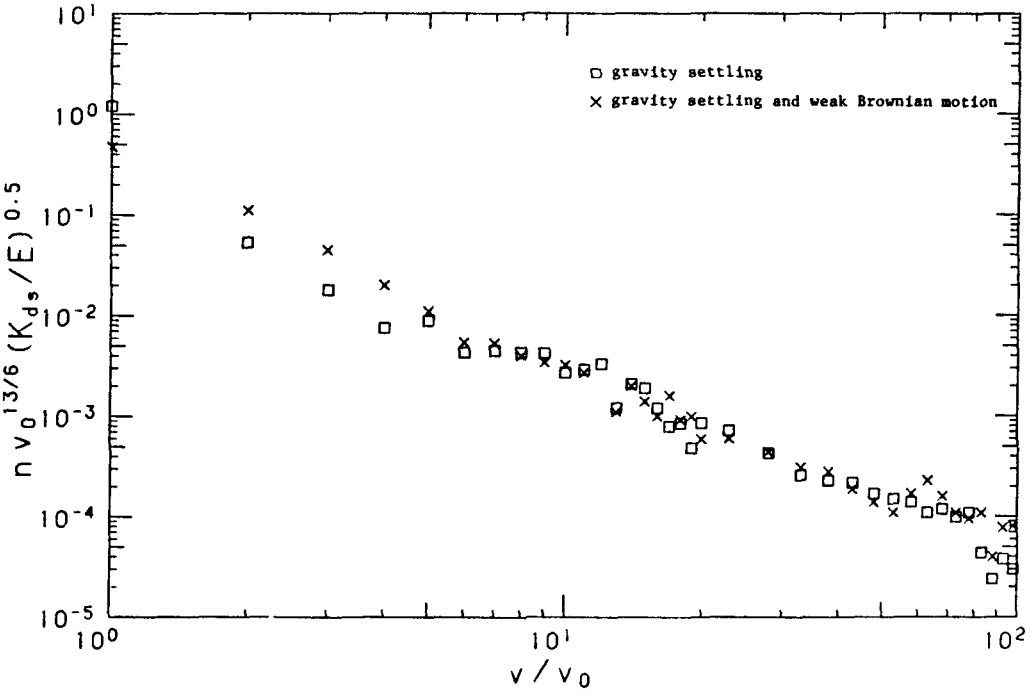

Fig. 5.3. Comparison of the steady state normalised size distribution for differential settling and Brownian motion with differential settling. K_{ds}=50, r_o=0.075, Δt=0.25, N_A=1, r_{max}=0.375; □ D_o=0; × D_o=0.005.

size distribution at the small size range. The steady state size distribution of the population of particles subjected to weak Brownian motion and gravity settling (Figure 5.3) is allowed to evolve in the presence of settling only. The steady state size distribution attained and averaged over 1000 time-steps, is compared with the initial one in Figure 5.3. The numerical results are statistically identical in the largest part of the size spectrum. When only differential settling operates as a volume-transferring mechanism through the size spectrum, the shape of the size distribution near the small size range reflects the ineffectiveness of differential settling to coagulate particles of similar size. Particles of equal size subjected to gravity settling do not collide. However, since the flux of particle volume into the size range from coagulation of particles smaller than v_o is represented in the simulation by a constant addition of unit particles it is apparent that this scheme cannot represent properly the collisions of particles larger than v_o with particles smaller than v_o ; hence the awkwardly high number of unit particles in the size distribution shown in Figure 5.3.

Figures 5.4 and 5.5 show two stages in the development of the size distribution of an initially monodisperse system of particles undergoing Brownian diffusion and settling. The relative strength of the two coagulation mechanisms can be assessed from the ratio of their respective rectilinear collision functions β_b and β_{ds} (see Table 1)

$$\frac{\beta_b}{\beta_{ds}} = 18 \frac{D_o}{K_{ds}} \frac{1}{r_o^3} \frac{1}{p(p^2 - 1)}$$

where p is the particle radius non-dimensionalised with the radius r_o of

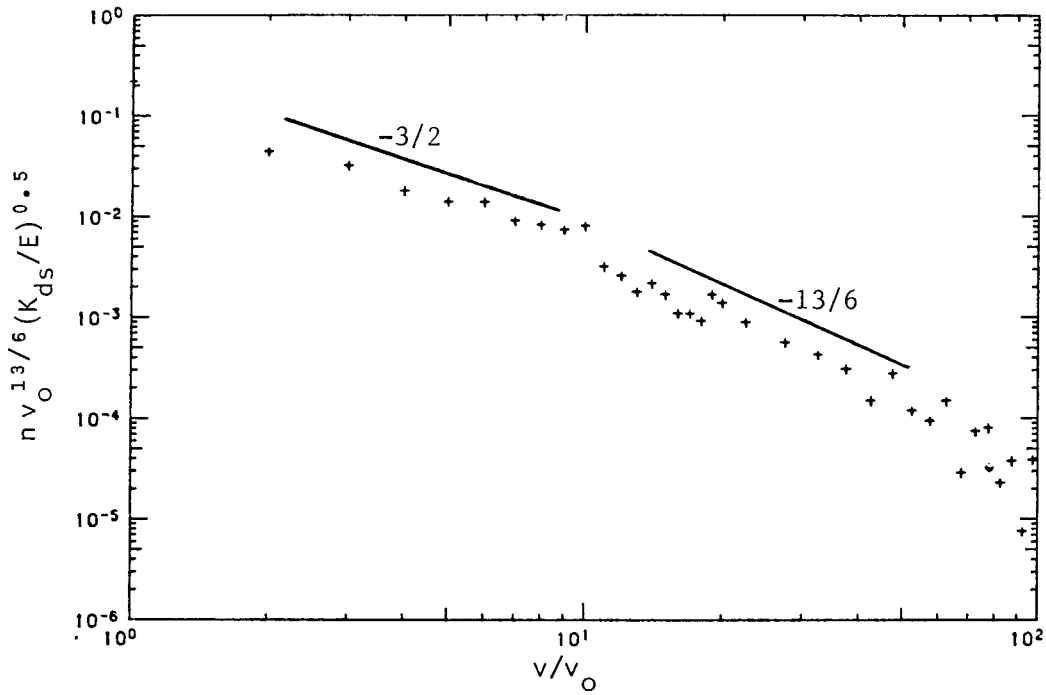

Fig. 5.4. Non-dimensional size distribution for differential sedimentation and weak Brownian motion at 1200 time steps. K_{ds}=10, D_o=0.005, V=128, r_o=0.075, Δt=0.25, $N_{initial}$=200, N_A=1, r_{max}=0.375.

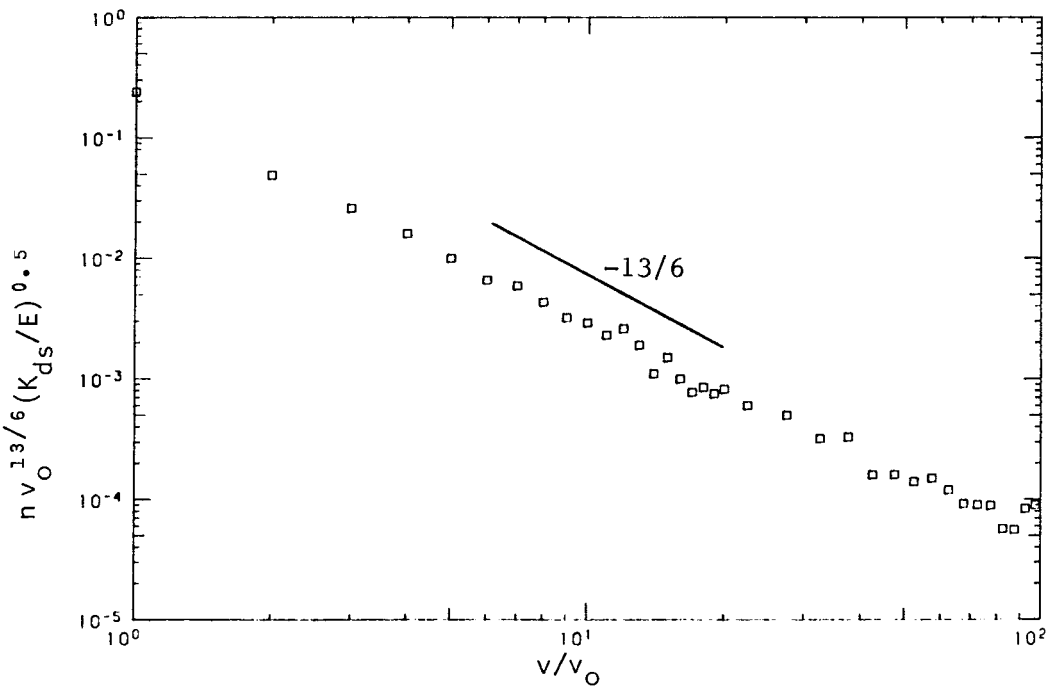

Fig. 5.5. Non-dimensional steady state size distribution for differential sedimentation and weak Brownian motion. K_{ds}=10, D_o=0.005, V=128, r_o=0.075, Δt=0.25, $N_{initial}$=200, N_A=1, r_{max}=0.375.

the unit particle and D_o the diffusivity of the unit particle. The transition in dominance of the two mechanisms in the particle system shown in Figures 5.4 and 5.5 is at v/v_o=24: the collision rates of particles of volume ($24 \cdot v_o$) with particles of volume v_o due to Brownian motion and differential settling are equal. Figure 5.4 shows the particle size distibution after 1200 time steps, only about 200 time steps before a steady state is attained. The -3/2 and -13/6 slopes are clearly distinguishable, but the transition point is shifted from v/v_o =24 indicating that the influence of the large particles undergoing differential settling induced coagulation tends to propagate to smaller size ranges in the size spectrum. The statistically steady state attained is shown in Figure 5.5, where the data points are averaged over 3000 time steps. The dominance of differential settling is evident.

So far hydrodynamic interactions were ignored. We turn now to more realistic particle systems in which hydrodynamic forces between two approaching particles exist. The time-evolution of the normalised size distribution of an initially mono-disperse suspension subjected to gravity settling and weak Brownian diffusion is shown in Figure 5.6. The data of five simulation runs, for a r_o corresponding to an actual particle radius of 40μm, are averaged and smoothed to give the curves shown. For a unit particle with radius 40μm and a density excess ratio $\frac{\rho_p - \rho_f}{\rho_f}$=0.1 the time step used in the simulation corresponds to about 0.05 seconds. The development pattern is strikingly similar to the Brownian and shear systems, but the change in the number of unit particles is more significant. This indicates that large particles formed at progressively later times influence significantly the particle size distribution at the small end of the spectrum.

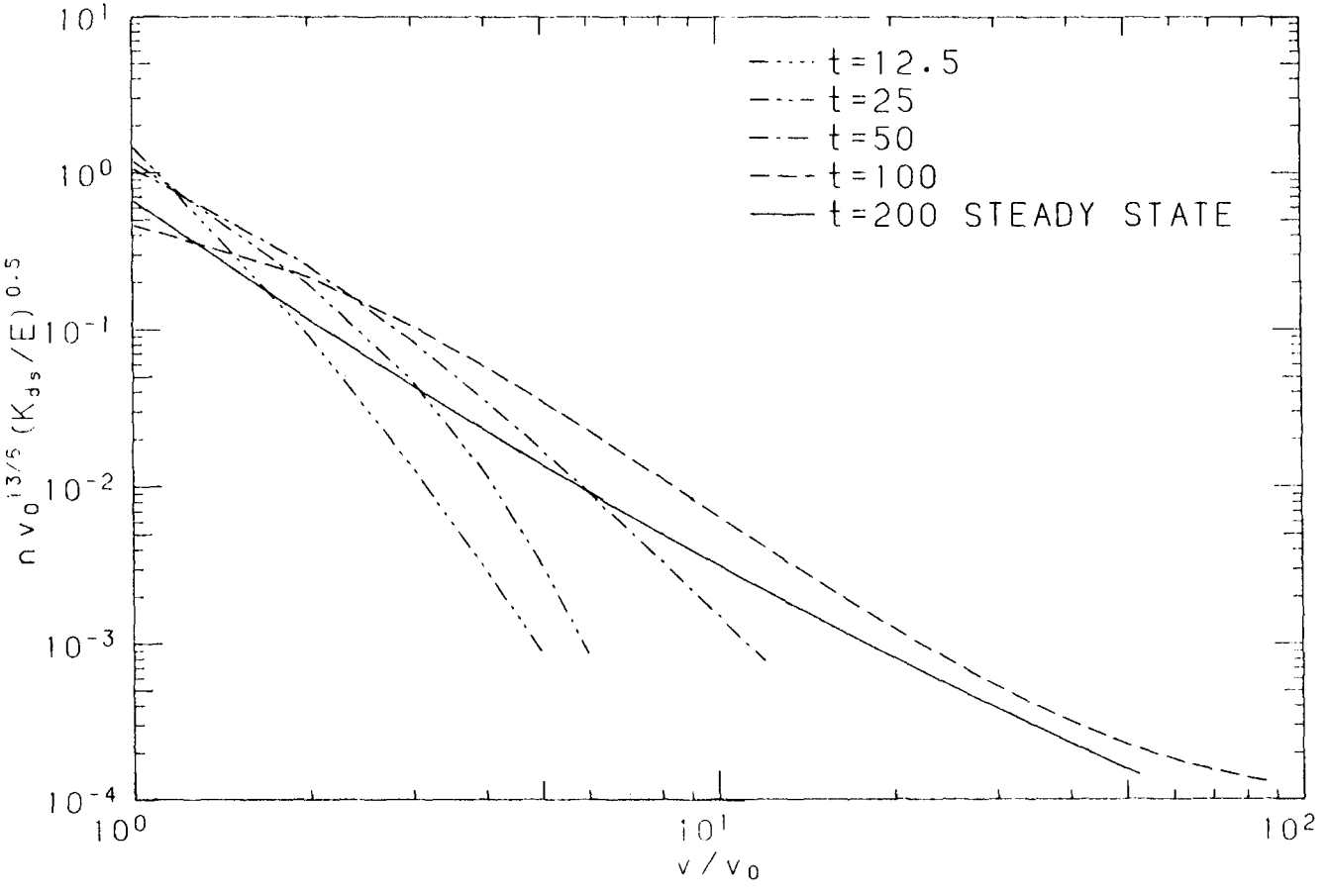

Fig. 5.6. Evolution of the normalised size distribution for differential sedimentation. K_{ds}=50, D_o=0.005, V=128, r_o=0.075, Δt=0.25, N_A=1, r_{max}=0.375.

The functional dependence of the effective collision cross-section on r_1(Figure 5.1) suggests that the shape of the size distribution will depend on the absolute size of the particles. This is illustrated in Figure 5.7 where the normalised size distributions of two particle systems differing in the size of the unit particles are compared. The two sets of data correspond to actual unit particle sizes of 20μm and 40μm, all other parameters being equal. The plotted points are numerical data averaged over 1000 time steps and normalised as suggested by Eq. 1.4. Weak Brownian diffusion is allowed to operate in order to smooth the size distribution at the smaller particle size range. The smaller the size of the unit particles the steeper the final steady state size distribution becomes. In Figure 5.8 two 'interacting' populations of particles with r =20μm and 80μm are compared with a 'non-interacting' system. Note that for the latter the absolute size of the particles is irrelevant. The size distribution with r_o =80μm levels off at v/v_o=15 where the cutoff in the respective efficiency curve occurs (see Figure 5.1). From Figures 5.7 and 5.8 we conclude that the slope of the size distribution of a coagulating system of suspended particles subjected to differential settling depends on the size of the particles. When the radius of the smallest particles involved in the simulation is less than about 40μm, the steady state size distribution has a slope steeper than -13/6; in simulations with larger r_o the size spectrum is flatter.

In simulations performed with r_o less than 15μm a steady state size distribution was not attained. Irrespective of the shape of the initial particle spectrum the number of unit particles in the control volume constantly increased. This is due to the shape of the efficiency curve

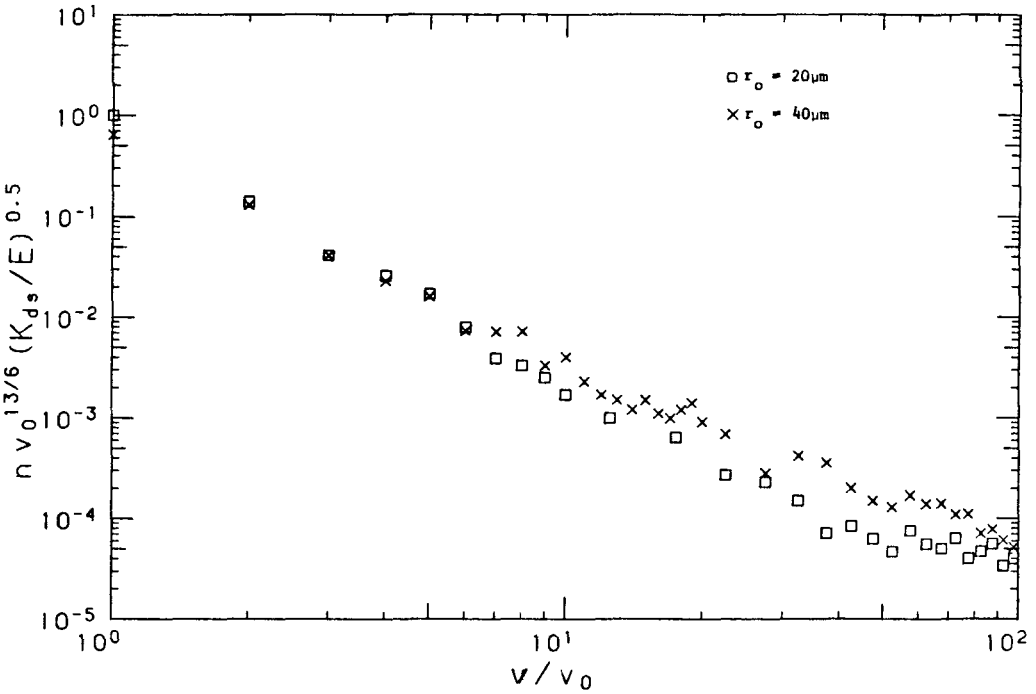

Fig. 5.7. Comparison of the steady state normalised size distribution for differential sedimentation and weak Brownian motion when different collision efficiences are used. K_{ds}=50, D_o=0.005, V=128, r_o=0.075 Δt=0.25, N_A=1, r_{max}=0.375; □ when r_o corresponds to an actual radius of 20μm; × when r_o corresponds to an actual radius of 40μm.

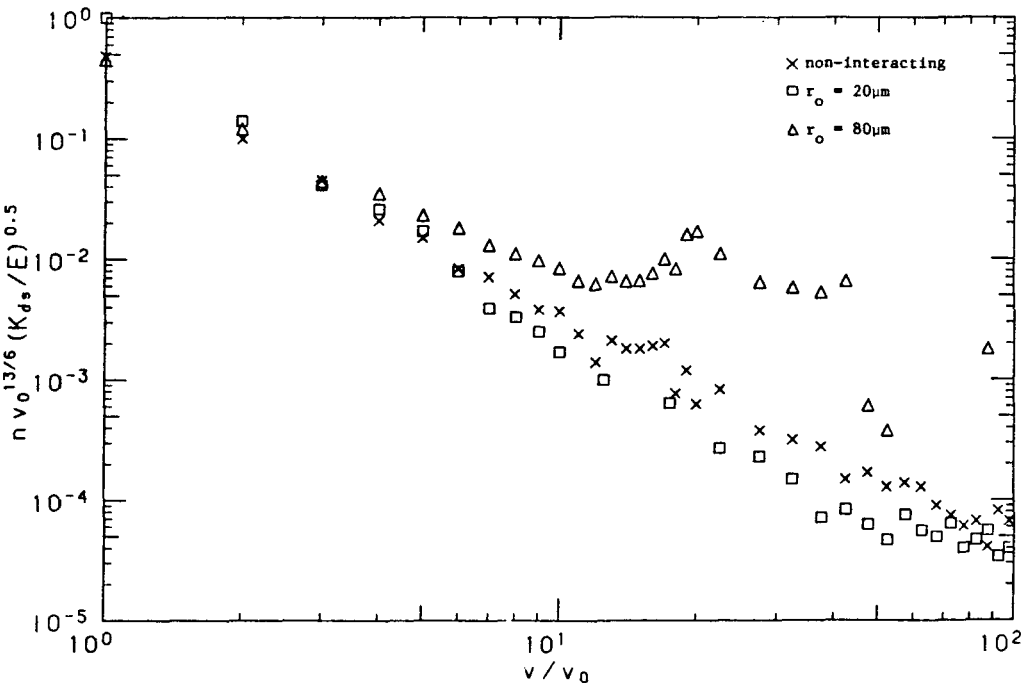

Fig. 5.8. Comparison of the steady state normalised size distribution for differential sedimentation and weak Brownian motion for a non-interacting system and two realistic ones. K_{ds}=50, D_o=0.005, V=128, r_o=0.075, Δt-0.25, N_A=1, r_{max}=0.375; × non-interacting; □ realistic with r_o corresponding to an actual radius of 20μm; Δ realistic with r_o corresponding to an actual radius of 80μm.

for r_1 less than about 15μm: collisions simply do not occur for particles close in size and widely different in size. However, for particles less than 15μm shearing motion is more effective in inducing collisions (Hunt, 1980).

Simulations performed for a non-interacting system of particles gave

$$A_{ds} = 0.45 \pm 0.02$$

for the dimensionless constant A_{ds} in Eq. 1.4. Hydrodynamic interactions between the approaching particles steepen or flatten the steady state size distribution, depending on the particle size range considered. However, computational cost effectively prohibited the direct simulation of a more extended particle size range. The simulations performed therefore involve overlapping sections of the size spectrum. The numerical results indicate that the size distibution becomes the steeper the smaller the size of the particles considered; for unit particles smaller than about 15 μm the computer model suggests that no steady state can exist as a result of the shape of the efficiency curve for such particles. Thus, no power-law expression of the form of Eq. 1.4 with a unique exponent can represent the particle size distribution in the size range where differential settling dominates. Unlike shearing induced coagulation (see Section 4) hydrodynamic interactions cannot be incorporated solely in the dimensionless coefficient A_{ds}.

6. CONCLUSIONS AND DISCUSSION

The direct simulation of the physical processes of particle collision and coalescence was undertaken in order to investigate Friedlander's (1960a,b) and Hunt's (1980) theory regarding the existence of a quasi-stationary particle size distribution in aerosols and hydrosols. Observations in the atmosphere (Friedlander, 1960ab) and in oceanic waters and wastewater sludges (Hunt, 1980) and Hunt's experiments partly support the theory. The numerical simulations of Pearson, Valioulis and List (1983) showed that, provided hydrodynamic and other interparticle forces are ignored, a population of coagulating particles can reach a state of dynamic equilibrium sustained by the flux of mass through the size space, when the collision mechanism is Brownian motion, simple shear or isotropic turbulent shear. The steady state size distributions obtained by Pearson et al. were in agreement with Hunt's dimensional results.

This study reexamined the kinetics of a population of coagulating particles accounting for the influence of interparticle forces on the collision rate. Such forces can arise from the disturbance the presence of the particle causes in the fluid (hydrodynamic forces), from the cloud of ions which surround an electrically charged particle (double layer forces), or they can be of molecular origin (van der Waals' forces). These forces modify the trajectory of two approaching particles, increasing or decreasing the probability of collision and subsequent coalescence. The significance of these interactions for the validity of the theory lies in the functional dependence of the

collision efficiency - which multiplies the rectilinear collision rate and incorporates the effect of all interparticle forces on the collision process - on the relative size of the interacting particles. For underlying Hunt's dimensional arguments is the notion that the coagulation process is mainly 'local' in size space.

For Brownian motion induced coagulation collision efficiencies were computed for two spherical particles of different size assuming Stokes' flow and taken into account the attractive van der Waals' and the double layer forces. The latter are assumed dispersive, since suspended particles in natural waters usually carry a negative charge. The results suggest that double layer electrostatic forces determine the onset of coagulation, but, once collisions occur, the coagulation rate depends only on the hydrodynamic and the van der Waals' forces. The onset of coagulation is abrupt, and so a quantitative criterion of stability was derived. The combined action of hydrodynamic and van der Waals' forces reduces the collision rate of all particle pairs, but it decreases the collision rate more between particles of similar size. As a result, contrary to the 'non-interacting' system of Pearson et al., the simulations performed here showed that the size range covered influences the final steady state size distribution. In Brownian diffusion the rectilinear collision rate increases with the ratio of the interacting particles; for the 'non-interacting' system of Pearson et al. this effect is counterbalanced by the relatively small number of large particles. Hydrodynamic and van der Waals' forces tend to reduce the collision efficiency relatively more between particles of equal size. Collisions between particles widely different in size therefore

become important in determining the evolution of the size distribution. The coagulation process is no longer 'local' in size space, external parameters like the particle size range do become important and so dimensional analysis cannot be used to describe the development of the size distribution.

Adler (1981) computed the collision efficiency for two unequal spheres in simple shear flow under the action of van der Waals' attractive forces. For particles very different in size the collision rate is negligible. As a result, the dynamic equilibrium obtained in the simulated population of coagulating particles does not depend on the size range considered. The power law expression for the steady state size distribution suggested by dimensional analysis is verified in the simulations, but the level of the equilibrium size distribution depends on the relative strength of the shear and the van der Waals' energy of attraction.

Simulations for turbulent induced coagulation were not performed. Pearson et al. showed that, for particles much smaller than the Kolmogorov microscale, isotropic turbulent shear is equivalent in coagulating power to a rectilinear laminar shear of magnitude 1.72 times the characteristic turbulent strain rate $(\varepsilon/\nu)^{1/2}$. Adler's (1981) collision efficiencies then can be used for isotropic turbulent shear induced coagulation. The equivalence with the simple shear is apparent and the same conclusions hold.

The rectilinear collision function for differential sedimentation induced coagulation was verified in this study using the non-coagulating

version of the model. This is illustrated in Figure 6.1 where the computed number of collisions, for several collision mechanisms, is plotted against the number of collisions predicted by the theoretical models. The data points shown are results from simulations involving a variety of different situations, such as monodisperse systems or suspensions with two particle sizes and systems with different densities and/or with different values of the dimensional parameters K_b , G and K_{ds} (which represent the strength of the collision mechanisms). Simulations with a non-interacting sedimenting population of particles gave steady state size distributions in agreement with the theory. Published collision efficiencies derived from theoretical computations assuming Stokes' flow and corrected to be consistent with experimental results (Neiburger et al., 1974) depend both on the relative and the absolute size of the interacting particles. For large particles (larger than about 80μm) the collision efficiency decreases as the particles become of increasingly different size; for smaller particles collisions between both similar and widely different in size particles are unlikely. Equilibrium size distributions were obtained only in simulations where the smallest particle in suspension was larger than about 15 μm. The steady state size distributions attained by the coagulating particles had a slope varying about -13/6, which is the slope predicted by dimensional arguments, and depending on the size range considered. Measured size distributions of particles in aerosols (Pruppacher and Klett, 1978, pg.212) and in sewage sludges (Faisst, 1976) in the size range 10-100μm have a slope varying about -13/6. The larger slope of the size distribution has been attributed erroneously in the past to a 'settling' dominated regime where particles settle out of

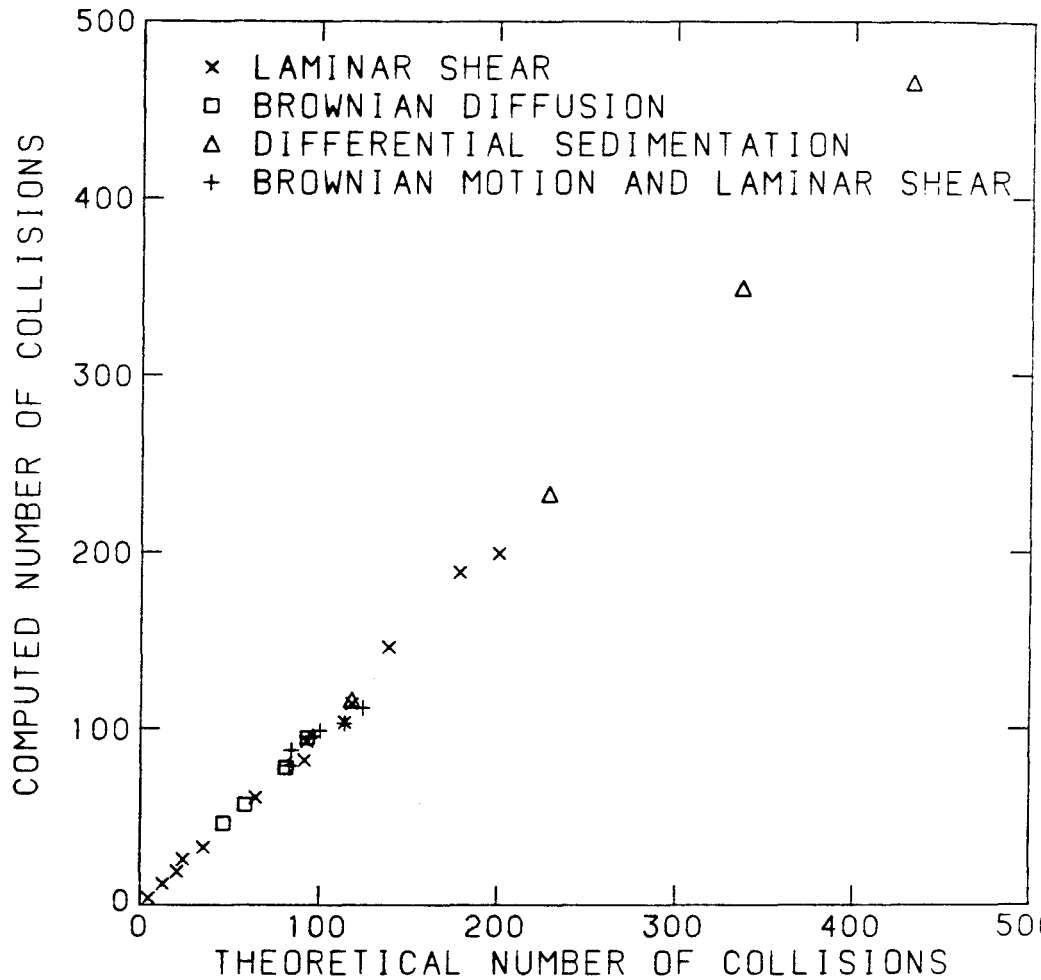

Fig. 6.1. Comparison of theoretical and computed collision rates.

the system. Settling, however, represents a spatially non-homogeneous mass flux (or volume flux, if the particle density is assumed to remain constant after coalescence) which cannot be sustained unless another mechanism operates simultaneously to input mass into the volume of fluid under consideration. The results of the computer simulation help to explain both the steeper slopes of the particle size distributions observed and their variability.

In conclusion, the results of the simulations suggest that a dynamic equilibrium, sustained by the flux of mass through the size spectrum, exists, but a power law expression of the form predicted by Hunt and Friedlander can be expected only in the shear induced coagulation regime. The limited size range covered by the simulations did not allow confirmation or otherwise of the hypothesis that different collision mechanisms act independently over separate regions of the size spectrum. The functional dependence of the collision efficiency on the relative size of the sedimenting particles suggest that differential settling induced coagulation does not influence the small end of the size spectrum; and Brownian motion is too weak as a coagulating mechanism to affect large particles. To further elucidate this point, information is needed on the influence of hydrodynamic, van der Waals' and electrostatic forces on the collision probability of two particles when two or more of the collision mechanisms examined here act simultaneously.

The simulation described here can also be used to give insight into the spatial fluctuations in particle number and size which occur in a

real system. Such information cannot be obtained from the numerical solution of the General Dynamic Equation (GDE) which is a deterministic phenomenological equation and describes the behavior of the suspension averaged over some volume of fluid. Furthermore, there is a good reason to question the suitability of the GDE to describe the evolution of a coagulating suspension. The GDE assumes a completely mixed system and ignores correlations between the particles induced by the coagulation process. For example, as particles of a given size in a region of fluid coagulate, a local reduction in their number occurs, so fewer particles of this size remain for further coalescence. If the suspension of particles is poorly mixed or the number of particles is small, then the average behavior of the suspension predicted by the GDE may not represent the true average of the local coalescence processes. Gillespie (1972) and Bayewitz et al. (1974) developed the full stochastic equation of the coalescence process and showed that the solution obtained from the GDE approaches the true stochastic average provided certain correlations are neglected and that coagulation between particles of equal size are unimportant. The computer model developed by Pearson et al. is a direct simulation of the processes of collision and coalescence of particles and, as such, it accounts for all correlations between particle properties. It does not only predict the average spectrum, but it also gives information on higher order moments of properties of the suspension. This is important since the size distribution predicted by the GDE will be valid when the standard deviation of the various properties of the suspension is a small fraction of the mean. The Monte Carlo simulation thus provides a unique tool to evaluate the validity of the GDE to describe the dynamics of a

coagulating population of particles and such work is in progress. The small number of particles which are employed in the simulation restricts its application to small regions of the fluid. However, since the coagulation process is mainly local, this may not be a serious defect. Ensemble averages over repeated runs can then represent the true stochastic average of the coagulation process in a larger fluid volume.

NOTATION

a	Correction for the curvilinear collision cross-section in laminar shear.
A	Van der Waals' energy of attraction
A_b	Dimensionless constant for Brownian diffusion.
A_{sh}	Dimensionless constant for shear.
A_{ds}	Dimensionless constant for differential sedimentation.
b	Particle mobility
c	Number of ion pairs
D_o	Diffusivity of unit size particle in the simulation
D_i	Diffusivity of particle with radius r_i
D_{ij}	Relative diffusivity of particles i and j
e	Electron charge
E	Particle volume flux through the size spectrum
$E_b(r_1,r_2)$	Collision efficiency of particles r_1 and r_2 in Brownian diffusion.
$E_{sh}(r_1,r_2)$	Collision efficiency of particles r_1 and r_2 in shear.
$E_{ds}(r_1,r_2)$	Collision efficiency of particles r_1 and r_2 in differential sedimentation.
f,F	Interparticle forces
g	Gravitational acceleration
G	Rate of strain (strength of the shear)
h	Dimensionless particle separation, $h=(r-r_2-r_1)/r_1$.
H	Dimensionless parameter for shear induced collisions.
I	Number of unit particles in a cluster of size v_i in the simulation.
I	Ionic strength
J_D	Number density flux due to diffusion
J_F	Number density flux due to a conservative force
k	Boltzmann's constant

NOTATION (continued)

K_b	Brownian coagulation parameter
K_{ds}	Differential sedimentation coagulation parameter
$n(v)$	Particle size distribution function
N	Particle number density
N_A	Number of particles added per time step in the simulation.
N_v	Avogadro number
r_i	Particle radius
t_i	Particle radius
T	Absolute temperature
u	Relative velocity of particles
v	Volume of particle
v_i	Volume of cluster with i monomers in the simulation
v_o	Volume of unit particle in the simulation
v_{max}	Volume of particle with maximum size in the simulation
V	Fluid volume used in the simulation
V_P	Potential energy between particles
V_A	Attractive potential between particles
V_F^{σ}	Electrostatic potential at constant surface charge between two flat double layers
V_F^{Ψ}	Electrostatic potential at constant surface potential between two flat double layers
V_R^{σ}	Electrostatic potential at constant surface charge between spherical particles
$w(v)$	Stokes' settling velocity of particle with volume v
z	Valence of the ionic species in solution

NOTATION (continued)

Greek letters

α	Dimensionless retardation parameter.
$\beta(r_1, r_2)$	Collision function for particles r_1 and r_2.
$\dot{\gamma}$	Rate of extension in pure straining motion
ε	Turbulent energy dissipation rate per unit mass of fluid
κ^{-1}	Debye-Huckel length
λ	London wave-length
μ	Fluid dynamic viscosity
ν	Fluid kinematic viscosity
ρ_f	Fluid density
ρ_p	Particle density
σ	Particle surface charge
Φ, Ψ	Dimensionless particle electrostatic potentials.
ω	Frequency

References

Adler, P.M. 1981 Heterocoagulation in shear flow. J. Colloid Interf. Sci. 83, 106-115.

Arp, P.A. and Mason, S.G. 1976 Orthokinetic collisions of hard spheres in simple shear flow. Can. J. Chem. 54, 3769-3774.

Batchelor, G.K. and Green, J.T. 1972 The hydrodynamic interactions of two small freely-moving spheres in a linear flow field. J. Fluid Mech. 56(2), 375-400.

Batchelor, G.K. 1976 Brownian diffusion of particles with hydrodynamic interactions. J. Fluid Mech. 74, 1-29.

Bayewitz, M.H., Yershalmi, J., Katz, S. and Shinnar, R. 1974 The extent of correlations in a stochastic coalescence process. J. Atmos. Sci. 31, 1604-1614.

Bell, G.M. and Peterson, G.C. 1972 Calculation of the electric double-layer force between unlike spheres. J. Interf. Sci. 41, 542-566.

Bell, G.M., Levine, S. and McCartney, L.N. 1970 Approximate methods of determining the double-layer free energy of interaction between two charged colloidal spheres. J. Colloid Interf. Sci. 33, 335-359.

Brenner, H. 1966 Hydrodynamic resistance of particles at small Reynolds numbers. Advan. Chem. Eng. 6, 287-438.

Derjaguin, B.V. 1954 A theory of the heterocoagulation, interaction and adhesion of dissimilar particles in solution of electrolysis. Discuss. Faraday Soc. 18, 85-98.

Einstein, A. 1926 The Theory of the Brownian Movement. Dover Publications, New York.

Faisst, W.K. 1976 Digested sewage sludge: characteristics of a residual and modeling for its disposal in the ocean off Southern California. EQL Rep. No 13, California Inst. of Tech., Pasadena.

Findheisen, W. 1939 Zur Frage der Regentropfenbildung in reinem Wasserwolken. Meteor. Z. 56, 365-368.

Frens G. and Overbeek, J.T.G. 1971 Repeptization and the theory of electrostatic colloids. J. Colloid Interf. Sci. 38, 376-387.

Friedlander, S.K. 1960a On the particle size spectrum of atmospheric aerosols. J. Meteorol. 17, 373-374.

Friedlander, S.K. 1960b Similarity considerations for the particle-size spectrum of a coagulating, sedimenting aerosol. J. Metereol. 17, 479-483.

Fuchs, N.A. 1964 The Mechanics of Aerosols. Pergamon Press, New York.

Gillespie, D.T. 1975 An exact method for numerically simulating the stochastic coalescence process in a cloud. J. Atmos. Sci. 29, 1977-1989.

Gregory, J. 1969 The calculation of Hamaker constants. Adv. Colloid Interf. Sci. 2, 396-417.

Hamaker, H.C. 1937 The London-van der Waals' attraction between spherical particles. Physica 4, 1058-1072.

Hogg, R., Healy, T.W. and Fuerstenau, D.W. 1965 Mutual coagulation of colloidal dispersions. Trans. Faraday Soc. 18, 1638-1651.

Honig, E.P., Roeberson, G.J. and Wiersema, D.H. 1971 Effect of hydrodynamic interaction on the coagulation rate of hydrophobic colloids. J. Colloid Interf. Sci. 36, No 1, 97-109.

Honig, E.P. and Mull, P.M. 1971 Tables and equations of the diffuse double layer repulsion at constant potential and at constant charge. J. Colloid Interf. Sci. 36, No 2, 258-272.

Hunt, J.R. 1980 Coagulation in continuous particle size distributions: theory and experimental verification. Report No. AC-5-80. W.M. Keck Lab. California Inst. of Tech., Pasadena.

Jeffrey, D.J. 1981 Quasi-stationary approximations for the size distribution of aerosols. J. Atmos. Sci. 38, 2440-2443.

Kiefer, J.E., Parsegian, V.A. and Weiss, G.H. 1978 Some convenient bounds and approximations for the many body van der Waals' attraction between two spheres. J. Colloid Interf. Sci. 67, 140-153.

Langbein, D. 1971 Non-retarded dispersion energy between macroscopic spheres. J. Phys. Chem. Solids 32, 1657-1667.

Lifshitz, E.M. 1956 The theory of molecular attractive forces between solids. Sov. Phys. JETP 2, 73-83.

Lyklema, J. 1968 Principles of stability of lyophobic colloidal dispersions in non-aqueous media. Advan. Colloid Sci. 2, 65-114.

Monin, A.S. and Yaglom A.M. 1975 Statistical Fluid Mechanics, Vol. 2. Cambridge Mass., The MIT Press.

Neiburger, M., Lee, I.Y., Lobl, E. and Rodriguez, L.Jr. 1974 Computed collision efficiencies and experimental collection efficiencies on cloud drops. Conference on Cloud Physics of the American Metereological Society, 73-78, Tucson, Arizona.

O' Melia, C.R. 1980 Aquasols: the behavior of small particles in aquatic systems. Environ. Sci. Techn. 14, 9, 1052-1060.

Ottewill, R.H. and Show, J.N. 1966 Stability of monodisperse polystyrene latex dispersions of various sizes. Disc. Faraday Soc. 42, 154-163.

Parsegian, V.A. and Nigham, B.W. 1970 Temperature dependent van der Waals' forces. Biophys. J. 10, 664-674.

Pearson, H.J., Valioulis, I.A. and List, E.J. 1983 Monte Carlo simulation of coagulation in discrete particle size distributions. Part I: Brownian motion and fluid shearing. J. Fluid Mech., in press.

Pruppacher, H.R. and Klett, J.D. 1978 Microphysics of Clouds and Precipitation. Dordrecht, Holland, Reidel.

Saffman, P.G. and Turner, J.S. 1956 On the collision of drops in turbulent clouds. J. Fluid Mech. 1, 16-30.

Schenkel,J.H. and Kitchener, J.A. 1960 A test of the Derjaguin-Verwey-Overbeek theory with a colloidal suspension. Trans. Faraday Soc. 56, 161-173.

Schmidt-Ott, A. and Burtscher, H. 1982 The effect of van der Waals' forces on aerosol coagulation. J. Colloid Interf. Sci. 89, No 2, 353-357.

Smith, D.L., Mitchell, D.J. and Ninham, B.W. 1973 Deviations of the van der Waals' energy for two interacting spheres from the predictions of Hamaker theory. J. Colloid Interf. Sci. 45, 55-68.

Smoluchowski, M. 1916 Drei Vorträge uber Diffusion, brownsche Bewegung and Koagulation von Kolloidteilchen. Physik Z. 17, 557-585.

Smoluchowski, M. 1917 Versuch einer mathematischen Theorie der Koagulationskinetic kolloider Losungen. Z. Phys. Chem. 92, 129.

Spielman, A.L. 1970 Viscous interactions in Brownian coagulation. J. Colloid Interf. Sci. 33, 562-571.

Stimson, M. and Jeffery, G.B. 1926 The motion of two spheres in a viscous fluid. Proc. Roy. Soc. London Ser. A 111, 110-116.

Stumm, W. and Morgan, J.J. 1981 Aquatic Chemistry. Wiley-Interscience.

Tag, P.M. 1974 The effect of utilizing empirically derived values of coalescence efficiency in a microphysical cloud model. Conference on Cloud and Physics of the American Metereological Society, 73-78, Tucson, Arizona.

Twomey, S. 1977 Atmospheric Aerosols. Elsevier, New York, N.Y.

Verwey, E.J.W. and Overbeek, J.T.G. 1948 Theory of the Stability of Lyophobic Colloids. Elsevier, New York, N.Y.

Zeichner, G.R. and Schowalter, W.R. 1977 Use of trajectory analysis to study the stability of colloidal dispersions in flow fields. AIChE J. 23, 243-254.

Zeichner, G.R. and Schowalter, W.R. 1979 Effects of hydrodynamic and colloidal forces on the coagulation of dispersions. J. Colloid Interf. Sci. 71, 237-253.

CHAPTER II: NUMERICAL SIMULATION OF A SEDIMENTATION BASIN

1. INTRODUCTION

1.a. Small- and Large-Scale Modeling

Direct simulation of particle coagulation processes in a natural system is not feasible with current computer technology. Instead, we attempt to describe the collisions and coalescences of particles by continuum mathematical models, trying to incorporate into them the physics which determine particle behavior. However, in the process of translating physical phenomena to mathematical language we are forced to make several approximations. Some of these are due to the 'translation' itself, for instance rendering the random process of coagulation deterministic. Others are a consequence of the limited availability of computer resources and could be avoided if, for example, it were possible to decrease the computational mesh-size both in physical space and in particle size-space. Nevertheless, mathematical models, if carefully constructed, can provide the investigator with the essential features of the natural system, thus becoming a valuable tool for design purposes.

The Monte Carlo simulation of coagulation described in Chapter I gives insight to small scale phenomena and extracts information useful for application in large scale modeling. Such information (the collision functions) will be used here to develop a mathematical model for a sedimentation basin. The numerical model developed incorporates

the basic kinetics of particle collision and coagulation processes, including floc break-up due to shear, and accounts for transport processes such as particle advection and settling, turbulent mixing and particle resuspension. Experimental results available in the literature are used extensively in an attempt to improve the realism of the model. Some common fallacies with regard to the influence of certain characteristics of the suspension (e.g. particle size-density relationship, particle collision efficiencies) on the efficiency of the tank are revealed and the parameters which play a major role in the operation of a settling basin are pointed out.

1.b. Historical Review

Settling is the most common unit treatment process in a wastewater treatment plant. Settling basins are used both as primary clarifiers to remove particulate matter and oil drops and as secondary tanks following the activated sludge unit for biological floc removal. They are also used to settle the chemical floc in the chemical coagulation process.

Camp (1945) presented in a compendium all physical processes which are important for the economic design of a settling tank. Later investigators focused successfully on the experimental evaluation of some of the parameters indicated by Camp, such as the design of inlets and outlets and the optimum dimensions of the basin (see, for example, Ingersoll et al., 1956, and Kawamura, 1981). The investigations on other physical processes, such as flocculation and the effect of the properties of the suspension upon it, or the scouring of deposits from

the bottom of the tank by turbulent eddies, although numerous, have been less successful in providing tools for design purposes, mainly because of the complexity of the mechanisms involved. Thus, most settling tanks are currently designed on the basis of detention times (circular tanks) and overflow rates (rectangular tanks). Pilot units, or data from actual plants, are often used to develop relations between loading and performance. The significance of physical processes such as particle flocculation and resuspension is widely recognized, but they are not well understood and subsequently modeled, so that the successful design of a settling tank relies heavily on the experience of the engineer. However, the performance of tanks might be improved if different design and operation schemes could be evaluated by a numerical simulation which would include all of the physical processes in the tank, such as turbulent mixing, particle settling, advection, coalescence, resuspension and deaggregation by turbulent shearing.

Numerous mathematical and numerical models for the performance of settling tanks under steady and unsteady conditions have been developed (Alarie et al., 1980). Regression models (Tebbutt and Christoulas, 1975) are empirical. They use data from operating tanks to derive a relationship between loading and effluent characteristics. Hydraulic scale-models (Kawamura, 1981), if successful, are applicable only to the sedimentation basins they simulate. Dispersion models (El-Baroudi, 1969, Humphreys, 1975) are based on the solution of a two-dimensional diffusion equation obtained by Dobbins (1944) and Camp (1946) and use an experimentally determined longitudinal eddy dispersion coefficient to characterize the departure from plug flow in the tank. Mechanistic models (Shiba and Inoue, 1975, Alarie et al., 1980) assume a vertically

well-mixed settling basin and use a one-dimensional unsteady diffusion equation to predict the effluent quality under variable load. The physical configuration of the tank is taken into account and the resuspension of sediment related empirically to the longitudinal dispersion coefficient. Ramaley et al. (1981) incorporated coagulation in simulating the settling basin in their numerical model for integral water treatment plant design. Their model does not account for scouring, vertical turbulent transport and dispersion of mass through the tank, it assumes a constant density for all particle sizes and uses a collision efficiency of unity. Dick (1982) noted that the utility of the Ramaley et al. model is limited because of the simplifications involved.

Hazen's (1904) early theory predicts that all particles with settling velocity greater than Q/A, where Q is the flow rate and A the surface area of the tank, are removed provided that the flow is uniform, no short-circuiting currents or scouring occur, and particles of uniform density and shape settle discretely. In reality, inlets, outlets, wind and density differences induce currents or create dead regions in the tank. High forward velocities near the bottom of the tank resuspend the deposits and reduce the efficiency of the basin. Regardless of surface loading coagulation is essential in achieving high suspended solids removal (Camp, 1945). Rigorous analysis of the performance of a settling basin must be based on the detailed spatial behavior of the fluid and the particles in the tank and take into account the fluid-particle and particle-particle interactions.

The aim of this computer simulation of a rectangular settling basin is to describe the spatial and temporal development of the particle size

distribution from the influent towards the outlet of the tank. It is based on the fundamental mechanisms which govern particle motion and growth. The model accounts for the variability of the flow-field and the particle size distribution in the tank and, from the local development of the particle size spectrum, predicts the overall performance of the settling basin.

2. FUNDAMENTAL MECHANISMS

In this section we discuss the basic features of the model.

2.a. Flow field

Any empirical or observed velocity distribution in the tank can be incorporated into the model. However, for this analysis the logarithmic velocity profile is used to demonstrate the model capabilities. We assume that the local mean longitudinal velocity through the tank is given by

$$u = \overline{u} + \frac{u_*}{\kappa} \left[1 + \log_e\left(\frac{z}{H}\right)\right] \qquad (2.1)$$

where $\overline{u}$ is the cross-sectional mean velocity, u_* is the shear velocity, H is the depth of the tank, u the time averaged velocity at the vertical coordinate z, and $\kappa = 0.38$ is von Karman's constant, reduced to account

for the suspended mass (Vanoni and Brooks, 1957).

The cross-sectional turbulent mixing coefficient $\hat{E}$ can be derived from the logarithmic velocity profile (Fischer et al., 1979)

$$\hat{E} = u_* z \left(1 - \frac{z}{H}\right) \tag{2.2}$$

where it is assumed that particles have the same diffusive properties as the fluid momentum. Longitudinal turbulent mixing is neglected because it is insignificant when compared with the shear flow dispersion caused by the vertical velocity gradient (Fischer et al., 1979).

An estimate of the rate of turbulent energy dissipation ε, per unit mass of fluid, can be obtained from (Blackadar, 1962)

$$\varepsilon = \hat{E} \left(\frac{du}{dz}\right)^2 \tag{2.3}$$

which agrees well with experimental results (Tennekes and Lumley, 1972). ε is needed in the collision function for turbulent shear induced coagulation and for determining the maximum allowable floc size for a given shear strength.

For the simulations performed and presented below typical values of the parameters defining the velocity field are as follows:

$\overline{u} = 0.5$ cm/sec,

$u_* = 0.05$ cm/sec,

$\hat{E} = 1.9$ cm^2/sec,

$\varepsilon = 0.25 \cdot 10^{-4}$ cm^2/sec^3.

2.b. Coagulation

Particles in wastewater are classified as (Rudolfs and Balmat, 1952)

settlable	>100μm
supracolloidal	1μm to 100μm
colloidal	10^{-3}μm to 1μm
soluble	<10^{-3}μm

In the absence of coagulation a settling basin operating at a detention time of practical interest will remove only the settlable and some of the supracolloidal particles. However, flocculation transfers mass through the particle size spectrum towards larger particle sizes with a subsequent increase in the removal efficiency of the tank. Thus particles in the size range traditionally referred to as suspended solids (> 1 μm) may be generated within the tank from coagulation of colloidal material.

Brownian motion, fluid shear and differential settling cause relative motion of the particles through the fluid and bring them into close proximity. Short-range interfacial forces act then between the particles to bring about their coalescence. Analytic estimates of the probability (collision function) $\beta(r_i, r_j)$ that two spherical particles of radii r_i and r_j in a unit volume of fluid will collide in unit time are shown in Table 4; $\beta(r_i, r_j)$ represents the geometry and dynamics of the collision mechanisms. The collision efficiency $E(r_i, r_j)$ reflects the influence of hydrodynamic and van der Waals' forces on the collision probability of two approaching particles.

Table 4

	Collision Function $\beta(r_i,r_j)$	Source
Brownian Motion	$\frac{2kT}{3\mu}\frac{(r_i+r_j)^2}{r_i r_j}E_b(r_i,r_j)=4\pi(D_i+D_j)(r_i+r_j)E_b(r_i,r_j)$	Smoluchowski (1916)
Turbulent Shear	$2.3(r_i+r_j)^3(\frac{\varepsilon}{\nu})^{\frac{1}{2}}E_{sh}(r_i,r_j)$	Pearson, Valioulis and List (1983)
Differential Sedimentation	$\frac{0.7g(\rho_p-\rho_w)}{\mu}(r_i+r_j)^2\lvert r_i^2-r_j^2\rvert E_{ds}(r_i,r_j)$	Findheisen (1939)

Collision functions for the three particle collision mechanisms considered. Values of β are for collision mechanisms acting individually. E_b, E_{sh} and E_{ds} express the influence of hydrodynamic and other interparticle forces on the collision process.

Notation

k - Boltzmann constant, T - absolute temperature, r_i,r_j - particle radii, μ - coefficient of fluid viscosity, D_i - particle diffusivity, ε - viscous dissipation rate per unit mass, ν - kinematic viscosity of fluid ($=\mu/\rho_f$), ρ_f - fluid density, ρ_p - particle density, g - acceleration of gravity.

Published work on E deals with interactions between hard spherical particles. For Brownian diffusion induced collisions the best-fit approximation to the numerical calculations obtained from Table 3 can be used

$$E_b(r_i,r_j) = 0.4207 + 0.031\left(\frac{r_i}{r_j}\right) - 0.0009\left(\frac{r_i}{r_j}\right)^2, \quad \text{for } \frac{r_i}{r_j} \lesssim 20$$

$$E_b(r_i,r_j) = 0.652 + 0.0055\left(\frac{r_i}{r_j}\right) - 3.035 \times 10^{-5}\left(\frac{r_i}{r_j}\right)^2, \quad \text{for } 20 \lesssim \frac{r_i}{r_j} \lesssim 100 \tag{2.4}$$

where $r_i > r_j$ and for $A/(kT)=1$; A is the van der Waals' energy of attraction, k Boltzmann's constant and T the absolute temperature. For particle size ratios larger than 100, where r_j =0.1 μm is the minimum particle size considered here, Brownian diffusion is no longer important in inducing particle collisions (Hunt, 1980).

Adler (1981a) used Stokes' equations to compute the collision efficiency $E_{sh}(r_i,r_j)$ for two unequal hard spheres in simple shear flow. His results are a function of the ratio of the size of the interacting particles r_i/r_j, where $r_i > r_j$, and, either the van der Waals' energy of attraction (Table 5), or the distance between the spheres at which collision is assumed to occur. The Monte Carlo simulation of the evolution of the particle size distribution by Pearson et al. (1983) showed that, for particles much smaller than the Kolmogorov microscale, isotropic turbulent shear is equivalent in coagulating power to a rectilinear laminar shear with a strain rate, G, of magnitude 1.72 times the characteristic strain rate $(\varepsilon/\nu)^{1/2}$ given by the rate of dissipation of turbulent kinetic energy, ε, per unit mass of fluid and the fluid

Table 5

Collision efficiencies E_{sh} for hard spherical particles in laminar shear (Adler, 1981a)

$$E_{sh} = \frac{a+bx}{1+cx+dx^2} \cdot \frac{8}{(1+\frac{1}{x})^3} \quad , \quad x = \frac{r_i}{r_j} \quad , \quad r_i \geq r_j$$

$\frac{A}{144\pi\mu r_i^3 G}$	a	b	c	d
10^{-2}	-1.189	0.118	-3.431	0.331
10^{-3}	0.766	0.007	-0.006	1.547
10^{-4}	0.145	-0.0006	-1.137	0.775
10^{-5}	0.0017	-0.0001	-1.442	0.557

kinematic viscosity ν. In primary clarifiers, even at high forward velocities, $(\varepsilon/\nu)^{1/2}$ is rarely larger than 10 sec^{-1} (Camp, 1945); ε is then of order 10^{-4} m^2/sec^3 and the Kolmogorov length microscale $(\nu^3/\varepsilon)^{1/4} = 3 \cdot 10^{-4}$ m. This suggests the use of Adler's (1981a) results with $G = 1.72\,(\varepsilon/\nu)^{1/2}$ for turbulent shear induced collisions between particles with sizes up to 100 μm. For larger particles differential settling induced coagulation becomes dominant.

Neiburger et al. (1974) obtained an analytic expression for theoretical collision efficiencies induced by differential sedimentation of hard spherical particles, computed assuming Stokes' flow (with the slip-flow correction) and modified to be consistent with experimental results

$$E_{ds}(r_i, r_j) = E_0 + E_1 + E_2 + E_3 + E_4 \qquad (2.5)$$

where

$$E_0 = 0.95 - (0.7 - 0.005\, r_i)^4 (7.92 - 0.12\, r_i + 0.001\, r_i^2)$$

$$E_1 = -\left(\frac{r_j}{r_i}\right) - 0.5^{\,2}$$

$$E_2 = -1.5\left[\exp -(0.0015\, r_i^2 + 8)\,\frac{r_j}{r_i}\right]$$

$$E_3 = -(1 - 0.007\, r_i)\,\exp\left[-0.65\, r_i\,\left(1 - \frac{r_j}{r_i}\right)\right]$$

$$E_4 = \begin{cases} 0 & \text{when } r_i < 20\ \mu m \\ \exp\left[-30\left(1 - \dfrac{r_j}{r_i}\right)\right] & \text{when } r_i \geq 20\ \mu m \end{cases}$$

where $r_i > r_j$ and r_i, r_j are in μm. This expression can be used for $r_i > 10$ μm. Davis (1972) computed collision efficiencies for two spherical particles smaller than 10 μm. His results suggest that

efficiencies for collisions between particles r_i and r_j such that $r_j < r_i < 10\,\mu m$ are essentially equal to those with $r_j < r_i = 10\,\mu m$.

In hydrosols only the smaller particles can be assumed nearly spherical. These particles coalesce and form loose aggregates rather than solid masses. The volume of the aggregate is larger than the sum of the volumes of primary particles it contains due to inclusion of water. The size-density relationship and the structure of the flocs depend on their physical and chemical characteristics. This has important implications with regard to particle-particle and fluid-particle interactions. Floc densities observed (Tambo and Watanabe, 1979, Dick, 1982), or computed numerically (Void, 1963, Sutherland and Goodarz-Nia, 1971, Tambo and Watanabe, 1979), indicate almost neutrally buoyant flocs for sizes larger than about $100\,\mu m$. For this model particles smaller than $4\,\mu m$ are considered solid spheres with a density of $2650\ kg/m^3$. For larger particles the empirical size-density relationship proposed by Tambo and Watanabe (1979) is used:

$$\rho_f - \rho_w = \frac{1.3}{(200\ r_i)^{0.9}} \tag{2.6}$$

where ρ_f and ρ_w are the densities of the floc and the water, respectively.

The very low aggregate densities are characteristic of particles with an expanded structure. Sutherland's (1967) computer simulation of floc formation and observations under an electron microscope by Thiele and Levern (1965) revealed an open network of filaments joining denser regions. Collisions of such clusters creates a chain-like framework. Void (1963) and Sutherland and Goodarz-Nia (1971) characterized their

numerically generated flocs by a core radius, where about 60% of the primary particles are contained, and by branches or tentacles with a mean length from 0.2 to 1 times the diameter of the core. Vold (1963) suggested that coagulation of such particle formations can involve only mechanical entanglement of their branches.

The above discussion suggests that the collision efficiencies for hard spheres can be used in the simulation of particles smaller than 4 μm but will underestimate the collision frequency between flocs. The increased chances of collisions of such aggregates are accounted for in the simulation by assuming that they behave like solid spheres with a 20% larger effective coalescence radius. The collision rate of Brownian diffusion induced collisions is not altered by this assumption, since both the collision function and the efficiency depend only on the size ratio of the interacting particles. For shear induced collisions and for particles larger than 4 μm, the best-fit approximation to Adler's (1981a) graphical results for the collision efficiency (assuming that coalescence occurs at interparticle separation of $0.2r_i$) is used

$$E_{sh}(r_i,r_j) = -0.4036 + 9.423\left(\frac{r_j}{r_i}\right) - 17.214\left(\frac{r_j}{r_i}\right)^2 + 9.444\left(\frac{r_j}{r_i}\right)^3 \qquad (2.7)$$

where $r_i > r_j$. Hocking (1970) showed that the efficiency for differential settling induced collisions is a weak function of the interparticle separation at which coalescence is assumed to occur. Thus the collision efficiencies for hard spheres can be used.

The open structure of the aggregate indicates that flow streamlines will cross the aggregate. Small particles moving on these streamlines are likely to be captured by purely hydrodynamic effects. Adler (1981b)

computes the streamlines around a porous sphere of radius r and permeability p. A reasonable approximation is that, when the two approaching particles are very different in size, the flow field is determined solely by the presence of the larger one. For such particle encounters Adler's (1981b)drainage cross-section, i.e. the cross-section at infinity for streamlines which cross the aggregate, is equivalent to the collision cross-section of the particles.

Using the argument advanced by Pearson, Valioulis and List (1983), Adler's (1981b)tabulated numerical results for simple laminar shear are used here for turbulence induced coagulation. Adler's (1981) results are approximated with

$$E_{sh}(r_i,r_j) = 1.1616 - 0.228\ \xi + 0.0112\ \xi^2, \quad r_i >> r_j \tag{2.8}$$

where $\xi = r_i/\sqrt{p}$.

For differential settling the collision efficiencies for particles with large difference in size are computed from (Adler, 1981b)

$$E_{ds}(r_i,r_j) = 1 - \frac{b}{\zeta} - \frac{a}{\zeta^3}, \quad r_i >> r_j \tag{2.9}$$

where $$\zeta = 2\xi^2 + 3 - 3\,\frac{\tanh\xi}{\xi}$$

$$a = -\frac{1}{\zeta}\left[\xi^5 + 6\xi^3 - \frac{\tanh\xi}{\xi}\left(3\xi^5 + 6\xi^3\right)\right]$$

$$b = \frac{1}{\zeta}\,3\xi^3\left(1 - \frac{\tanh\xi}{\xi}\right)$$

For aggregates with high porosity the permeability p can be estimated from Brinkman's equation applicable to a cloud of spherical particles

(Sutherland and Tan, 1970)

$$p = \frac{c^2}{18}\left(3 + \frac{4}{1-e} - 3\sqrt{\frac{8}{1-e} - 3}\right) \tag{2.10}$$

where c is the radius of the primary particles (or denser regions) in the aggregate, assumed to be 1/20 of its diameter, and e its porosity computed from

$$e = \frac{\rho_p - \rho_f}{\rho_p - \rho_w} \tag{2.11}$$

where ρ_p is the density of the primary particles (or denser formations) which compose the aggregate.

The efficiencies given by Eqs. 2.8 and 2.9 have been used for particle encounters with relative size less than 0.1 and when the larger particle possesses a relative density lower than 2.65, that is, it is considered a floc. Collision efficiencies of two porous spheres of comparable size do not appear to be known. Since such particles will interact hydrodynamically as they approach each other, it is assumed that the collision efficiencies of hard spheres (with the 20% increased coalescence radius assumption) can be used.

Summarizing, the following hypotheses are used here with regard to particle dynamics: Particles smaller than 4 μm are assumed to behave as solid spheres. Larger particles are considered flocs with reduced density and an amorphous shape which increases the collision radius of the sphere equivalent in mass by 20%. The increased chances of collisions between a porous aggregate and a floc or a solid particle are taken into account only for encounters between particles with relative size less than 0.1.

For this simulation the collision mechanisms are assumed additive, although this may not be strictly true (van de Ven and Mason 1977), and only binary particle encounters are assumed to occur. In most wastewater applications the ionic strength of the suspension is large enough that double-layer electrostatic forces do not influence the coagulation rate.

2.c Particle size distribution

The size distribution function n(d) of a population of coagulating particles is defined by

$$\Delta N = n(d)\ \Delta d$$

where ΔN is the number of particles with a diameter d in the size interval $(d, d+\Delta d)$, per unit volume of fluid. Atmospheric aerosols (Friedlander, 1960) and hydrosols (Faisst, 1976) are found to exhibit the power law

$$n(d) = (\Delta N / \Delta d) = A\ d^{-\alpha}$$

where the exponent α is a constant and the constant A depends on the total particle mass per unit volume of fluid. The surface ΔS, volume ΔV and mass ΔQ of particles in the size range Δd, per unit volume of fluid, are then expressed as

$$\begin{aligned} \Delta S &= A \frac{\pi}{4} d^{-\alpha+2}\ \Delta d \\ \Delta V &= A \frac{\pi}{6} d^{-\alpha+3}\ \Delta d \\ \Delta Q &= A \frac{\pi}{6} \rho(d)\ d^{-\alpha+3}\ \Delta d \end{aligned} \qquad (2.12)$$

where the particle density $\rho(d)$ is in general a function of particle size as discussed in the previous section.

In hydrosols α ranges from 2.5 to 5.6 (Hunt, 1980), and depends on one or more physical mechanisms which induce particle collisions. Lawler et al. (1980) stressed the significance of α for water quality: some pollutants are expressed as mass concentrations (suspended solids), some concentrate on surfaces (trace metals) and for others the total number is important (pathogenic organisms).

2.d. Resuspension

Strong fluid shear near the bottom of the tank results in resuspension of material previously deposited. Work on entrainment of sediments has focused on the determination of the critical conditions for the initiation of motion of the deposits (for an extended review see Vanoni, 1977). Individual particles resist resuspension by their weight while fine, cohesive sediments (incorporating fractions of silt or clay, for example) offer additional resistance to entrainment due to cohesive forces. It is widely accepted that the critical shear stress for the initiation of motion of noncohesive sediments can be obtained from Shields' curve (Vanoni, 1977). The critical velocity near the bottom is, in general, an increasing function of the grain size.

Knowledge of the resuspension of cohesive sediments is primitive. Experimental data for the critical conditions for the entrainment of cohesive sediments is not consistent, mainly because the cohesive forces depend on factors such as shear strength, mineral content, plasticity

and electrochemical condition of the deposits. Results of several experimental studies suggest that cohesive sediments exhibit increasing resistance to erosion with decreasing grain size (Vanoni, 1977).

For the simulation model the resuspension flux of the deposits is needed. To the knowledge of the author, published information on the amount of entrained material from cohesive or noncohesive purpose of testing the sensitivity of the results to scouring, a reduced deposition mass flux per unit volume of fluid is defined

$$\text{deposition mass flux} = -w_p(1-s)\, Q_p \qquad (2.13)$$

where w_p is the Stokes' settling velocity of particles with mass concentration Q_p and s is a scouring parameter. For s=0 only deposition takes place; for $0 < s < 1$ partial scouring occurs; s=1 implies that deposition is balanced by scouring; $s > 1$ implies that scouring dominates. For a typical simulation run a value of s=0.15 was chosen; this value of s agrees well with the experimental results of Takamatsu et al. (1974) in a model settling tank. In addition, simulation runs with s=0, s=0.4 and s=0.8 were performed.

2.e. Floc break-up

Strong local fluid shear may cause the aggregates to break up. The effect is more important in the flocculation basin which often precedes the settling tank, but can be significant in regions of the clarifier where turbulence levels are high.

Two floc break-up mechanisms are distinguished (Parker et al., 1972): Inorganic flocs tend to disintegrate due to surface erosion; in organic flocs the polymer bridge holding primary particles on the floc surface breaks when the shear strength of the polymer bridge is exceeded (filament fracture). Parker et al. (1972) obtained experimental relationships between the maximum size of the aggregate and the local shear. For inorganic flocs they found

$$\text{ferric floc:} \quad r_{max} = \frac{3.6 \times 10^5}{G^2}, \quad 100\mu m < r_{max} < 15{,}000\ \mu m \tag{2.14}$$

$$\text{alum floc:} \quad r_{max} = \frac{6 \times 10^3}{G}, \quad 15\ \mu m < r_{max} < 250\ \mu m$$

and for conventional activated sludge flocs

$$r_{max} = \frac{2{,}250}{G^{0.35}}, \quad 400\ \mu m < r_{max} < 1{,}000\ \mu m \tag{2.15}$$

where $G=(\varepsilon/\nu)^{1/2}$ and r_{max} is in μm.

3. THE COMPUTER MODEL

For the purpose of modeling these processes a settling tank is segmented into k equal rectangular cells with length x and height z (Figure 3.1). The flow field and the size distribution of the particles are assumed uniform across the width of the tank and the suspension is spatially homogeneous within each cell. The continuous particle size (radius) spectrum is divided into q logarithmically equal spaced

sections within each of which the mass concentration of particles is constant (Gelbard and Seinfeld, 1980). This procedure reduces the number of conservation equations to be integrated and renders the problem tractable for computer solution.

The discrete conservation equation for the development of the particle size distribution in any cell k=(m,n) at time t is

$$
\begin{aligned}
\frac{dQ_{\ell,m,n}}{dt} = \Bigg[& \frac{1}{2}\sum_{i=1}^{\ell-1}\sum_{j=1}^{\ell-1}\left({}^{1a}\bar{\beta}_{i,j,\ell}\, Q_j Q_i + {}^{1b}\bar{\beta}_{i,j,\ell}\, Q_i Q_j\right) && (1)\\
& - \sum_{i=1}^{\ell-1}\left({}^{2a}\bar{\beta}_{i,\ell}\, Q_i Q_\ell - {}^{2b}\bar{\beta}_{i,\ell}\, Q_\ell Q_i\right) && (2)\\
& - \frac{1}{2}\,{}^{3}\bar{\beta}_{\ell,\ell}\, Q_\ell Q_\ell && (3)\\
& - Q_\ell \sum_{i=\ell+1}^{q} {}^{4}\bar{\beta}_{i,\ell}\, Q_i \Bigg]_{m,n} && (4)\\
& + \bar{S}_{\ell,m,n+1} && (5)\\
& - \bar{S}_{\ell,m,n} && (6)\\
& + \frac{u_{m-1,n}\, Q_{\ell,m-1,n}}{x} - \frac{u_{m,n}\, Q_{\ell,m,n}}{x} && (7)\\
& + \hat{E}_{n,n+1}\,\frac{Q_{\ell,m,n+1} - Q_{\ell,m,n}}{z^2} + \hat{E}_{n-1,n}\,\frac{Q_{\ell,m,n-1} - Q_{\ell,m,n}}{z^2} && (8)
\end{aligned}
\qquad (3.1)
$$

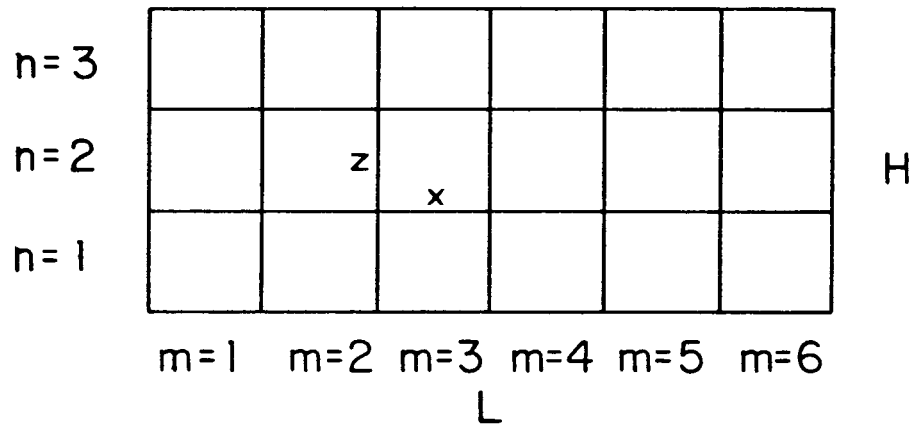

Fig. 3.1. Schematic diagram of tank partition.

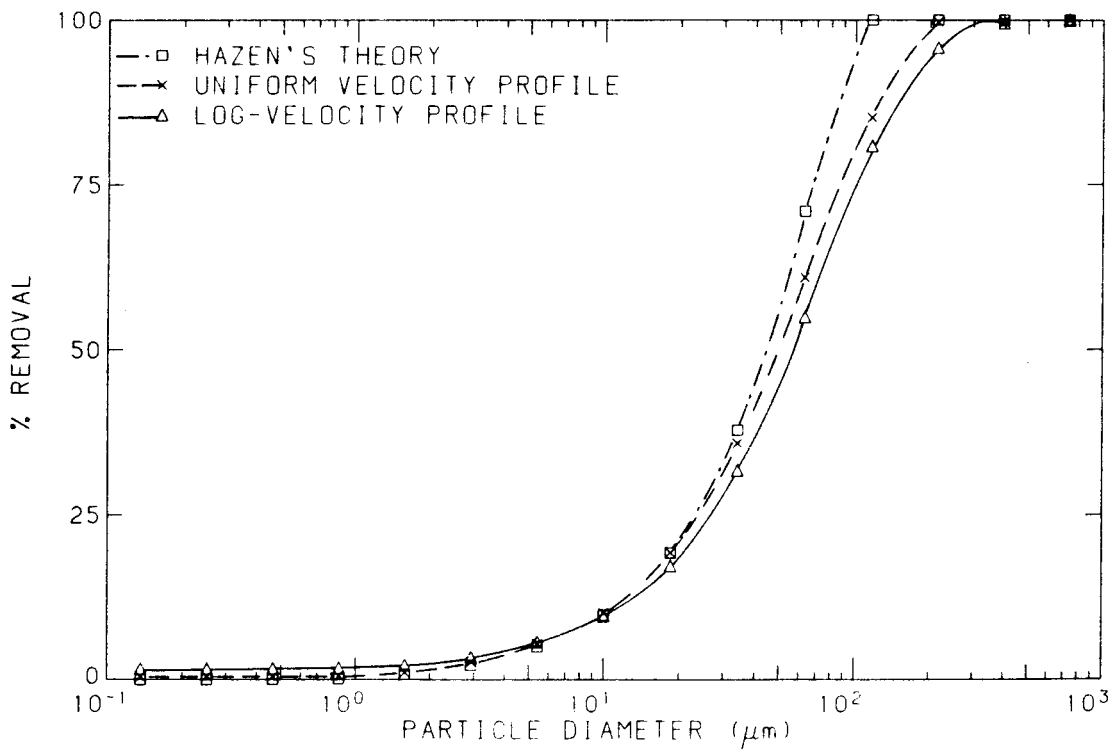

Fig. 3.2. Numerical diffusion. The removal efficiencies for a non-coagulating suspension are compared with the predictions of Hazen's theory.

Table 6

Sectional Coagulation Coefficients with Geometric Constraint ($v_{i+1} \geq 2v_i$, $i = 0,1,2,\ldots q-1$)

Symbol	Remarks	Coefficient
$^{1a}\bar{\beta}_{i,j,\ell} = {}^{1b}\bar{\beta}_{i,j,\ell}$	$i < \ell - 1$ $j < \ell - 1$	0
$^{1a}\bar{\beta}_{i,\ell-1,\ell} = {}^{1b}\bar{\beta}_{\ell-1,i,\ell}$	$1 < \ell \leq q$ $i < \ell - 1$	$\int_{x_{i-1}}^{x_i} \int_{f(v_{\ell-1}-v)}^{x_{\ell-1}} \frac{u\beta(u,v)}{uv(x_i - x_{i-1})(x_{\ell-1} - x_{\ell-2})}\, dydx$
	$1 < \ell \leq q$ $i = \ell - 1$	$\int_{x_{i-1}}^{f(v_i-v_{i-1}} \int_{f(v_{\ell-1}-v)}^{x_{\ell-1}} \frac{u\beta(u,v)}{uv(x_{\ell-1} - x_{\ell-2})^2}\, dydx + \int_{f(v_i-v_{i-1})}^{x_i} \int_{x_{\ell-2}}^{x_{\ell-1}} \frac{u\beta(u,v)}{uv(x_{\ell-1} - x_{\ell-2})^2}\, dydx$
$^{1b}\bar{\beta}_{i,\ell-1,\ell} = {}^{1a}\bar{\beta}_{\ell-1,i,\ell}$	$1 < \ell \leq q$ $i < \ell - 1$	$\int_{x_{i-1}}^{x_i} \int_{f(v_{\ell-1}-v)}^{x_{\ell-1}} \frac{v\beta(u,v)}{uv(x_i - x_{i-1})(x_{\ell-1} - x_{\ell-2})}\, dydx$
$^{2a}\bar{\beta}_{i,\ell} = {}^{1a}\bar{\beta}_{i,\ell,\ell+1}$	$1 < \ell \leq q$ $1 \leq i < \ell$	$\int_{x_{i-1}}^{x_i} \int_{f(v_\ell-v)}^{x_i} \frac{u\beta(u,v)}{uv(x_i - x_{i-1})(x_\ell - x_{\ell-1})}\, dydx$
$^{2b}\bar{\beta}_{i,\ell}$	$1 < \ell \leq q$ $1 \leq i < \ell$	$\int_{x_{i-1}}^{x_i} \int_{x_{\ell-1}}^{f(v_\ell-v)} \frac{v\beta(u,v)}{uv(x_i - x_{i-1})(x_\ell - x_{\ell-1})}\, dydx$
$^{3}\bar{\beta}_{\ell,\ell} = {}^{2}\bar{\beta}_{\ell,\ell,\ell+1}$	$1 \leq \ell \leq q$	$\int_{x_{i-1}}^{f(v_\ell-v_{\ell-1})} \int_{f(v_\ell-v)}^{x_\ell} \frac{(u+v)\beta(u,v)}{uv(x_\ell - x_{\ell-1})^2}\, dydx + \int_{f(v_\ell-v_{\ell-1})}^{x_\ell} \int_{x_{\ell-1}}^{x_\ell} \frac{(u+v)\beta(u,v)}{uv(x_\ell - x_{\ell-1})^2}\, dydx$
$^{4}\bar{\beta}_{i,\ell}$	$1 \leq \ell < q$ $\ell < i \leq q$	$\int_{x_{i-1}}^{x_i} \int_{x_{\ell-1}}^{x_\ell} \frac{u\beta(u,v)}{uv(x_i - x_{i-1})(x_\ell - x_{\ell-1})}\, dydx$
$\bar{S}_\ell$	$1 \leq \ell < q$	$Q_\ell \int_{x_{\ell-1}}^{x_\ell} \frac{w(v)}{(x_\ell - x_{\ell-1})}\, dx$

where $x_i = \log v = f(v_i)$, $u_i = \exp(y_i)$, $v_i = \exp(x_i)$ and u, v denote particle mass per unit volume of fluid, $\beta(u,v)$ is the collision function obtained from Table I and w(v) is the Stokes' settling velocity of particles with mass concentration v.

*adapted from Gelbard and Seinfeld (1980)

where m and n denote, respectively, the horizontal and vertical index of the cell and are subscripts to all variables in the square brackets. $Q_{\ell,m,n}$ is the concentration of the suspension in section ℓ in cell (m,n). The coagulation coefficients $^{1a}\bar{\beta}_{i,j,\ell}$, $^{1b}\bar{\beta}_{i,j,\ell}$, $^{2a}\bar{\beta}_{i,\ell}$, $^{2b}\bar{\beta}_{i,\ell}$, $^{3}\bar{\beta}_{\ell,\ell}$, $^{4}\bar{\beta}_{i,\ell}$ and settling coefficient $\bar{S}_{\ell}$ are listed in Table 6. $E_{n,n+1}$ is the vertical turbulent mixing coefficient for the exchange of momentum and mass between cells (m,n) and (m,n+1) and is computed on the line separating the two cells. $u_{m,n}$ is the horizontal velocity assigned to the cell (m,n), calculated at its center.

Term (1) represents the flux of mass into section ℓ by coagulation of particles from lower sections (i.e. particles of smaller size). Term (2) accounts for the loss of mass from section ℓ when a particle in section ℓ coagulates with a particle from lower sections. Term (3) represents the loss of mass from section ℓ due to intrasectional coagulation and term (4) the loss of mass from section ℓ when a particle from section ℓ coagulates with a particle from a higher section. Terms (5) and (6) represent, respectively, gain and loss of mass for the cell (m,n) resulting from particles sedimenting at their Stokes' settling velocity $w=\frac{2}{9} g \frac{\rho_f-\rho_w}{\mu} r^2$. Terms (7) correspond to the advective transfer of mass and terms (8) to the turbulent transport of mass from cell to cell.

The accumulation of particle mass per unit area at the bottom of the tank is obtained from

$$\frac{dQ^{\circ}_{\ell,m,1}}{dt} = (1 - s)\, Q^{\circ}_{\ell,m,1}\, \bar{S}_{\ell,m,1} \qquad (3$$

where $Q^{\circ}_{\ell,m,1}$ is the deposited mass per unit volume of fluid in section

ℓ from cell (m,1). Thus the computer model predicts the particle size distribution in the deposits and the thickness of the sludge blanket along the length of the tank. For simplicity it is assumed that the tank volume does not change due to sludge accumulation throughout the calculations.

Due to coagulation particles may exceed the maximum size allowed by the local shear. Their mass is then distributed equally among the smaller size fractions.

Incoming particles of a given size distribution can be introduced selectively at any height. Particles reaching the end of the tank are removed in the effluent from one or more cells.

The basis of the computer program is the MAEROS code developed by Gelbard (1982) at Sandia National Laboratories. This code simulates the evolution of the size distribution of a multicomponent aerosol in a completely mixed air chamber. The code is adapted here to water suspensions and modified to incorporate the spatial inhomogeneity of the tank and the exchange of particle mass and fluid volume between the cells.

For k cells and q sections a system of $k \times q$ first-order ordinary differential equations results. The Runge-Kutta-Fehlberg (4,5) integration routine that MAEROS uses proved to be inefficient, because the introduction of convective and turbulent mass fluxes renders the system of equations stiff. Instead, Gear's (1971) modification of Adams's multistep variable order predictor-corrector method is used. Gear's (1971) method uses information from previous steps to predict the derivative functions and extrapolate them into the next interval, therefore allowing a larger step size.

The geometric constraint $v_{i+1} > 2\ v_i$ (i=0,1,....q-1), where v_i is the upper limit of section i, is imposed in the code on the sectionalization of particle mass, thus minimizing the number of sectional coefficients to be computed (Gelbard et al., 1980). The latter depend on the section boundaries, the collision function $\beta(r_i, r_j)$ and the physical dimensions of the cells. Normally 15 sections are used covering the particle size range from 10^{-7}m to 10^{-3}m. The higher size range contains insignificant mass throughout the calculations, so the particle mass is essentially conserved.

From the three coagulation mechanisms listed in Table 4 only shear induced particle collisions are influenced by the flow. For the cells where turbulent shear induced collisions are comparatively unimportant, the same sectional coefficients are used, thus reducing the computational work.

The ability of the computer model to reproduce the actual operating characteristics of a settling basin depends on the mesh size used, both in the physical space and in the particle size-space. A finite cell size introduces an artificial mixing in the tank. Increased vertical and reduced longitudinal mixing enhance the settling rate. The selection of the number of cells and particle size sections represents a compromise between accuracy and computational cost. 18 cells (3 rows and 6 columns) and 15 particle size sections are used, thus a total of 270 ordinary differential equations are integrated simultaneously requiring about 12 minutes of Central Processor Unit (CPU) time on an IBM 370/3032 computer for 5 hrs of settling. The numerical diffusion is evaluated by passing a non-coagulating suspension through the basin. Particles enter the tank uniformly distributed with height and are

subjected to a uniform velocity field. The removal efficiencies obtained under steady state operation are compared in Figure 3.2 with the ones obtained when a logarithmic velocity profile is used and with the predictions of Hazen's (1904) theory. The plotted data points represent the removal efficiencies of the 15 particle size sections used in the simulation. It is seen that both numerical diffusion and flow induced mixing cause some suspended particles, which would have settled according to Hazen's theory, to be carried in the effluent. Numerical diffusion influences strongly the removal of particles in the size range 50μm to 100μm; for smaller or larger particles dispersion and turbulent mixing are more important.

Mixing coeficients in sedimentation tanks depend also on parameters which are not considered here, such as density currents, high inlet velocities, three-dimensional effects and sludge removal facilities. All these mechanisms increase the mixing in the tank, so that the dispersion and vertical mixing caused by the logarithmic velocity profile represents a lower bound to the actual dispersion characteristics of the tank. In the following sections we use the mesh size described above to illustrate the capabilities of the computer model developed, being aware of the additional mixing caused by numerical diffusion and regarding it as if it were due to the aforementioned mechanisms. However, in order to reproduce the characteristics of an operating settling tank with known mixing coefficients a finer mesh size both in physical and in particle size space is needed.

4. SENSITIVITY ANALYSIS

A standard wastewater treatment plant with parameters representative of treatment practice (Table 7) is selected to illustrate the capabilities of the model. A logarithmic velocity profile is assumed. The influent particle mass flux is proportional to the influent fluid flux. Particles are removed as deposits when they reach the bottom of the tank, or as effluent from all three cells at the end of the basin. Suspended solids, as traditionally defined, include all particles with diameters larger than 1μm; colloidal particles range in size from 0.1μm to 1μm.

It is common practice to evaluate the performance of a settling tank by the fraction R_{SS} of suspended solids removed; this is because in the field suspended solids analysis only captures particles larger than 1μm. This is only one measure of tank efficiency since the effectiveness of the settling process depends on how the mass is distributed in size-space. R_{SS} is reported here for all cases examined together with the total solids removal efficiency R_{TS} . The relative magnitude of R_{SS} and R_{TS} indicates the importance of flocculation in transferring particle mass from the colloidal particle size range (<1 μm) to the suspended size range (>1 μm).

Sensitivity analysis is performed to determine the influence of selective variables on the steady state plant performance. For the standard plant steady state operation is reached after about 5 hrs of constant inflow. In Section II.6 the dynamic response of the sedimentation basin to a temporally variable flow rate and concentration of inflow is examined.

TABLE 7

Characteristics of the tank configuration, flow conditions and the influent suspensions used in the simulation

Standard Plant

depth	4 m
length	40 m
detention time	2 hrs
overflow rate	48 m^3/m^2-day

Influent Suspensions

Raw Water	Total Solids Concentration	Slope parameter α[†]	Density
Suspension A	400 mg/ℓ	4	variable[§]
Suspension B	400 mg/ℓ	4	constant
Suspension C	200 mg/ℓ	4	variable
Suspension D	400 mg/ℓ	3	variable

[†]The size distribution function n(d) of the influent suspension follows the power law $n(d) = (\Delta N/\Delta d) = A.d^{-\alpha}$, where ΔN is the number of particles with a diameter in the size range Δd, per unit volume of fluid, the exponent α is a constant and the constant A depends on the influent mass concentration.

[§]The relationship proposed by Tambo and Watanabe (1979) is used: $\rho_f - \rho_w = \frac{1.3}{(100d)^{0.9}}$

where ρ_f and ρ_w are the densities of the floc and the water, respectively.

The output of the computer program is a histogram in particle size space. The curves of mass and number concentration against particle size shown in the following paragraphs are best-fit approximations to the histograms. The geometric mean of the diameters which define the size section is taken as the representative diameter of the section.

5. STEADY STATE OPERATION

5.a. Constant/Variable Particle Density

The effluent particle size distribution of two suspensions, one following the size-density relationship of Tambo and Watanabe (1979) (suspension A, standard case), and one with a constant particle density of 2000 kg/m^3 for all particles sizes (suspension B) are compared in Figures 5.1 and 5.2. The curves are best-fit approximations to the results of the simulation. For both suspensions the efficiencies for collisions between flocs are used. The influent size distribution has a slope parameter of α=4 which gives the same influent number size distribution but different influent mass distributions. The solids removal efficiencies are R_{TS} =61% and R_{SS} =44% for the variable density suspension and R_{TS} =53% and R_{SS} =45% for the constant density suspension. Large particles (larger than 20 μm) are removed less effectively in the case of the variable density suspension because of their reduced density. Their presence, however, increases the coagulation rate and the transfer of mass towards larger size sections. As a result, the number of particles in the size fraction 0.5 μm to

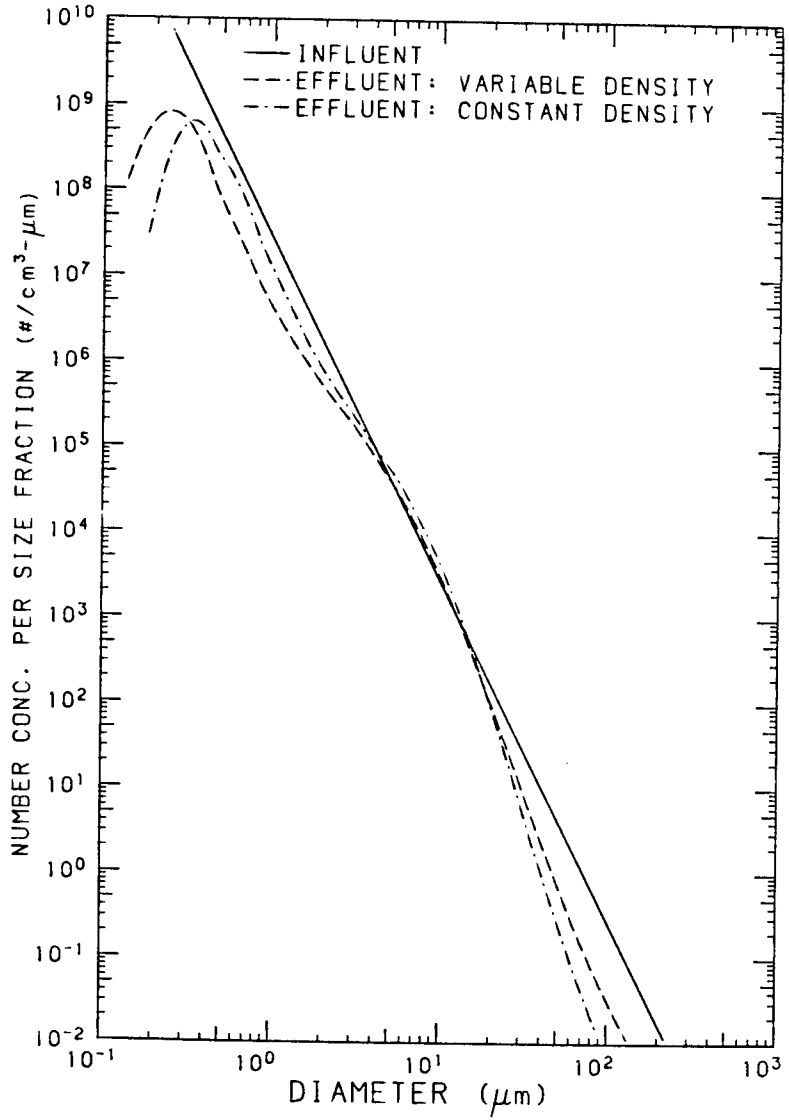

Fig. 5.1. Comparison of the variable density suspension A with the constant density suspension B. Number distribution function.

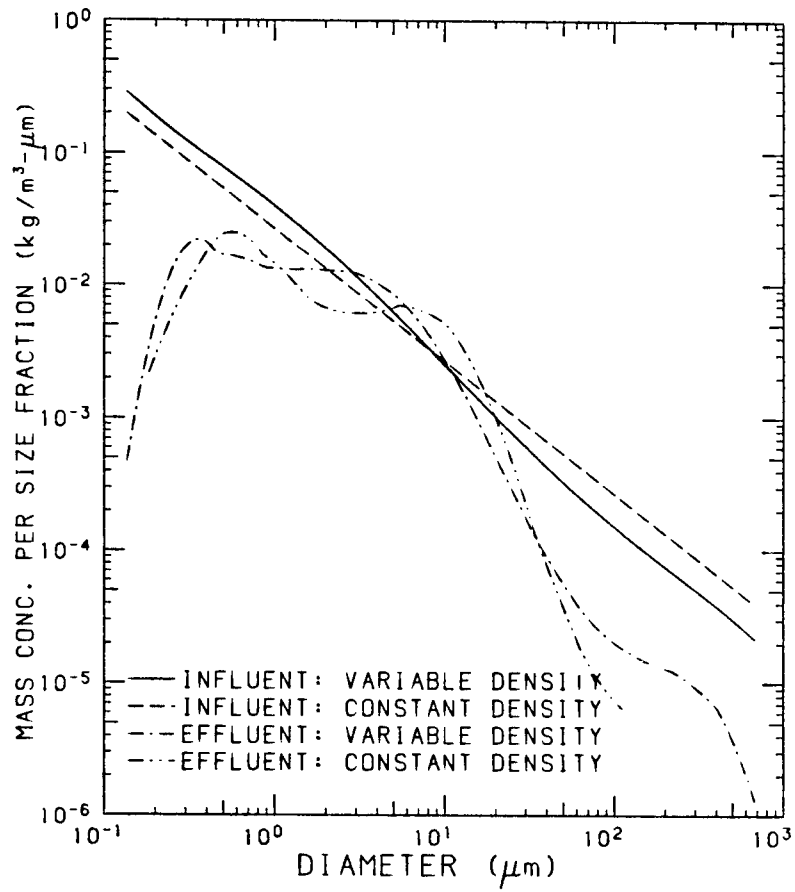

Fig. 5.2. Comparison of the variable density suspension A with the constant density suspension B. Mass distribution function.

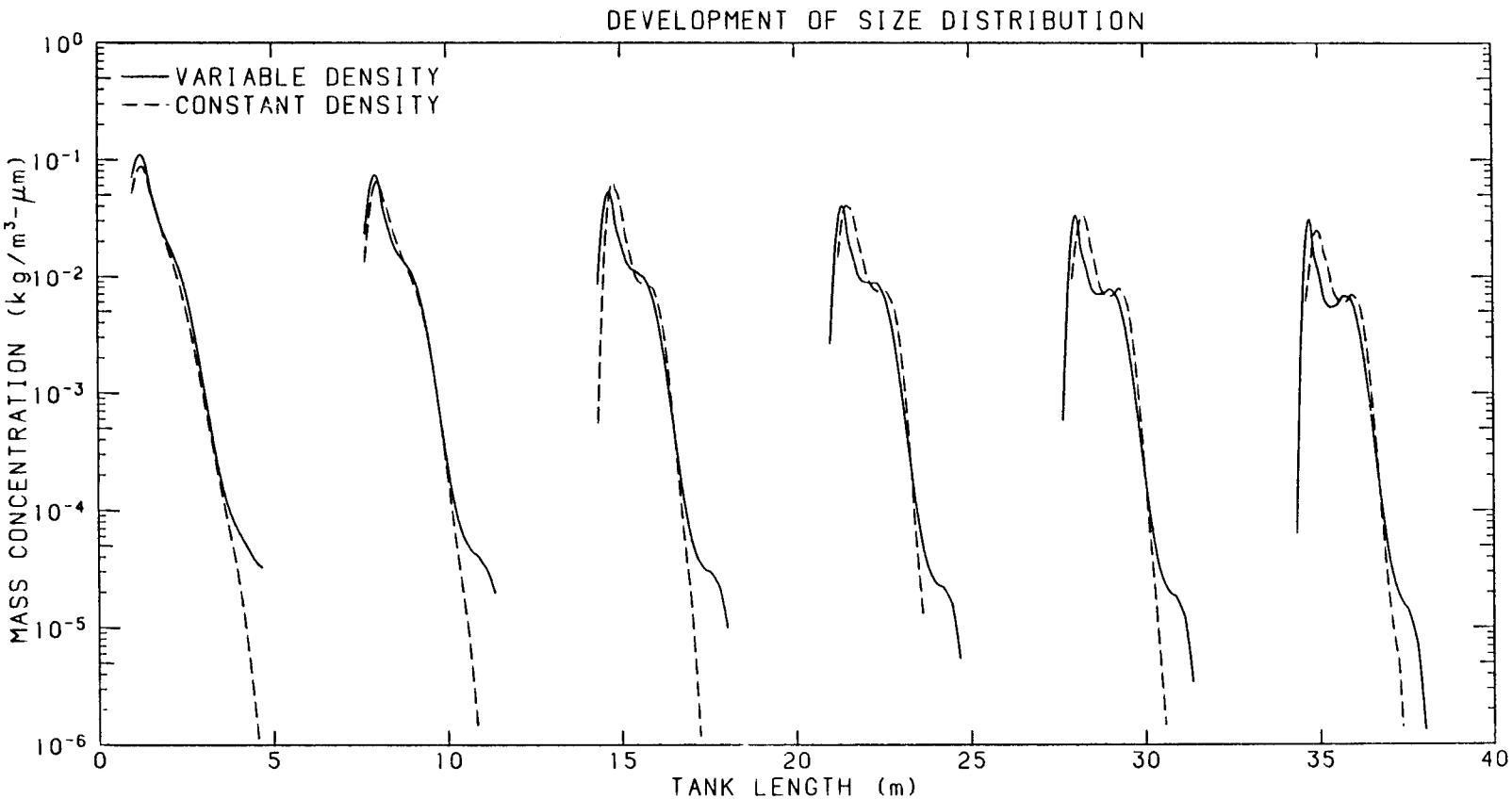

Fig. 5.3. Evolution of the mass distribution functions of the variable density suspension A and the constant density suspension B through the tank.

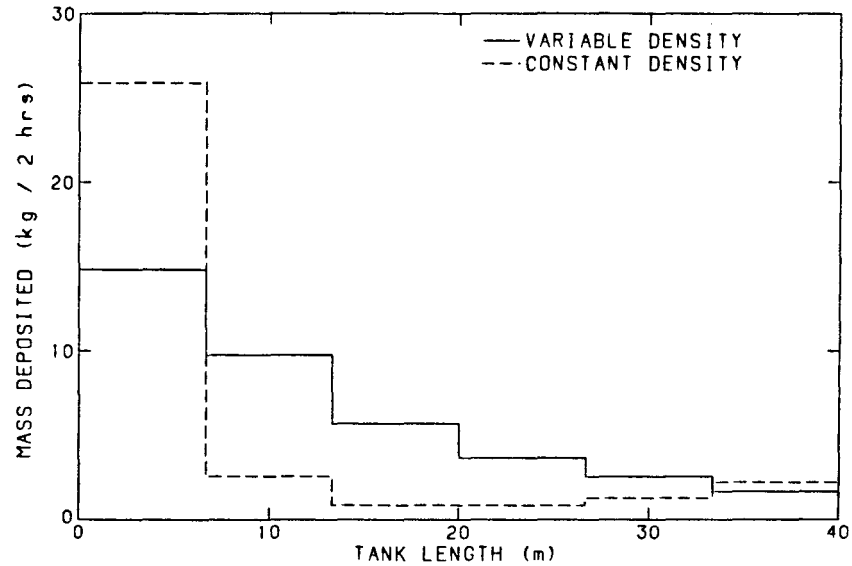

Fig. 5.4. Mass accumulated at the bottom of the tank (per unit width) when the variable density suspension A and the constant density suspension B are treated under steady state conditions.

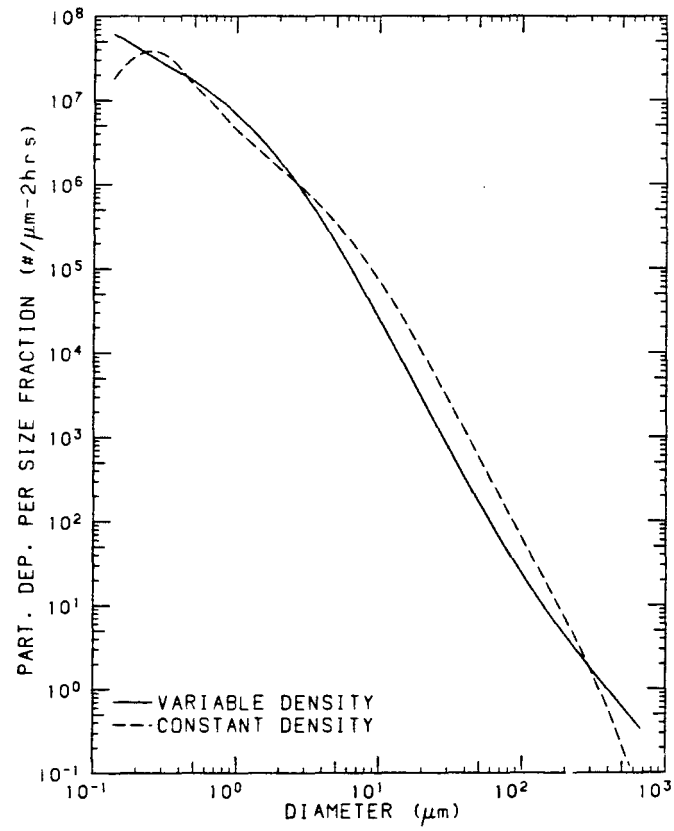

Fig. 5.5. Number distribution in the deposits when the variable density suspension A and the constant density suspension B are treated under steady state conditions.

20 μm remaining in the effluent is lower for the variable density suspension and the overall mass removal efficiency higher. However, note that in-field suspended solids analysis would, contrary to this result, indicate a better tank performance when the constant density suspension is treated.

The development of the mass size distribution of suspensions A and B along the tank, averaged over its cross-section, is shown in Figure 5.3. Two distinctive peaks in both mass size distributions develop near the particle sizes 0.5 μm and 10 μm. The constant density suspension loses all particles larger than 10 μm by the time it reaches the midpoint of the tank but coagulation recreates such particles near the end of the basin. This is further illustrated in Figure 5.4 where the total mass (per unit width) deposited along the tank during the 2 hrs detention time under steady state conditions is shown. For both suspensions most of the removal takes place in the first quarter of the tank length. Depletion of the large particles in suspension reduces the deposition rate of the constant density suspension near the middle of the tank and some time is required before settlable particles are created and precipitated. In contrast, a sludge blanket of decreasing thickness accumulates when the variable density suspension is treated.

The average particle number distribution in the deposits is depicted in Figure 5.5. Clearly this is not the particle size distribution expected in the sludge since hindered motion and compression settling in the high density zone near the bottom of the tank will alter the sludge size distribution. It provides the input parameters, however, for the modeling of these settling processes. Information on the quantity and quality of the sludge blanket is useful

in designing the sludge removal facilities of the tank.

5.b. Hydrodynamic Efficiencies

In modeling particle coagulation in hydrosols the collision efficiencies are commonly either assumed unity or constant, independent of the absolute and relative sizes of the interacting particles. A variable density suspension (suspension C) with half the total solids concentration of the standard case is used to evaluate the importance of employing the proper collision efficiencies. Two cases are compared in Figures 5.6 and 5.7, one using the rectilinear coagulation functions (efficiency unity) and one the collision efficiencies for flocs (Eqs. 2.8 and 2.9). The effluent particle size distributions are completely different in shape and the reduction in the removal efficiency of the tank is dramatic. When the collision efficiencies for flocs are used only 16% of the suspended and 39% of the total solids are removed, compared with 87% and 82%, respectively, for the hydrodynamically non-interacting suspension.

It is interesting to compare the removal efficiencies of the tank with suspensions B and C (where in both cases the collision efficiencies for flocs are used). Suspension A has a total solids concentration of 400mg/ℓ of which 250mg/ℓ is defined as suspended solids. For this influent 61% of the total solids are removed in the tank and 44% of the influent particles larger than 1 μm (the suspended solids), i.e. R_{SS} =44%. For the influent suspension C with 200mg/ℓ of total solids and 125mg/ℓ of suspended solids, 39% of the total solids are removed and

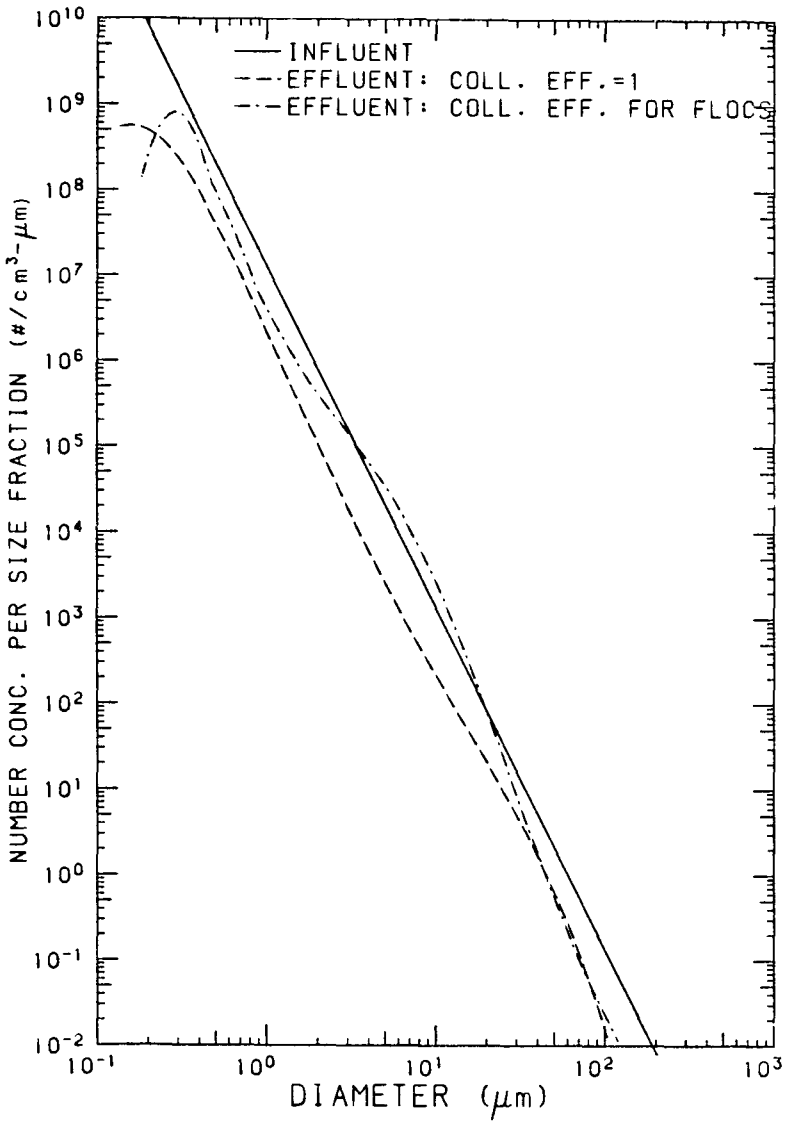

Fig. 5.6. Effect of the collision efficiency on the effluent number distribution function of the variable density suspension C.

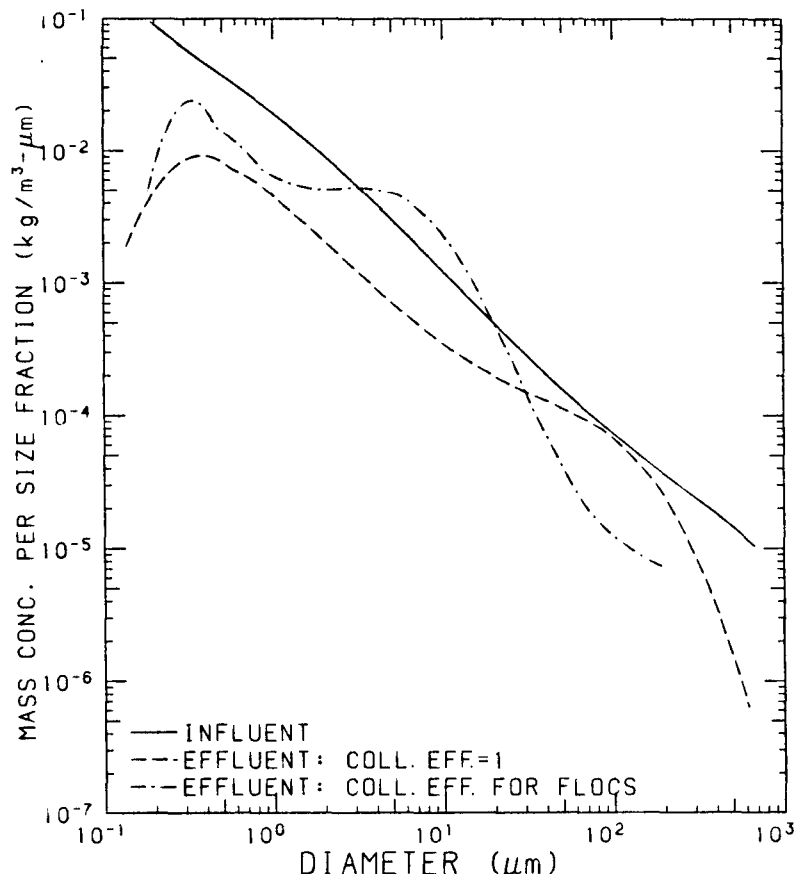

Fig. 5.7. Effect of the collision efficiency on the effluent mass distribution function of the variable density suspension C.

16% of the suspended solids (R_{SS} =16%). This low figure is indicative of the production of suspended solids by the coagulation process. A non-coagulating suspension gives removal efficiencies R_{TS} =20% and R_{SS} =33%. Coagulation transfers mass through the particle size spectrum toward settleable particle sizes so that the total solids removal efficiency is increased but the suspended solids removal efficiency is reduced. Coagulation is responsible for this paradox. For the hydraulic conditions and the size density relationship used here only particles larger than about 20 μm are precipitated. Coagulation accumulates particle mass in the size range 1 μm to 40 μm and this is characteristic of all simulations presented above. The rate of mass transfer to particle sizes larger than 40 μm is slow since the number of large particles which will extract mass from the immediately smaller size fractions is reduced because of settling. Hence the remarkable reduction in suspended solids removal efficiency for the coagulating suspensions.

5.c. Influent Particle Size Distribution

Suspension D has a total solids concentration of 400 mg/ℓ , as for suspension A, but a flatter particle size distribution with α =3. This value of α implies a uniform surface area concentration distribution and increasing volume and mass concentrations with increasing particle size (see Eqs. 2.12 in Chapter II). Both coagulation and settling are enhanced and so 98% of the solids are removed when suspension D is treated under the standard hydraulic conditions. Figures 5.8 and 5.9

illustrate the change in the mass and number distributions, respectively, when suspension D passes through the settling tank. For all particles smaller than about 8 μm the particle number distribution is merely shifted downwards, retaining the influent slope; for larger particles the slope is altered to -3.5.

The development of the volume average diameter, defined as

$$d = \left(\frac{6}{\pi} \frac{\sum Nv}{\sum N} \right)^{1/3}$$

where N and v are, respectively, the number and volume concentrations of the particles, along the length of the tank for suspensions A and D is shown in Figure 5.10. The volume average diameter increases continuously in the case of suspension A indicating that coagulation transfers mass to large particle size sections at a faster rate than sedimentation removes suspended mass. The situation is reversed for suspension D which has relatively more mass at large particle sizes.

5.d. Longer Tank

For the same detention time a longer but more shallow tank with reduced overflow rate can be used. Longitudinal dispersion is enhanced and vertical turbulent mixing reduced. Large particles spend less time suspended, collecting fewer particles as they fall.

Suspension B was treated in a settling basin 64m long and 2.5m deep. The solids removal efficiencies were R_{TS} =50% and R_{SS} =27% indicating a reduction in the removal efficiency of the basin. Figure 5.11 compares the effluent characteristics for the standard basin and

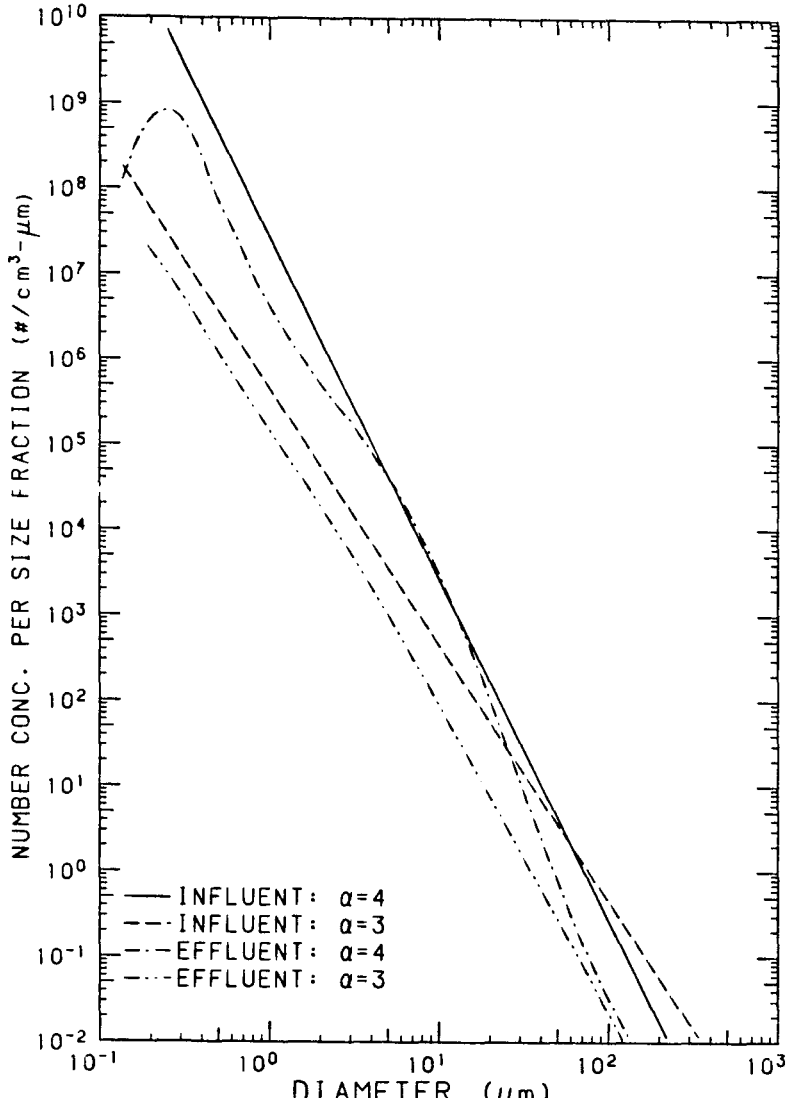

Fig. 5.8. Comparison of the effluent number distribution functions of suspension A with slope parameter α=3 and suspension D with slope parameter α=4.

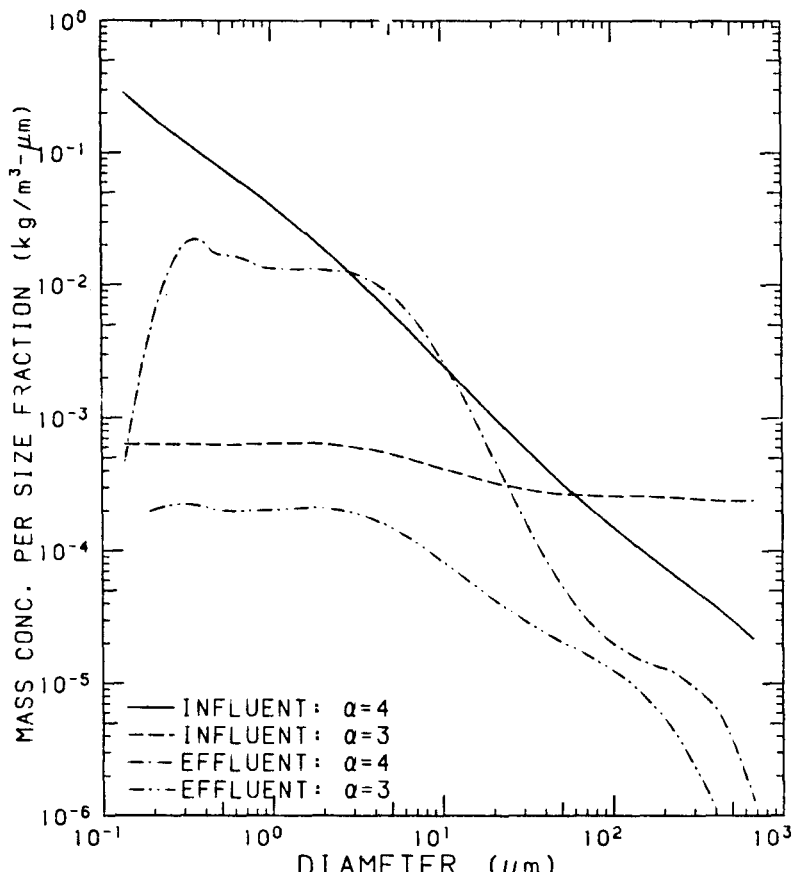

Fig. 5.9. Comparison of the effluent mass distribution functions of suspension A with slope parameter α=3 and suspension D with slope parameter α=4.

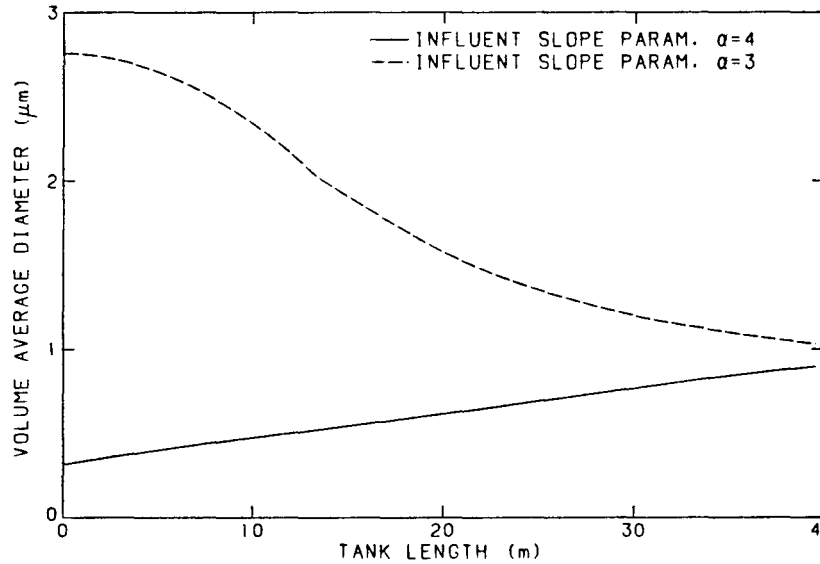

Fig. 5.10. Evolution of the volume average diameter of the variable density suspensions A (α=3) and D (α=4).

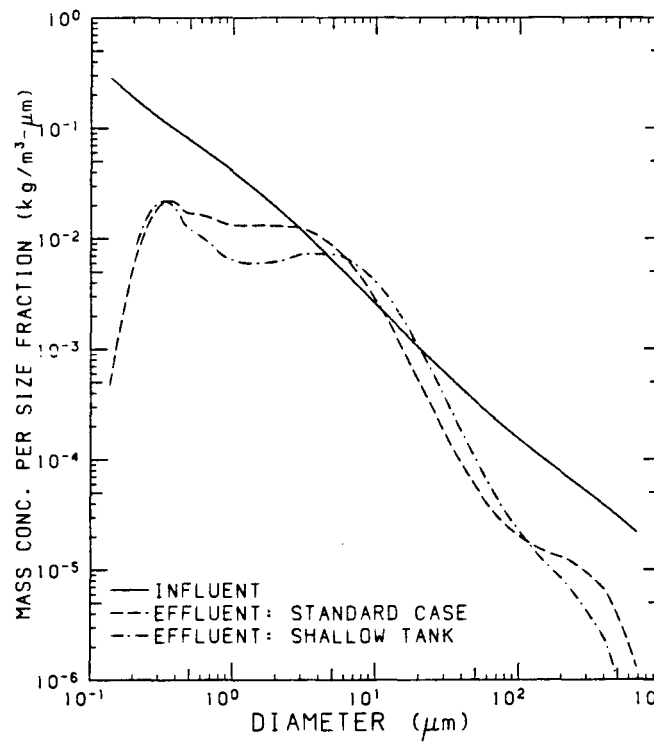

Fig. 5.11. Comparison of the effluent mass distribution functions for the standard and the shallow tank both treating the variable density suspension A.

the longer one, both treating suspension A. The stronger shearing in the shallow tank promoted coagulation of particles in the size range 0.5 μm to 10 μm, but larger particles, whose coagulation rate depends largely on differential settling induced collisions, tend to remain in suspension.

5.e. Recirculation

The logarithmic velocity distribution is not realistic near the inlet and outlet of the basin and has been used above only to provide a convenient flow regime in order to examine other parameters of interest. Published data on the flow fields in settling tanks do not satisfy continuity of fluid mass. Thus, a flow field is assumed, including a circulation current, as shown in Figure 5.12. This is obviously one of an infinite number of possible flow patterns which can develop in a sedimentation tank and assumes that the inflow has a jet-like behavior.

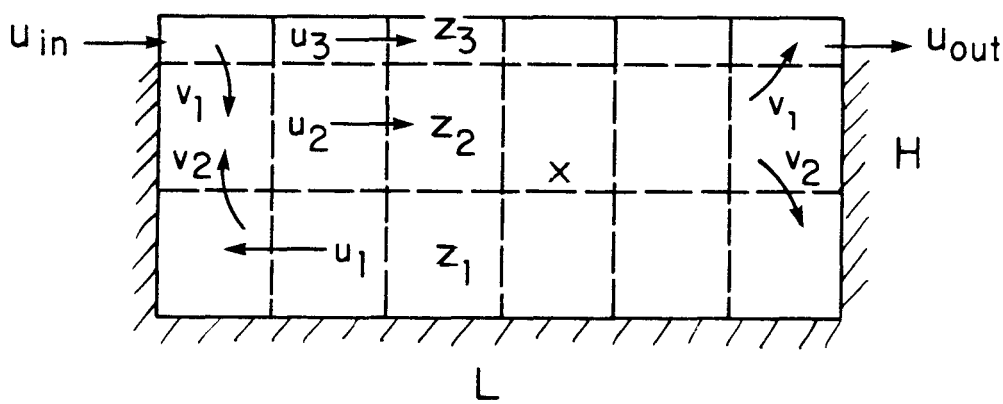

Fig. 5.12. Schematic diagram of the recirculating flow pattern.

A variable mesh size is used in the vertical direction and it is assumed, first, that one fourth of the inflow moves horizontally along the upper row of cells, and second, that all vertical velocities in the tank are equal. This crude flow pattern enhances the mixing and the turbulence intensity at the lower section of the tank. The vertical mixing coefficient is estimated using the mixing-length argument from

$$E = (z_n + z_{n+1})(u_n + u_{n+1}), \quad n=1,2$$

where z_n and u_n are, respectively, the depth and the horizontal velocity in the cells in row n. The turbulent energy dissipation rate, per unit mass of fluid, is estimated using Eq. 2.3 in Chapter II. The intense local shearing enhances the coagulation rate but also breaks up any flocs which, according to Eq. 2.15 in Chapter II, grow larger than about 1000 μm.

Figures 5.13 and 5.14 compare the tank effluent when suspension A is subjected to the recirculating flow field with the effluent of the standard case. The increased mixing in the tank, induced by the circulating current, causes more large particles to be carried over the effluent weir. Enhanced coagulation rates and the break-up of flocs exceeding 1000 μm in diameter - their mass is equally distributed among the other sections - result in smoother number and mass distributions in the effluent. The total solids removal efficiency remains 61% but the suspended solids removal efficiency is increased to 54%, as compared with the standard case.

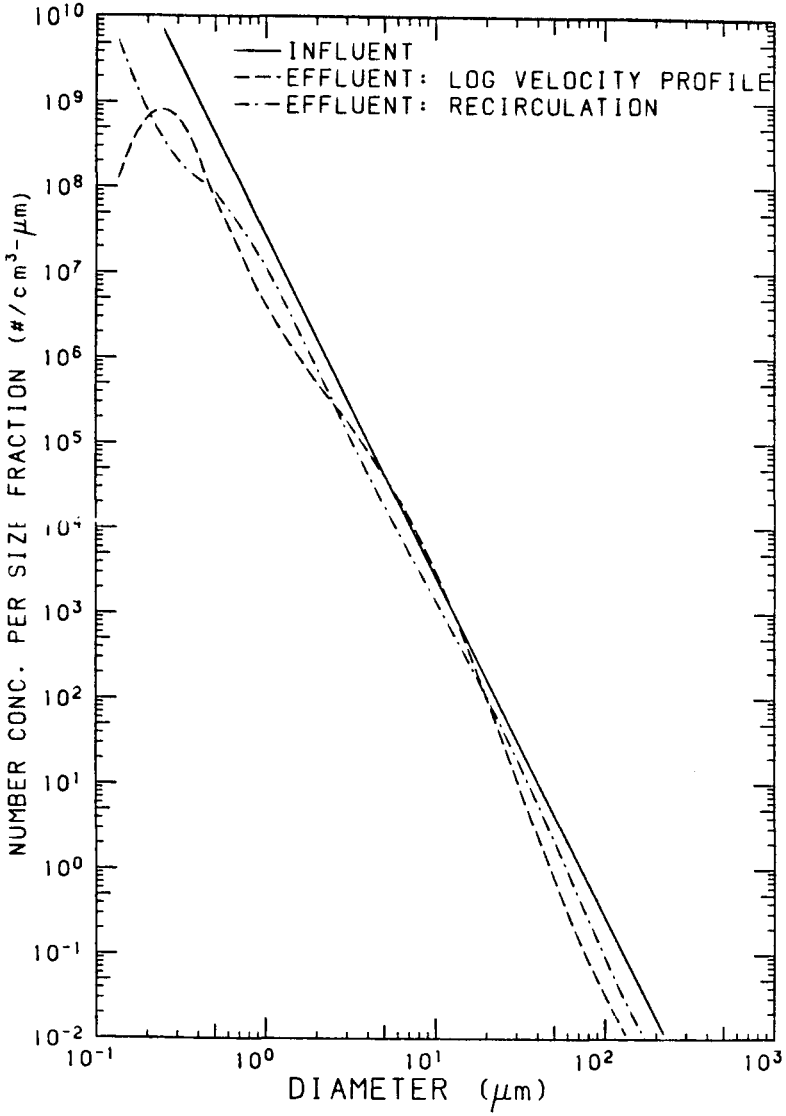

Fig. 5.13. Effect of the flow field on the effluent number distribution function of the variable density suspension A.

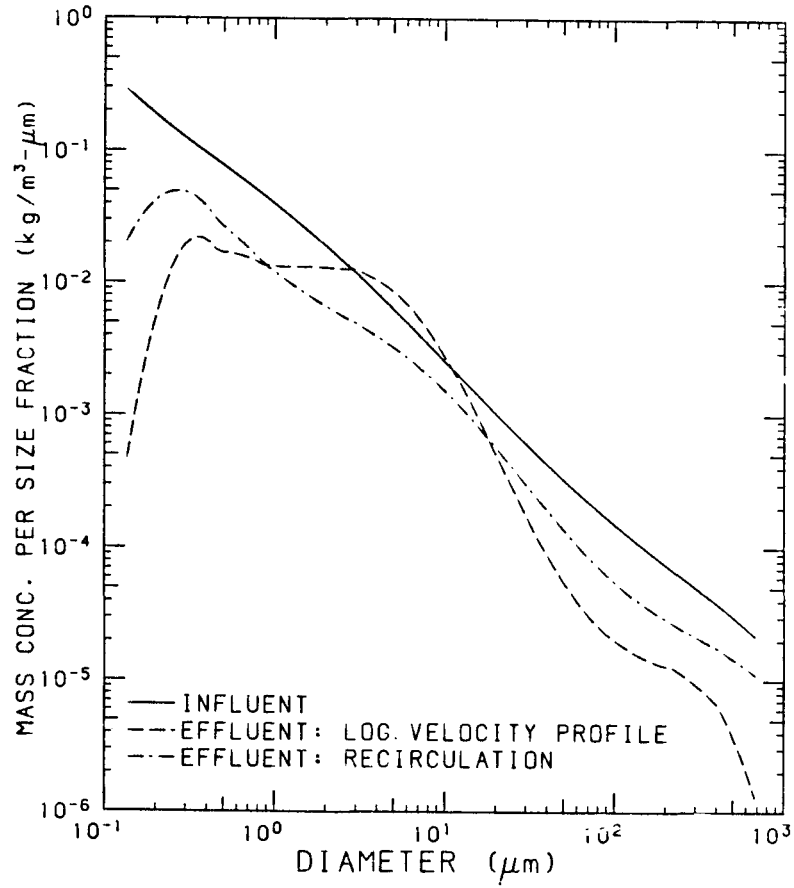

Fig. 5.14. Effect of the flow field on the effluent mass distribution function of the variable density suspension A.

5.f. Scouring

The sensitivity of the tank performance to scouring was investigated by performing simulation runs at various values of the resuspension parameter s, all other parameters remaining the same. The removal efficiencies obtained when suspension A was treated are listed in Table 8. Included in the same table are the results for a non-coagulating suspension with the same characteristics as suspension A. In the case of the non-coagulating suspension the tank performance deteriorates as the rate of resuspension increases. The sensitivity of the solids removal efficiency to s is in accordance with the results of Takamatsu et. al. (1974) for a non-flocculating suspension. On the contrary, when a suspension which undergoes coagulation is treated, resuspension of the deposits improves slightly the tank performance for small values of the resuspension parameter s; for large s the tank perfomance deteriorates.

Coagulation in the high mass concentration regions near the bottom of the tank, resulting from resuspension of previously deposited material, transfers mass toward larger particle size sections with a subsequent improvement in the tank performance. As the resuspension flux increases, however, a critical situation is reached, where coagulation cannot compensate for the reduced settling rates and so the solids removal efficiency of the basin is reduced.

Table 8: Sensitivity of the tank performance to scouring

	Resuspension Parameter S	% Total Solids Removed R_{TS}	% Suspended Solids Removed R_{SS}
Coagulating suspension	0	60.1	42.8
	0.15	60.6	43.6
	0.4	60.8	44.1
	0.8	55.7	38.2
Non-coagulating suspension	0	21.6	33.9
	0.15	20.0	33.0
	0.4	18.8	29.7
	0.8	13.8	21.3

6. UNSTEADY RESPONSE

In actual wastewater treatment plants the flow rate and the concentration in the inflow may vary considerably with time. The computer simulation is capable of predicting the dynamic response of the settling tank to a temporally variable input. For the purpose of demonstrating the capabilities of the computer model the effluent characteristics are investigated when a top-hat discontinuity or a sinusoidal variation in the influent concentration or the flow rate occurs.

6.a. Top-hat Discontinuity

A sedimentation tank is assumed operating with a detention time of 2 hrs. It is taken to be treating the variable density suspension A in a steady state mode. Then, either the influent concentration, or the overflow rate is doubled for 30 minutes, the discontinuity occurring at 360 minutes after start-up time, with the latter marked as time zero. The ratio of the total mass concentration in the effluent at a given time to the steady state effluent concentration is plotted in Figure 6.1 as a function of time for the two cases examined. The change in the effluent concentration due to an impulse in the concentration in the inflow is small. After a time lag of about 30 minutes the effluent concentration increases, reaches its maximum value at 60 minutes after the initial change in the influent concentration and then decreases for

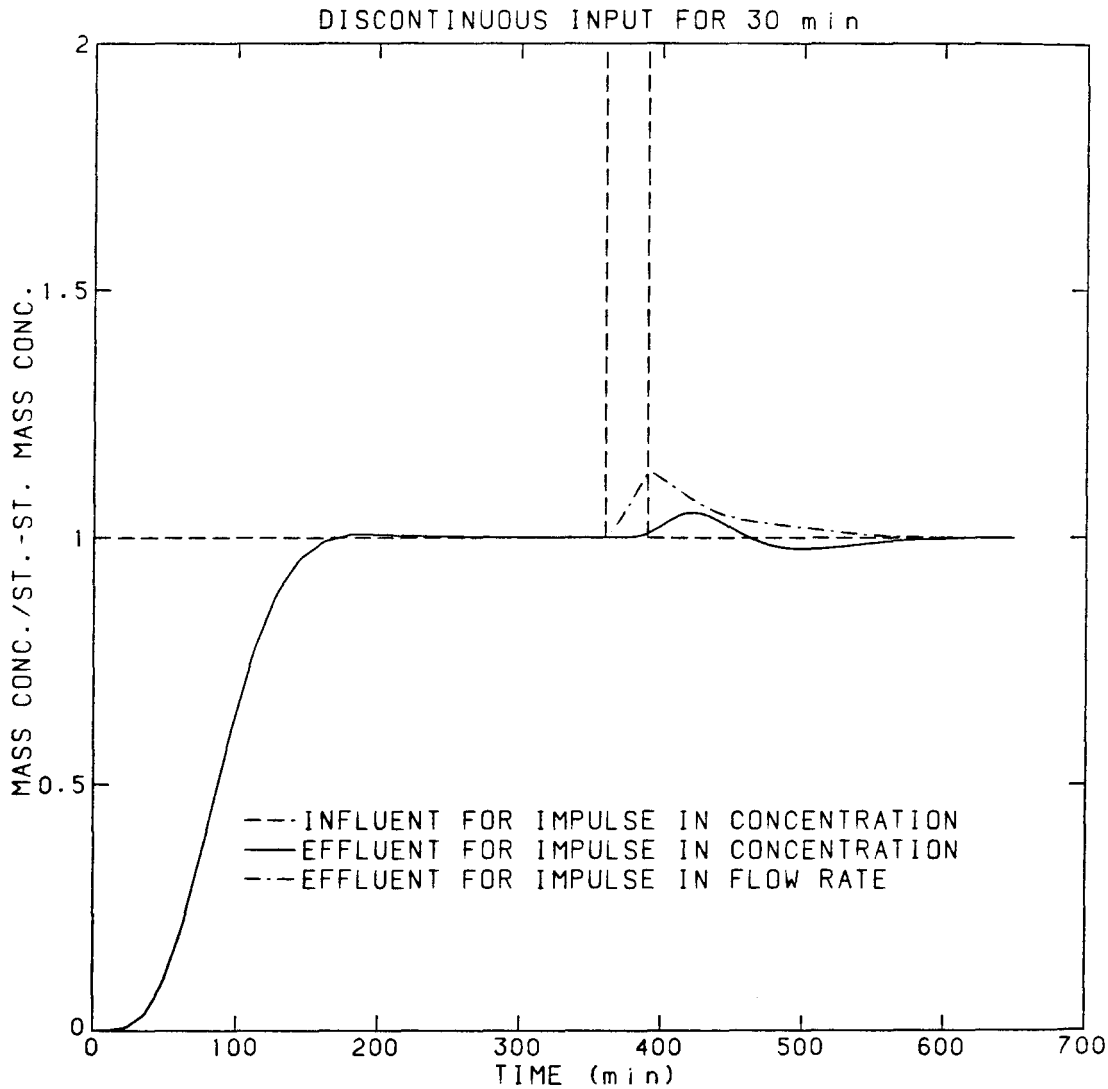

Fig. 6.1. Effluent response to an impulse in concentration of the inflow or the flow rate.

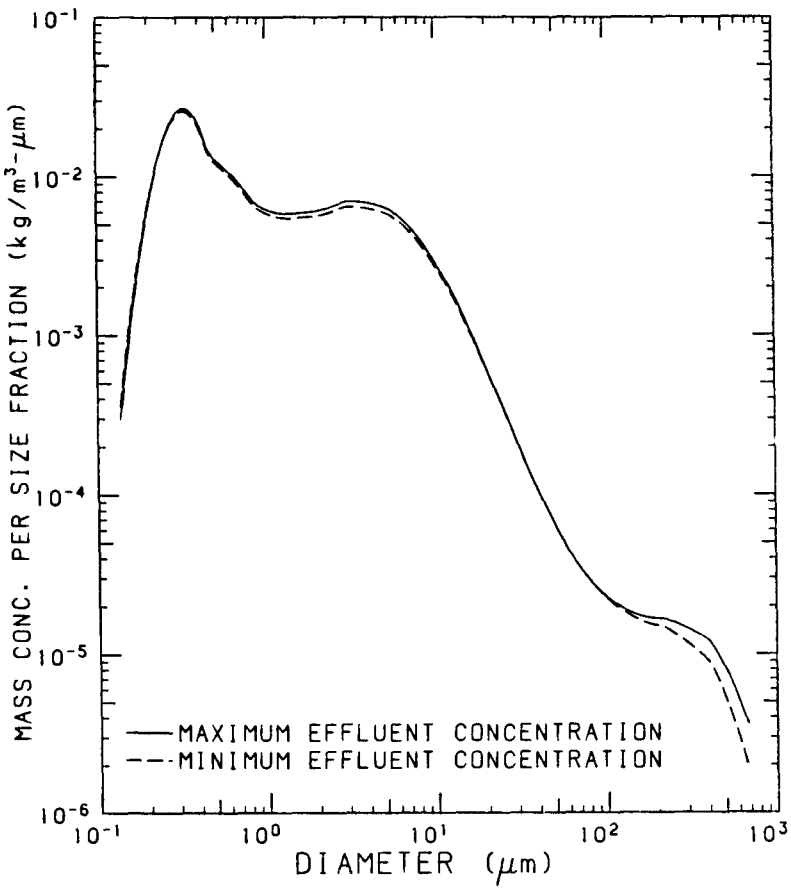

Fig. 6.2. Effluent mass distribution functions for an impulse in the influent concentration.

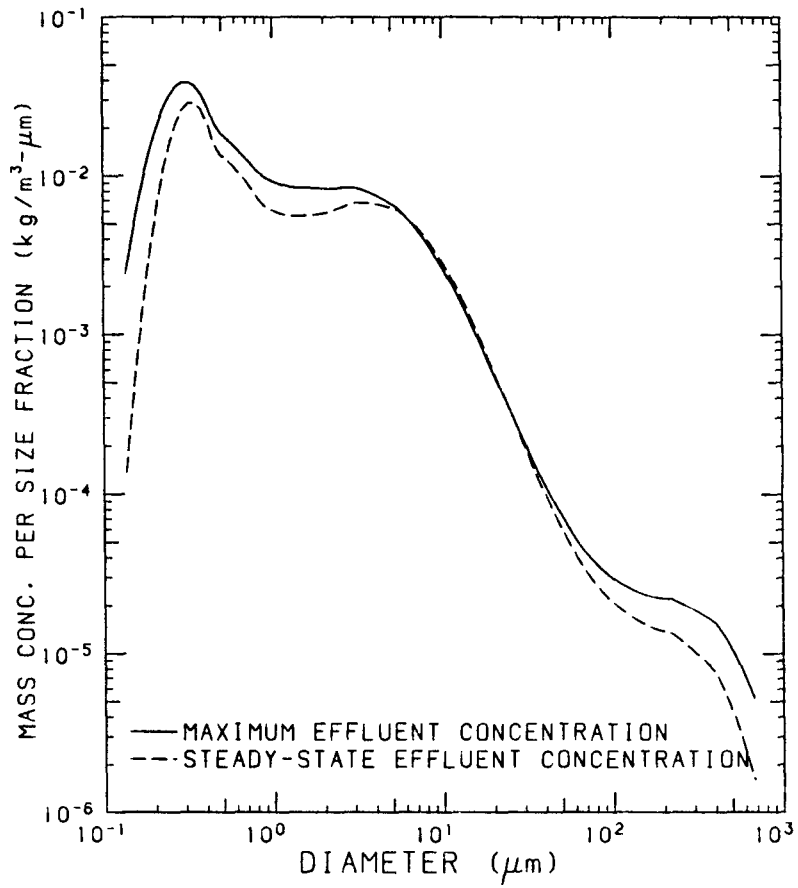

Fig. 6.3. Effluent mass distribution functions for an impulse in the flow rate.

some time below its steady state value. The shape of the effluent curve reflects the trade-off between the increased influent mass load, which suggests that more mass will be carried in the effluent, and coagulation, which is a second order function of concentration and promotes settling and therefore mass loss from the effluent. The response of the tank to the impulse in the flow rate is immediate; this is because it is assumed that the flow field in the tank adjusts instantaneously to the change in the inflow rate. In both cases the increase in the effluent concentration is small because of the dumping effects of numerical diffusion, turbulent mixing and coagulation.

The next two figures compare the effluent particle mass distribution curves at the peak effluent mass concentration with that for the steady state effluent. Figure 6.2 is for the case when there is an impulse in the influent mass concentration and it can be seen that the effects are mainly on particles larger than 100 μm. In Figure 6.3, which is for the case of an impulse in flow rate, the effects are more severe. There is a significant rise in the concentration of larger particles in the effluent.

6.b. Periodic Input

The variable density suspension A is used to investigate the response of the tank to a periodic variation in the influent concentration or the flow rate. The frequency of the sinusoidal input is equal to the inverse of the residence time of the suspension in the tank (2 hrs) and its amplitude equal to half the steady state input.

Figure 6.4 shows the temporal variation in the effluent concentration when the mass concentration in the inflow varies sinusoidally with time. The tank acts as a filter and smooths the variations in the influent concentration. The effluent characteristics of a non-coagulating suspension, plotted in the same figure, indicate that numerical diffusion and turbulent dispersion and mixing are mainly responsible for the filtering action of the tank, while coagulation reduces significantly the time-averaged effluent concentration. Coagulation also reduces the time between the effluent and influent peak concentrations (modal time) from 90 minutes for the non-coagulating suspension to about 60 minutes. In both cases the modal time is smaller than the theoretical detention time; observed dispersion curves in model settling tanks show the same trend (El-Baroudi, 1969, Kawamura, 1981).

Figure 6.5 illustrates the effluent response to a sinusoidally varying flow rate. In this figure the flow rate, non-dimensionalised with its time-averaged value, and the effluent mass concentration, non-dimensionalised with the steady state effluent concentration obtained when the flow rate is steady and equal to the time-averaged flow rate, are plotted against time. Note the very short modal time, about 30 minutes, and that the time-averaged effluent concentration is slightly higher than the one obtained when the flow rate is steady.

The next two Figures 6.6 and 6.7 show the mass distribution at the maximum and minimum effluent concentrations for the two time variable input simulations performed. As in the case of the top-hat discontinuities, the variation in the mass concentration function is larger when the flow rate varies with time.

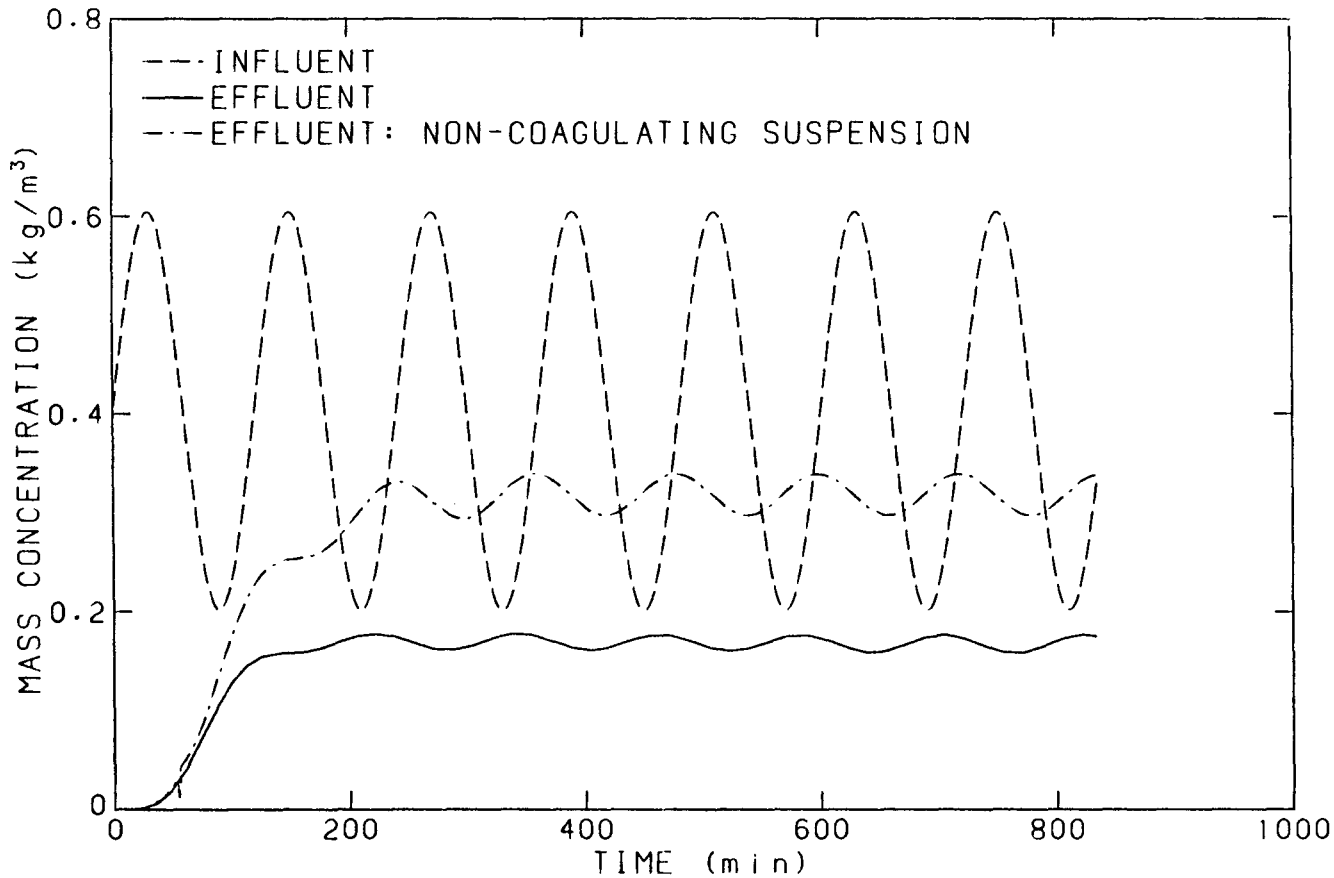

Fig. 6.4. Temporal variation of the effluent mass concentration for a sinusoidally varying concentration in the inflow. The frequency of the sinusoidal input is equal to the inverse of the detention time (2 hrs) and its amplitude equal to half the steady state influent concentration.

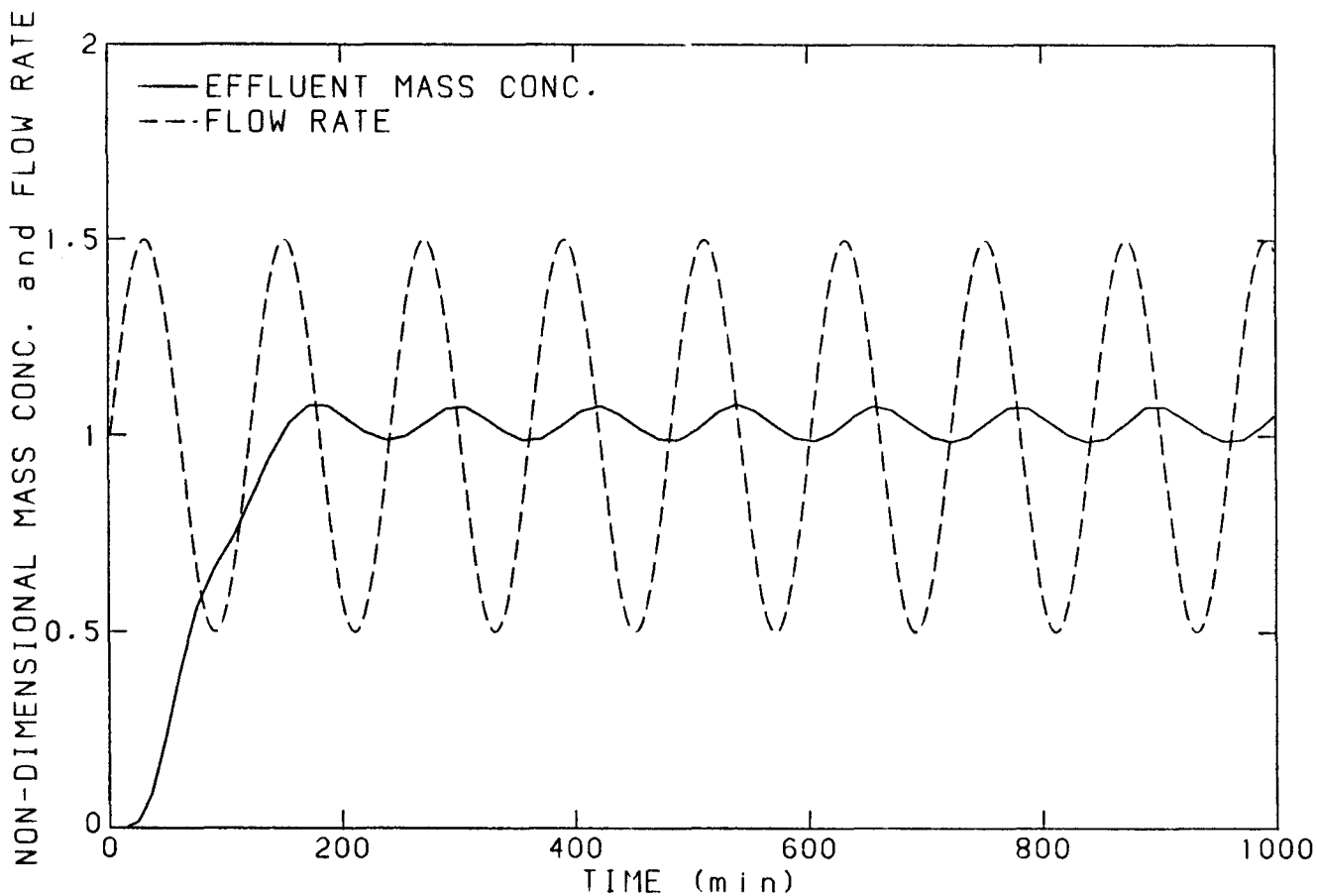

Fig. 6.5. Non-dimensional flow rate and effluent mass concentration. The flow rate is non-dimensional with its time-averaged value and the concentration with the steady state effluent concentration obtained when the flow rate is steady and equal to the time-averaged flow rate. The frequency of the sinusoidal input is equal to the inverse of the detention time (2 hrs) and its amplitude equal to half the steady state flow rate.

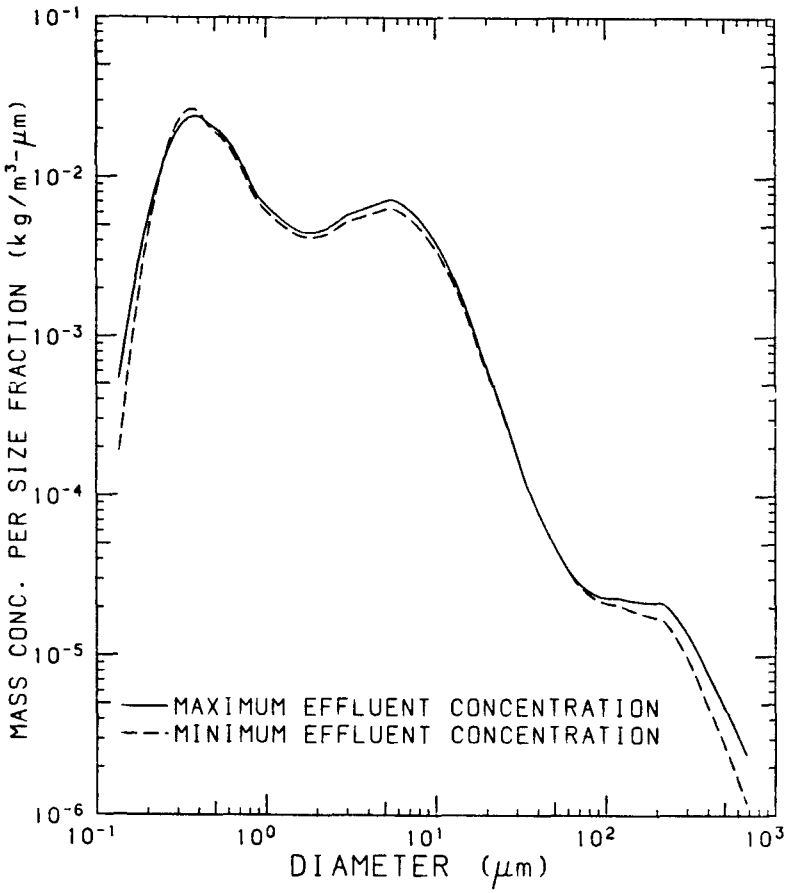

Fig. 6.6. Effluent mass distribution functions for a sinusoidally varying influent concentration.

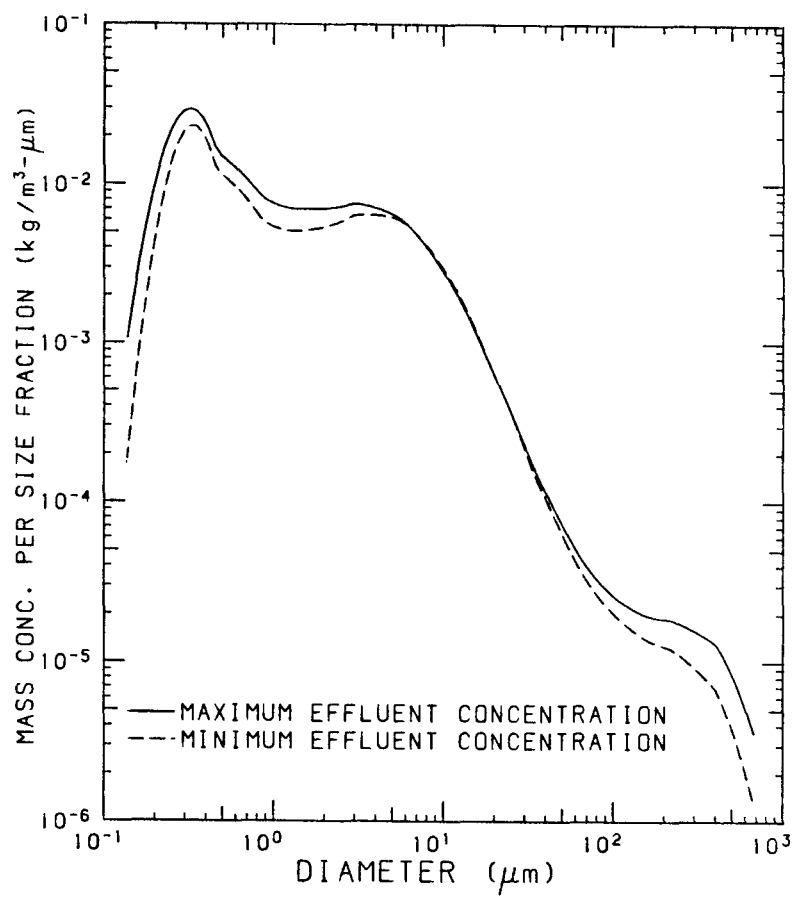

Fig. 6.7. Effluent mass distribution functions for a sinusoidally varying flow rate.

7. CONCLUSIONS

The basic aim of this study has been to develop a numerical model simulating the operation of a rectangular sedimentation basin. The model is based on a computer solution of an extended General Dynamic Equation and includes all of the basic kinetics of particle collision and coagulation processes, including Brownian motion, turbulent shear and differential sedimentation. Also included are estimates for the modification to particle collision efficiencies by van der Waals' forces and hydrodynamic interactions between particles. Specific attention is directed to transport processes such as particle advection, turbulent diffusion and particle resuspension. The influence of the particle size-density relationship and floc deaggregation by turbulent shearing are also modeled. Of necessity, modeling of some of these processes has been somewhat empirical since the physical and biochemical nature of the flocs produced are often unique to a particular suspension. Nevertheless, the model developed is capable of predicting the evolution of a particle size distribution in flow through a sedimentation tank under both steady and unsteady operating conditions, and within reasonable computation time.

For the purpose of elucidating features of the model, it has been applied to a specific sedimentation tank design. From the limited number of simulations presented here it is evident that particle collision efficiencies, the particle size-density relationship and the shape of the influent particle size distribution affect dramatically both the characteristics of the effluent size distribution and the overall tank performance. The collision efficiencies between particles

and the particle size-density relationship were modeled somewhat arbitrarily, since, to the knowledge of the writer, no related published results exist; both depend on the physical and biochemical nature of the flocs and will be unique for a particular suspension, so their determination requires experimental work.

The collision efficiencies used in the simulation runs are valid only if it is assumed that the ionic strength of the suspension is sufficiently large for coagulation to occur. Repulsive double layer forces may inhibit flocculation, as suggested by Figures 3.9, 3.10 and 3.11 in Chapter I. For a non-coagulating suspension the removal efficiency R_{SS} of suspended solids is larger than the removal efficiency R_{TS} of the total solids (see the results in Section II.5.b); the reverse is true for a coagulating suspension in most simulation runs performed. This indicates that coagulation tranfers mass through the size spectrum toward settleable particle sizes. This phenomenon is more likely to occur in polymer-added sedimentation. Coagulants help precipitate particles with sizes less than 1μm (phosphorus (Long and Nesbitt, 1975) or bacteria (Waite, 1979), for instance) and have been found to increase the relative contribution of suspended solids in the total solids of the effluent (Hunter and Heukelekian, 1965). The above suggest that the simulation runs performed here are applicable to situations where the suspension has been destabilized by some coagulating agent.

Moderate resuspension of the deposits may improve the performance of a basin when a coagulating suspension is treated. For a non-flocculating suspension scouring reduces the solids removal efficiency. Since , however, scouring and resuspension of sediments were modeled empirically, definite conclusions cannot be drawn.

However, experimental and theoretical work on resuspension of cohesive sediments is in progress (NOAA, 1982) and the results can be easily incorporated in the simulation.

The simulations of tank operation under unsteady state inflow conditions suggest that coagulation smooths moderate variations in the inflow concentration and flow rate. A finer mesh size than the one used here in physical space is required in order to reduce the effect of numerical diffusion.

Clearly, further modifications, improvements and trials will be necessary before the model can be used with confidence in the design of new facilities. At this juncture, it appears that more experimental work on the nature of the particle size-density relationship, the resuspension of deposits and the particle collision efficiencies are the crucial next steps in improving the realism of the model. Also, information on the properties of the suspension in the influent and effluent of operating sedimentation tanks will allow the testing and subsequent improvement of the simulation model.

NOTATION

A	Van der Waals' energy of attraction
c	Density of dense regions in the floc
d	Particle diameter
D_i	Diffusivity of particle with radius r_i
e	Porosity
E	Particle volume flux through the size spectrum
$E_b(r_1,r_2)$	Collision efficiency of particles r_1 and r_2 in Brownian diffusion.
$E_{sh}(r_1,r_2)$	Collision efficiency of particles r_1 and r_2 in shear
$E_{ds}(r_1,r_2)$	Collision efficiency of particles r_1 and r_2 in differential sedimentation
F	Froude number
g	Gravitational acceleration
G	Strain rate
H	Depth of tank
k	Boltzmann's constant
K	Average cross-sectional mixing coefficient
L	Length of tank
$n(d)$	Particle size distribution function
N	Particle number density
p	Permeability
$Q_{\ell,m,n}$	Mass concentration of the particle size section ℓ in cell number (m,n)
ΔQ	Particle mass concentration in the size range $(d, d+\Delta d)$
r_i	Particle radius
r_{max}	Maximum particle radius for a given shear rate
R_{SS}	Suspended solids removal efficiency, %
R_{TS}	Total solids removal efficienct, %

NOTATION (continued)

s	Resuspension parameter, dimensionless
$\overline{S}_{\ell}$	Settling coefficient
ΔS	Particle surface concentration in the size range $(d, d+\Delta d)$
T	Absolute temperature
$u_{m,n}$	Mean horizontal velocity in cell (m,n)
$\overline{u}$	Vertically averaged horizontal velocity in the tank
u_{*}	Shear velocity
ΔV	Particle volume concentration in the size range $(d, d+\Delta d)$
w	Stokes' settling velocity
x	Horizontal dimension of the cell
z	Vertical dimension of the cell

Greek letters

α	Slope parameter for particle size distribution
$\beta(r_i, r_j)$	Collision function for particles r_i and r_j
$\overline{\beta}_{i,j,k}$	Coagulation coefficient
ε	Turbulent energy dissipation rate per unit mass of fluid
κ	Von Karman's constant
μ	Fluid dynamic viscosity
ν	Fluid kinematic viscosity
ρ_f	Density of floc
ρ_p	Density of particle
ρ_w	Density of water

References

Adler, P.M. 1981 Heterocoagulation in shear flows. Journal of Colloid and Interface Science, Vol 83, 106-115.

Adler, P.M. 1981 Streamlines in and around porous particles. Journal of Colloid and Interface Science, Vol 81, No 2, 531-535.

Alarie, R.L., McBean, E.A., Farquhar, G.J. 1980 Simulation modeling for primary clarifiers. Journal of the Environmental Engineering Division, ASCE, Vol 106, No EE2, 293-309.

Blackadar, A.K. 1962 The vertical distribution of wind and turbulent exchange in a neutral atmosphere. Journal of Geophysical Research, Vol 67, No 8, 3095-3102.

Camp, T.R. 1945 Sedimentation on the design of settling tanks. Transactions, ASCE, Vol 111, Paper No 2285, 146, 895-936.

Davis, M.H. 1972 Collisions of small cloud droplets: Gas kinetic effects. Journal of the Atmospheric Sciences, Vol 29, 911-915.

Dick, R.I. 1982 Discussion on 'Integral analysis of water plant performance'. Journal of the Environmental Engineering Division, ASCE,Vol 108, No EE2, 430-432.

Dobbins, W.E. 1944 The effect of turbulence on sedimentation. Transactions ASCE, Vol 109, Paper No. 2218, 629-656.

El-Baroudi, H.M. 1969 Characterization of settling tanks by eddy diffusion. Journal of the Sanitary Engineering Division, ASCE, Vol 95, No SA3, 527-544

Faisst, W.K. 1976 Digested sewage sludge: characteristics of a residual and modeling for its disposal in the ocean off Southern California. EQL Rep. No 13, California Institute of Technology, Pasadena, CA.

Findheisen, W. 1939 Zur Frage der Regentropfenbildung in reinem Wasserwolken. Meteor. Z. 56, 365-368.

Fischer, H.B., List, E.J., Koh, R.C.Y, Imberger, J., Brooks, N.H. 1979 Mixing in Inland and Coastal Waters. Academic Press, New York, N.Y.

Friedlander, S.K. 1960 On the particle size spectrum of atmospheric aerosols. Journal of Metereology, Vol 17, 373.

Gelbard, F. and Seinfeld, J. 1980 Simulation of multicomponent aerosol dynamics. Journal of Colloid and Interface Science, Vol 78, No 2, 485-501.

Gelbard, F. 1982 private communication.

Gear, C.W. 1971 Numerical Initial Value Problems in Ordinary Differential Equations. Prentice-Hall, Inc., Englewood Cliffs, N.J.

Hazen, A. 1904 On sedimentation. Transactions ASCE, Vol 53, No 980, 45-88.

Hocking, L.M. and Jonas, P.R. 1970 The collision efficiencies of small drops. Quarterly Journal of Royal Metereological Society, Vol 96, 722-729.

Humphreys, H.W. 1975 Hydraulic model study of a settling basin. Journal of the Americal Water Works Association, Vol 67, No 7, 367-372.

Hunt, J.R. 1980 Coagulation in continuous particle size distributions: theory and experimental verification. Report No. AC-5-80. W.M. Keck Lab. California Institute of Technology, Pasadena, CA.

Hunter, J.V. and Heukelekian, H. 1965 The composition of domestic sewage fraction. Journal of the Water Pollution Control Federation, Vol 37, 1142.

Ingersoll, A.C., McKee, J.E. and Brooks, N.H. 1956 Fundamental concepts of rectangular settling tanks. Transactions ASCE, Vol 121, Paper No. 2837, 1179-1218.

Kawamura, S. 1981 Hydraulic scale-model simulation of the sedimentation process. Journal of the American Water Works Association, Vol 73, No 7, 372-379.

Lawler, D.F., O'Melia, C.R., Tobiason, J.E. 1980 Integral water treatment plant design: From particle size to plant performance, in 'Particulates in Water: Characterization, Fate, Effects and Removal', Chemistry Series No 189, Americam Chemical Society, Washington, D.C.

Long, D.A. and Nesbitt, J.B. 1975 Removal of soluble phosphorus in an activated sludge plant. Journal of the Water Pollution Control Federation, Vol 47, 170-185.

Neiburger, M., Lee, I.Y., Lobl, E., Rodriguez, L.Jr. 1974 Computed collision efficiencies and experimental collection efficiencies on cloud drops. Conference on Cloud Physics of the American Metereological Society, 73-78, Tucson, Arizona.

NOAA 1982 Proceedings of a pollutant transfer by particulates workshop. Published by the National Oceanic and Atmospheric Administration, Seattle, Wa.

Parker, D.S., Kaufman, W.J., Jenkins,D. 1972 Floc breakup in turbulent flocculation processes. Journal of Sanitary Engineering Division, ASCE, Vol 98, No SA1, Proc. Paper 8702, 79-99.

Pearson, H.J., Valioulis, I.A., List, E.J. 1983 Monte Carlo simulation of coagulation in discrete particle size distributions. I. Brownian motion and fluid shearing. Journal of Fluid Mechanics, in press.

Ramaley, B.L., Desmond, F.L., Wright, W.C., O'Melia, C.R. 1981 Integral analysis of water plant performance. Journal of the Environmental Engineering Division, ASCE, Vol 107, No EE3, 547-561.

Rudolfs, W. and Balmat, J.L. (1952) Colloids in sewage. Sewage and Industrial Wastes, Vol 24, No 3.

Shiba, S. and Inoue, Y. 1975 Dynamic response of settling basins. Journal of the Environmental Engineering Division, ASCE, Vol 101, No EE5, 741-757.

Smoluchowski, M. 1916 Drei Vortrage uber Diffusion, brownsche Bewegung and Koagulation von Kolloidteilchen. Physic Z., 17, 557-585.

Sutherland, D.N. 1967 A theoretical model of floc structure. Journal of Colloid and Interface Science, Vol 25, 373-380.

Sutherland, D.N. and Tan, C.T. 1970 Sedimentation of a porous sphere. Chemical Engineering Science ,Vol 25, 1948-1950.

Sutherland, D.N. and Goodarz-Nia, I. 1971 Floc simulation: the effect of collision sequence. Chemical Engineering Science, Vol 26, 2071-2085.

Tambo, N., Watanabe, Y. 1979 Physcial characteristics of flocs. I. The floc density function and aluminum floc. Water Research, Vol 13, 409-419.

Takamatsu, T., Naito, M., Shiba, S. and Veda, Y. 1974 Effects of deposit resuspension on settling basin. Journal of the Environmental Engineering Division, ASCE, Vol 100, 883-903.

Tebbutt, T.H. and Christoulas, D.G. 1975 Performance relationships for primary sedimentation. Water Research, Vol 9, 347-356.

Tennekes, H. and Lumley, J.L. 1972 A First Course in Turbulence. The MIT Press, Cambridge, MA.

Thiele, H. and Levern, H.S. 1965 Synthetic protective colloids. Journal of Colloid Science,Vol 20, 679-694.

van de Ven, T.G.M. and Mason S.G. 1977 The microrheology of colloidal dispersions. VIII. Effect of shear on perikinetic doublet formation. Colloid and Polymer Science, Vol 255, 794-804.

Vanoni, V.A. 1977 in "Sedimentation Engineering", Vanoni, V.A. Editor, ASCE, New York, N.Y.

Vanoni, V.A. and Brooks, N.H. 1957 Laboratory studies of the roughness and suspended load of alluvial streams. Report No E-68, Sedimentation Laboratory, California Institute of Technology, Pasadena, CA.

Vold, J.M. 1963 Computer simulation of floc formation. Journal of Colloid Science, Vol 18, 684-695.

Waite, T.D. 1979 Feasability of wastewater treatment with ferrate. Journal of Environmental Engineering Division, ASCE, Vol 105, 1023-1034.

Wallace, A.T. 1967 Design and analysis of sedimentation basins. Water and Sewage Works, Vol 114, 219-222.

APPENDIX A

MONTE CARLO SIMULATION OF COAGULATION IN DISCRETE PARTICLE SIZE DISTRIBUTIONS. I. BROWNIAN MOTION AND FLUID SHEARING.

H. J. Pearson, I. A. Valioulis and E. J. List

W. M. Keck Laboratory of Hydraulics and Water Resources,
Division of Engineering and Applied Science,
California Institute of Technology,
Pasadena, California 91125,
U.S.A.

December 1981

ABSTRACT

A method for the Monte Carlo simulation, by digital computer, of the evolution of a colliding and coagulating population of suspended particles is described. Collision mechanisms studied both separately and in combination are: Brownian motion of the particles, and laminar and isotropic turbulent shearing motions of the suspending fluid. Steady state distributions are obtained by adding unit size particles at a constant rate and removing all particles once they reach a pre-set maximum volume. The resulting size distributions are found to agree with those obtained by dimensional analysis (Hunt, 1980a,b, 1982). Isotropic turbulent shear is shown, for particles much smaller than the Kolmogorov microscale, to be equivalent in coagulating power to a rectilinear laminar shear, G, of magnitude 1.72 times the characteristic strain rate $(\varepsilon/\nu)^{\frac{1}{2}}$ given by the rate of dissipation of kinetic energy per unit mass and the fluid viscosity.

1. INTRODUCTION

In many fluid systems with a continuous size distribution of suspended particles the primary mechanism for the production of larger particles from smaller particles, over much of the size range, is coagulation, the process of collision and coalescence of particles. These coagulating particles can be solid or liquid with the suspending medium gaseous or liquid, for example: atmospheric aerosols, cloud water droplets, colloidal suspensions in water or emulsions of one liquid in another. The computations described in this paper are primarily concerned with suspensions of solid particles in water but the techniques used have general applications.

In describing the dynamics of continuous size distributions it is convenient to introduce the particle size distribution, n(v), defined by

$$dN = n(v)dv$$

so that dN is the number of particles per fluid volume whose sizes (volumes) lie in the range v to v+dv. The collision rate, per unit volume of fluid, of particles of volumes v_i and v_j is given by the product of their respective concentrations and a collision function, $\beta(v_i,v_j)$, representing the geometry and dynamics of the collision mechanism, so that

$$\text{collision rate} = \beta(v_i,v_j)n(v_i)n(v_j)dv_i dv_j \ .$$

Then the change with time of the particle size distribution is given by the general dynamic equation (GDE)

$$\frac{\partial n(v)}{\partial t} = I(v) + \frac{1}{2}\int_0^v \beta(v',v-v')\, n(v')n(v-v')dv' - \int_0^\infty \beta(v,v')n(v)n(v')dv' + S(v)\frac{\partial n(v)}{\partial z}$$

Here I(v) is a source of particles (through condensation, for example) and $S(v)\frac{\partial n}{\partial z}$ is a particle sink resulting from particles sedimenting in the z direction at their Stokes' settling velocity, S(v). If we restrict attention to size ranges where the source term is negligible, and to homogeneous situations (so that spatial derivatives may be neglected) then (1) reduces to the coagulation equation

$$\frac{\partial n(v)}{\partial t} = \frac{1}{2}\int_0^v \beta(v',v-v')n(v')n(v-v')dv' - \int_0^\infty \beta(v,v')n(v)n(v')dv' \qquad (2)$$

The two terms on the r.h.s. of (2) represent, respectively, the rate of gain of particles of volume v by coagulation of pairs of smaller particles, conserving volume, and the loss of particles, v, due to their coagulation with particles of all sizes.

A variety of techniques have been used to investigate (1) and (2) and an extensive literature has resulted (see Pruppacher and Klett, 1978 for a recent account). In most of these techniques some simple analytic form for β is used. The heart of the coagulation problem is to provide an accurate model for this collision kernel and the study of two particle collisions has been mostly toward this end. In the present study both β and solutions to (2) are directly simulated at the same time by a Monte Carlo method. Direct numerical solutions of equation (2) such as developed by Gelbard, Tambour and Seinfeld (1980) must assume forms for the β functions.

For particles to coagulate two processes are required: (a) a mechanism to develop relative motion of the particles through the fluid which will bring them into close proximity, and (b) short-range interfacial forces acting between the particles to bring about their

coalescence. Relative motion of particles in a fluid can be due to one or a combination of the following:

1. Brownian or thermal motion.
2. Laminar or turbulent fluid shear or straining.
3. Particle inertia in turbulent flows.
4. Differential sedimentation of different size particles.

As a first step, the hydrodynamic interactions between particles are often ignored. In this case, relatively simple analytic estimates for β are available for each of these collision mechanisms acting independently and these are summarized in Table 1. The table also includes the dimensional parameters that characterize the mechanisms and determine, in any given situation, the characteristic size of particle that they affect.

Note that all the collision functions depend on properties of the suspending fluid, the structure of its velocity field, and the size of the particles. However, only the functions for the final two collision mechanisms depend on a physical property of the particles: the difference between their density and that of the fluid. If the particle density excess ratio $(\rho_p - \rho_f)/\rho_f$ is small then sedimentation and inertia will only be important for larger particles. In a turbulent flow sedimentation will dominate inertial effects unless the characteristic acceleration $(\varepsilon^3/\nu)^{1/4}$ is comparable with g, the gravitational acceleration. In this paper we will be concerned only with the first two collision mechanisms. Differential sedimentation and interfacial forces will be the subject of a sequel.

For a coagulating system more than one collision mechanism can be important for a given size range of particles. However, if there is a

Table 1. Various mechanisms for particle collisions.

Mechanism	Collision Function β	Source	Dimensional Parameter
Brownian Motion	$\frac{2kT}{3\mu}\frac{(r_i+r_j)^2}{r_i r_j} = 4\pi\,(D_i+D_j)(r_i+r_j)$	Smoluchowski (1916)	$K_b = \frac{kT}{\mu}$
Laminar Shear	$1.33G\,(r_i+r_j)^3$	Smoluchowski (1917)	G
Pure Strain (extension)	$4.89\dot{\gamma}\,(r_i+r_j)^3$	Zeichner and Schowalter (1977)	$\dot{\gamma}$
Isotropic Turbulent Shear	$2.3^*(r_i+r_j)^3(\epsilon/\nu)^{1/2}$	Saffman and Turner (1956)	$\left(\frac{\epsilon}{\nu}\right)^{1/2}$
Turbulent Inertia	$\frac{1.27(\rho_p-\rho_f)}{\mu}\left(\frac{\epsilon^3}{\nu}\right)^{1/4}(r_i+r_j)^2\lvert r_i^2-r_j^2\rvert$	Saffman and Turner (1956)	$\frac{(\rho_p-\rho_f)}{\mu}\left(\frac{\epsilon^3}{\nu}\right)^{1/4}$
Differential Sedimentation	$\frac{0.7g(\rho_p-\rho_f)}{\mu}(r_i+r_j)^2\lvert r_i^2-r_j^2\rvert$	Findheisen (1939)	$K_{ds} = \frac{g(\rho_p-\rho_f)}{\mu}$

* corrected from original, see text.

particle size subrange in which the coagulation is dominated by only one collision mechanism, and this subrange is in a state of dynamic equilibrium, then the theory of Friedlander (1960a,b) and Hunt (1980a,b) predicts the local size distribution given a constant flux of mass through the particle size distribution. The theory depends on two basic hypotheses: an equilibrium size distribution being established and non-interference of particles of a size characteristic of one collision mechanism with those of another collision mechanism.

Hunt's (1980a)* experimental results generally support the predictions of the theory for Brownian motion and laminar shear but are limited by uncertainty over the effects of the unsteadiness in the experiments due to particle sedimentation and loss from the system. In the present work these limitations are overcome by performing a computer "experiment" in which particle collisions are directly simulated by Monte Carlo techniques. The size evolution of a population of particles is followed. This allows the effects of each collision mechanism to be evaluated independently, and, by combining mechanisms, the hypothesis of non-interference of characteristic particle sizes to be tested. Collision rates as well as the approach to and the final form of an equilibrium size distribution are studied. The method could also be used to study the "aging" of an initially fixed number of particles as they collide and grow.

Monte Carlo simulations have been used by Nowakowski and Sitarski (1981) to model the collision function for Brownian coagulation of aerosol particles and by Husar (1971) and Gartrell and Friedlander (1975) to find solutions to the coagulation equation (2). In addition to

*See also Hunt (1982).

simulating directly the collision function, the Monte Carlo method accounts properly for correlations which are ignored in the derivation of the general dynamic equation (Gillespie, 1975).

In this paper we first briefly describe Hunt's theory and experimental results. Subsequent sections describe in detail the simulation techniques used to model Brownian, laminar shear and turbulent shear induced coagulation and the results obtained. The results are then compared with previous experiments and theory, and the success of the method evaluated.

2. HUNT'S WORK

Friedlander (1960a,b) explained observed regularities in the size distributions of atmospheric aerosols by assuming that a state of dynamic equilibrium existed between production, coagulation and loss through sedimentation of particles. He then employed methods analogous to those developed by Kolmogorov for the analysis of turbulence spectra. If it is assumed that the size distribution in some subrange depends only on the particle volume, v, the constant flux of particle volume through the size distribution, E, and a dimensional parameter, C, characterizing the sole dominant coagulation mechanism (see Table 1) so that

$$n(v) = n(v,E,C) \ ,$$

then the form of n(v) can be determined by dimensional analysis alone. This is analogous to postulating an inertial subrange of scales in which the turbulent energy spectrum is determined solely by the wavenumber and the flux of energy through the subrange (equal to the rate

of energy dissipation by viscous stresses at the smallest scales). (See, for example, Monin and Yaglom, 1975, Ch. 21).

Hunt (1980a,b) extended these ideas to hydrosols and compared the predictions of his theory with both laboratory and field measurements. In particular, he performed experiments on Brownian and laminar shear induced coagulation. His theory predicts the following size distributions for regions dominated by Brownian, shear and differential sedimentation coagulation

Brownian

$$n(v) = a_b (E/K_b)^{1/2} v^{-3/2} , \tag{3}$$

Shear

$$n(v) = a_{sh} (E/G)^{1/2} v^{-2} , \tag{4}$$

Differential Sedimentation

$$n(v) = a_{ds} (E/K_{ds})^{1/2} v^{-13/6} , \tag{5}$$

He shows (Hunt 1980b, Figure 1) that it is plausible, for a typical coagulating hydrosol, that these three mechanisms could dominate in regions of successively increasing particle size.

Hunt's measurements indicated that his system was in a quasi-dynamic equilibrium where size distributions taken at progressively later times were similar in shape but decreasing in magnitude. This unsteadiness was due to the overall particle concentration decreasing as a result of the larger aggregates settling to the bottom. Hunt measured the varying total suspended volume by light absorbance and used the computed rate of volume loss as an estimate for E. He

explains why this will be an overestimate for the quantity (see Hunt, 1980a for details), but it is still a useful approximation. The measured value of $E^{\frac{1}{2}}$ can then be used to normalize size distributions (c.f. equations (3) - (5)) partially correcting for the effects of unsteadiness.

Hunt successfully collapsed much of his data at various times and for different experiments at different shear rates by normalizing the size distributions not just with $E^{\frac{1}{2}}$, but with the ratio $(E/G)^{\frac{1}{2}}$ and non-dimensionalizing the particle volume with the characteristic volume at which particles have both Brownian collisions and shear induced collisions at the same rate. This characteristic volume, found by putting $r_i = r_j$ in the expressions for the relevant collision rates in Table 1, is seen to be $v = \pi K_b/(3G)$, proportional to the ratio of the Brownian and shear parameters.

For some of the particle types tested the normalized volume distributions expressed as functions of nondimensional size provide support for the relations (3) and (4) (see in particular Hunt, 1980a, Figure 4.9). However, as we have already noted, there are some reservations about the experiments, complicated as they are by instrumental difficulties and uncertainties about the effects of unsteadiness. Also, no one single experiment exhibits a size distribution having regions with the equilibrium power laws corresponding to both Brownian and shear dominated mechanisms. One of the main aims of the present study, then, is to provide support or otherwise for Hunt's results by means of a computer "experiment". This allows a genuine steady state to be set up and detailed probing of the interaction between Brownian and shear collision mechanisms.

3. COMPUTER SIMULATION

3.1 General Technique

Simulation of solutions to the coagulation equation (2) proceeds by tracking the positions and sizes of a variable number, N, of spherical particles (typically $50 < N < 600$). Whenever two particles collide they are coagulated to form a larger (still spherical) particle, conserving particle volume, thereby reducing N by one. The population of particles studied therefore consists of particles of unit volume, v_o, and integral multiples, $v_i = i.v_o$ of the unit volume. In this paper the suffix i is used to denote properties of i-fold particles made up from i elemental particles. The collision simulation algorithm is programmed for a digital computer.

The program can also function in a different mode in which collisions are counted but particles are not coagulated. On collision, one of the particles is randomly repositioned so as to avoid repeated collisions of the same pair of particles. This allows direct measurement of the collision function, β, for any given mechanism. These results can be used both to verify the analytic solutions given in Table 1 and as a check on the correct operation of the simulation.

Particle motions take place in a cubical box or "control volume" of side L and volume V (Figure 1 gives a schematic representation of this box and a definition of the rectangular coordinate system used). Particle positions are denoted by $\underset{\sim}{P}(i) = (P_1(i),P_2(i),P_3(i))$. The simulation employs what are essentially periodic boundary conditions, so that particles that have left the control volume at the end of a time step are replaced, for the next time step, by image particles

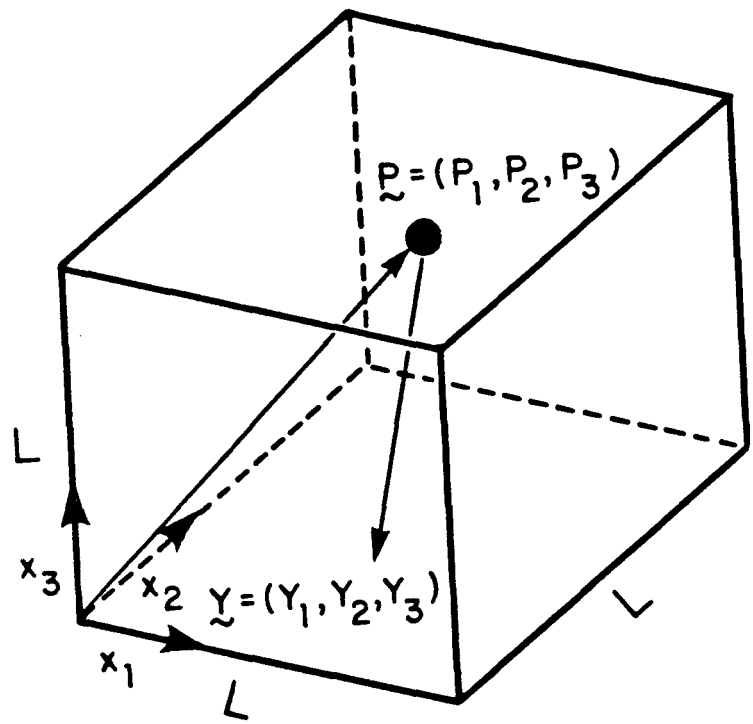

Figure 1. Schematic diagram of simulation box or "control volume" with cartesian coordiante system and representative particle at position (P_1, P_2, P_3). Displacement of particle in current time step is (D_1,D_2,D_3).

that enter from the opposite side. This type of boundary condition is commonly employed in Monte Carlo simulations (see Alder and Wainwright, 1959) and allows an infinite homogeneous system to be modeled approximately by a finite volume. Edge effects are reduced by allowing particles to interact with image particles just outside the control volume. The slight modifications to these boundary conditions required for laminar and turbulent shearing motions are described in §3.4 and §3.5 below.

In order to model a system in dynamic equilibrium, a fixed number N_c of particles of unit volume are added to the population at random each time step and any particles that have reached a preset maximum volume $v_{max} = i_{max}.v_o$ are removed from the population. (Typically, $i_{max} = 125$). The constant addition of small particles is a crude attempt to represent, indirectly, the flux of particles into the size range from the collision of particles smaller than v_o. The removal of large particles is necessary to limit the total volume density of particles in the simulation. It can be physically justified as a crude representation of the loss of larger particles from a region by the combined action of sedimentation and vertical concentration gradients. The procedure of adding small particles and extracting large ones is consistent with the hypothesis that collisions between particles of similar size are more important and is justified *a posteriori* by the success of the simulation in reproducing Hunt's (1980b) dimensional results.

A schematic representation of the logical sequence of the simulation is given in Figure 2. The simulation starts either by generating a monodisperse population of particles randomly distributed over the control volume, or by reading a set of particle positions and sizes

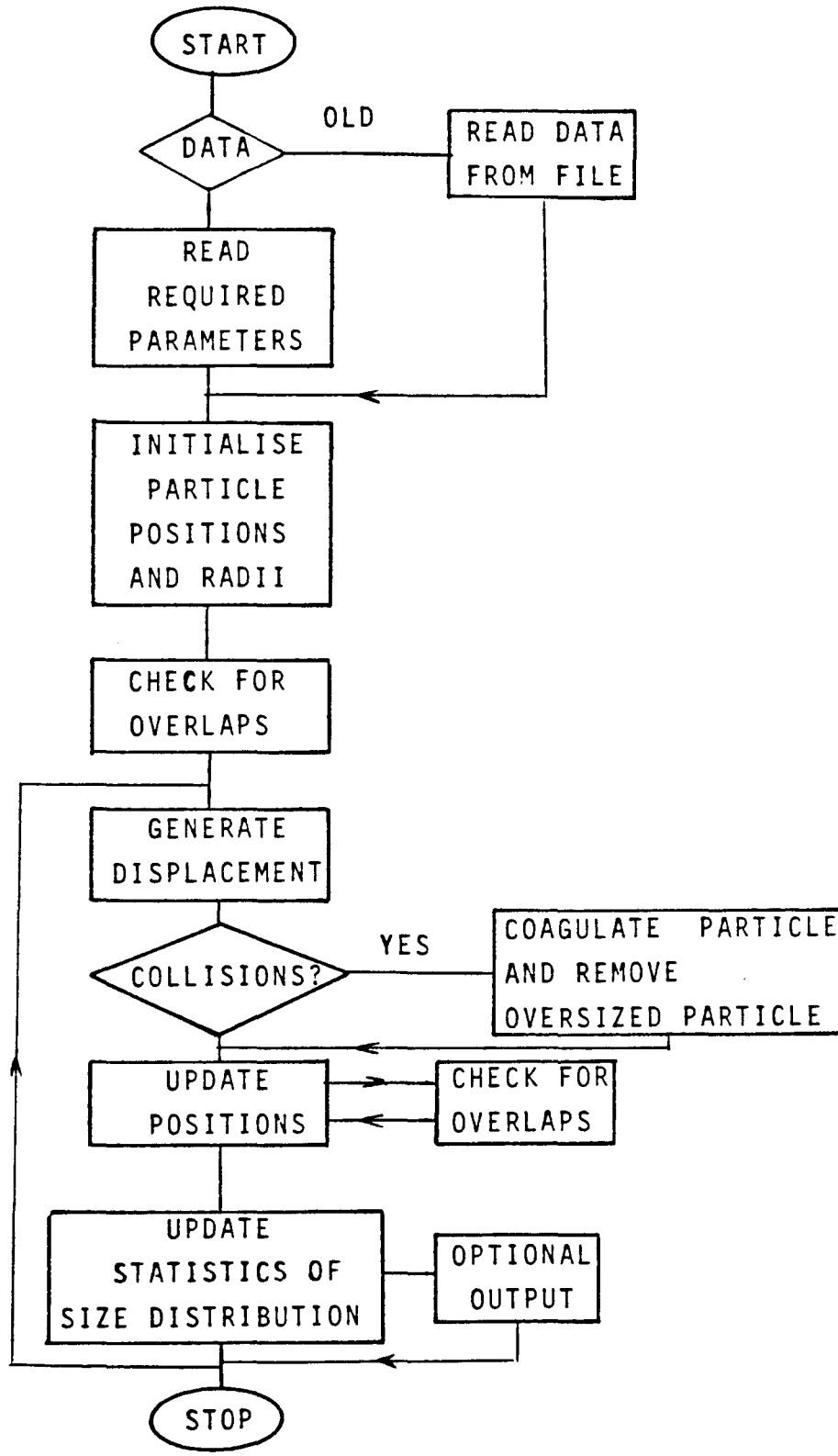

Figure 2. Summary of logical structure of simulation program.

from a preexisting file. This file is either a set of particles of given size distribution generated by an auxiliary program, or the end point of a previous simulation that is to be continued. Controlling parameters for the simulation run are either input manually or read from a file.

The particular methods for generating the particle displacements at each time step, $\underset{\sim}{Y}(i) = (Y_1(i), Y_2(i), Y_3(i))$, and updating their positions between time steps are described in detail below in connection with each physical collision mechanism. Each particle is assumed to travel on a straight line path at constant speed during each time step. The algorithm used to detect particle collisions is described in §3.2 below.

At the end of every time step the particle size distribution is computed. After a prescribed number k of time steps, the size distribution, averaged over time $t = k.\Delta t$, is output along with the positions and sizes of all the particles to a file in permanent computer storage. The particle positions and sizes are written over the previous copy to save storage space. The latest version is then always available to restart a run at a later time. The simulation continues until the required number of time steps have been completed.

Time averages are needed to provide reasonable particle size statistics as only a small number of particles are followed. Once a simulated system has reached a statistical steady state (dynamical equilibrium) then long time averages can be employed to produce well converged statistics. To follow the evolution of a rapidly changing system with any precision, it would be necessary to repeat the simulation many times and compute ensemble averages.

Most simulation runs were started with a monodisperse population of particles. The total volume of particles in the simulation increases continuously until the first particle grows by coagulation to v_{max} and is removed. In order to have reasonable computational times the volume concentration, ϕ, of suspended particles used in the simulations is larger than that occurring in many natural systems. (For example, typically ϕ is about 20 p.p.m. in Hunt's experiments but is about 10^3 larger in the simulation runs). Simulation results must therefore be checked for dependence on volume fraction of particles, before they are applied to more dilute systems.

The simulation requires the generation of relatively large numbers of (pseudo-) random numbers from both uniform and Gaussian distributions; details of the numerical methods used are given in Appendix A.

3.2 Collision algorithm

Detecting which particles have collided at each time step is very costly in computer time and so an efficient method is needed. To this end the basic control volume is divided into cubic sub-cells. The cells are chosen to be as small as possible consistent with the constraint that any particle can only collide, during the next time step, with particles in the same cell or the adjoining 26 cells. Each cell is given three integer coordinates that define its position in the control volume. For each particle the numbers of the cell it occupies are stored along with its actual position.

The first stage in checking for collisions is to determine for each pair of particles whether they are in the same or adjoining cells. Only if this is so, are they considered candidates for a collision and

a detailed calculation performed. Checking whether particles are in adjoining cells is performed by computationally fast integer arithmetic. Given two candidate particles their relative initial position, $\underset{\sim}{RP} = \underset{\sim}{P}(1) - \underset{\sim}{P}(2)$, and displacement, $\underset{\sim}{RY} = \underset{\sim}{Y}(2) - \underset{\sim}{Y}(1)$, are computed (note the different ordering of particles). Then the condition for collision is that the vector $\underset{\sim}{RY}$ enters the sphere of radius $\sigma = r_i + r_j$ around the point RP, a simple geometrical test. This corresponds to following the motion of the two particles in a frame of reference moving with the (1) particle (see Figure 3 for schematic illustration).

A further advantage of the sub-cell system is that it allows for easy implementation of periodic boundary conditions. Particles in cells along any of the boundaries of the control volume are allowed to interact with particles in the requisite cells on the opposite side of the volume.

3.3 Brownian motion

The thermal impact of molecules cause suspended particles to perform random motion relative to the bulk fluid. In contrast to the recent work of Nowakowski and Sitarski (1981), the particles studied here are much larger than the molecular free-path in the fluid and so are in the continuum regime of Brownian motion. Also the time step, Δt, of the simulation is very much larger than the particle viscous relaxation time, $t_r = 2r^2/9\nu$. Therefore, the relevant probability distribution function (p.d.f.) for the displacement, $\underset{\sim}{Y}$, of a particle during a time step is (Chandrasekhar, 1943)

$$W(\underset{\sim}{Y}) = \frac{1}{(4\pi D \cdot \Delta t)^{3/2}} \exp\left(-\frac{|\underset{\sim}{Y}|^2}{4D\Delta t}\right)$$

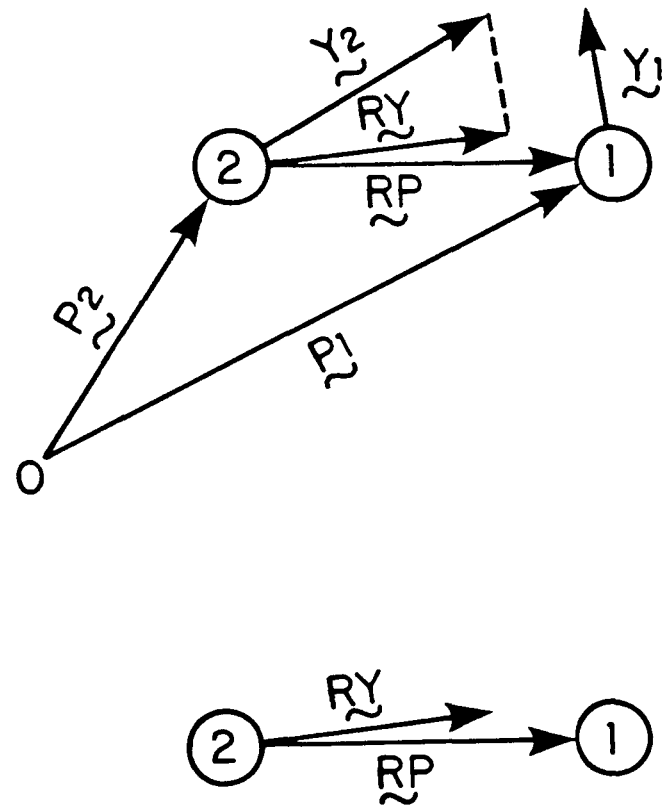

Figure 3. (a) Geometry for collision algorithm. (b) Viewed in frame of reference in which particle 2 is at rest.

where D is the diffusivity of the particle

$$D = kT/(6\pi\mu r) = K_b/6\pi r$$

Each component of $\underset{\sim}{Y}$ has an independent Gaussian p.d.f.

$$W(Y_k) = \frac{1}{(4\pi D\Delta t)^{1/2}} \exp\left(-\frac{Y_k^2}{4D\Delta t}\right) \qquad k = 1,2,3$$

and this is used to replace the Brownian motion of the particles by a finite random walk. At each time step three independent random components of displacement are generated for each particle from the corresponding Gaussian distribution (see Appendix A for details). The r.m.s. displacement in any direction, Δx, of an i-fold particle is

$$\Delta x_i = (2 \cdot D_i \cdot \Delta t)^{1/2}$$

where, $D_i = K_b/6\pi r_i$, is the particle diffusivity. D_i can be obtained in terms of the diffusivity D_o of an elemental particle by

$$D_i = D_o \cdot i^{-1/3}$$

Particle collisions are simulated on the basis of straight line trajectories during each time step. The question arises, therefore, of the validity of this as an approximation to Brownian induced coagulation. The r.m.s. displacement has been chosen correctly, but a particle of mass m undergoing Brownian motion actually travels along a tortuous path at r.m.s. speed $(kT/m)^{\frac{1}{2}}$. At first sight this suggests that the simulation would underpredict the collision rate. However, replacing Brownian motion by a finite random walk must change the pair distribution

function, that is to say the probability distribution function for the spacing between any given pair of particles. So, while modeling Brownian motion by a finite random walk introduces inefficiency into the basic collision process it can compensate by increasing the probability that any pair of particles are found close together at the beginning of a time step. Here, "close together" means a separation on the scale of the r.m.s. steplength of the random walk. These matters are investigated in detail in Appendix B. Tests with the non-coagulating form of the program have shown that satisfactory collision rates for monodisperse populations of particles are obtained when the ratio $\Delta x/r$ is about 0.5. It is important to use the maximum possible time step in order to minimize computation times.

3.4 Laminar shear

The coagulating effects of a velocity gradient are investigated by imposing a uniform shearing motion on the control volume:

$$u_1 = G.x_3$$

with G the shear rate. The particles are assumed to move with the fluid so their displacement in any time step is just

$$\underset{\sim}{Y}(i) = (Y_1(i),0,0); \quad Y_1(i) = G \cdot P_3(i) \cdot \Delta t \ .$$

This means that we are ignoring hydrodynamic interactions between particles. This is only defensible as the first stage towards a more realistic model. The large body of work on particle interactions in low Reynolds number flows (see e.g. Mason, 1976, for a review) shows that hydrodynamic forces will always come into play in a detailed analysis of collision dynamics. This is investigated in detail in a subsequent paper.

Figure 4 shows how a uniform shearing motion, on average, moves a fraction of the particles out of the control volume at every time step. If they were replaced in the control volume according to simple periodic boundary conditions ($P_1 = P_1 - L$, whenever $P_1 > L$) the simulation would be completely deterministic once initial positions had been chosen for the particles. Each particle would move in a straight line with fixed P_2 and P_3 coordinates. After a certain time all collisions between existing particles would cease as each particle would have swept out its own track through the control volume. In a real flow this would not occur as particles are continually meeting "new" particles. Therefore, in the simulation, when a particle leaves the volume it is replaced at a randomly chosen height P_3 on the other side of the control volume. The random value of the height P_3 must be chosen from a distribution that reflects the increasing flux of particles at larger values of P_3 (see Appendix A). This strategy leads to a further complication: particles may be replaced on top of one another, leading to spurious collisions. This is almost totally eliminated by checking for such particle overlaps at the end of each time step and randomly moving one of each overlapping pair. This may introduce a few further overlaps as no final check is made. An estimate of this number is available from the number of initial overlaps, which is recorded. This error is acceptable in the light of other approximations in the simulation. Overlaps are also introduced by the process of adding new elemental particles at each time step, whatever the collision mechanism. All types of overlaps are resolved simultaneously in the same manner.

3.5 Turbulent shear

We wish to simulate the coagulation of small particles by

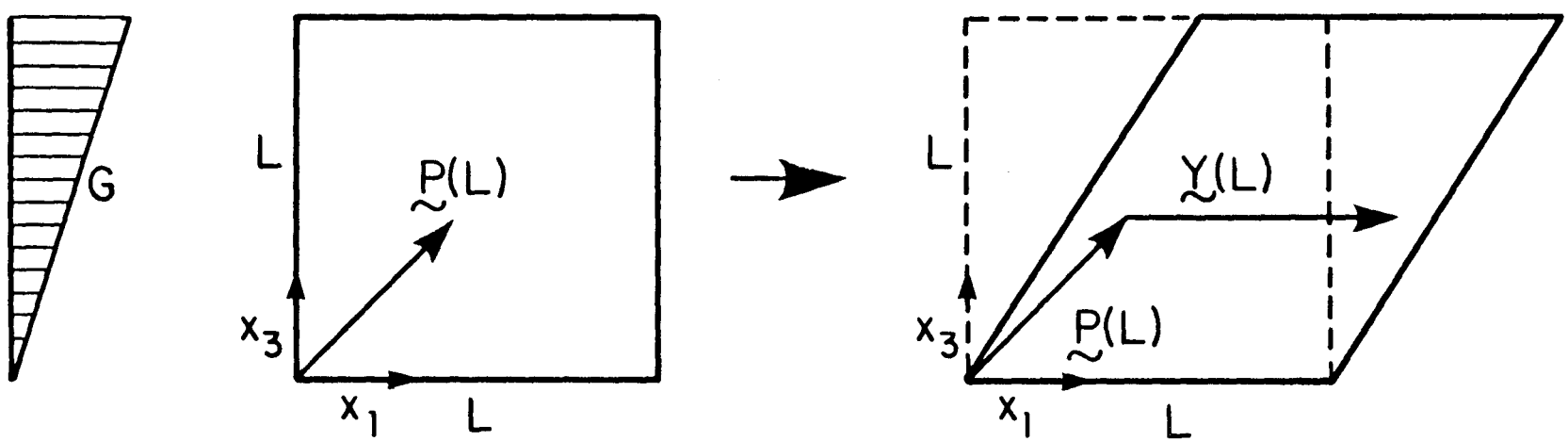

Figure 4. Action of laminar shearing motion, $u_1 = G \cdot x_3$, on control volume.

turbulent flow. The motion of a suspended particle can be identified with the motion of an adjacent fluid particle provided that the time scale of the (fluid) particle acceleration is much greater than the particle relaxation time, t_r, that is to say, if inertial effects are negligible, as will be the case here. Then for particles of radius smaller than the smallest scale of the turbulent motion (the Kolmogorov length scale, $(\nu^3/\varepsilon)^{\frac{1}{2}}$), coagulation rates are determined solely by the kinematics of the small scales of the turbulent flow field, in particular by the r.m.s. strain rate $(\varepsilon/\nu)^{\frac{1}{2}}/15^{\frac{1}{2}}$. These small scales are very nearly isotropic (Batchelor, 1953).

Under these conditions, two particles separated by a distance smaller than the Kolmogorov length scale are subjected to a motion that can be decomposed into a rigid body rotation representing the local vorticity, and a locally uniform three-dimensional straining motion. The rigid body rotation component of the motion has no effect on the collisions of non-interacting particles and so only the straining motion (with symmetric velocity gradient tensor) is modeled. The straining motion will be uniform over length scales smaller than the Kolmogorov micro-scale but there is no agreement as to the duration of this straining (Monin and Yaglom, 1975). Two time scales are important for the small scale straining: the rate of rotation of the principal axes of strain and the rate of change of the magnitude of the principal rates of strain. For turbulent flow at high Reynolds number the rate of change of the deformation fields of the small eddies is related to the Lagrangian time microscale α (Lumley, 1972). The time scale of the deformation field is λ/u', where λ is the Taylor microscale and u' the r.m.s. fluctuating velocity. Corrsin (1963) approximates the

ratio of the two as

$$\alpha\ u'/\lambda \simeq (R_\lambda/30)^{\frac{1}{2}}$$

and since by definition

$$\lambda^2 = 15\nu \frac{\overline{u'^2}}{\varepsilon} \quad \text{and} \quad R_\lambda = \frac{u'\lambda}{\nu}$$

we have

$$\frac{\alpha}{(\nu/\varepsilon)^{\frac{1}{2}}} \simeq (R_\lambda/2)^{\frac{1}{2}}$$

which implies that the strain and vorticity fields of the small eddies remain constant for a time interval at least equal to the Kolmogorov time scale, $t = (\nu/\varepsilon)^{\frac{1}{2}}$. This is just the inverse of the characteristic strain rate.

The effect of the rate of rotation of the principal axes of strain on the collision rate was investigated using the monodisperse, non-coagulating version of the simulation. The velocity gradient was simulated so that both the principal axes and principal rates of strain could be changed independently. The magnitude of the strain was kept constant for a time interval equal to the Kolmogorov time scale. No statistically significant difference in the collision rate was found, whatever the time scale of rotation of the principal axes of strain. Therefore in the coagulation simulation both principal axes and rates of strain were varied at the same rate.

Assuming homogeneous, isotropic, unbounded turbulence with a Gaussian velocity gradient field, the elements of the rate of strain tensor were chosen randomly to satisfy (Hinze, 1959)

$$\frac{\partial u_i}{\partial x_k}\frac{\partial u_j}{\partial x_l} \begin{cases} = \frac{1}{15}\frac{\varepsilon}{\nu} & i=j=k=l \\ = -\frac{1}{30}\frac{\varepsilon}{\nu} & j=l \text{ and } i=k \text{ or } i=l \text{ and } j=k \text{ and } i\neq j \\ = \frac{2}{15}\frac{\varepsilon}{\nu} & k=l \text{ and } i=j \text{ and } i\neq k \\ = 0 & \text{all other combinations} \end{cases}$$

subject to

$$\frac{\partial u_i}{\partial x_i} = 0$$

and kept constant for a time interval equal to the Kolmogorov time scale.

The simulation proceeds as in the case of laminar shear with particle displacements being given by the product of the time step (t_k) and the fluid velocity corresponding to the particle position. Now, however, as the motion is three-dimensional and stochastic, true periodic boundary conditions can be used. This corresponds to the control volume being surrounded by copies which are deformed with the original. Particles in the control volume at the end of one time step can then be used for the next. However, in preliminary simulations, random fluctuations in the number of particles were found to cause trouble. To avoid the program halting because of too many or no particles left in the control volume the total number was adjusted at each time step according to

$$N_{i+1} = N_i - N_{COL} + N_c$$

where N_{COL} is the number of collisions that had occurred during the time step and N_c the number of elemental particles added. In order to satisfy the above condition, either particles were removed at random,

or a particle whose volume had been chosen at random from the existing population was added at a random position. Finally, particle overlaps were resolved as explained in §3.4.

3.6 Multiple mechanisms

Simulations were performed in which the particle displacement was the linear sum of a fluid shearing and a Brownian component. The relative magnitude of the Brownian and shearing parameters could then be varied to investigate their interaction.

4. RESULTS

Figure 5 shows the effect of changing the r.m.s. steplength on collision rate in Brownian motion (see Appendix B for a discussion). There is some statistical scatter in the results but the general shape of the curve is correct. From these results a suitable time step can be chosen for simulations involving Brownian motion. Similar computations of collision rates in laminar and turbulent shear induced coagulation were performed to check that they yielded the values given by Table 1. This, indeed, was found to be the case. The result for turbulent shear due to Saffman and Turner (1956) has been amended by a factor of $\pi^{\frac{1}{2}}$ from that in the original paper, correcting an algebraic error.

The development of a size distribution in a typical simulation starting with particles all of unit volume v_o and undergoing Brownian induced coagulation is shown in Figure 6. The size distribution is non-dimensionalized according to equation (3) and plotted logarithmically against particle volume non-dimensionalized with the unit particle volume. The curves plotted are smoothed approximations to the actual

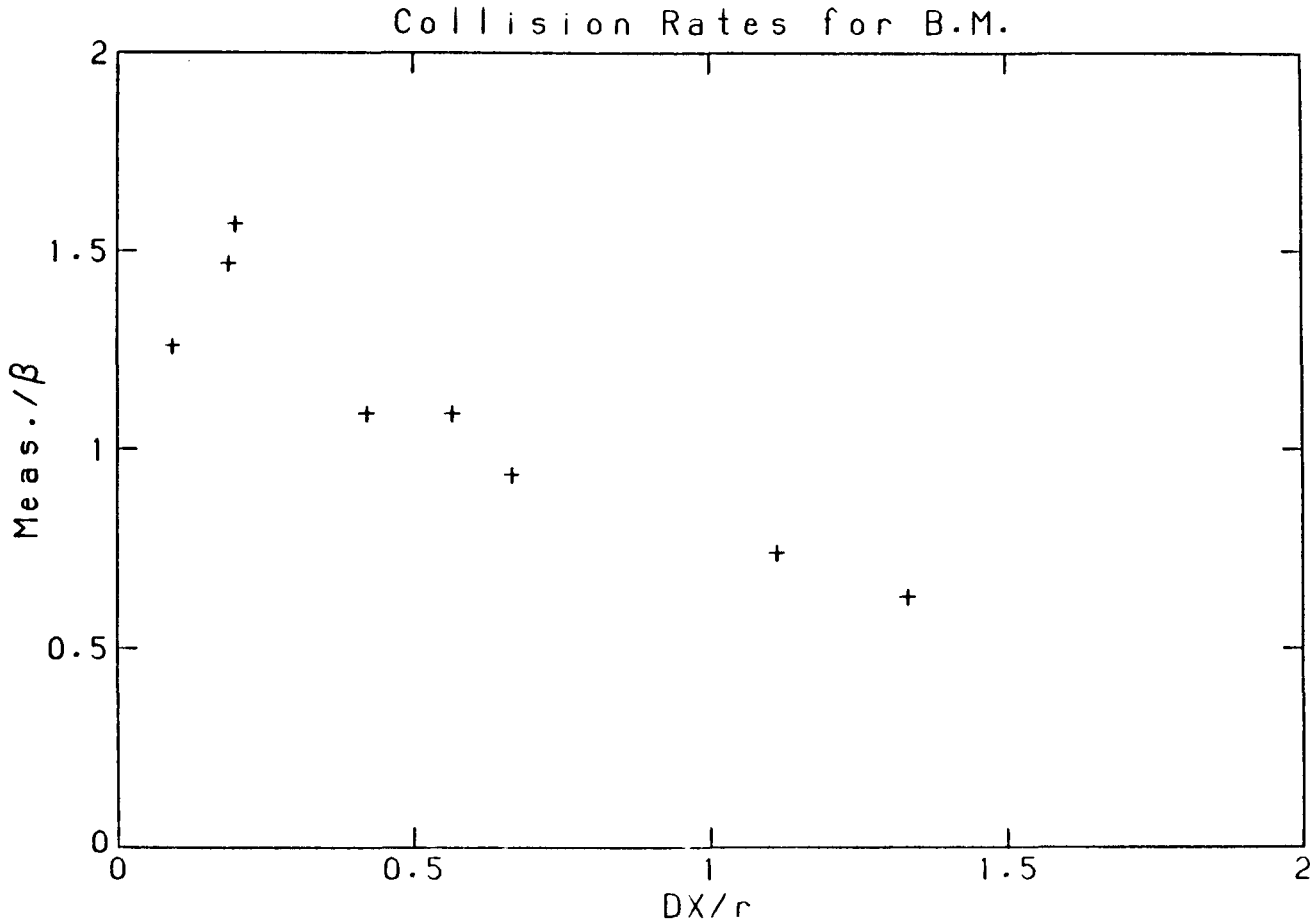

Figure 5. Simulated collision rate of monodisperse particles undergoing Brownian motion as a function of r.m.s. displacement. The ratio between measured collision rate and theoretical rate is plotted against the ratio of steplength to particle radius.

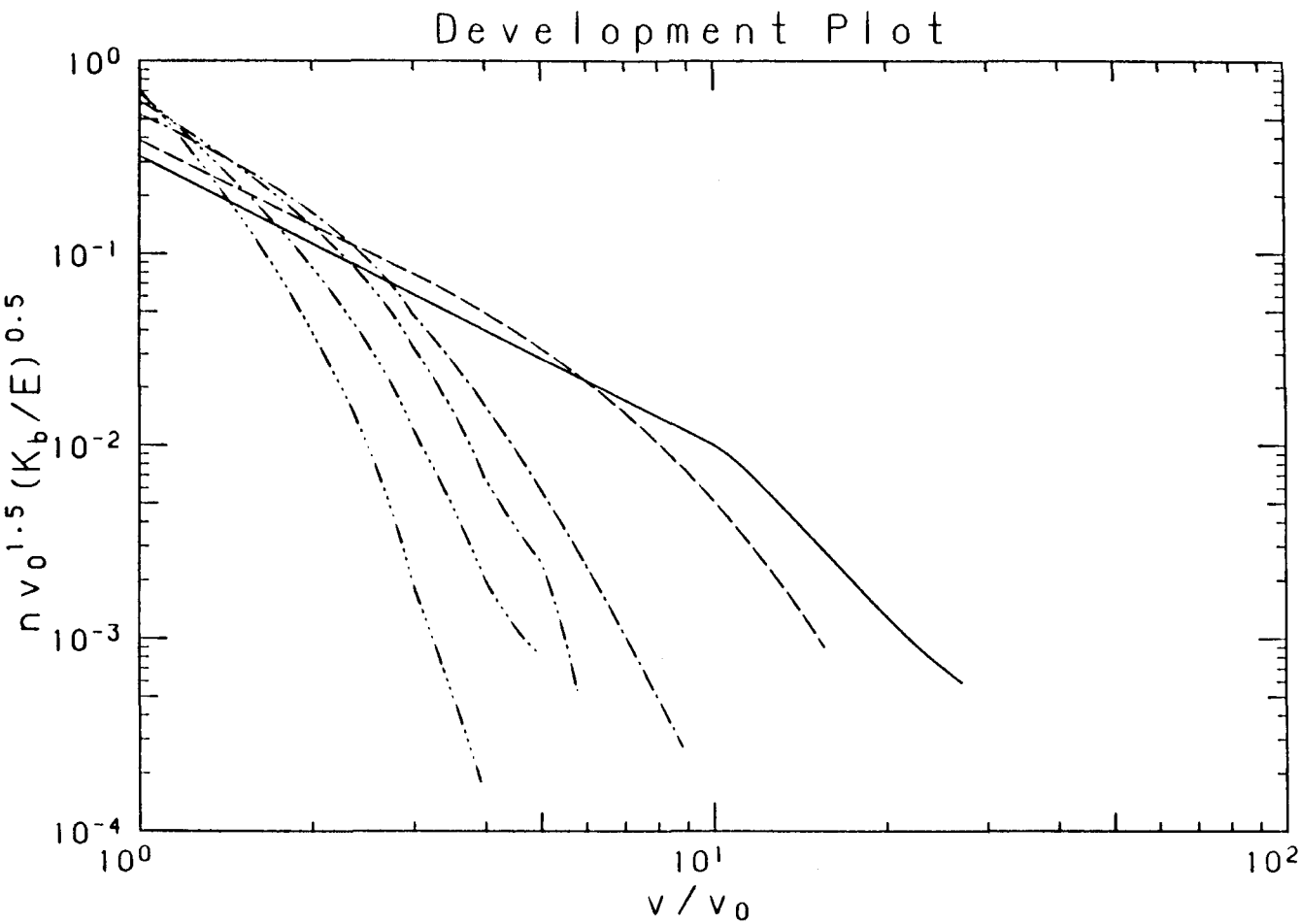

Figure 6. Development towards steady state of size distribution of initially monodisperse population undergoing Brownian induced coagulation. V=125, r_o=0.075, r_{max}=0.375, Δt=0.25, N_c=1, D_o=0.005, ϕ=0.0155; Averaging time: — ·•·•· —t=25; — ••• —t=50; — •• —t=100; — · —t=200; — —t=400; ———t=600.

data points, at $v=i.v_o$, which are rather scattered. The upper portion of the data attains a slope of -3/2 once a range of about one decade in volume has been reached. Then, as particles of increasing size are formed, the slope of the size distribution remains the same, but its absolute level declines gradually. It reaches a statistically steady state once the first large particle is lost from the system. The final steady state for this set of parameters is shown in Figure 7, along with that for a run at a higher final volume concentration ϕ (this is obtained by adding more particles at each time step). The points plotted are actual data from the simulations, averaged over 1000 time steps. Even with this time averaging there is still some statistical scatter in the data, especially at the lower end of size distribution where very small numbers of particles are actually involved. To further smooth the data in the region $v/v_o = 20\text{-}100$ they have been averaged in groups of 5.

For both these runs $v_{max} = 125.v_o$, although the volume distribution is only plotted out to $v/v_o=100$. Beyond this the data becomes erratic. The two sets of data are fully collapsed by the normalization used and very clearly exhibit the -3/2 power law expected from Hunt's (1980a,b) theory. The intercept of the best fit line of slope -3/2 with the axis $v/v_o=1$ gives the constant a_b in equation (3).

Figure 8 is a comparison of the steady state size distributions for laminar shear at two volume concentrations differing by an order of magnitude. Again the data points are averaged over 1000 time steps, and are collapsed onto a slope of -2 by the normalization suggested by dimensional arguments. Similar results are shown for turbulent shear in Figure 9, where the inverse of the Kolmogorov time scale, $(\varepsilon/\nu)^{\frac{1}{2}}$, is used in place of G in the normalization of the size distribution.

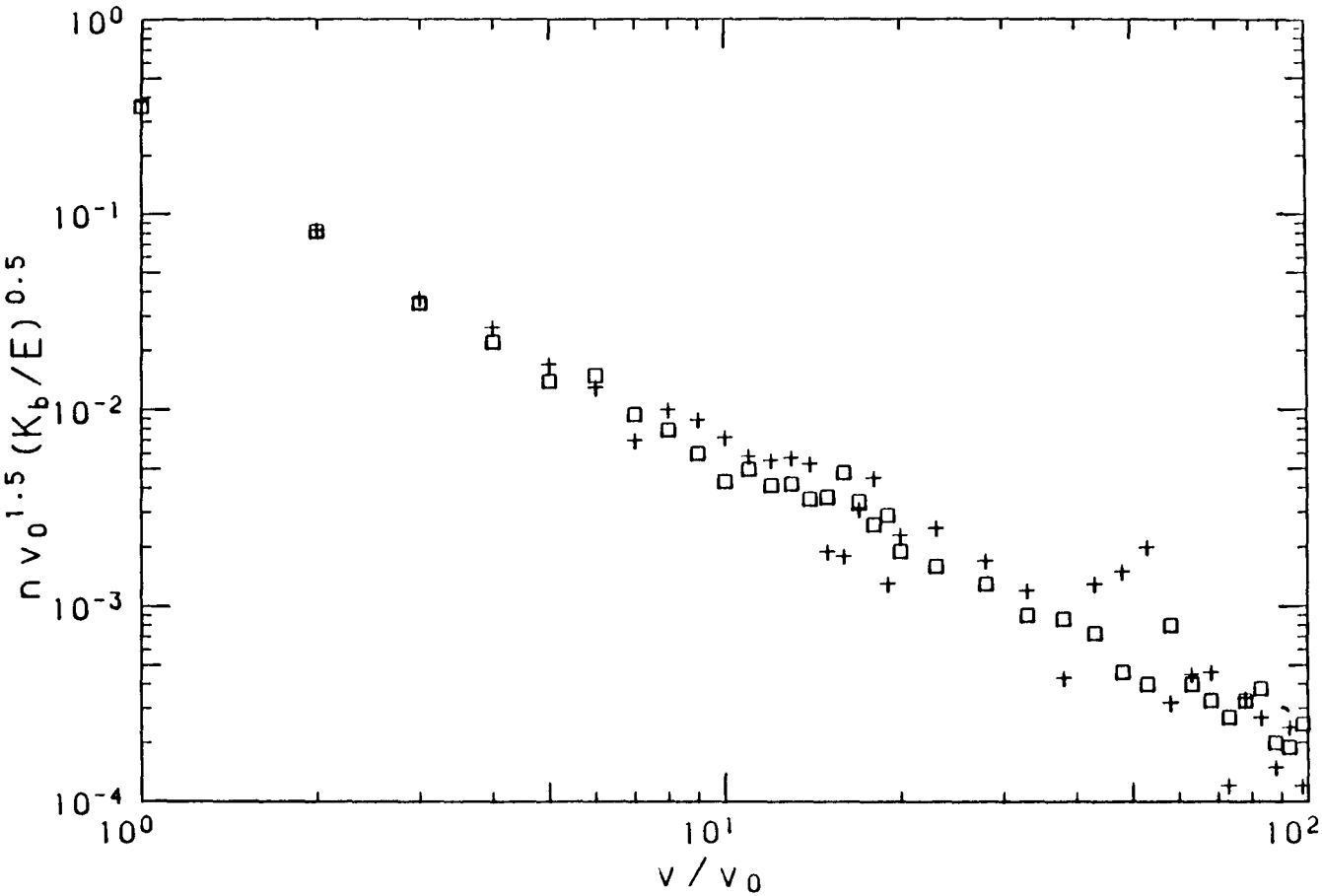

Figure 7. Steady state non-dimensional size distribution for Brownian motion. r_o=0.075, r_{max}=0.375, D_o=0.005, Δt=0.25; + V=125, N_c=1, ϕ=0.0155; □ V=64, N_c=4, ϕ=0.0204.

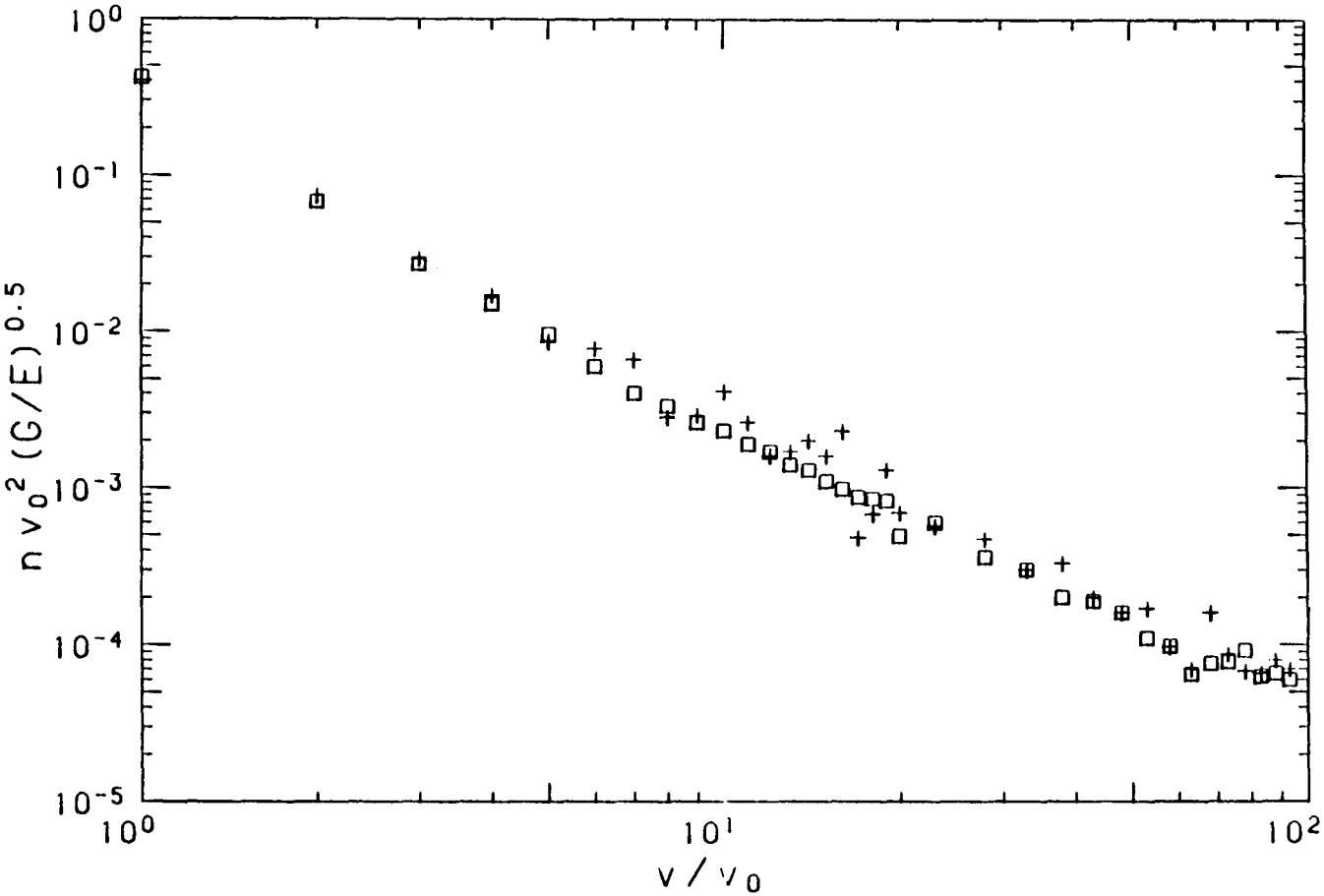

Figure 8. Steady state non-dimensional size distribution for laminar shear. G=1; + V=125, r_o=0.075, r_{max}=0.375, Δt=0.25, N_c=1, ϕ=0.0129; □ V=1, r_o=0.03, r_{max}=0.15, Δt=1, N_c=10, ϕ=0.195.

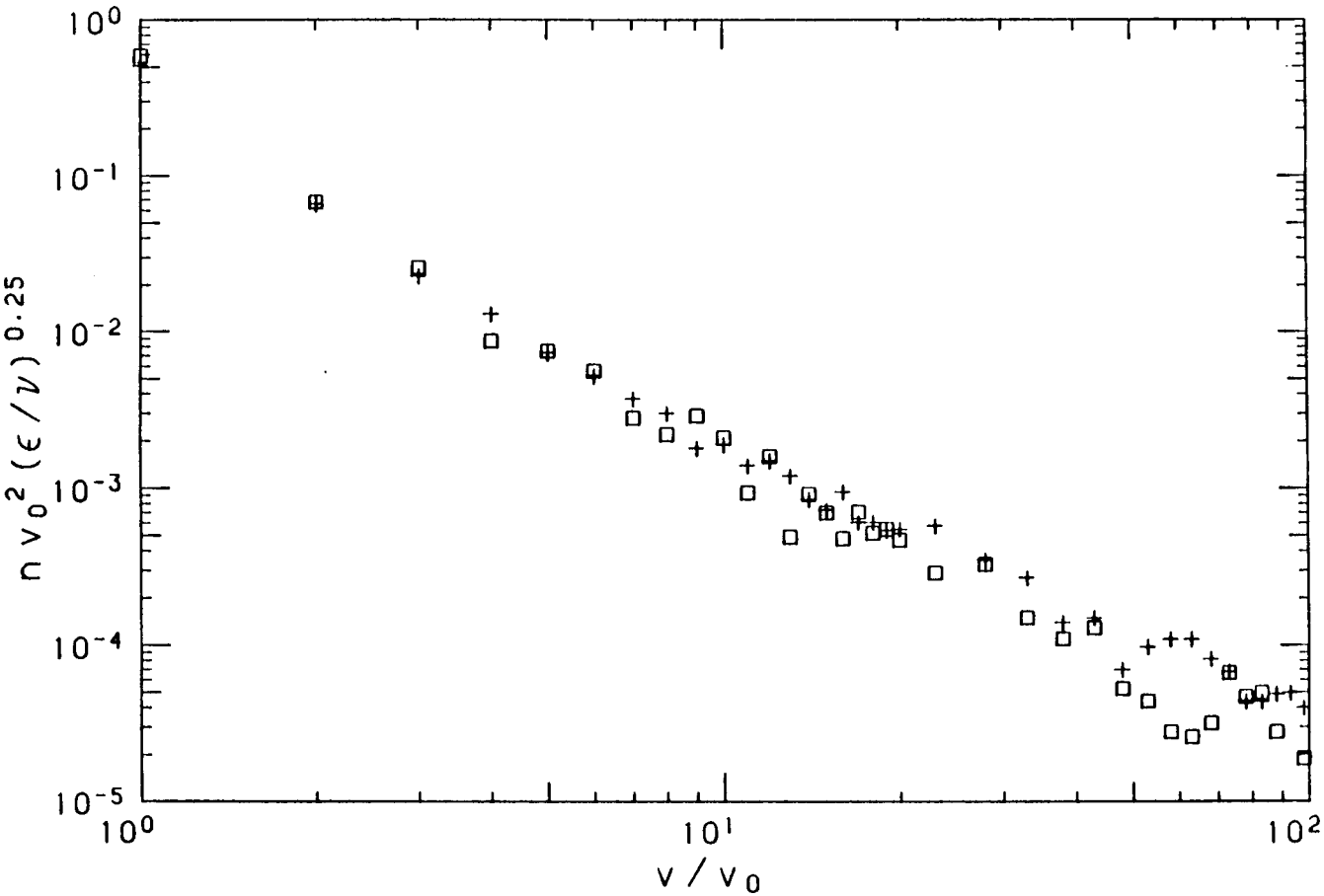

Figure 9. Steady state non-dimensional size distribution for turbulent shear. r_o=0.03, r_{max}=0.15, K_{sh}=1, Δt=0.5; + V=1, N_c=5, ϕ=0.0529; □ V=8, N_c=1, ϕ=0.0103.

Again a -2 power law is achieved at steady state and the normalized results are independent of the flux of particle volume through the size range. Note, however, that the intercept of the data with the axis v/v_o is larger by a factor of nearly 2 than in the case of laminar shear. This is simply a consequence of the collision functions given in Table 1: the expressions for laminar and isotropic turbulent shear are identical if G is replaced by $1.72\ (\varepsilon/\nu)^{\frac{1}{2}}$. With this scaling the data of figures 8 and 9 collapse. This result strongly suggests the equivalence of laminar rectilinear shear and three-dimensional turbulent shear as coagulating agents; a result previously suggested but not verified.

The next series of simulation runs illustrate the effect that the ratio v_{max}/v_o (i.e., the size range covered by the simulation) has on final steady state size distributions in Brownian motion and laminar shear. Figures 10 and 11 give size distributions for the three cases $v_{max}/v_o = 27, 125$, and 512; all other parameters remaining equal. In all cases the relevant -3/2 or -2 power law prevails. For Brownian motion the results for $v_{max}/v_o = 125$ and 512 are indistinguishable, while those for the smallest size range are slightly higher at the upper end of the size range. For laminar shear there is a slight but consistent decline in level with increasing size range. This reflects the extent to which the size distribution is affected by the collisions of the relatively small number of large particles. In laminar shear the collision function increases with the volume of the particles involved faster than in Brownian coagulation. Work on the effects of hydrodynamic interactions between particles on coagulation (see Adler, 1981 for most recent study) suggests that they act to reduce most the collision rate between particles of widely different sizes. This would probably result in weaker dependence of the

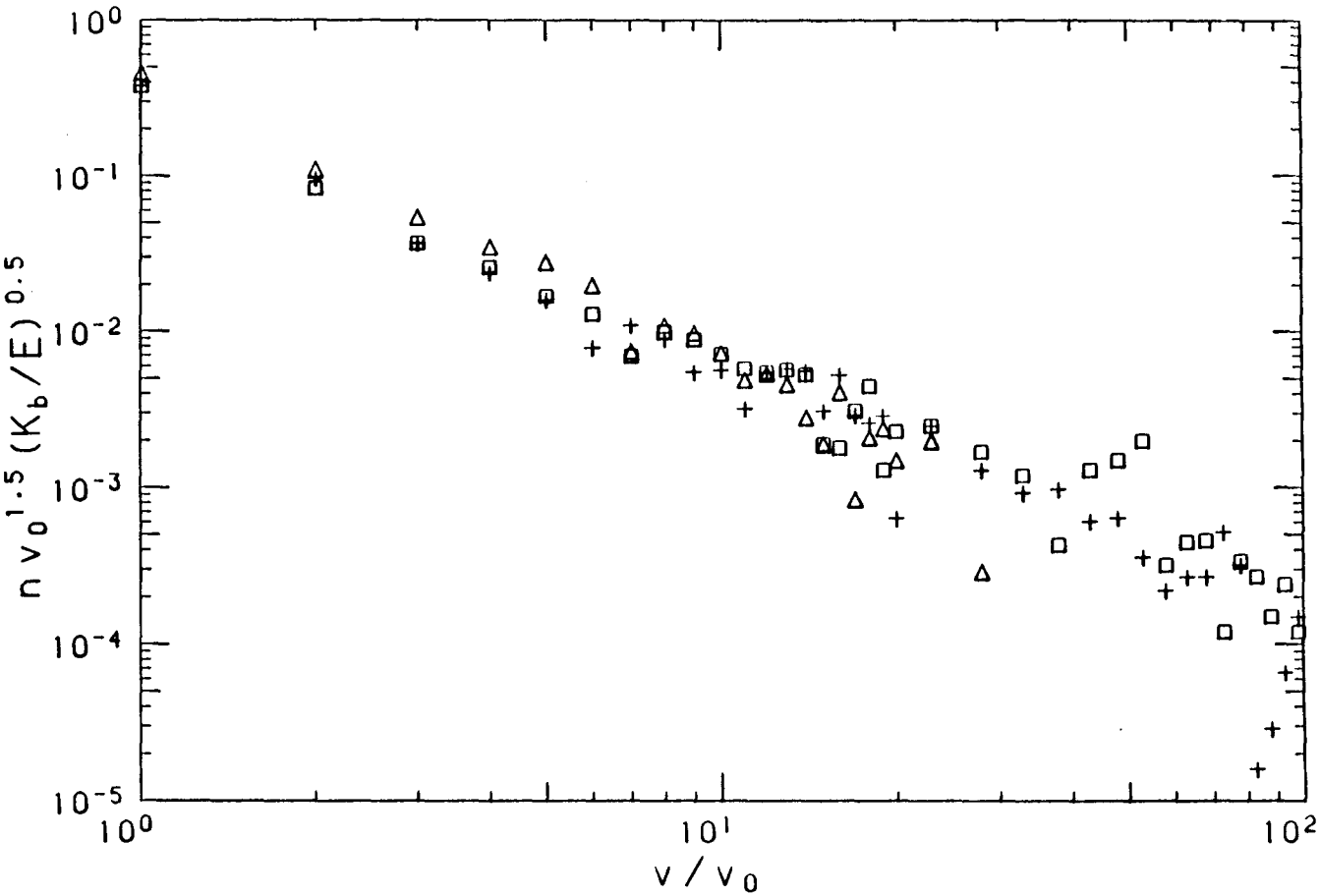

Figure 10. Comparison of steady state non-diminsional size distribution for Brownian motion for different r_{max}/r_o. V=125, r_o=0.075, D_o=0.005, Δt=0.25, N_c=1; □ r_{max}=0.225, ϕ=0.0105; Δ r_{max}=0.375, ϕ=0.0155; + r_{max}=0.6, ϕ=0.0139.

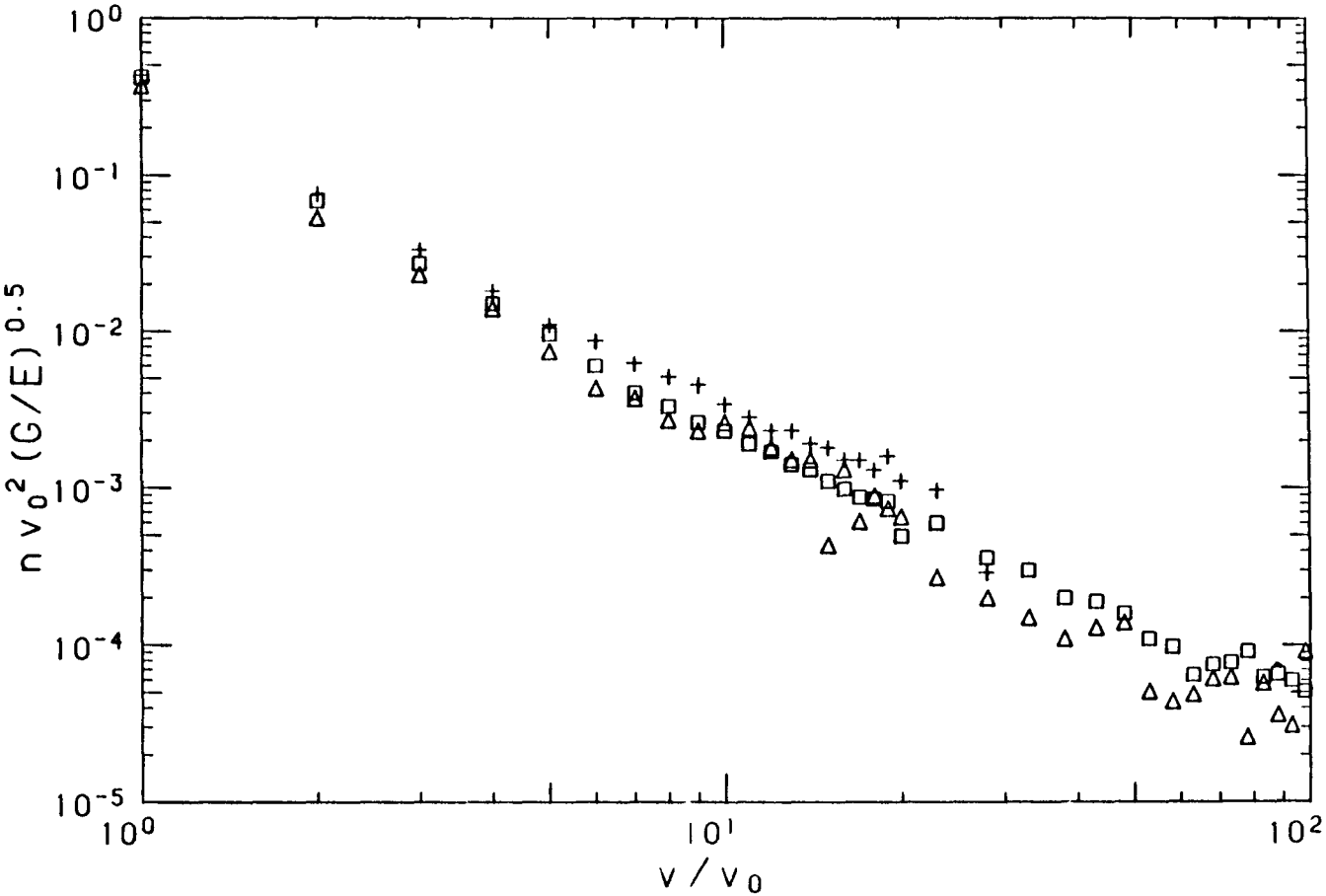

Figure 11. Comparison of steady state non-dimensional size distribution for laminar shear for different r_{max}/r_o. V=1, r=0.03, G=1, Δt=1, N_c=10; □ r_{max}=0.15, ϕ=0.195; + r_{max}=0.09, ϕ=0.128; Δ V=125, r_o=0.075, r_{max}=0.6, Δt=0.25, N_c=1, ϕ=0.014.

level of the size distribution (the value of a_{sh}) on the size range covered by the simulation. Further work, with a more sophisticated simulation incorporating hydrodynamic interactions, will elucidate this point.

A consensus of the simulations performed gives the values,

$$a_b = 0.2 \pm 0.04, \; a_{sh} = 0.24 \pm 0.05 \quad ,$$

which are close to the range of values found by Hunt (1980a) in his experiments. This comparability of "constants" is striking and supports the general validity of the study.

So far all the results have been for simulations in which only one collision mechanism has been present. We now turn to cases where both Brownian motion and fluid shearing operate. A new normalization of the size distribution and volume variable is now required to collapse all the data. Following Hunt (1980a) we define a non-dimensional volume

$$\chi = v.(K_{sh}/K_b) \quad ,$$

where K_{sh} represents G or $1.72(\varepsilon/\nu)^{\frac{1}{2}}$ and K_b is as before. This is such that the collision rates due Brownian motion and shear are equal for particles of size $\chi \simeq 1$. Then if a normalized size distribution is defined by

$$n^* = n(K_b/K_{sh})^2 \cdot (K_{sh}/E)^{\frac{1}{2}} \quad ,$$

equations (3) and (4) reduce to

$$n^*(\chi) = a_b \cdot \chi^{-3/2} \quad ,$$

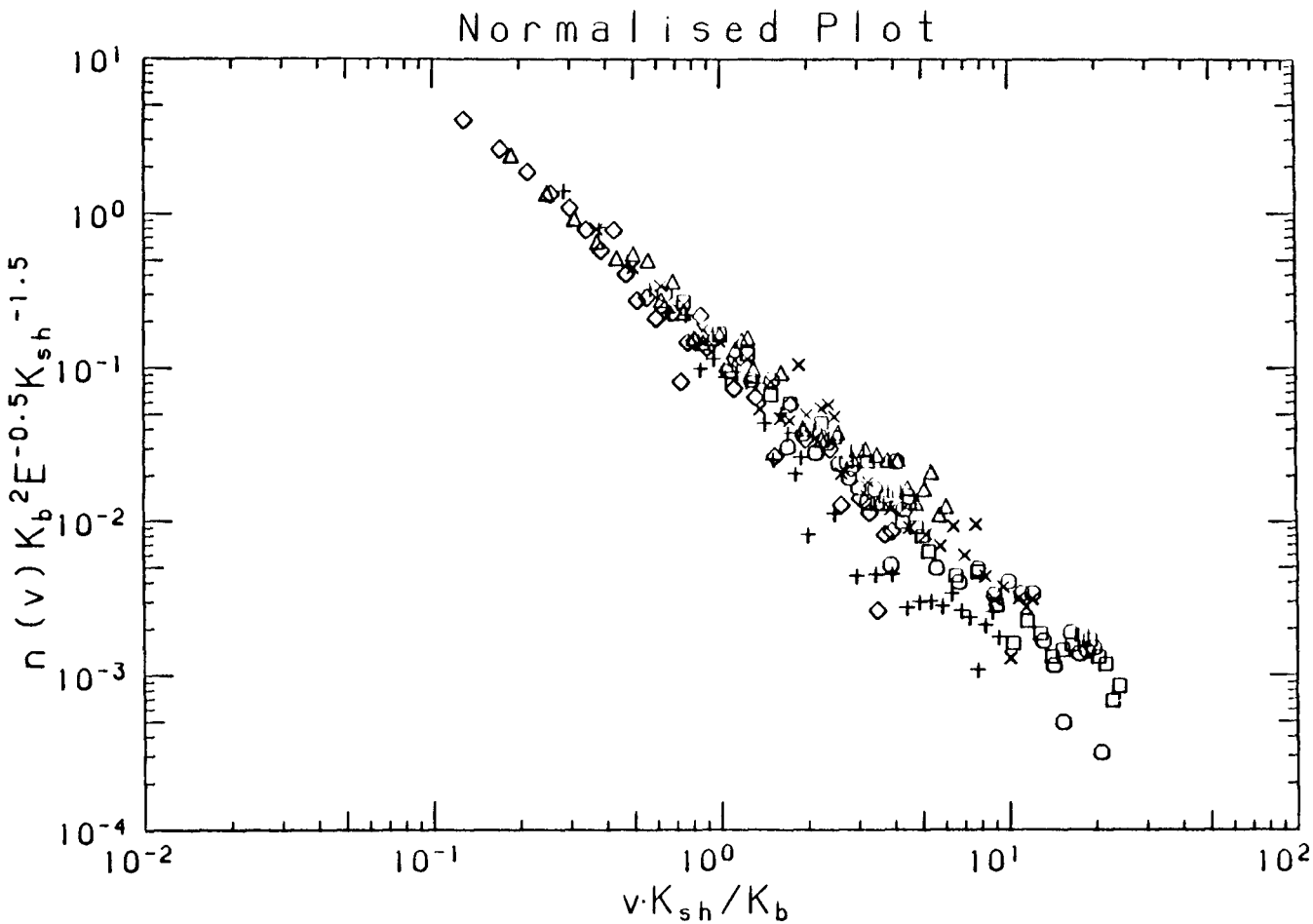

Figure 12. Steady state normalized size distribution for (i) Brownian motion and laminar shear, (ii) Brownian motion and turbulent shear. V=125, N_c=1. (i) r_o=0.075, r_{max}0.375, D_o=0.005, Δt=0.25; □ K_{sh}=1, ϕ=0.0081; × K_{sh}=0.5, ϕ=0.011; Δ K_{sh}=0.25, ϕ=0.013. (ii) + r_o=0.05, r_{max}=0.4, K_{sh}=1.72, D_o=0.01, Δt=0.2, ϕ=0.0096; ◇ r_o=0.075, r_{max}=0.375, K_{sh}=0.86, D_o=0.005, ϕ=0.0077; ○ r_o=0.075, r_{max}=0.375, K_{sh}=0.172, D_o=0.005, ϕ=0.013.

and

$$n^*(\chi) = a_{sh} \cdot \chi^{-2}$$

Results of three simulations each for laminar and turbulent shear with Brownian motion are plotted in this normalized form in Figure 12. Lines of slope -3/2 and -2 are plotted for comparison. There is some indication of a change in slope around χ=1 but it is not conclusive. Also, the constants a_b and a_{sh} obtained from (10), (11) and Figure 12 are the same (within statistical error) as those obtained from simulations with only one collision mechanism present, providing some support for the hypothesis of non-interference of mechanisms.

5. DISCUSSION

The main aims of this study have been:

1. to study the feasibility of a Monte Carlo simulation of both the collision function, β, and the coagulation equation, (2), for the evolution of a population of particles to a steady state;
2. the investigation of Hunt's (1980a,b) theory for the form of the resulting size distribution.

The simulation method described has proved most successful in modeling the coagulating powers of both Brownian and bulk shearing mechanisms and the development of steady state size distributions. This is in spite of the relatively restricted range of particle sizes that can be followed in any one computer run and the somewhat artificial strategy of adding new unit particles at each time step.

The results show that final steady state is rather insensitive to the size range covered, and that the size distribution at the upper end, (small particles), is not very disturbed by replacing the interactions of all small particles with the addition of unit particles at a constant rate. These observations are in accord with the striking success of dimensional analysis in predicting the observed size distributions. For dimensional analysis to be successful the dynamics of the coagulation process must be mainly "local" in size space so that further independent parameters (such as v_o and v_{max}) are not important. We expect that accounting for hydrodynamic interactions between particles will decrease the dependence of the level of the size distribution, for given volume flux, in shear-induced coagulation. Notice that the evolving populations of particles start to exhibit the relevant power-law over much of their size distribution long before a steady state is reached.

Hunt's further hypothesis that different collision mechanisms can act independently over separate size ranges has been partially confirmed. A slope of -3/2 is not very different from one of -2 when there is scatter in the data! However, complete resolution of this point would require the simulation to cover a greater range of particle sizes. This is not feasible with the available computer storage. The perturbation analysis of van de Ven and Mason (1977), for the effect of weak shear on Brownian coagulation, suggests that when hydrodynamic interactions are considered the two mechanisms may not be strictly additive.

In conclusion it can be said that, while simple in concept, and using acceptable computer resources, the simulation method has provided useful elucidation of Hunt's hypotheses and experimental results under carefully

controlled conditions. Further work on the technique to include hydrodynamic interactions and gravitational settling is in progress.

ACKNOWLEDGMENTS

Financial support for this work was provided by NOAA/Sea Grant NA80AA-D-00120, NOAA Grant NA80RA-DO-0084 and a Mellon Foundation Grant to the Environmental Quality Laboratory at Caltech. The authors would also like to thank Dr. R.C.Y. Koh for advice on many aspects of the computer code and Dr. R. C. Flagan for helpful discussions of the problem.

APPENDIX A

RANDOM NUMBER GENERATION

Each simulation requires very many ($\sim 10^6$) random numbers from both uniform and Gaussian distributions. A sequence of (pseudo-)random numbers distributed uniformly on the interval (0,1), denoted URN, are generated by the standard congruence method described in Abramowitz and Stegun (1964), §26.8 (henceforth referred to as AS). These random variates can then be scaled to any required uniform distribution. Random variates with Gaussian distribution are generated from URN by various algebraic manipulations and employing a 6 constant rational function approximation to the inverse of the Gaussian cumulative distribution function. Details are given in AS §26.2.23 and §26.8. The variates so computed are then scaled to the required variance. While the rest of the computer code is in FORTRAN the random number generator is written in assembler language, for efficient programming of the algorithm.

The random number generator produces a repeating sequence of variates whose maximum cycle length is restricted to 32,768 because the computer used (PDP 11/60) is a 16-bit machine. To avoid possible problems with the finite repetition time of the URN the sequence is restarted with a randomly generated seed number for each block of random numbers. The random seed is generated using an independent URN generator and the computer's internal clock. This guarantees different sequences of random variates even if the same program is rerun. Each block of random variates is a small fraction of the whole cycle.

In the simulation of laminar shearing motions, particles leaving the box must be replaced on the other side with a vertical coordinate (P_3) whose probability distribution reflects the differing fluxes of particles from the box at different heights. This flux is proportional to P_3 and a URN variate may be converted to this linear p.d.f. by taking its square-root.

APPENDIX B

FINITE STEPLENGTH AND COLLISION RATE IN BROWNIAN MOTION

The theoretical collision function, β, for Brownian induced collisions between particles of radii r_i and r_j given in Table 1 was computed (see e.g. Chandrasekhar, 1949) by solving a diffusion equation for the pair distribution function, w(s), where s is the distance between the particles. In particular, the collision function is given by the asymptotic flux to the surface of a fixed sphere of radius $\sigma = r_i + r_j$, with a total diffusivity $D = D_i + D_j$. The "concentration", w, is held at zero at $s=\sigma$ and unit at $s=\infty$. Initially, w is uniform outside the sphere. Then at large times the pair distribution function is given by

$$w = 1 - \sigma/s \ , \tag{A.1}$$

whence the required result:

$$\beta = 4\pi D(s^2 dw/ds)_{s=\sigma} = 4\pi D\sigma \ . \tag{A.2}$$

If the actual pair distribution function in the finite steplength simulation was identical to that in (A.1), then the collision rate measured would be no larger than one-half of that in (A.2), however small the steplength. This result can be obtained either by careful evaluation of the expected collision probability from the algorithms used for generating particle displacements and detecting collisions, or by the following simple argument. In the limit of $\Delta x << \sigma$, i.e., very small r.m.s steplength, but still with $\Delta t >> t_r$, two particles must be so close at the beginning of the time step in which they collide that the curvature of their surfaces may be neglected. The problem then reduces to that of the collision of a diffusing point with an adsorbing plane and we need only consider the component of the random walk perpendicular to the plane.

Consider now this one-dimensional problem. The particle is judged to have collided with the plane if its final position is on the far side of the plane. For any given final position on the far side of the plane there is a whole class of possible Brownian trajectories leading to it. Now each of these trajectories must cross the plane for the first time at some point. There will be an associated trajectory defined to be identical with the original until the first contact with the adsorbing plane and then the mirror image, in the plane, of the original. As the end-point of this associated trajectory lies on the near side of the plane it would not be judged a collision by the collision algorithm. Hence the 50 per cent inefficiency.

However, for the same reason, the pair distribution function will not be identical in the theoretical and simulated cases. In the finite steplength case, w will be larger within a distance of order Δx of s=c. This can compensate for the basic inefficiency of the collision algorithm. The actual form of w for a given distribution of steplengths and hence the collision function could be computed by solving the relevant integral equation. This has not been done as yet, but the non-coagulating form of the simulation has been used to determine the collision rate for a monodisperse population of particles as a function of the mean steplength. The results of this "experimental" determination are shown in Figure 5. The ratio of measured collision rate to that predicted from (A.2) is plotted against the ratio of r.m.s. displacement in any direction, Δx, and the particle radius r. The ratio is unity for $\Delta x/r$ about 0.6 and so Δx is chosen accordingly in all the coagulation simulations.

REFERENCES

Adler, P.M. 1981 Heterocoagulation in shear flows. *J. Coll. Interf. Sci.* 83, 106-115.

Alder, B.J. and Wainwright, T.E. 1959 Studies in Molecular Dynamics. I. General Method. *J. Chem. Phys.* 31, 459-466.

Batchelor, G.K. 1953 *The theory of homogeneous turbulence.* Cambridge University Press, London.

Chandrasekhar, S. 1943 Stochastic problems in physics and astronomy. *Rev. Mod. Phys.* 15, 1-89.

Corrsin, S. 1963 Estimates of the relations between Eulerian and Lagrangian scale in large Reynolds number turbulence. *J. Atmos. Sci.* 20, 115

Findheisen, W. 1939 *Meteor. Z.* 56, 356.

Friedlander, S.K. 1960a On the particle size spectrum of atmospheric aerosols. *J. Meteorol.* 17, 373-374.

Friedlander, S.K. 1960b Similarity considerations for the particle-size spectrum of a coagulating, sedimenting aerosol. *J. Meteorol.* 17, 479-483.

Gartrell, G. Jr. and Friedlander, S.K. 1975 Relating particulate pollution to sources: the 1972 California aerosol characterization study. *Atmos. Env.* 9, 279-294.

Gelbard, F., Tambour, Y. and Seinfeld, J.H. 1980 Sectional representations for simulating aerosol dynamics. *J. Coll. Interf. Sci.* 76, 541-556.

Gillespie, D.T. 1975 An exact method for numerically simulating the stochastic coalescence process in a cloud. *J. Atmos. Sci.* 29, 1977-1989.

Hinze, J.O. 1975 *Turbulence.* 2nd edition, McGraw-Hill, New York.

Hunt, J.R. 1980a Coagulation in continuous particle size distributions: theory and experimental verification. Report No. AC-5-80. W. M. Keck Lab, Calif. Inst. of Tech., Pasadena.

Hunt, J.R. 1980b Prediction of oceanic particle size distribution from coagulation and sedimentation mechanisms. In *Adv. in Chem. Series No. 189, Particulates in Water,* Kavanaugh, M.C. and Leckie, J.O., Eds.

Hunt, J.R. 1982 Self-similar particle-size distributions during coagulation: theory and experimental verification. *J. Fluid Mech.* 122, 169-185.

Husar, R.B. 1971 Coagulation of Knudsen aerosols. Ph.D. Thesis, The University of Minnesota, Minneapolis, Minn.

Lumley, J.L. 1972 On the solution of equations describing small scale deformation. In *Symposia Mathematica: Convegno sulla Teoria della Turbolenza al Instituto Nazionale di Alta Matematica.* Academic Press, New York.

Mason, S.G. 1977 Orthokinetic phenomena in disperse systems. *J. Coll. Interf. Sci.* 58, 275-285.

Monin, A.S. and Yaglom, A.M. 1975 *Statistical Fluid Mechanics, Vol. 2.* The MIT Press, Cambridge, Mass., 874 pp.

Nowakowski, R. and Sitarski, M. 1981 Brownian coagulation of aerosol particles by Monte Carlo simulation. *J. Coll. Interf. Sci.* 83, 614-622.

Pruppacher, H.R. and Klett, J.D. 1978 *Microphysics of Clouds and Precipitation.* Reidel, Dordrecht, Holland, 714 pp.

Saffman, P.G. and Turner, J.S. 1956 On the collision of drops in turbulent clouds. *J. Fluid Mech.* 1, 16-30.

Smoluchowski, M. 1916 *Physik Z.* 17, 557.

Smoluchowski, M. 1917 *Z. Phys. Chem.* 92, 129.

van de Ven, T.G.M. and Mason, S.G. 1977 The microrheology of colloidal dispersions. VIII. Effect of shear on perikinetic doublet formation. *Colloid and Polymer Sci.* 255, 794-804.

Zeichner, G.R. and Schowalter, W.R. 1977 Use of trajectory analysis to study the stability of colloidal dispersions in flow fields. *AIChE J.* 23, 243-254.

APPENDIX B

```
C     MAIN PROGRAM  FOR THE MONTE-CARLO SIMULATION OF PARTICLE
C     COAGULATION (REF: PEARSON, VALIOULIS AND LIST, 1983, AND
C     VALIOULIS' PH.D. THESIS, CHAPTER I).
C     BROWNIAN DIFFUSION, LAMINAR SHEAR AND DIFFERENTIAL SEDIMENTATION
C     INDUCED PARTICLE COLLISIONS. THE PROGRAM INCLUDES HYDRODYNAMIC
C     INTERACTIONS FOR SEDIMENTING PARTICLES.
C
C  THE COMPUTER CODE IS ADAPTED FOR CALTECH'S IBM 370/3032.
C
C  APTS: NUMBER OF PARTICLES ADDED PER TIME-STEP
C  D1,D2,D3: PARTICLE DISPLACEMENTS
C  DIFF: DIFFUSIVITY FOR MONOMER
C  DSK: DIFFERENTIAL SEDIMENTATION PARAMETER
C  DT: TIME STEP
C  GA: STRAIN RATE
C  JCOLL: NUMBER OF COLLISIONS
C  JSR(I): NUMBER OF INTEGRAL MULTIPLES
C  KB1(I),KB2(I),KB3(I): INTEGERS DEFINING THE SUB-CELL OF PARTICLE I
C  L1,L2,L3: NUMBER OF SUB-CELLS
C  N: NUMBER OF PARTICLES
C  NDT: TIME INTERVALS FOR OUTPUT
C  NT: TOTAL NUMBER OF TIME-STEPS
C  P1,P2,P3: PARTICLE POSITIONS
C  R: RADIUS OF MONOMER
C  RMAX: RADIUS OF LARGEST PARTICLE
C  UL(I): DIMENSIONS OF CONTROL VOLUME
C  VOL: CONTROL VOLUME
C  XR(I): RADIUS OF AGGREGATE CONSISTING OF I MONOMERS
C
        REAL*4 JSR,JCOLL
        COMMON/PART/ D1(1000),D2(1000),D3(1000),P1(1000),P2(1000),
     *               P3(1000),KB1(1000),KB2(1000),KB3(1000),XR(1000),
     *               JSR(100),UL(3),BL(3),NUM
        COMMON/VALI/ N,R,DT,JCOLL,GA,ANF,RMAX,L1,L2,L3,DSK,DX,RMICRO
        COMMON/FLAG/ KFLAG
C***  DEFINE CONSTANTS
        EPI=2.51327E+01
        KR2=0
        KR3=0
        KR4=0
        KR5=0
        NUM=456789
```

```
C***  CHECK INPUT MODE: TERMINAL, FILE OR RERUN,
        READ(5,81) KFLAG
  81    FORMAT(I1)
        IF(KFLAG.NE.0) GO TO 7
        READ(5,8,ERR=99) N,R,DIFF,GA,DT,NT,NDT,APTS,RMAX,RMICRO
  8     FORMAT(I3,4F6.4,2I4,2F5.2,F5.1)
        READ(5,10,ERR=99) DSK,MEFF
  10    FORMAT(F6.4,I2)
        READ(5,13,ERR=99)UL(1),UL(2),UL(3),L1,L2,L3
   13   FORMAT(3F5.2,3I2)
        RMAX=R*RMAX
        DX=SQRT(2.*DIFF*DT)
        GO TO 16
C***  INPUT DATA FOR RERUN
   7    CALL PAREAD
        READ(5,11,ERR=99) GA,DSK,RMICRO,MEFF
  11    FORMAT(2F6.4,F6.2,I2)
        READ(5,15,ERR=99) NT,NDT,APTS,RMAX
   15   FORMAT(2I4,2F5.2)
        READ(5,152,ERR=99) L1,L2,L3
  152   FORMAT(3I2)
        RMAX=R*RMAX
        DX=SQRT(2.*DT*DIFF)
C***  COMPUTE DERIVED PARAMETERS
   16   VOL=UL(1)*UL(2)*UL(3)
        XNC=N/VOL
        FT=DT
        ESPAC=EXP(-ALOG(XNC)/3.)
        SPACR=ESPAC/R
        FTAU=NT*FT
        DFR=DX/R
C***  OUTPUT PARAMETERS OF RUN AND INITIALISE
        WRITE(1,18)VOL,N,R,DIFF,GA,DSK,NT,NDT
   18   FORMAT(´   VOL ´,F10.4,´ N ´,I4,´ RAD ´,F10.4,´ DIFF ´,
     *       F10.4,´ GA ´,F10.4,´ DSK ´,F10.4,´ NT ´,I5,´ NDT ´,I4)
        WRITE(1,19)DT,APTS
   19   FORMAT(´   DT ´,E10.4,´   APTS ´,F8.4)
        WRITE(1,20)XNC,SPACR,FTAU,DFR
   20   FORMAT(´     NCONC ´,E10.4,´ SPACR ´,E10.4,´ FTAU ´,E10.4,
     *         ´ DFR ´,E10.4)
        CALL INIT3
        IN=0
        JCOLL=0.
        ISTEP=0
        CALL CCOLL3(IN,MEFF,KR2,KR3,KR4,KR5,ISTEP)
        IN=1
```

```
      WRITE(1,21) BL(1),BL(2),BL(3),RMAX
   21 FORMAT(' BLENG ',3(2X,E10.4),' RMAX ',F8.4)
      WRITE (1,22) JCOLL
   22 FORMAT('     INITIAL COLLS ',F8.0/)
      WRITE(1,25) RMICRO
   25 FORMAT(' RMICRO=',F8.2)
      JCOLL=0.
      NINIT=N
C***  MAIN LOOP
      DO 1 I=1,NT
C***  COMPUTE GRAVITY INDUCED DISPLACEMENT
      CALL DIFSED
      IF(DX.LE.0.1E-05) GO TO 261
C***  GENERATE RANDOM DISPLACEMENTS
      CALL DISPG(D1,XR,R,N,DX,NUM)
      CALL DISPG(D2,XR,R,N,DX,NUM)
      CALL DISPG(D3,XR,R,N,DX,NUM)
C***  COMPUTE SHEAR INDUCED DISPLACEMENT
261   IF(GA.LE.0.1E-05) GO TO 262
      CALL SHDISP
C***  CHECK FOR COLLISIONS
262   CALL CCOLL3(IN,MEFF,KR2,KR3,KR4,KR5,I)
C***  UPDATE POSITIONS AND BOX-NUMBERS
      CALL UPDATE(APTS,I,MEFF,KR2,KR3,KR4,KR5)
      CALL SZDIST(I,FT,NDT,NF)
    1 CONTINUE
C***  COMPUTE FINAL STATISTICS
      TV=APTS*NT+NINIT
      XNL=TV-JCOLL-NF
      FV=TV-XNL*(RMAX/R)**3
      FVOLC=FV*EPI*(R**3)/(6.*VOL)
      IF(TIM.LE.0.0) TIM=TIM+86400.
C***  PRINT FINAL RESULTS
      IF(APTS.LT. 1.) WRITE(1,24)
   24 FORMAT(//' FVOLC IN ERROR')
      WRITE(1,23)JCOLL,TIM,FVOLC
   23 FORMAT(/'     NCOLL ',F10.0,' RTIME ',F10.0,' FVOLC ',E12.4//)
      WRITE(1,251) KR2,KR3,KR4,KR5
  251 FORMAT(/' TIME STEPS FOR REMOVAL:  KR2',I4,'  KR3',I4,'  KR4',
     *        I4,'  KR5',I4)
   99 STOP
      END
```

```
C ***********************************************************************
C     ROUTINE TO DETERMINE WHETHER GIVEN PARTICLES HAVE COLLIDED
C     CALLS COAG
C
C
      SUBROUTINE MCOLL3(I1,I2,IN,MEFF,KR2,KR3,KR4,KR5,ISTEP)
      REAL*4 JSR,DT,JCOLL
      COMMON/PART/ D1(1000),D2(1000),D3(1000),P1(1000),P2(1000),
     *             P3(1000),KB1(1000),KB2(1000),KB3(1000),XR(1000),
     *             JSR(100),UL(3),BL(3),NUM
      COMMON/VALI/ N,R,DT,JCOLL,GA,ANF,RMAX,L1,L2,L3,DSK,DX,RMICRO
      DIMENSION RD(3),RP(3)
C***  COMPUTE COLLISION CROSS-SECTION
      SIG2=(XR(I1)+XR(I2))**2
      IF(IN.EQ.0) GO TO 12
      XR1=XR(I1)*RMICRO
      XR2=XR(I2)*RMICRO
      IF(XR2.GE.XR1) GO TO 14
      A=XR1
      PR=XR2/XR1
      GO TO 13
   14 A=XR2
      PR=XR1/XR2
   13 E0=0.95-(0.7-0.005*A)**4*(7.92-0.12*A+0.001*A**2)
      E1=-(PR-0.5)**2
      E2=-1.5*EXP(-(0.0015*A**2+8.)*PR)
      E3=-(1.-0.007*A)*EXP(-0.65*A*(1.-PR))
      E4=EXP(-30.*(1.-PR))
      IF(A.LT.20.) E4=0.
      EFF=E0+E1+E2+E3+E4
      IF(EFF.LT.0.0) EFF=0.
      SIG1=SIG2*EFF
C***  CHECK FOR WRAP-AROUND
      SHX=0.
      SHY=0.
      SHZ=0.
      LDX=KB1(I1)-KB1(I2)
      IF(IABS(LDX).LE.1) GO TO 3
```

```
      SHX=SIGN(UL(1),FLOAT(LDX))
3     LDY=KB2(I1)-KB2(I2)
      IF(IABS(LDY).LE.1) GO TO 5
      SHY=SIGN(UL(2),FLOAT(LDY))
5     LDZ=KB3(I1)-KB3(I2)
      IF(IABS(LDZ).LE.1) GO TO 4
      SHZ=SIGN(UL(3),FLOAT(LDZ))
4     P1(I2)=P1(I2)+SHX
      P2(I2)=P2(I2)+SHY
      P3(I2)=P3(I2)+SHZ
      D1(I2)=D1(I2)+GA*DT*SHZ
C*** CHECK FOR COLLISION
      IF(IN.NE.0) GO TO 11
12    D1(I1)=0.0
      D2(I1)=0.0
      D3(I1)=0.0
      D1(I2)=0.0
      D2(I2)=0.0
      D3(I3)=0.0
11    RD(1)=D1(I2)-D1(I1)
      RD(2)=D2(I2)-D2(I1)
      RD(3)=D3(I2)-D3(I1)
      RP(1)=P1(I1)-P1(I2)
      RP(2)=P2(I1)-P2(I2)
      RP(3)=P3(I1)-P3(I2)
      RD2=RD(1)**2+RD(2)**2+RD(3)**2
      RP2=RP(1)**2+RP(2)**2+RP(3)**2
      IF(IN.EQ.0) GO TO 10
      DDOTP=RD(1)*RP(1)+RD(2)*RP(2)+RD(3)*RP(3)
      IF(DDOTP.LT.0.0E+00)GO TO 1
      IF(RD2.LE.0.0E+00) GO TO 1
      IF((RP2-DDOTP**2/RD2).GT.SIG1) GO TO 1
      IF(RD2.GE.DDOTP) GO TO 2
      IF((RP2+RD2-2.*DDOTP).GT.SIG1) GO TO 1
 2    CALL COAG(I1,I2,KR2,KR3,KR4,KR5,ISTEP)
      GO TO 6
 1    P1(I2)=P1(I2)-SHX
      P2(I2)=P2(I2)-SHY
      P3(I2)=P3(I2)-SHZ
      D1(I2)=D1(I2)-GA*DT*SHZ
 6    RETURN
10    IF(RP2.GT.SIG2) GO TO 6
      CALL PINIT(I2,IN)
      JCOLL=JCOLL+1.
      GO TO 6
      END
```

```
C*********************************************************************
C     FINDS AND COUNTS COIIISIONS
C
        SUBROUTINE CCOLL3(IN,MEFF,KR2,KR3,KR4,KR5,ISTEP)
        REAL*4 JSR,JCOLL
        COMMON/PART/ D1(1000),D2(1000),D3(1000),P1(1000),P2(1000),
     *               P3(1000),KB1(1000),KB2(1000),KB3(1000),XR(1000),
     *               JSR(100),UL(3),BL(3),NUM
        COMMON/VALI/ N,R,DT,JCOLL,GA,ANF,RMAX,L1,L2,L3,DSK,DX,RMICRO
        N1=N-1
        L11=L1-1
        L22=L2-1
        L33=L3-1
        DO 100 LI=1,N1
        IX1=KB1(LI)
        IY1=KB2(LI)
        IZ1=KB3(LI)
        LIP=LI+1
        DO 1 LT=LIP,N
C***  CHECK FOR NULL PARTICLES
        IF(KB1(LI).EQ.0) GO TO 100
        IF(KB1(LT).EQ.0) GO TO 1
C*** TEST FOR ADJACENT BOX-NUMBERS
        IDX=IABS(IX1-KB1(LT))
        IF(IDX.EQ.L11) IDX=1
        IF(IDX.GT.1) GO TO 1
        IDY=IABS(IY1-KB2(LT))
        IF(IDY.EQ.L22) IDY=1
        IF(IDY.GT.1) GO TO 1
        IDZ=IABS(IZ1-KB3(LT))
        IF(IDZ.EQ.L33) IDZ=1
        IF(IDZ.GT.1) GO TO 1
        CALL MCOLL3(LI,LT,IN,MEFF,KR2,KR3,KR4,KR5,ISTEP)
    1   CONTINUE
  100   CONTINUE
        RETURN
        END
C
C*********************************************************************
C     INITIALISES POSITIONS AND/OR BOX NUMBERS
C
        SUBROUTINE INIT3
        REAL*4 JSR,JCOLL
        COMMON/PART/ D1(1000),D2(1000),D3(1000),P1(1000),P2(1000),
     *               P3(1000),KB1(1000),KB2(1000),KB3(1000),XR(1000),
     *               JSR(100),UL(3),BL(3),NUM
        COMMON/VALI/ N,R,DT,JCOLL,GA,ANF,RMAX,L1,L2,L3,DSK,DX,RMICRO
        COMMON/FLAG/ KFLAG
```

```
C***  COMPUTE BOX DIMENSIONS
        BL(1)=UL(1)/FLOAT(L1)
        BL(2)=UL(2)/FLOAT(L2)
        BL(3)=UL(3)/FLOAT(L3)
        IF(KFLAG.EQ.1) GO TO 3
        DO 1 I=1,N
        NUM=NUM*65539
        IF(NUM.LT.0) NUM=NUM+2147483647+1
        URN=NUM*0.465661E-9
        P1(I)=UL(1)*URN
        NUM=NUM*65539
        IF(NUM.LT.0) NUM=NUM+2147483647+1
        URN=NUM*0.465661E-9
        P2(I)=UL(2)*URN
        NUM=NUM*65539
        IF(NUM.LT.0) NUM=NUM+2147483647+1
        URN=NUM*0.465661E-9
        P3(I)=UL(3)*URN
        XR(I)=R
    1   CONTINUE
    3   DO 2 I=1,100
    2   JSR(I)=0.
        ANF=0.E+00
        DO 4 I=1,N
        KB1(I)=1+INT(P1(I)/BL(1))
        IF(XR(I).LE.1.E-07) KB1(I)=0
        KB2(I)=1+INT(P2(I)/BL(2))
        KB3(I)=1+INT(P3(I)/BL(3))
    4   CONTINUE
        RETURN
        END
C
C*********************************************************************
C     GENERATES GAUSSIAN RANDOM DISPLACEMENTS
C
        SUBROUTINE DISPG(D,XR,R,N,DX,NUM)
        DIMENSION D(1000),XR(1000)
        DO 1 I=1,N
        IF(XR(I).LT.1.E-09) GO TO 1
        CALL GRAN(RN,NUM)
        D(I)=DX*SQRT(R/XR(I))*RN+D(I)
    1   CONTINUE
        RETURN
        END
```

```
C*********************************************************************
      SUBROUTINE DIFSED
      REAL*4 JSR,JCOLL
      COMMON/PART/ D1(1000),D2(1000),D3(1000),P1(1000),P2(1000),
     *             P3(1000),KB1(1000),KB2(1000),KB3(1000),XR(1000),
     *             JSR(100),UL(3),BL(3),NUM
      COMMON/VALI/ N,R,DT,JCOLL,GA,ANF,RMAX,L1,L2,L3,DSK,DX,RMICRO
      DO 1 I=1,N
      IF(KB1(I).EQ.0.0) GO TO 1
      D3(I)=-(2./9.)*XR(I)**2*DSK*DT+D3(I)
      D1(I)=0.0
      D2(I)=0.0
    1 CONTINUE
      RETURN
      END
C
C*********************************************************************
C    GENERATES STANDARD NORMALLY DISTRIBUTED RANDOM NUMBERS
C    USING I AS SEED, RANDOM NUMBER IS XN.
C
      SUBROUTINE GRAN(XN,NUM)
      DATA C0,C1,C2,D1,D2,D3/ 2.515517,0.802853,.010328,1.432788,
     *      .189269,.001308/
      NUM=NUM*65539
      IF(NUM.LT.0) NUM=NUM+2147483647+1
      URN=NUM*0.465661E-9
      XH=URN-0.5E00
      IF(ABS(XH).LE.1.E-04) GO TO 2
      T=SQRT(-ALOG(XH*XH))
      XNT=T-(C0+T*(C1+C2*T))/(1.+T*(D1+T*(D2+T*D3)))
    1 XN=SIGN(XNT,XH)
      RETURN
    2 XNT=3.719124
      GO TO 1
      END
C
C*********************************************************************
C     COAGULATES PARTICLES
C
      SUBROUTINE COAG(I1,I2,KR2,KR3,KR4,KR5,ISTEP)
      REAL*4 JSR,JCOLL
      COMMON/PART/ D1(1000),D2(1000),D3(1000),P1(1000),P2(1000),
     *             P3(1000),KB1(1000),KB2(1000),KB3(1000),XR(1000),
     *             JSR(100),UL(3),BL(3),NUM
      COMMON/VALI/ N,R,DT,JCOLL,GA,ANF,RMAX,L1,L2,L3,DSK,DX,RMICRO
C***  UPDATE TOTAL NUMBER OF COLLISIONS
      JCOLL=JCOLL+1.
```

```
C*** COMPUTE RADIUS OF AGGREGATE
        R3=XR(I1)**3+XR(I2)**3
        XR(I1)=EXP(ALOG(R3)/3.E+00)
        IF(KR5.NE.0) GO TO 15
        IF(KR4.NE.0) GO TO 16
        IF(KR3.NE.0) GO TO 17
        IF(KR2.NE.0) GO TO 18
        IF(XR(I1).GE.2.*R) KR2=ISTEP
        GO TO 15
  18    IF(XR(I1).GE.3.*R) KR3=ISTEP
        GO TO 15
  17    IF(XR(I1).GE.4.*R) KR4=ISTEP
        GO TO 15
  16    IF(XR(I1).GE.5.*R) KR5=ISTEP
C***  CHECK FOR AND REMOVE LARGE PARTICLE
  15    IF(XR(I1).LT.RMAX) GO TO 1
        XR(I1)=0.0E-10
        KB1(I1)=0
        KB2(I1)=0
        KB3(I1)=0
C***  ZERO PARTICLE
    1   XR(I2)=0.0E-10
        KB1(I2)=0
        KB2(I2)=0
        KB3(I2)=0
        RETURN
        END
C
C**********************************************************************
C     CALCULATES SIZE DISTRIBUTION AS FUNCTION OF RADIUS
C
        SUBROUTINE SZDIST(IT,FT,NDT,NF)
        REAL*4 JSR,JCOLL
        COMMON/PART/ D1(1000),D2(1000),D3(1000),P1(1000),P2(1000),
     *               P3(1000),KB1(1000),KB2(1000),KB3(1000),XR(1000),
     *               JSR(100),UL(3),BL(3),NUM
        COMMON/VALI/ N,R,DT,JCOLL,GA,ANF,RMAX,L1,L2,L3,DSK,DX,RMICRO
        NF=0
        JM=0
        DO 2 I=1,N
        IF(KB1(I).EQ.0) GO TO 2
        IM=I
        NF=NF+1
        JR=INT(1.E-04+(XR(I)/R)**3)
        JM=MAX0(JR,JM)
        IF(JR.GT.100) GO TO 2
        JSR(JR)=JSR(JR)+1.
    2   CONTINUE
```

```
      N=IM
      ANF=ANF+NF
      IF(IT-NDT*INT(FLOAT(IT)/FLOAT(NDT)+1.E-04).NE.0) GO TO 3
      DO 4 I=1,100
    4 JSR(I)=JSR(I)/NDT
      ANF=ANF/NDT
      CALL SZDOUT(IT,FT,NF,JM)
      DO 5 I=1,100
    5 JSR(I)=0.
      ANF=0.0E+00
    3 RETURN
      END
C*********************************************************************
C     OUTPUTS SIZE DISTRIBUTION
C
      SUBROUTINE SZDOUT(IT,FT,NF,JM)
      REAL*4 JSR,JCOLL
      COMMON/PART/ D1(1000),D2(1000),D3(1000),P1(1000),P2(1000),
     *             P3(1000),KB1(1000),KB2(1000),KB3(1000),XR(1000),
     *             JSR(100),UL(3),BL(3),NUM
      COMMON/VALI/ N,R,DT,JCOLL,GA,ANF,RMAX,L1,L2,L3,DSK,DX,RMICRO
      RTIME=IT*FT
      WRITE(1,20) RTIME,JCOLL,N,NF,ANF,JM,JSR
   20 FORMAT(//,'   TIME=',F10.4,'   NCOLL=',F8.0,'  N=',I4,
     *     '   NF=',I4,'   ANF=',F6.1,'  VMAX=',I6,//,(10F8.3))
C***  OUTPUT INTERMEDIATE DATA FOR POSSIBLE RERUN
      REWIND 3
      WRITE (3)N,UL,R,DT,DX,P1,P2,P3,XR
      RETURN
      END
C
C*********************************************************************
C     ADDS NEW PARTICLES
C
      SUBROUTINE PADD(APTS)
      REAL*4 JSR,JCOLL
      COMMON/PART/ D1(1000),D2(1000),D3(1000),P1(1000),P2(1000),
     *             P3(1000),KB1(1000),KB2(1000),KB3(1000),XR(1000),
     *             JSR(100),UL(3),BL(3),NUM
      COMMON/VALI/ N,R,DT,JCOLL,GA,ANF,RMAX,L1,L2,L3,DSK,DX,RMICRO
      IF(APTS.GE.1.) GO TO 1
      NUM=NUM*65539
      IF(NUM.LT.0) NUM=NUM+2147483647+1
      URN=NUM*0.465661E-9
      IF(URN.GT.APTS) GO TO 3
      NADD=1
      GO TO 4
    1 NADD=INT(APTS+1.E-04)
    4 J=0
      IN=1
      DO 2 I=1,N
      IF(KB1(I).NE.0) GO TO 2
```

```
          CALL PINIT(I,IN)
          J=J+1
          IF(J.EQ.NADD) GO TO 3
      2   CONTINUE
          NN=N+NADD-J
          IF(NN.GT.1000) GO TO 5
          N1=N+1
          DO 6 I=N1,NN
      6   CALL PINIT(I,IN)
          N=NN
      3   RETURN
      5   WRITE(1,7)
      7   FORMAT(//'     STOPPING BECAUSE N>1000')
          STOP
          END
C*********************************************************************
C     INITIALISES PARTICLE
C
          SUBROUTINE PINIT(I,IN)
          REAL*4 JSR,JCOLL
          COMMON/PART/ D1(1000),D2(1000),D3(1000),P1(1000),P2(1000),
     *               P3(1000),KB1(1000),KB2(1000),KB3(1000),XR(1000),
     *               JSR(100),UL(3),BL(3),NUM
          COMMON/VALI/ N,R,DT,JCOLL,GA,ANF,RMAX,L1,L2,L3,DSK,DX,RMICRO
          NUM=NUM*65539
          IF(NUM.LT.0) NUM=NUM+2147483647+1
          URN=NUM*0.465661E-9
          P1(I)=UL(1)*URN
          NUM=NUM*65539
          IF(NUM.LT.0) NUM=NUM+2147483647+1
          URN=NUM*0.465661E-9
          P2(I)=UL(2)*URN
          NUM=NUM*65539
          IF(NUM.LT.0) NUM=NUM+2147483647+1
          URN=NUM*0.465661E-9
          P3(I)=UL(3)*URN
          KB1(I)=1+INT(P1(I)/BL(1))
          KB2(I)=1+INT(P2(I)/BL(2))
          KB3(I)=1+INT(P3(I)/BL(3))
          IF(IN.NE.0) XR(I)=R
          RETURN
          END
```

```
C*********************************************************************
C     READS STORED RESULTS
C
        SUBROUTINE PAREAD
        REAL*4 JSR,JCOLL
        COMMON/PART/ D1(1000),D2(1000),D3(1000),P1(1000),P2(1000),
     *               P3(1000),KB1(1000),KB2(1000),KB3(1000),XR(1000),
     *               JSR(100),UL(3),BL(3),NUM
        COMMON/VALI/ N,R,DT,JCOLL,GA,ANF,RMAX,L1,L2,L3,DSK,DX,RMICRO
        REWIND 2
        READ(2)N,UL,R,DT,DIFF,P1,P2,P3,XR
        RETURN
        END
C*********************************************************************
C     COMPUTES SHEAR INDUCED DISPLACEMENT
C
        SUBROUTINE SHDISP
        REAL*4 JSR,JCOLL
        COMMON/PART/ D1(1000),D2(1000),D3(1000),P1(1000),P2(1000),
     *               P3(1000),KB1(1000),KB2(1000),KB3(1000),XR(1000),
     *               JSR(100),UL1,UL2,UL3,BL1,BL2,BL3,NUM
        COMMON/VALI/ N,R,DT,JCOLL,GA,ANF,RMAX,L1,L2,L3,DSK,DX,RMICRO
        DO 1 I=1,N
        IF(KB1(I).EQ.0) GO TO 1
        D1(I)=D1(I)+DT*GA*(P3(I)+0.5*D3(I))
    1   CONTINUE
        RETURN
        END
C*********************************************************************
C     UPDATES POSITIONS AND BOX-NUMBERS
C
        SUBROUTINE UPDATE(APTS,IT,MEFF,KR2,KR3,KR4,KR5)
        REAL*4 JSR,JCOLL
        COMMON/PART/ D1(1000),D2(1000),D3(1000),P1(1000),P2(1000),
     *               P3(1000),KB1(1000),KB2(1000),KB3(1000),XR(1000),
     *               JSR(100),UL1,UL2,UL3,BL1,BL2,BL3,NUM
        COMMON/VALI/ N,R,DT,JCOLL,GA,ANF,RMAX,L1,L2,L3,DSK,DX,RMICRO
        DO 1 I=1,N
        IF(KB1(I).EQ.0) GO TO 1
        P2(I)=P2(I)+D2(I)
        IF(P2(I).LE.0.0E+00) P2(I)=P2(I)+UL2
```

```
      IF(P2(I).GT.UL2) P2(I)=P2(I)-UL2
      P1(I)=P1(I)+D1(I)
      IF(P1(I).LE.0.0E+00) P1(I)=P1(I)+UL1
      IF(P1(I).GT.UL1) GO TO 2
      GO TO 9
8     P1(I)=P1(I)-UL1
9     P3(I)=P3(I)+D3(I)
      IF(P3(I).LE.0.1E-5) GO TO 7
      GO TO 3
7     NUM=NUM*65539
      IF(NUM.LT.0) NUM=NUM+2147483647+1
      URN=NUM*0.465661E-9
      P1(I)=UL1*URN
      NUM=NUM*65539
      IF(NUM.LT.0) NUM=NUM+2147483647+1
      URN=NUM*0.465661E-9
      P2(I)=UR2*URN
      F=-P3(I)
      IK=INT(F/UL3+1.E-5)
      P3(I)=P3(I)+(IK+1)*UL3
      GO TO 3
  2   IF(GA.LE.0.1E-05) GO TO 8
      NUM=NUM*65539
      IF(NUM.LT.0) NUM=NUM+2147483647+1
      URN=NUM*0.465661E-9
      P3(I)=UL3*SQRT(URN)
      P1(I)=DT*GA*P3(I)*(P1(I)-UL1)/D1(I)
  3   KB1(I)=1+INT(P1(I)/BL1)
      KB2(I)=1+INT(P2(I)/BL2)
      KB3(I)=1+INT(P3(I)/BL3)
  1   CONTINUE
      IF (APTS.LE.1.E-04) GO TO 4
      CALL PADD(APTS)
  4   XJC=JCOLL
      IN=0
      CALL CCOLL3(IN,MEFF,KR2,KR3,KR4,KR5,IT)
      XNJ=JCOLL-XJC
      JCOLL=XJC
      RETURN
      END
$
```

APPENDIX C

```
C COMPUTER PROGRAM FOR THE SIMULATION OF A RECTANGULAR SEDIMENTATION BASIN
C
C Solves the General Dynamic Equation (Ref: Valioulis, Ph.D. Thesis)
C using the sectional approximation to the particle size spectrum
C as developed by Gelbard and Seinfeld, 1980. The collision
C functions are appropriate for a flocculant suspension in water
C as described in Valioulis' Thesis, Chapter II. The time-integration
C is performed using Gear's subroutine on Caltech's IBM 370/3032.
C The arrays are dimensioned for 24 equal cells (settling tank partitions)
C and 21 particle size sections.
C
      DIMENSION Q(362),SOURCE(24),TOUT(2),DIAM(21),QEFFL(2000)
      COMMON/PHYSPT/AFLROV,VOLUME,EPS
      COMMON/TANK/BL1,BL2,UAVE,USTAR,UL1,UL2,SCOUR,FREQ
      COMMON/VELOC/U1,U2,U3,U4
      DATA TOUT/16200.E+00,18000.E+00/
C
      DATA IPRNT/4/
C
C Initialize parameters and flags
C IDISC: =0 for continuous input, =1 for discontinuous input (step
C        input), =2 for sinusoidal input with frequency FREQ)
C ISCOUR: =0 No scour
C NEWCOF: =0 Use coagulation coefficients from file, =12 Compute
C         new coagulation coefficients
C
      START=0.
      IDISC=0
      FREQ=0.
      ISCOUR=0
      NEWCOF=0
      TWAT=288.
C
C Set number of sections (M), minimum (Diam(1)) and maximum (Diam(M+1))
C particle diameter, length of tank (UL1), depth of tank (UL2),
C number of horizontal cells (NB1), number of vertical cells (NB2).
      M=15
      DIAM(1)=1.E-7
      DIAM(M+1)=1.E-3
      UL1=40.
      UL2=4.
      NB1=6
      NB2=3
```

```
C Logarithmic velocity profile: UAVE is the mean horizontal velocity
C and USTAR the shear velocity
      UAVE=0.0053
      USTAR=0.00055
C
C Check for scour
      IF(ISCOUR.LE.0) GO TO 53
      FROUDE=UAVE/(SQRT(9.81*UL2))
      COEFDI=3.59*EXP(58.5*FROUDE)
      SCOUR=1.17*(EXP(-8.05/COEFDI))
      GO TO 54
 53   SCOUR=0.
 54   CONTINUE
C
C Compute dimensions of cells
C
      BL1=UL1/NB1
      BL2=UL2/NB2
      VOLUME=BL1*BL2*1.
      AFLROV=1./BL2
C
C  Initialise mass concentrations
C  The mass concentations are stored in Q(MKS) in a sequential manner
C  so that IBOX=I+(J-1)*NB1 is the index of cell IBOX and
C  MKS=IBOX+(L-1)*KBOX is the mass concentration of section L in cell IBOX.
C  Q(MKBOX+1) is the mass concentration in the effluent.
C  Q(MKBOX+2) is the mass (per unit volume of tank) deposited.
C
      IFILE=0
      KBOX=NB1*NB2
      MKBOX=M*KBOX
      IF(IFILE.EQ.1) GO TO 509
      DO 1 I=1,MKBOX
    1 Q(I)=START
      GO TO 507
 509  DO 508 I=1,NB1
      DO 508 J=1,NB2
      IBOX=(J-1)*NB1+I
 508  READ(4,406,ERR=99) (Q((L-1)*KBOX+IBOX),L=1,M)
 406  FORMAT(5E15.10)
C
 507  Q(MKBOX+1)=0.
      Q(MKBOX+2)=0.
C
      TIME=0.
C
C Compute section boundaries
C
      DO 2 I=2,M
  2   DIAM(I)=DIAM(1)*(DIAM(M+1)/DIAM(1))**(FLOAT(I-1)/FLOAT(M))
C
      IF(IDISC.NE.1 .AND. IDISC.NE.2) GO TO 681
```

```
C  Discontinuous input
C  Request output every 100 sec
C
      HEXT=100.
      MAXTIM=INT(TOUT(4)/HEXT)
      ISTEP=4
      GO TO 682
C
C  Continuous input
 681  ISTEP=2
 682  IFLAG=1
C
C  Round is set for IBM 370/3032
      ROUND=5.E-7
C
C  Output initial parameters
C
      WRITE(IPRNT,60) M,NB1,NB2
 60   FORMAT(' NUMBER OF SECTIONS=',I3/' NUMBER OF BOXES: NB1=',I2,
     *1X,'NB2=',I2/)
      WRITE(IPRNT,61) UL1,UL2,BL1,BL2
 61   FORMAT(' TANK LENGTH=',F5.1,' TANK HEIGHT=',F5.1/' BOX LENGTH=
     *',F5.1,' BOX HEIGHT=',F5.1/)
      WRITE(IPRNT,62) UAVE,USTAR,SCOUR
 62   FORMAT(' AVERAGE VELOCITY=',F7.5,' SHEAR VELOCITY=',F7.5,
     *       ' SCOURING PAR.=',F7.5/)
      WRITE(IPRNT,610) TOUT(1),TOUT(2),TOUT(3),TOUT(4)
 610  FORMAT(' TIME STEPS=',4E12.4/)
      M1=M+1
      WRITE(IPRNT,63) (DIAM(I),I=1,M1)
 63   FORMAT(15X,'SECTION BOUNDARIES (DIAMETERS)'/(5E13.8))
      WRITE(IPRNT,64) START
 64   FORMAT(/' INITIAL MASS=',E13.8/)
      WRITE(IPRNT,65) TWAT,ROUND
 65   FORMAT(' WATER TEMPERATURE=',F5.1,' K',5X,'ROUND=',E13.8//)
C
C  Set parameter for turbulence induced coagulation
      EPS=1.
C
      IF(NEWCOF.EQ.12) WRITE(2,8) M,DIAM(1),DIAM(M+1)
8     FORMAT(' NUMBER OF SECTIONS=',I3,4X,' DIAM RANGE: ',E10.5,' - ',
     *E10.5/)
C*
      H=26.*ROUND
      SOUOLD=0.
```

```
C  Main loop
C
      DO 3 ITIME=1,ISTEP
      DELTIM=TOUT(ITIME)-TIME
      CALL SOR(NB1,NB2,ITIME,TIME,TOUT(ISTEP),SOURCE,FLOW,SMASS,IDISC)
      IF(SOURCE(1).NE.SOUOLD) GO TO 7
      GO TO 18
 7    DO 77 I=1,NB1
      DO 77 J=1,NB2
      IBOX=I+(J-1)*NB1
 77   WRITE(IPRNT,9)I,J,SOURCE(IBOX)
  9   FORMAT(10X,'BOX=',2I3,'  SOURCE=',E13.5,'KG/SEC')
      WRITE(IPRNT,91) FLOW,U1,U2,U3,U4
  91  FORMAT(//' FLOW RATE=',E10.4,' U1=',E10.4,' U2=',E10.4,
     *       ' U3=',E10.4,' U4=',E10.4)
      IFLAG=1
      SOUOLD=SOURCE(1)
 18   IF((TOUT(1)-16200.E+00).GT.10.E+00) GO TO 99
      CALL AERSL(M,NB1,NB2,TIME,DELTIM,Q,SOURCE,DIAM,ROUND,IPRNT,
     *IFLAG,NEWCOF,H,ITIME,SMASS,PERSUS,HEXT,IDISC,TOUT,QEFFL,FLOW)
      CALL PRAERO(Q,DIAM,DELTIM,TIME,VOLUME,M,NB1,NB2,IPRNT,SMASS,
     *FLOW,PERSUS,MAXTIM,IDISC,HEXT,TOUT(4),TOUT(2),QEFFL,SOURCE)
  3   CONTINUE
  99  STOP
      END
C**********************************************************************
      SUBROUTINE PRAERO(Q,DIAM,DELTIM,TIME,VOLUME,M,NB1,NB2,IPRNT,
     *SMASS,FLOW,PERSUS,MAXTIM,IDISC,HEXT,TIMEND,TDISIN,QEFFL,SOURCE)
C
C  This routine prints results every time step
C
      DIMENSION Q(362),QT(362),DIAM(21),QEFFL(2000),QINFL(2000),
     *SOURCE(24)
      COMMON/OUTX/DUM1(362),DUM2(362),DEPSIT(362),OUTMAS(362)
      COMMON/TANK/BL1,BL2,UAVE,USTAR,UL1,UL2,SCOUR,FREQ
      COMMON/RDEQU/RNUM(20),DNUM(20)
      COMMON/VELOC/U(4)
      COMMON/DISCO/SUMAX(20),SUMIN(20),TIMAX,TIMIN,TSRMAX,SSRMAX,
     *             TSRMIN,SSRMIN,QEFMAX,QEFMIN,OUTDIR,SINUS
      DATA TOTOUT,TOTDEP,DEPDIR/3*0.E+00/
```

```
      TIMEFF=HEXT
      IF(IDISC.EQ.0) TIMEFF=DELTIM
      IF((TIME+20.).LT.TIMEND .OR. IDISC.EQ.0) GO TO 101
      TDIS=0.
      MAX1=MAXTIM+1
      IF(IDISC.EQ.1) GO TO 108
      DO 120 L=1,MAX1
      SUM=0.
      DO 130 J=1,NB2
      IBOX=(J-1)*NB1+1
      TD=TDIS+FLOAT(L)*HEXT
  130 SUM=SUM+SOURCE(IBOX)*(1.+0.5*SIN(2.*3.14*FREQ*TD))
      SUM=SUM/FLOW
  120 WRITE(IPRNT,103) TD,QEFFL(L)
  103 FORMAT(' TIME=',F10.2,'  EFFLUENT CONC.=',E10.4,
     *'  INFLUENT CONC=',E10.4)
      DO 1200 L=1,MAX1
      SUM=0.
      DO 1300 J=1,NB2
      IBOX=(J-1)*NB1+1
      TD=TDIS+FLOAT(L)*HEXT
 1300 SUM=SUM+SOURCE(IBOX)*(1.+0.5*SIN(2.*3.14*FREQ*TD))
      SUM=SUM/FLOW
 1200 WRITE(3,406) TD,QEFFL(L),SUM
  406 FORMAT(3E15.10)
      GO TO 109
  108 DO 122 L=1,MAX1
      TD=TDIS+FLOAT(L)*HEXT
  122 WRITE(IPRNT,110) TD,QEFFL(L)
  110 FORMAT(' TIME=',F10.2,'  EFFLUENT CONC.=',E10.4)
  109 WRITE(IPRNT,104) TIMAX,TSRMAX,SSRMAX,TIMIN,TSRMIN,SSRMIN
  104 FORMAT(' TIME FOR MAX CONC=',F8.2,' % TS REMOVAL=',E10.4,
     *' % SS REMOVAL=',E10.4/' TIME FOR MIN CONC=',F8.2,
     *' % TS REMOVAL=',E10.4,' % SS REMOVAL=',E10.4//
     *' MAXIMUM CONC. (KG/M3)','   MINIMUM CONC. (KG/M3)'/)
C
      DO 105 L=1,M
  105 WRITE(IPRNT,106)SUMAX(L),SUMIN(L)
  106 FORMAT(5X,E10.4,10X,E10.4)
C
      WRITE(IPRNT,107)QEFMAX,QEFMIN
  107 FORMAT(' TOTAL MAX CONC.=',E10.4,'  TOTAL MIN CONC.=',E10.4)
```

```
 101  KBOX=NB1*NB2
      MKBOX=KBOX*M
C
      DO 100 I=1,MKBOX
      IF(OUTMAS(I).LE.0.0) OUTMAS(I)=0.
 100  IF(DEPSIT(I).LE.0.0) DEPSIT(I)=0.
C
      SUM=0.
      DO 1 L=1,M
      QT(L)=0.
      DO 2 I=1,NB1
      DO 2 J=1,NB2
      IBOX=NB1*(J-1)+I
   2  QT(L)=QT(L)+Q(IBOX+(L-1)*KBOX)
   1  SUM=SUM+QT(L)
C
      S1=SUM*VOLUME
      WRITE(IPRNT,312)TIME,S1
 312  FORMAT(1H1,20X,'TIME=',E10.5,' SEC'/20X,' TOTAL MASS=',E12.5,
     *' KG',//12X,'AVERAGE MASS, NUMBER AND VOL CONCENTRATIONS')
      WRITE(IPRNT,314)
 314  FORMAT(//12X,'DIAMETER RANGE (M)',8X,'KG/M3',4X,'#/CM3',
     *8X,'PPM'/)
      DO 313 I=1,M
      S1=QT(I)/KBOX
      S2=S1/(3.14/6.*RNUM(I)*DNUM(I)**3)*1.E-6
      S3=S1/RNUM(I)*1.E+6
 313  WRITE(IPRNT,3)DIAM(I),DIAM(I+1),S1,S2,S3
   3  FORMAT((10X,E10.4,' -',E10.4,E12.5,3X,E10.4,3X,E10.4)/)
C
      WRITE(IPRNT,36)
 36   FORMAT(/15X,' MASS IN EACH BOX'/)
      DO 4 I=1,NB1
      DO 4 J=1,NB2
      SUM=0.
      IBOX=NB1*(J-1)+I
      DO 5 L=1,M
 5    SUM=SUM+Q((L-1)*KBOX+IBOX)
      S1=SUM*VOLUME
 4    WRITE(IPRNT,6)SUM,S1,I,J
 6    FORMAT(10X,'TOTAL=',E13.4,'(KG/M3)',1X,E13.4,'KG',
     *'  BOX=',I2,1X,I2)
C
      WRITE(IPRNT,37)
 37   FORMAT(//10X,' MASS DISTRIBUTION ALONG THE TANK'/)
```

```
      DO 38 I=1,NB1
      TSREM=0.
      SSREM=0.
      SUM3=0.
      SUM4=0.
      DO 383 L=1,M
      SUM1=0.
      DO 381 J=1,NB2
      IBOX=NB1*(J-1)+I
      MKS=IBOX+(L-1)*KBOX
 381  SUM1=SUM1+Q(MKS)
      SUM2=SUM1/(3.14/6.*RNUM(L)*DNUM(L)**3)/NB2
      S1=SUM1/NB2
      TSREM=TSREM+S1
      IF(L.GE.5) SSREM=SSREM+S1
      S2=S1/RNUM(L)*1.E+6
      S3=SUM2*1.E-6
      WRITE(IPRNT,382) I,L,S1,S2,S3
 382  FORMAT(' POSIT=',I2,' SECTION=',I2,' MASS CONC=',E10.4,
     *' KG/M3',' VOL CONC=',E10.4,' PPM',' NUM CONC=',E10.4,' #/CM3'/)
      SUM3=SUM2+SUM3
 383  SUM4=SUM4+SUM1/NB2/RNUM(L)
      SUM=(6./3.14*SUM4/SUM3)**(1./3.)
      TSREM=1.-TSREM*FLOW/SMASS
      SSREM=1.-SSREM*FLOW/(SMASS*PERSUS)
  38  WRITE(IPRNT,384) SUM,TSREM,SSREM
 384  FORMAT(' EQUIVALENT DIAMETER=',E10.4,' % TS REMOVAL=',E10.4,
     *       ' %SS REMOVAL=',E10.4//)
C
C  Optional output for detailed information on particle size distribution
C  in the tank
C      WRITE(IPRNT,37)
C 37   FORMAT(//15X,' MASS DISTRIBUTION IN TANK'/)
C      DO 38 I=1,NB1
C      DO 38 J=1,NB2
C      IBOX=NB1*(J-1)+I
C      DO 38 L=1,M
C  38  WRITE(IPRNT,39) I,J,L,Q(KBOX*(L-1)+IBOX),Q(KBOX*(L-1)+IBOX)/
C     *                (3.14/6.*RNUM(L)*DNUM(L)**3)*1.E-6
C  39  FORMAT(' BOX=',2I3,' SECTION=',I3,' MASS CONC.=',E10.4,' KG/
C     *M3',  NUM CONC.=',E10.4,' #/CM3'/)
C
C  Compute total (approximate) mass concentration in deposits
C
      DEPTIM=0.
      DO 111 I=1,NB1
      DO 111 L=1,M
      MKS=KBOX*(L-1)+I
 111  DEPTIM=DEPTIM+DEPSIT(MKS)
      IF(DEPTIM.LT.1.E-15) GO TO 1110
      CORDEP=(Q(MKBOX+1)-DEPDIR)/DEPTIM
 1110 TOTDEP=TOTDEP+DEPTIM
```

```
C  Compute total (approximate) mass concentration in effluent
C
      SUM2=0.
      DO 112 J=1,NB2
      IBOX=NB1*(J-1)+NB1
      DO 112 L=1,M
      MKS=KBOX*(L-1)+IBOX
 112  SUM2=SUM2+OUTMAS(MKS)
      IF(SUM2.LT.1.E-12) GO TO 1120
      COROUT=(Q(MKBOX+2)-OUTDIR)/SUM2
 1120 TOTOUT=TOTOUT+SUM2
C
C  Output deposited mass
C
      S1=Q(MKBOX+1)*VOLUME
      S2=DEPTIM*CORDEP*VOLUME
      WRITE(IPRNT,22)  S1,S2
 22   FORMAT(//'  CUMULATIVE DEPOSITED MASS=',E12.4,' KG'/,
     *        '  DEPOSITED MASS FOR THE TIME STEP=',E12.4,' KG'//)
C
C  Output deposition rates during last time step
C
      IF(DEPTIM.LT.1.E-15) GO TO 1111
      J=1
      DO 11 I=1,NB1
      SUM1=0.
      SUM=0.
      DO 16 L=1,M
      MKS=KBOX*(L-1)+I
      SUM1=SUM1+DEPSIT(MKS)/RNUM(L)
 16   SUM=SUM+DEPSIT(MKS)
      S1=SUM*CORDEP/DELTIM
      S2=SUM1*CORDEP/DELTIM*1.E+6
      WRITE(IPRNT,13) I,J,S1,S2
 13   FORMAT('  BOX',I3,1X,I3,' MASS DEP RATE=',E13.4,' KG/(M3-SEC)',
     *       ' VOLUME DEP RATE=',E13.4,' #/(CM3-SEC)'/)
 11   CONTINUE
C*
C      WRITE(IPRNT,21)
C 21   FORMAT(/8X,'  DEPOSITION RATES FROM BOXES'/)
C
C      DO 12 I=1,NB1
C      DO 12 L=1,M
C      MKS=KBOX*(L-1)+I
C      SUM=DEPSIT(MKS)/(3.14/6*RNUM(L)*DNUM(L)**3)/DELTIM
C  12  WRITE(IPRNT,14) I,J,L,DEPSIT(MKS)*CORDEP/DELTIM,SUM*CORDEP*1.E-6
C  14  FORMAT('  BOX=',2I3,' SECTION=',I2,'  MASS DEP. RATE=',E10.5,
C     *' KG/M3-SEC',' NUM DEP. RATE=',E10.4,' #/CM3-SEC')
```

```
      WRITE (IPRNT,19)
   19 FORMAT(/12X,'AVERAGE DEPOSITION RATES'/)
      DO 17 L=1,M
      SUM=0.
      DO 18 I=1,NB1
      MKS=KBOX*(L-1)+I
   18 SUM=SUM+DEPSIT(MKS)/DELTIM*CORDEP
      SUM3=SUM/(3.14/6.*RNUM(L)*DNUM(L)**3)/NB1*1.E-6
      S1=SUM/NB1
      S2=S1/RNUM(L)*1.E+6
   17 WRITE(IPRNT,20) L,S1,S2,SUM3
   20 FORMAT(' SECTION=',I3,' MASS DEP RATE=',E10.4,' KG/M3-SEC',
     *' VOL DEP RATE=',E10.4,' PPM-SEC',' NUM DEP RATE=',E10.4,
     *'#/CM3-SEC'/)
C
C  Output effluent mass
C
 1111 S1=Q(MKBOX+2)*VOLUME
      S2=SUM2*COROUT*VOLUME
      WRITE(IPRNT,23) S1,S2
   23 FORMAT(//' CUMULATIVE MASS IN EFFLUENT=',E12.4,' KG'/,
     *       ' EFFLUENT MASS FOR THE TIME STEP=',E12.4,' KG'//)
C
      I=NB1
      DO 24 J=1,NB2
      SUM=0.
      DO 25 L=1,M
      MKS=KBOX*(L-1)+J*NB1
   25 SUM=SUM+OUTMAS(MKS)
      S1=SUM*COROUT/(U(J)*BL2*TIMEFF)*VOLUME
C
   24 WRITE(IPRNT,26) I,J,S1
   26 FORMAT(' BOX=',2I3,' EFFLUENT CONC.=',E10.4,' KG/M3'/)
C
C  Optional output for detailed information on effluent particle size
C  distribution
C      WRITE(IPRNT,27)
C 27   FORMAT(//9X,' MASS DISTRIBUTION IN EFFLUENT FROM EACH BOX'/)
C      DO 28 J=1,NB2
C      DO 28 L=1,M
C      MKS=KBOX*(L-1)+J*NB1
C      SUM3=VOLUME/(U(J)*L2*TIMEFF)
C      SUM=OUTMAS(MKS)/(3.14/6.*RNUM(L)*DNUM(L)**3)*SUM3
C      S1=OUTMAS(MKS)*COROUT*SUM3
C      S2=SUM*COROUT*1.E-6
C  28  WRITE(IPRNT,29) I,J,L,S1,S2
C  29  FORMAT(' BOX=',2I3,' SECTION=',I3,' MASS CONC=',E10.4,' KG/M3',
C     *' NUM CONC=',E10.4,' #/CM3'/)
C
      IF(S2.LT.1.E-15) GO TO 1112
```

```
      WRITE(IPRNT,30)
   30 FORMAT(//9X,' AVERAGE MASS CONC. IN EFFLUENT FROM TANK'/)
      TSREM=0.
      SSREM=0.
      SUM5=0.
      SUM7=0.
      DO 31 L=1,M
      SUM=0.
      DO 32 J=1,NB2
      MKS=KBOX*(L-1)+J*NB1
      SUM4=VOLUME/(U(J)*BL2*TIMEFF*NB2)*COROUT
      SUM9=SUM9+OUTMAS(MKS)
   32 SUM=SUM+OUTMAS(MKS)*SUM4
      TSREM=TSREM+SUM
      IF(L.GE.5) SSREM=SSREM+SUM
      SUM3=SUM/(3.14/6*RNUM(L)*DNUM(L)**3)*1.E-6
      SUM7=SUM7+SUM3
      SUM6=SUM/RNUM(L)
      SUM5=SUM5+SUM6
      S1=SUM6*1.E+6
   31 WRITE(IPRNT,33) L,SUM,S1,SUM3
   33 FORMAT(' SECTION=',I3,' MASS CONC=',E10.4,' KG/M3',
     *' VOL CONC=',E10.4,' PPM',' NUM CONC=',E10.4,' #/CM3'//)
      SUM=(6./3.14*SUM5/SUM7)**(1./3.)
      S1=SUM5*1.E+6
      TSREM=1.-TSREM*FLOW/SMASS
      SSREM=1.-SSREM*FLOW/(SMASS*PERSUS)
      WRITE(IPRNT,42) S1,SUM,TSREM,SSREM
 42   FORMAT(' TOTAL VOLUMETRIC CONC IN EFFLUENT=',E10.4,' PPM'/,
     *       ' EQUIVALENT DIAMETER=',E10.4,' M','   % TS REMOVAL=',
     *       E10.4,' % SS REMOVAL=',E10.4//////)
C
C  Initialise effluent and deposition parameters
C
 1112 DO 41 I=1,NB1
      DO 41 J=1,NB2
      IBOX=NB1*(J-1)+I
      DO 41 L=1,M
      MKS=(L-1)*KBOX+IBOX
      DEPSIT(MKS)=0.
   41 OUTMAS(MKS)=0.
C
C  Store cumulative deposited and effluent mass concentrations
C
      OUTDIR=Q(MKBOX+2)
      DEPDIR=Q(MKBOX+1)
C
      RETURN
   99 STOP
      END
```

```
C*****************************************************************
      SUBROUTINE AERSL(M,NB1,NB2,TIME,DELTIM,Q,SOURCE,DIAM,ROUND,
     *IPRNT,IFLAG,NEWCOF,H,ITIME,SMASS,PERSUS,HEXT,IDISC,TOUT,QEFFL,
     *FLOW)
C
C  This routine calls COEF, to compute the coagulation coefficients,
C  and then GEAR for the time integration
C
      DIMENSION Q(362),SOURCE(24),WORK(90000),IWORK(362),DIAM(21),
     *V(21),QT(24),X(21),TOUT(4),QEFFL(2000)
      COMMON/AVGCOF/COEFAV(781,24),SRATE(362),MPASS,KPAS1,KPAS2,NB2A,
     *NB2B,NB3,NB4,NDEPST
      COMMON/PHYSPT/AFLROV,VOLUME
      COMMON/RDEQU/RNUM(20),DNUM(20)
      COMMON/OUTX/DUM1(362),DUM2(362),DUM3(362),OUTMAS(362)
      COMMON/VELOC/U(4)
      COMMON/DISCO/SUMAX(20),SUMIN(20),TIMAX,TIMIN,TSRMAX,SSRMAX,
     *             TSRMIN,SSRMIN,QEFMAX,QEFMIN,QSTORE,SINUS
      COMMON/TANK/BL1,BL2,UAVE,USTAR,UL1,UL2,SCOUR,FREQ
      EXTERNAL DIFFUN
      DATA JTIME/0/
      DATA SINOLD,SINNEW/2*0.E+00/
C
      KBOX=NB1*NB2
      MKBOX=M*KBOX
C
C  Set pointers
C
      MPASS=M
      KPAS1=NB1
      KPAS2=NB2
      NB2A=((M-2)*(M-1))/2
      NB2B=((M-1)*M)/2+NB2A
      NB3=NB2B+((M-1)*M)/2
      NB4=NB3+M
      NDEPST=NB4+((M-1)*M)/2
      NUMCOF=NDEPST+M
      MP1=M+1
C
      IF((TOUT(1)-16200.E+00).GT.10.E+00) GO TO 100
      IF(NEWCOF.LT.0) GO TO 1
```

```
C  Compute the geometric means of the diameters and the densities
C  of the boundaries of the particle size spectrum
C
      V(1)=0.
      CALL RHODD(V(1),DIAM(1),RHO)
      R1=RHO
      DO 18 I=2,MP1
      V(I)=0.
      CALL RHODD(V(I),DIAM(I),RHO)
      RNUM(I-1)=SQRT(R1*RHO)
      R1=RHO
      DNUM(I-1)=SQRT(DIAM(I-1)*DIAM(I))
  18  CONTINUE
C
C  Compute coagulation coefficients
C
      IF(NEWCOF.EQ.0) GO TO 777
C
      CALL COEF(NEWCOF,M,V,ROUND,IPRNT)
      DO 20 I=1,NB1
      DO 20 J=1,NB2
      IBOX=NB1*(J-1)+I
      DO 20 K=1,NUMCOF
      COEFAV(K,IBOX)=COEFAV(K,1)
   20 CONTINUE
      WRITE(2,300) (COEFAV(K,1),K=1,NUMCOF)
 300  FORMAT(5E15.8)
      GO TO 100
 777  DO 303 I=1,NB1
      DO 303 J=1,NB2
      IBOX=NB1*(J-1)+I
      READ(3,300) (COEFAV(L,IBOX),L=1,NUMCOF)
 303  CONTINUE
C
      NEWCOF=12
C
  1   NEWCOF=-IABS(NEWCOF)
C
C  Fractionate the input mass
C
      CALL DIVIDE(M,NB1,NB2,VOLUME,SOURCE,SRATE,DIAM,IPRNT,ITIME,
     *            PERSUS)
```

```
C  Set parameters for the integration subroutine
C
      REL=.001E+00
      METH=1
      MITER=2
      MKBOX2=MKBOX+2
C
      TEND=TIME+DELTIM
C
C  Check for type of input
C
      IF(IDISC.NE.1 .AND. IDISC.NE.2) GO TO 6
      PROD=VOLUME/(FLOW*HEXT)
      TEND=TIME+HEXT
C
 7    QSTORE=Q(MKBOX2)
      SINOLD=SINNEW
      DO 120 I=1,MKBOX
 120  OUTMAS(I)=0.
      CALL DGEAR(MKBOX2,DIFFUN,FCNJ,TIME,H,Q,TEND,REL,METH,MITER,
     *IFLAG,IWORK,WORK,IER,COEFAV,NDEPST,M,NB1,NB2,NSTEP,NFE,SCOUR)
C
      IF(IFLAG.NE.2 .AND. IFLAG.NE.0) GO TO 8
      TEND=TIME+HEXT
C
C  Optional for sinusoidal input
C     IF((TIME+1.E-2).LT.TOUT(2)) GO TO 11
C     SINNEW=1.+0.5*SIN(2.*3.14*TIME*FREQ)
C     SINUS=0.5*(SINNEW+SINOLD)
C      PROD1=PROD/SINUS
      PROD1=PROD
      JTIME=JTIME+1
      QEFFL(JTIME+1)=(Q(MKBOX2)-QSTORE)*PROD1
      IF((TIME+5.).LT.TOUT(2)) GO TO 11
      IF(QEFFL(JTIME+1).GT.QEFMAX)GO TO 9
      IF(QEFFL(JTIME+1).LT.QEFMIN)GO TO 10
      GO TO 11
```

```
C  Determine maximum and minimum mass concentrations in effluent
C
  9    OUTALL=0.
       DO 12 J=1,NB2
       IBOX=NB1*(J-1)+NB1
       DO 12 L=1,M
       MKS=KBOX*(L-1)+IBOX
       IF(OUTMAS(MKS).LT.0.) OUTMAS(MKS)=0.
 12    OUTALL=OUTALL+OUTMAS(MKS)
       IF(OUTALL.LT.1.E-15) GO TO 11
       COROUT=(Q(MKBOX2)-QSTORE)/OUTALL
       TSREM=0.
       SSREM=0.
       SUM5=0.
       SUM7=0.
       DO 13 L=1,M
       SUMAX(L)=0.
       DO 14 J=1,NB2
       MKS=KBOX*(L-1)+J*NB1
       SUM4=VOLUME/(U(J)*BL2*HEXT*NB2)*COROUT
 14    SUMAX(L)=SUMAX(L)+OUTMAS(MKS)*SUM4
       TSREM=TSREM+SUMAX(L)
       IF(L.GE.5) SSREM=SSREM+SUMAX(L)
       SUM3=SUMAX(L)/(3.14/6*RNUM(L)*DNUM(L)**3)
       SUM7=SUM7+SUM3
       SUM6=SUMAX(L)/RNUM(L)
 13    SUM5=SUM5+SUM6
C
       SUM=(6./3.14*SUM5/SUM7)**(1./3.)
       TSRMAX=1.-TSREM*FLOW/SMASS
       SSRMAX=1.-SSREM*FLOW/(SMASS*PERSUS)
       TIMAX=TEND
       QEFMAX=QEFFL(JTIME+1)
       GO TO 11
  10   OUTALL=0.
       DO 15 J=1,NB2
       IBOX=NB1*(J-1)+NB1
       DO 15 L=1,M
       MKS=KBOX*(L-1)+IBOX
       IF(OUTMAS(MKS).LT.0.) OUTMAS(MKS)=0.
 15    OUTALL=OUTALL+OUTMAS(MKS)
       IF(OUTALL.LT.1.E-15) GO TO 11
       COROUT=(Q(MKBOX2)-QSTORE)/OUTALL
       TSREM=0.
       SSREM=0.
       SUM5=0.
       SUM7=0.
```

```
      DO 16 L=1,M
      SUMIN(L)=0.
      DO 17 J=1,NB2
      MKS=KBOX*(L-1)+J*NB1
      SUM4=VOLUME/(U(J)*BL2*HEXT*NB2)*COROUT
 17   SUMIN(L)=SUMIN(L)+OUTMAS(MKS)*SUM4
      TSREM=TSREM+SUMIN(L)
      IF(L.GE.5) SSREM=SSREM+SUMIN(L)
      SUM3=SUMIN(L)/(3.14/6*RNUM(L)*DNUM(L)**3)
      SUM7=SUM7+SUM3
      SUM6=SUMIN(L)/RNUM(L)
 16   SUM5=SUM5+SUM6
C
      SUM=(6./3.14*SUM5/SUM7)**(1./3.)
      TSRMIN=1.-TSREM*FLOW/SMASS
      SSRMIN=1.-SSREM*FLOW/(SMASS*PERSUS)
      TIMIN=TEND
      QEFMIN=QEFFL(JTIME+1)
C
 11   IF(TEND.GT.(1.+1.E-4)*TOUT(ITIME)) GO TO 200
      GO TO 7
C
C  Continuous input
C
 6    CALL DGEAR(MKBOX2,DIFFUN,FCNJ,TIME,H,Q,TEND,REL,METH,MITER,
     *IFLAG,IWORK,WORK,IER,COEFAV,NDEPST,M,NB1,NB2,NSTEP,NFE,SCOUR)
      QEFFL(1)=Q(MKBOX2)*VOLUME/(FLOW*TIME)
C
      IF(IFLAG.EQ.2.OR.IFLAG.EQ.0.OR.IFLAG.EQ.3)RETURN
   8  WRITE(IPRNT,27)IER,TIME
   27 FORMAT(' GEAR ERROR NUMBER',I4,3X,
     *  3X,'TIME REACHED =',E11.4)
      WRITE(IPRNT,29)(Q(I),I=1,MKBOX2)
  29  FORMAT(' VALUES OF Q ARRAY'/(5E15.4))
 100  STOP
      END
C*****************************************************************
      SUBROUTINE COEF(NEWCOF,M,V,ROUND,IPRNT)
C
C  This routine computes the sectional coagulation coefficients
C  (Gelbard and Seinfeld, 1980)
C
      DIMENSION V(21),X(21),DEL(20)
      COMMON/AVGCOF/COEFAV(781,24),SRATE(362),MPASS,NB1,NB2,NB2A,
     *NB2B,NB3,NB4,NDEPST
      EXTERNAL DEPOST,BETCAL
```

```
C
      MM1=M-1
      MP1=M+1
      DO 10 I=1,MP1
      X1=V(I)
 10   X(I)=ALOG(X1)
C
      DO 2 L=1,M
 2    DEL(L)=X(L+1)-X(L)
      REL=5.E-3
      ABSER=1.E-20
      TWAT=288.
C
C
C
C
C     NBTYPE = TYPE OF COEFFICIENT CALCULATED
C     INNER  = 0 INNER LIMITS OF INTEGRATION ARE CONSTANT
C              1 CHANGE LOWER INNER LIMIT OF INTEGRATION TO
C                ALOG(BASESZ-OUTER INTEGRATION VARIABLE). IN THIS
C                CASE FIXSZ IS THE INNER UPPER LIMIT OF INTEGRATION.
C              2 CHANGE UPPER LIMIT OF INTEGRATION TO
C                ALOG(BASESZ-OUTER INTEGRATION VARIABLE). IN THIS
C                CASE FIXSZ IS THE INNER LOWER LIMIT OF INTEGRATION.
C
C
C
C
C       CALCULATE BETA(SUPER-1B,SUB-I,L-1,L)
C       STORE WITH I VARYING FIRST FROM 1 TO L-2
C
      IBOX=1
C
C
C
      NBTYPE=1
      INNER=1
      DO 13 L=3,M
      LM2=L-2
      LIBEF=(LM2*(L-3))/2
      DO 13 I=1,LM2
      IER=1
      BASESZ=V(L)
      FIXSZ=X(L)
      CALL GAUSBT(BETCAL,X(I),X(I+1),REL,ABSER,ROUND,ANS,IER,IPRNT,
     *FIXSZ,BASESZ,INNER,TWAT,NBTYPE)
      IF(IER.NE.0)GO TO 31
 13   COEFAV(I+LIBEF,IBOX)=ANS/(DEL(I)*(X(L)-X(L-1)))
```

```
C       CALCULATE BETA(SUPER-2A,SUB-I,L) AND BETA(SUPER-2B,SUB-I,L)
C       STORE WITH I VARYING FIRST FROM 1 TO L-1
C
      DO 14 L=2,M
      LM1=L-1
      LIBEF=(LM1*(L-2))/2
      DO 14 I=1,LM1
      NBTYPE=2
      IER=1
      INNER=1
      BASESZ=V(L+1)
      FIXSZ=X(L+1)
      CALL GAUSBT(BETCAL,X(I),X(I+1),REL,ABSER,ROUND,ANS,IER,IPRNT,
     *FIXSZ,BASESZ,INNER,TWAT,NBTYPE)
      IF(IER.NE.0)GO TO 31
      COEFAV(NB2A+I+LIBEF,IBOX)=ANS/(DEL(I)*DEL(L))
      NBTYPE=3
      IER=1
      INNER=2
      BASESZ=V(L+1)
      FIXSZ=X(L)
      CALL GAUSBT(BETCAL,X(I),X(I+1),REL,ABSER,ROUND,ANS,IER,IPRNT,
     *FIXSZ,BASESZ,INNER,TWAT,NBTYPE)
      IF(IER.NE.0)GO TO 31
   14 COEFAV(NB2B+I+LIBEF,IBOX)=ANS/(DEL(I)*DEL(L))
C
C       CALCULATE BETA(SUPER-3,SUB-L,L)
C
      DO 15 L=1,M
      LP1=L+1
      NBTYPE=4
      IER=1
      INNER=1
      REL=1.E-2
      BASESZ=V(LP1)
      FIXSZ=X(LP1)
      ALV=V(LP1)
      ALV=ALOG(.5*ALV)
      CALL GAUSBT(BETCAL,X(L),ALV,REL,ABSER,ROUND,ANS,IER,IPRNT,
     *FIXSZ,BASESZ,INNER,TWAT,NBTYPE)
      IF(IER.NE.0)GO TO 31
C
      IER=1
      COEFAV(NB3+L,IBOX)=ANS
      NBTYPE=4
      INNER=1
      ALV2=V(LP1)-V(L)
      ALV2=ALOG(ALV2)
      BASESZ=V(LP1)
      FIXSZ=X(LP1)
      CALL GAUSBT(BETCAL,ALV,ALV2,REL,ABSER,ROUND,ANS,IER,IPRNT,
     *FIXSZ,BASESZ,INNER,TWAT,NBTYPE)
```

```
      IF(IER.NE.0)GO TO 31
      COEFAV(NB3+L,IBOX)=ANS+COEFAV(NB3+L,IBOX)
C
      IER=1
      NBTYPE=5
      INNER=0
      BASESZ=X(L)
      FIXSZ=X(LP1)
      CALL GAUSBT(BETCAL,ALV2,X(LP1),REL,ABSER,ROUND,ANS,IER,IPRNT,
     *FIXSZ,BASESZ,INNER,TWAT,NBTYPE)
      ANS=ANS+COEFAV(NB3+L,IBOX)
      IF(IER.NE.0)GO TO 31
   15 COEFAV(NB3+L,IBOX)=.5*ANS/DEL(L)**2
C
C       DETERMINE THE SECTIONAL COAGULATION COEFFICIENTS FOR
C       SCAVENGING OF PARTICLES IN SECTION L BY THOSE IN SECTION I
C       I.E. BETA(SUPER-4,SUB-I,L)
C       STORE WITH I VARYING FIRST FROM L+1 TO M
C
C
      NBTYPE=6
      INNER=0
      DO 12 L=1,MM1
      LP1=L+1
      NBEFR=((L-1)*(2*M-L))/2
      DO 12 I=LP1,M
      INNER=0
      BASESZ=X(L)
      FIXSZ=X(LP1)
      CALL GAUSBT(BETCAL,X(I),X(I+1),REL,ABSER,ROUND,ANS,IER,IPRNT,
     *FIXSZ,BASESZ,INNER,TWAT,NBTYPE)
      IF(IER.NE.0)GO TO 31
   12 COEFAV(NB4+I-L+NBEFR,IBOX)=ANS/(DEL(I)*DEL(L))
C
C       DETERMINE THE SECTIONAL DEPOSITION COEFFICIENTS OF THE L-TH
C       SECTION ON THE J-TH DEPOSITION SURFACE
C
      REL=1.E-3
      DO 1 L=1,M
      NBTYPE=7
      IER=1
      CALL GAUS2(DEPOST,X(L),X(L+1),REL,ABSER,ROUND,ANS,IER,DUM,TWAT,
     *NBTYPE)
      IF(IER.NE.0)GO TO 31
 1    COEFAV(NDEPST+L,IBOX)=ANS/DEL(L)
C
C
      RETURN
C
C
 31   WRITE(IPRNT,3)IER,NBTYPE
  3   FORMAT(//' OUTER INTEGRATION ERROR NUMBER',I3,
     *'   FOR COEFFICIENT TYPE',I3)
      STOP
      END
```

```
C*****************************************************************
      SUBROUTINE DIFFUN(MKBOX2,TIME,Q,DQDT)
C
C  This routine calculates the time derivatives of the General
C  Dynamic Equation

      DIMENSION Q(MKBOX2),DQDT(MKBOX2)
      COMMON/AVGCOF/COEFAV(781,24),SRATE(362),M,NB1,NB2,NB2A,
     *NB2B,NB3,NB4,NDEPST
      COMMON/VELOC/U(4)
      COMMON/TANK/BL1,BL2,UAVE,USTAR,UL1,UL2,SCOUR,FREQ,ADIS
      COMMON/OUTX/OUTMAS(362),DEPTUB(362),DEPSIT(362),DUM(362)
C
C
      KBOX=NB1*NB2
      MKBOX=MKBOX2-2
C
      DO 3 L=1,M
      LM1=L-1
      LM2=L-2
      LM1KBF=LM1*KBOX
      LM2KBF=LM2*KBOX
      L1BF=((L-3)*LM2)/2
      L2BF=(LM1*LM2)/2
C
C  Coagulation
C
      DO 3 I=1,NB1
      DO 3 J=1,NB2
      K=NB1*(J-1)+I
      SUM=0.
      IF(L.LT.3)GO TO 4
      DO 5 N=1,LM2
      NL=(N-1)*KBOX+K
    5 SUM=SUM+Q(KBOX*(N-1)+K)*(COEFAV(NB2A+N+L1BF,K)*Q(K+LM2KBF)
     *  -COEFAV(NB2A+N+L2BF,K)*Q(K+LM1KBF))
     *  +Q(KBOX*(N-1)+K)*(COEFAV(N+L1BF,K)*Q((LM1-1)*KBOX+K)
     *  +COEFAV(NB2B+N+L2BF,K)*Q((L-1)*KBOX+K))
    4 IF(L.GT.1)SUM=SUM+Q((LM1-1)*KBOX+K)*(COEFAV(NB3+LM1,K)*Q(K+LM2KBF)
     *  -COEFAV(NB2A+LM1+L2BF,K)*Q(K+LM1KBF))
     *  + COEFAV(NB2B+LM1+L2BF,K)*Q((L-1)*KBOX+K)*Q(K+LM2KBF)
      DQDT(K+LM1KBF)=SUM-COEFAV(NB3+L,K)*Q((L-1)*KBOX+K)*Q(K+LM1KBF)
  3   CONTINUE
```

```
C  Removal rate from a section due to scavenging by higher sections
C
      MM1=M-1
      DO 6 I=1,NB1
      DO 6 J=1,NB2
      K=NB1*(J-1)+I
      DO 6 L=1,MM1
      LM1=L-1
      LM1KBF=LM1*KBOX
      LBF=(LM1*(2*M-L))/2
      SUM=0.
      LP1=L+1
      DO 7 N=LP1,M
    7 SUM=SUM+COEFAV(NB4+N-L+LBF,K)*Q((N-1)*KBOX+K)
      DQDT(K+LM1KBF)=DQDT(K+LM1KBF)-SUM*Q(K+LM1KBF)
    6 CONTINUE
C
C
C  Spatial sources and sinks of particle mass
C
      SINUS=1.+0.5*SIN(2*3.14*TIME*FREQ)
C
      DO 8 L=1,M
      DO 8 I=1,NB1
      DO 8 J=1,NB2
      K=NB1*(J-1)+I
      MKS=K+(L-1)*KBOX
      DQDT(MKS)=DQDT(MKS)+SRATE(MKS)*SINUS
     *          -COEFAV(L+NDEPST,K)*Q(MKS)
  8   CONTINUE
C
C  Correct for adjacent cells
C
C      1. Settling
C
      NB22=NB2-1
      DO 9 I=1,NB1
      DO 9 J=1,NB22
      K=NB1*(J-1)+I
      DO 9 L=1,M
      MKS=K+(L-1)*KBOX
      DQDT(MKS)=DQDT(MKS)+COEFAV(L+NDEPST,K)*Q(MKS+NB1)
 9    CONTINUE
```

```
      SIG=0.
      J=1
      DO 90 I=1,NB1
      K=NB1*(J-1)+I
      DO 90 L=1,M
      MKS=K+(L-1)*KBOX
C
C  Scouring
C
      DEPTUB(MKS)=-COEFAV(L+NDEPST,K)*Q(MKS)*SCOUR
      DQDT(MKS)=DQDT(MKS)-DEPTUB(MKS)
      SIG=SIG+COEFAV(L+NDEPST,K)*Q(MKS)+DEPTUB(MKS)
   90 DEPTUB(MKS)=0.
      DQDT(MKBOX+1)=SIG
C
C       2. Advection
C
      SUM=0.
      DO 10 I=2,NB1
      DO 10 J=1,NB2
      IBOX=NB1*(J-1)+I
      DO 10 L=1,M
      MKS=IBOX+(L-1)*KBOX
      OUTMAS(MKS)=0.
      DQDT(MKS)=DQDT(MKS)+(Q(MKS-1)-Q(MKS))*U(J)/BL1*SINUS
C
C  Compute the rate (kg/(sec-m3)) at which mass leaves the tank
C
      IF(I.EQ.NB1) OUTMAS(MKS)=U(J)*Q(MKS)/BL1
   10 SUM=SUM+OUTMAS(MKS)
      DQDT(MKBOX2)=SUM
C
C  For the first column of cells
C
      I=1
      DO 12 J=1,NB2
      IBOX=NB1*(J-1)+I
      DO 12 L=1,M
      MKS=IBOX+(L-1)*KBOX
      DQDT(MKS)=DQDT(MKS)-U(J)*Q(MKS)/BL1*SINUS
12    CONTINUE
C
C       3. Vertical turbulent mixing
C
      IF(NB22.LT.2) GO TO 19
      DO 13 I=1,NB1
      DO 13 J=2,NB22
      Z1=(J-1)*BL2
      Z2=J*BL2
      TUDIF1=0.3*USTAR*Z1*(1.-Z1/UL2)*ADIS*SINUS
      TUDIF2=0.3*USTAR*Z2*(1.-Z2/UL2)*ADIS*SINUS
```

```
      IBOX=(J-1)*NB1+I
      DO 13 L=1,M
      MKS=IBOX+(L-1)*KBOX
      DQDT(MKS)=DQDT(MKS)-((Q(MKS)-Q(MKS+NB1))*TUDIF2+
     *          (Q(MKS)-Q(MKS-NB1))*TUDIF1)/(BL2**2)
 13   CONTINUE
C
C  For the lowest (first) row of cells
C
  19  J=1
      Z=BL2
      TUDIF=0.3*USTAR*Z*(1.-Z/UL2)*ADIS*SINUS
      SIG=0.
      DO 14 I=1,NB1
      IBOX=NB1*(J-1)+I
      DO 14 L=1,M
      MKS=IBOX+(L-1)*KBOX
      DQDT(MKS)=DQDT(MKS)-(Q(MKS)-Q(MKS+NB1))*TUDIF/BL2**2
  14  CONTINUE
C
C  For the upper (last) row of cells
C
      J=NB2
      Z=(J-1)*BL2
      TUDIF=0.3*USTAR*Z*(1.-Z/UL2)*ADIS*SINUS
      DO 15 I=1,NB1
      IBOX=(J-1)*NB1+I
      DO 15 L=1,M
      MKS=IBOX+(L-1)*KBOX
      DQDT(MKS)=DQDT(MKS)-(Q(MKS)-Q(MKS-NB1))*TUDIFZ/BL2**2
 15   CONTINUE
C
      RETURN
      END
C*********************************************************************
      SUBROUTINE FCNJ(N,X,Y,PD)
      INTEGER N
      REAL Y(N),PD(N,N),X
      RETURN
      END
C*********************************************************************
      BLOCK DATA
      COMMON/OUTX/OUTMAS(362),DEPTUB(362),DEPSIT(362),OUT(362)
      COMMON/DISCO/SUMAX(20),SUMIN(20),TIMAX,TIMIN,TSRMAX,SSRMAX,
     *             TSRMIN,SSRMIN,QEFMAX,QEFMIN,QSTORE,SINUS
      DATA QSTORE,QEFMAX,QEFMIN,SINUS/0.,0.,100.,0./
      DATA OUT,DEPSIT/724*0.E+00/
      END
```

```
C***********************************************************************
C
      SUBROUTINE DGEAR  (N,FCN,FCNJ,X,H,Y,XEND,TOL,METH,MITER,INDEX,
     1                   IWK,WK,IER,COEFAV,NDEPST,MSECT,NB1,NB2,
     2                   NNSTEP,NNFE,SCOUR)
C                                 SPECIFICATIONS FOR ARGUMENTS
      INTEGER           N,METH,MITER,INDEX,IWK(1),IER
      REAL              X,H,Y(N),XEND,TOL,WK(1)
C                                 SPECIFICATIONS FOR LOCAL VARIABLES
      INTEGER           NERROR,NSAVE1,NSAVE2,NPW,NY,NC,MFC,KFLAG,
     1                  JSTART,NSQ,NQUSED,NSTEP,NFE,NJE,I,NO,NHCUT,KGO,
     2                  JER,KER,NN,NEQUIL,IDUMMY(21),NLC,NUC
      REAL              SDUMMY(4)
      REAL              T,HH,HMIN,HMAX,EPSC,UROUND,EPSJ,HUSED,TOUTP,
     1                  AYI,D,DN,SEPS,DUMMY(39)
C
      INTEGER NDEPST,MSECT,NB1,NB2
      REAL COEFAV(781,24),YOLD(362),DEPOLD(362)
C
      EXTERNAL          FCN,FCNJ
      COMMON /DBAND/    NLC,NUC
      COMMON /GEAR/     T,HH,HMIN,HMAX,EPSC,UROUND,EPSJ,HUSED,DUMMY,
     1                  TOUTP,SDUMMY,NC,MFC,KFLAG,JSTART,NSQ,NQUSED,
     2                  NSTEP,NFE,NJE,NPW,NERROR,NSAVE1,NSAVE2,NEQUIL,
     3                  NY,IDUMMY,NO,NHCUT
C
      COMMON/OUTX/OUTMAS(362),DEPTUB(362),DEPSIT(362),OUT(362)
C
      DATA              SEPS/Z3C100000/
C              FIRST EXECUTABLE STATEMENT
C
      KBOX=NB1*NB2
      DO 400 I=1,NB1
      DO 400 J=1,NB2
      IBOX=(J-1)*NB1+I
      DO 400 LS=1,MSECT
      MKS=(LS-1)*KBOX+IBOX
      YOLD(MKS)=0.
 400  DEPOLD(MKS)=0.
C
C
      IF (MITER.GE.0) NLC = -1
      KER = 0
      JER = 0
      UROUND = SEPS
```

```
C                                       COMPUTE WORK VECTOR INDICIES
      NERROR = N
      NSAVE1 = NERROR+N
      NSAVE2 = NSAVE1+N
      NY = NSAVE2+N
      IF (METH.EQ.1) NEQUIL = NY+13*N
      IF (METH.EQ.2) NEQUIL = NY+6*N
      NPW = NEQUIL + N
      IF (MITER.EQ.0.OR.MITER.EQ.3) NPW = NEQUIL
      MFC = 10*METH+IABS(MITER)
C                                       CHECK FOR INCORRECT INPUT PARAMETERS
C
      IF (MITER.LT.-2.OR.MITER.GT.3) GO TO 85
      IF (METH.NE.1.AND.METH.NE.2) GO TO 85
      IF (TOL.LE.0.) GO TO 85
      IF (N.LE.0) GO TO 85
      IF ((X-XEND)*H.GE.0.) GO TO 85
      IF (INDEX.EQ.0) GO TO 10
      IF (INDEX.EQ.2) GO TO 15
      IF (INDEX.EQ.-1) GO TO 20
      IF (INDEX.EQ.3) GO TO 25
      IF (INDEX.NE.1) GO TO 85
C                                       IF INITIAL VALUES OF YMAX OTHER THAN
C                                         THOSE SET BELOW ARE DESIRED, THEY
C                                         SHOULD BE SET HERE. ALL YMAX(I)
C                                         MUST BE POSITIVE. IF VALUES FOR
C                                         HMIN OR HMAX, THE BOUNDS ON
C                                         DABS(HH), OTHER THAN THOSE BELOW
C                                         ARE DESIRED, THEY SHOULD BE SET
C                                         BELOW.
      DO 5 I=1,N
         WK(I) = ABS(Y(I))
         IF (WK(I).EQ.0.) WK(I) = 1.
         WK(NY+I) = Y(I)
    5 CONTINUE
      NC = N
      T = X
      HH = H
      IF ((T+HH).EQ.T) KER = 33
      HMIN = ABS(H)
      HMAX = ABS(X-XEND)*10.
      EPSC = TOL
      JSTART = 0
      NO = N
      NSQ = NO*NO
      EPSJ = SQRT(UROUND)
      NHCUT = 0
      DUMMY(2) = 1.0
      DUMMY(14) = 1.0
      GO TO 30
```

```
C                                     TOUTP IS THE PREVIOUS VALUE OF XEND
C                                       FOR USE IN HMAX.
   10 HMAX = ABS(XEND-TOUTP)*10.
      GO TO 45
C
   15 HMAX = ABS(XEND-TOUTP)*10.
      IF ((T-XEND)*HH.GE.0.) GO TO 95
      GO TO 50
C
   20 IF ((T-XEND)*HH.GE.0.) GO TO 90
      JSTART = -1
      NC = N
      EPSC = TOL
C
   25 IF ((T+HH).EQ.T) KER = 33
C
   30 NN = N0
      CALL DGRST (FCN,FCNJ,WK(NY+1),WK,WK(NERROR+1),WK(NSAVE1+1),
     1 WK(NSAVE2+1),WK(NPW+1),WK(NEQUIL+1),IWK,NN)
C
      KGO = 1-KFLAG
      GO TO (35,55,70,80), KGO
C                                   KFLAG = 0, -1, -2, -3
   35 CONTINUE
C                                   NORMAL RETURN FROM INTEGRATOR. THE
C                                     WEIGHTS YMAX(I) ARE UPDATED. IF
C                                     DIFFERENT VALUES ARE DESIRED, THEY
C                                     SHOULD BE SET HERE. A TEST IS MADE
C                                     FOR TOL BEING TOO SMALL FOR THE
C                                     MACHINE PRECISION. ANY OTHER TESTS
C                                     OR CALCULATIONS THAT ARE REQUIRED
C                                     AFTER EVERY STEP SHOULD BE
C                                     INSERTED HERE. IF INDEX = 3, Y IS
C                                     SET TO THE CURRENT SOLUTION ON
C                                     RETURN. IF INDEX = 2, HH IS
C                                     CONTROLLED TO HIT XEND (WITHIN
C                                     ROUNDOFF ERROR), AND THEN THE
C                                     CURRENT SOLUTION IS PUT IN Y ON
C                                     RETURN. FOR ANY OTHER VALUE OF
C                                     INDEX, CONTROL RETURNS TO THE
C                                     INTEGRATOR UNLESS XEND HAS BEEN
C                                     REACHED. THEN INTERPOLATED VALUES
C                                     OF THE SOLUTION ARE COMPUTED AND
C                                     STORED IN Y ON RETURN.
C                                     IF INTERPOLATION IS NOT
C                                     DESIRED, THE CALL TO DGRIN SHOULD
C                                     BE REMOVED AND CONTROL TRANSFERRED
C                                     TO STATEMENT 95 INSTEAD OF 105.
```

```
      D = 0.
      DO 40 I=1,N
         AYI = ABS(WK(NY+I))
         WK(I) = AMAX1(WK(I),AYI)
   40 D = D+(AYI/WK(I))**2
      D = D*(UROUND/TOL)**2
      DN = N
      IF (D.GT.DN) GO TO 75
      IF (INDEX.EQ.3) GO TO 95
      IF (INDEX.EQ.2) GO TO 50
   45 IF((T-XEND)*HH.LT.0.) GO TO 255
      NN = NO
      CALL DGRIN (XEND,WK(NY+1),NN,Y)
      X = XEND
      GO TO 1055
C
 255  DO 113 IB=1,NB1
      DO 113 JB=1,NB2
      IBOX=(JB-1)*NB1+IB
      DO 113 LS=1,MSECT
      MKS=(LS-1)*KBOX+IBOX
      AVEMAS=0.5*(WK(NY+MKS)+YOLD(MKS))*(1.-SCOUR)
      DEPTUB(MKS)=COEFAV(LS+NDEPST,IBOX)*AVEMAS*HUSED
      DEPSIT(MKS)=DEPTUB(MKS)+DEPSIT(MKS)
      AVEOUT=0.5*(OUTMAS(MKS)+DEPOLD(MKS))
      OUT(MKS)=AVEOUT*HUSED+OUT(MKS)
      DEPOLD(MKS)=OUTMAS(MKS)
      YOLD(MKS)=WK(NY+MKS)
  113 CONTINUE
      GO TO 25
C
   50 IF (((T+HH)-XEND)*HH.LE.0.) GO TO 255
      IF (ABS(T-XEND).LE.UROUND*AMAX1(10.*ABS(T),HMAX)) GO TO 95
      IF ((T-XEND)*HH.GE.0.) GO TO 95
      HH = (XEND-T)*(1.-4.*UROUND)
      JSTART = -1
      GO TO 255
C                                    ON AN ERROR RETURN FROM INTEGRATOR,
C                                      AN IMMEDIATE RETURN OCCURS IF
C                                      KFLAG = -2, AND RECOVERY ATTEMPTS
C                                      ARE MADE OTHERWISE. TO RECOVER, HH
C                                      AND HMIN ARE REDUCED BY A FACTOR
C                                      OF .1 UP TO 10 TIMES BEFORE GIVING
C                                      UP.
```

```
   55 JER = 66
   60 IF (NHCUT.EQ.10) GO TO 65
      NHCUT = NHCUT+1
      HMIN = HMIN*.1
      HH = HH*.1
      JSTART = -1
      GO TO 25
C
   65 IF (JER.EQ.66) JER = 132
      IF (JER.EQ.67) JER = 133
      GO TO 95
C
   70 JER = 134
      GO TO 95
C
   75 JER = 134
      KFLAG = -2
      GO TO 95
C
   80 JER = 67
      GO TO 60
C
   85 JER = 135
      GO TO 110
C
   90 JER = 136
      NN = NO
      CALL DGRIN (XEND,WK(NY+1),NN,Y)
      X = XEND
      GO TO 110
C
   95 X = T
      DO 100 I=1,N
  100 Y(I) = WK(NY+I)
C
 1055 HSTEP=HUSED-(T-XEND)
C
      KBOX=NB1*NB2
      DO 114 IB=1,NB1
      DO 114 JB=1,NB2
      IBOX=(JB-1)*NB1+IB
      DO 114 LS=1,MSECT
      MKS=(LS-1)*KBOX+IBOX
      AVEMAS=0.5*(Y(MKS)+YOLD(MKS))*(1.-SCOUR)
      DEPTUB(MKS)=COEFAV(LS+NDEPST,IBOX)*AVEMAS*HSTEP
      DEPSIT(MKS)=DEPTUB(MKS)+DEPSIT(MKS)
      AVEOUT=0.5*(OUTMAS(MKS)+DEPOLD(MKS))
      OUT(MKS)=AVEOUT*HSTEP+OUT(MKS)
      DEPOLD(MKS)=OUTMAS(MKS)
      YOLD(MKS)=Y(MKS)
  114 CONTINUE
      NNFE=NFE
      NNSTEP=NSTEP
```

```
  105 IF (JER.LT.128) INDEX = KFLAG
      TOUTP = X
      H = HUSED
      IF (KFLAG.NE.0) H = HH
  110 IER = MAX0(KER,JER)
 9000 CONTINUE
      IF (KER.NE.0.AND.JER.LT.128) CALL UERTST (KER,6HDGEAR )
      IF (JER.NE.0) CALL UERTST (JER,6HDGEAR )
 9005 RETURN
      END
C*********************************************************************
      SUBROUTINE RHODD(V,D,RHO)
C
C  This routine computes the density of the flocs assuming the
C  size-density relationship Eq. 2.6, Chapter II, in Valioulis' Thesis.
C
      RHOWAT=1000.
      IF (V.LE.0.) GO TO 1
      RHO=2650.
      IF(V.GT.8.8802E-14) GO TO 5
      D=(6.*V/(3.141592654*RHO))**(1./3)
      RETURN
   5  D=4.E-6
      DO 10 I=1,1000
      F1=RHOWAT+1.3/(100.*D)**0.9
      F=F1*0.5235987757*D*D*D-V
      DF=F1*1.5707963*D*D-0.0097092232*D*D/D**0.9
      D=D-F/DF
      IF(ABS(F).LE.(0.001*V)) GO TO 14
  10  CONTINUE
      GO TO 15
  14  RHO=RHOWAT+1.3/(100.*D)**0.9
      RETURN
  1   IF(D.LT.4.E-6) GO TO 2
      RHO=RHOWAT+1.3/(D*100.)**0.9
      GO TO 3
  2   RHO=2650.
  3   V=0.5235987757*D*D*D*RHO
      RETURN
  15  STOP
      END
```

```
C*********************************************************************
C       SUBROUTINE RHODD(V,D,RHO)
C  This routine computes the density of the flocs assuming a constant
C  density of 2000kg/m3 for all floc sizes
C
C       RHO=2000.
C       IF(V.LE.0.) GO TO 1
C       D=(6.*V/(3.141592654*RHO))**(1./3.)
C       RETURN
C    1  V=0.5235987757*D*D*D*RHO
C       RETURN
C       END
C
C*********************************************************************
      SUBROUTINE DIVIDE(M,NB1,NB2,VOLUME,SOURCE,SRATE,DIAM,IPRNT,IT,
     *                  PERSUS)
C
C  This routine fractionates the source (kg/m3) according to the
C  power law: Number=constant*(particle volume)**(-bslope)
C  and stores the input mass concentration in SRATE (kg/sec-m3)

      DIMENSION SOURCE(24),SRATE(362),DENS(21),DIAM(21),V(21),
     *CONSTA(24),ROMEAN(21),DIMEAN(21)
      COMMON/VELOC/U(4)
      COMMON/TANK/BL1,BL2,UAVE,USTAR,UL1,UL2,SCOUR
      KBOX=NB1*NB2
      BSLOPE=3.
      MAX=15
      SUMFRA=0.
      MK=M+1
      DO 1 I=1,MK
      V(I)=0.
 1    CALL RHODD(V(I),DIAM(I),DENS(I))
     DO 2 I=1,M
      ROMEAN(I)=SQRT(DENS(I+1)*DENS(I))
 2    DIMEAN(I)=SQRT(DIAM(I+1)*DIAM(I))
      DO 21 I=1,MAX
      SUMFRA=ROMEAN(I)*DIMEAN(I)**(3.-BSLOPE)*3.14/6.+SUMFRA
 21   CONTINUE
      WRITE(IPRNT,900)M,SOURCE(1),DIAM(1),DENS(1)
900   FORMAT(' DIV=',I3,2X,3(2X,E10.4))
      DO 3 I=1,NB1
      DO 3 J=1,NB2
      K=NB1*(J-1)+I
 3    CONSTA(K)=SOURCE(K)/SUMFRA
      IF(IT.NE.1) GO TO 12
      WRITE(IPRNT,10)
 10   FORMAT('  MASS CONC. ',3X,' NUMBER CONC.',3X,
     * ' VOLUME CONC.',3X,' MEAN DIAMETER',3X,' MEAN DENSITY',
     * 3X,' SECTION'/'  KG/M3    ',6X,'#/CM3    ',5X,'  PPM.     ',
     * 12X,'M',16X,'KG/M3'//)
```

```
 12   SUM1=0.
      TOTVOL=0.
      DO 41 L=1,MAX
      SUM=0.
      PARNUM=0.
      PARVOL=0.
      DO 4 I=1,NB1
      DO 4 J=1,NB2
      K=NB1*(J-1)+I
      SUM2=1./(U(J)*BL2*NB2)
      PARVOL=PARVOL+CONSTA(K)*DIMEAN(L)**(3.-BSLOPE)*SUM2*3.14/6.
      SRATE(KBOX*(L-1)+K)=CONSTA(K)*DIMEAN(L)**(3.-BSLOPE)
     *                    *ROMEAN(L)/VOLUME*3.14/6.
      SUM=SUM+SRATE(KBOX*(L-1)+K)*VOLUME*SUM2
      SUM1=SUM1+SRATE(KBOX*(L-1)+K)
   4  PARNUM=PARNUM+CONSTA(K)*DIMEAN(L)**(-BSLOPE)*SUM2
      IF(IT.NE.1) GO TO 41
      S1=PARNUM*1.E-6
      S2=PARVOL*1.E+6
      WRITE(IPRNT,11) SUM,S1,S2,DIMEAN(L),ROMEAN(L),L
  11  FORMAT(1X,E10.4,6X,E10.4,6X,E10.4,7X,E10.4,6X,E10.4,
     *       7X,I3//)
      TOTVOL=TOTVOL+PARVOL
  41  CONTINUE
      IF(IT.NE.1) RETURN

C  Compute equivalent diameter in effluent
C
      SUM2=0.
      SUM3=0.
      DO 50 J=1,NB2
      SUM=0.
      SUM4=0.
      IBOX=NB1*(J-1)+1
      DO 51 L=1,M
      MKS=IBOX+(L-1)*KBOX
      SUM=SRATE(MKS)/ROMEAN(L)+SUM
  51  SUM4=SRATE(MKS)/(3.14/6.*ROMEAN(L)*DIMEAN(L)**3)+SUM4
      SUM2=SUM+SUM2
  50  SUM3=SUM3+SUM4
      SUM2=(6./3.14*SUM2/SUM3)**(1./3.)
C
C  Compute the % suspended solids in effluent
C
      SUM=0.
      DO 88 I=1,NB1
      DO 88 J=1,NB2
      IBOX=NB1*(J-1)+I
      DO 88 L=5,M
      MKS=IBOX+(L-1)*KBOX
 88   SUM=SUM+SRATE(MKS)
```

```
      PERSUS=SUM/SUM1
      S1=TOTVOL*1.E+6
C
      WRITE(IPRNT,48) S1,SUM2,PERSUS
 48   FORMAT(' TOTAL VOLUMETRIC CONC IN INFLUENT=',E10.4/,
     *       ' EQUIVALENT DIAMETER=',E10.4/,' % SUSPENDED SOLIDS IN',
     *       ' INFLUENT=',E10.4/)
C
       RETURN
       END
C*************************************************************
      SUBROUTINE SOR(NB1,NB2,IT,TIME,TDISIN,SOURCE,FLOW,START,IDISC)
C
C  This routine computes the velocity field and the input
C  mass in SOURCE (kg/sec)
C
      COMMON/TANK/BL1,BL2,UAVE,USTAR,UL1,UL2,SCOUR,FREQ,ADIS
      COMMON/VELOC/U1,U2,U3,U4
      DIMENSION SOURCE(24)
      KBOX=NB1*NB2
      ADIS=1.
      IF(IT.NE.1) GO TO 7
      START=0.00888
      Z1=0.5*BL2
      Z2=1.5*BL2
      Z3=2.5*BL2
C      Z4=3.5*BL2
C      V4=UAVE+USTAR/0.3*(1.+ALOG(Z4/UL2))
      V1=UAVE+USTAR/0.3*(1.+ALOG(Z1/UL2))
      V2=UAVE+USTAR/0.3*(1.+ALOG(Z2/UL2))
      V3=UAVE+USTAR/0.3*(1.+ALOG(Z3/UL2))
      V4=0.
      V=V1+V2+V3+V4
      VFLOW=V*BL2
      V=1./V
      A1=V1*V
      A2=V2*V
      A3=V3*V
      A4=V4*V
  7   IF(IDISC.EQ.1 .AND. TIME.EQ.TDISIN) ADIS=2.
      SOURCE(1)=A1*START*ADIS
      SOURCE(NB1+1)=A2*START*ADIS
      SOURCE(2*NB1+1)=A3*START*ADIS
C      SOURCE(3*NB1+1)=A4*START
```

```
      U1=V1
      U2=V2
      U3=V3
      U4=V4
      FLOW=VFLOW
      DO 11 J=1,NB2
      DO 11 I=2,NB1
 11   SOURCE(NB1*(J-1)+I)=0.
      RETURN
      END
C*****************************************************************
      FUNCTION BETCAL(X,RELER,ABSER,ROUND,IPRNT,FIXSZ,BASESZ,INNER,
     *TWAT,NBTYPE)
      EXTERNAL BETA
C
C  This routine calculates the inner integral of the sectional
C  coagulation coefficients.
C
      YU=FIXSZ
      YL=BASESZ
      IF(INNER.EQ.0) GO TO 3
      YL=ALOG(BASESZ-EXP(X))
      IF(INNER.EQ.1) GO TO 20
      YU=YL
      YL=FIXSZ
C
   3  IER=1
      ABE=ABSER*ABSER
      REL=.5*RELER
      CALL GAUS2(BETA,YL,YU,REL,ABE,ROUND,ANSWR,IER,X,TWAT,NBTYPE)
  10  BETCAL=ANSWR
      IF(IER.EQ.0) RETURN
C
      WRITE(IPRNT,4) NBTYPE,X,YL,YU,IER,REL,ABE
  4   FORMAT(' INNER INTEFRATION ERROR, INTEGRAL TYPE',I3,
     */' OUTER VARIABLE=',E12.4,' INNER DOMAIN=',2E12.4,' ERROR=',
     *I3,' REL='E12.4,' ABE=',E12.4)
C
      STOP
  20  ETEST=ABS(YU-YL)/(DABS(YU)+DABS(YL))
      IF(ETEST.GT.500.*ROUND) GO TO 3
      DELVL=EXP(X)/BASESZ
      YMEAN=0.5*(YU+YL)
      ANSWR=(DELVL+0.5*DELVL*DELVL)*BETA(YMEAN,X,TWAT,NBTYPE)
      GO TO 10
C
      END
```

```
C*****************************************************************
      FUNCTION BETA(Y,X,TWAT,NBTYPE)
C  This routine computes the coagulation coefficients due
C  to Brownian diffusion, turbulent shear and gravity settling
C  The collision efficiencies are computed as outlined in Valioulis'
C  Thesis, Section II.2.b.
C
      COMMON/PHYSPT/AFLROV,VOLUME,EPS
      COMMON/TANK/BL1,BL2,UAVE,USTAR,UL1,UL2
C
      V=EXP(X)
      U=EXP(Y)
      DX=0.
      DY=0.
      CALL RHODD(V,DX,RHOX)
      CALL RHODD(U,DY,RHOY)
C
C  Determine the physical properties of water
C
      RHOWAT=1000.
      VISCOS=1.002E-03
      VISCKI=VISCOS/RHOWAT
      BKT=4.1E-22
      HYEFF=1.
C
      DX=1.2*DX
      DY=1.2*DY
      IF(DX.GT.DY) GO TO 9
      R2=DY*0.5
      RATIO=DY/DX
      DENS=RHOY
      GO TO 10
  9   R2=DX*0.5
      DENS=RHOX
      RATIO=DX/DY
 10   RATINV=1./RATIO
C
C  Brownian coagulation
C
      IF(RATIO.GT.20.) GO TO 6
      HYEFF=0.4207+0.031*RATIO-9.E-4*RATIO**2
      GO TO 5
  6   HYEFF=0.652+0.0055*RATIO-3.035*E-5*RATIO**2
  5   BETABR=(2./3.)*BKT/VISCOS*(DX+DY)**2/(DX*DY)*HYEFF
```

```
C  Turbulent shear coagulation
C
      Z=(EPS-0.5)*BL2
C
C  For the log-velocity profile
C
      EPSILO=USTAR**3/(0.3*Z)*(1.-Z/UL2)
C
C
C
C
      G=SQRT(EPSILO/VISCKI)
C
      IF(R2.LT.1.E-6) GO TO 201
      POROS=(2650.-DENS)/(2650.-RHOWAT)
      IF(POROS.LT.1.E-2) GO TO 20
      XI=SQRT(3.+4./(1.-POROS)-3.*SQRT(8./(1.-POROS)-3.))
      XI=SQRT(1800.)/XI
      IF(XI.GT.10.89) XI=10.89
      HEFSH1=1.16156-0.22776*XI+0.0111864*XI*XI
      GO TO 203
 20   HEFSH1=0.
 203  RATI2=RATINV*RATINV
      RATI3=RATI2*RATINV
      HEFSH2=-0.403611+9.42306*RATINV-17.2139*RATI2+9.444*RATI3
      HEFFSH=AMAX1(HEFSH1,HEFSH2)
      GO TO 202
 201  HEFFSH=(-0.9798-1.09705E-3*RATIO+2.2377E-5*RATIO**2-
     *       1.3297E-7*RATIO**3)/(1.-2.79224*RATIO)
 202  IF(HEFFSH.LT.0.) GO TO 35
      BETATU=2.3/8.*(DX+DY)**3*G
      BETATU=BETATU*HEFFSH
      GO TO 36
   35 BETATU=0.
C
C  Gravitational coagulation
C
 36   IF(R2.LE.7.E-6) GO TO 21
      POROS=(2650.-DENS)/(2650.-RHOWAT)
      XI=SQRT(3.+4./(1.-POROS)-3.*SQRT(8./(1.-POROS)-3.))
      XI=SQRT(1800.)/XI
      XI2=XI*XI
      XI3=XI*XI*XI
      XI5=XI*XI*XI3
```

```
      JEY=2.*XI2+3.-3./XI
      CJEY=-(XI5+6.*XI3-(3.*XI5+6.*XI3)/XI)/JEY
      DJEY=3.*XI3*(1.-1./XI)/JEY
      HEFPOR=1.-DJEY/XI-CJEY/XI3
      IF(R2.LE.15.E-6) GO TO 205
      IF(R2.LE.20.E-6) R2=20.E-6
      R22=R2*1.E+6
      IF(R22.GT.140.) R22=140.
      E0=0.95-(0.7-0.005*R22)**4*(7.92-0.12*R22+0.001*R22**2)
      E1=-(RATINV-0.5)**2
C
C  Correct E2 for particles larger than 140.E-6 m.
C
      E2=-1.5*EXP(-(0.0015*(R2*1.E+6)**2+8)*RATINV)
      E3=-(1.-0.007*R22)*EXP(-0.65*R22*(1.-RATINV))
      E4=EXP(-30.*(1.-RATINV))
      HEFFDS=E0+E1+E2+E3+E4
      GO TO 206
 205  HEFFDS=0.5*RATINV**2/(1.+RATINV)**2
 206  HEFFDS=DMAX1(HEFFDS,HEFPOR)
      IF(HEFFDS.LT.0.0) HEFFDS=0.0
      GO TO 31
 21   HEF=0.5*RATINV**2/(1.+RATINV)**2
 31   IF(RATINV.GE.0.4) HEFFDS=DMAX1(HEFFDS,0.4D-1)
      IF(RATINV.LE.0.1 .AND. R2.GE.1.E-6) HEFFDS=DMAX1(HEFFDS,0.6D-1)
      BETAGR=0.7/16.*9.81/VISCOS*(DX+DY)**2
      BETAGR=BETAGR*ABS((RHOX-RHOWAT)*DX**2-(RHOY-RHOWAT)*DY**2)
      BETAGR=BETAGR*HEFFDS
C
C  Add all coagulation mechanisms
C
      BETA=BETABR+BETAGR+BETATU
C
C  Convert the integrand for sectionalization by mass
C
      GO TO (2,1,2,3,3,1),NBTYPE
   1  BETA=BETA/V
      RETURN
   2  BETA=BETA/U
      RETURN
    3 BETA=1.E20*BETA*(U+V)/(U*1.E20*V)
      RETURN
      END
```

```
C*********************************************************************
      FUNCTION DEPOST(X,DUMMY,TWAT,NBTYPE)
C
C  This routine computes the deposition coeficients
C
      COMMON/PHYSPT/AFLROV,VOLUME
C
      V=EXP(X)
      D=0.
      CALL RHODD(V,D,RHO)
C
C  Determine the physical properties of water
C
      RHOWAT=1000.
      VISCOS=1.002E-03
C
      D1=1.2*D
      VTERM=(1./18.)*9.81*(RHO-RHOWAT)/VISCOS*D1*D1
      IF(NBTYPE.EQ.7) DEPOST=AFLROV*DMAX1(0.D+00,VTERM)
      RETURN
      END

C*********************************************************************
      SUBROUTINE GAUS2(F,XL,XU,RELER,ABSER,ROUND,ANSWR,IER,EXTRA1,
     *  EXTRA2,NEXTRA)
C
C
C     THIS ROUTINE COMPUTES THE INTEGRAL OF F(X,EXTRA1,EXTRA2,EXTRA3,
C     NEXTRA) FROM XL TO XU.  A TWO POINT GAUSS-LEGENDRE QUADRATURE
C     FORMULA IS USED. CONVERGENCE IS CHECKED BY DIVIDING THE DOMAIN IN
C     HALF AND REAPPLYING THE FORMULA IN EACH HALF.  IF THE VALUE OF THE
C     INTEGRAL CALCULATED OVER THE ENTIRE DOMAIN IS NOT EQUAL TO THE
C     SUM OF THE INTEGRALS IN EACH HALF (WITHIN THE
C     USER SPECIFIED ERROR TOLERANCE), EACH HALF IS FURTHER DIVIDED
C     INTO HALVES AND THE GAUSS-LEGENDRE FORMULA IS REAPPLIED. THE
C     PROCEDURE WILL CONTINUE ITERATING (I.E. SUBDIVIDING),UNTIL
C     CONVERGENCE IS ACHIEVED OR THE MAXIMUM NUMBER OF ITERATIONS IS
C     REACHED.  THE MAXIMUM NUMBER OF ITERATIONS IS EITHER THE SET
C     DEFAULT VALUE OF 30 (WHERE THE FIRST ITERATION IS FOR EVALUATION
C     OVER THE ENTIRE DOMAIN), OR THE LARGEST NUMBER OF ITERATIONS
C     POSSIBLE WITHOUT SEVERE MACHINE ROUND-OFF ERRORS, WHICHEVER IS
C     SMALLER.  THE MACHINE ROUND-OFF ERROR CHECK IS MADE TO INSURE
C     THAT THE INTEGRATION DOMAIN IS NOT TOO SMALL SO AS TO BE
C     INSIGNIFICANT.  SINCE THE PROCEDURE IS ADAPTIVE, ONLY THE REGIONS
C     WHICH ARE NONCONVERGENT ARE DIVIDED INTO HALVES. THIS CODE WAS
C     WAS WRITTEN BY FRED GELBARD, FEBRUARY, 1982.
C
```

```
      DIMENSION A(2,21),X(21),H(21),ISIDE(21)
      FUN(XD,HD)=0.5*HD*(F(XD+.2113248654052*HD,EXTRA1,EXTRA2,
     *  NEXTRA)+F(XD+.788675134598*HD,EXTRA1,EXTRA2,NEXTRA))
      NMAX=21
C
      H(1)=XU-XL
      A(2,1)=FUN(XL,H(1))
      IF(IER.NE.1) GO TO 2
      IF(10.*ABS(H(1))/RELER.LT.AMAX1(ABS(XU),ABS(XL))) GO TO 7
C
C      CHECK THAT THE SIZE DOMAIN IS NOT TOO SMALL
C
  2   IF(ABS(XU-XL).GT.4.*ROUND*AMAX1(ABS(XL),ABS(XU))) GO TO 8
      ANSWR=A(2,1)
      IER=-2
      RETURN
C
C      DETERMINE THE MAXIMUM NUMBER OF SUBDIVISIONS BEFORE ROUND OFF
C      ERROR WOULD MAKE IT DIFFICULT TO DISTINGUISH POINTS IN THE DOMAIN
C
  8   RATIO=AMAX1(ABS(XU/H(1)),ABS(XL/H(1)))
      N1=2-IFIX(1.4427*ALOG(RATIO*ROUND))
C-      N1=-IFIX(1.4427*ALOG(RATIO*ROUND))
C+  ALLOW TWO EXTRA ITERATIONS TO INCREASE CHANCE OF CONVERGENCE
      NMAX=MIN0(NMAX,N1)
      IF(NMAX.GT.1) GO TO 10
      IER=-1
      RETURN
C
 10   ISIDE(1)=2
      DO 1 I=2,NMAX
      ISIDE(I)=2
  1   H(I)=.5*H(I-1)
C
      X(2)=XL
      N=2
C
  4   SUM=0.
      A(1,N)=FUN(X(N),H(N))
      A(2,N)=FUN(X(N)+H(N),H(N))
      SUM=A(1,N)+A(2,N)
C
      IF(ABS(SUM-A(ISIDE(N),N-1))/RELER.LT.ABS(SUM)+ABSER) GO TO 3
      IF(N.EQ.NMAX) GO TO 9
      N=N+1
      ISIDE(N)=1
      X(N)=X(N-1)
      GO TO 4
```

```
  3      A(ISIDE(N),N-1)=SUM
         IF(ISIDE(N).EQ.1) GO TO 5
  6      IF(N.EQ.2) GO TO 7
         N=N-1
         A(ISIDE(N),N-1)=A(1,N)+A(2,N)
         IF(ISIDE(N).EQ.2) GO TO 6
C
C
  5      ISIDE(N)=2
         X(N)=X(N-1)+H(N-1)
         GO TO 4
C
C
  9      IER=N-1
         XL=X(N)
         XU=X(N)+2.*H(N)
         RELER=SUM
         ABSER=A(ISIDE(N),N-1)
         RETURN
C
  7      IER=0
         ANSWR=A(2,1)
         RETURN
         END
C
C*********************************************************************
C
         SUBROUTINE GAUSBT(F,XL,XU,RELER,ABSER,ROUND,ANSWR,IER,IPRNT,
     *   FIXSZ,BASESZ,INNER,TGAS,NBTYPE)
C
         DIMENSION A(2,21),X(21),H(21),ISIDE(21)
         FUN(XD,HD)=0.5*HD*(F(XD+.2113248654052*HD,RELER,ABSER,ROUND,
     *   IPRNT,FIXSZ,BASESZ,INNER,TWAT,NBTYPE)+
     *   F(XD+.788675134598*HD,RELER,ABSER,ROUND,
     *   IPRNT,FIXSZ,BASESZ,INNER,TWAT,NBTYPE))
         NMAX=21
         H(1)=XU-XL
         A(2,1)=FUN(XL,H(1))
         IF(IER.NE.1) GO TO 2
         IF(10.*ABS(H(1))/RELER.LT.AMAX1(ABS(XU),ABS(XL))) GO TO 7
  2      IF(ABS(XU-XL).GT.4.*ROUND*AMAX1(ABS(XL),ABS(XU))) GO TO 8
         ANSWR=A(2,1)
```

```
      IER=-2
      RETURN
 8    RATIO=AMAX1(ABS(XU/H(1)),ABS(XL/H(1)))
      N1=2-IFIX(1.4427*ALOG(RATIO*ROUND))
C-    N1=-IFIX(1.4427*ALOG(RATIO*ROUND))
C+   ALLOW TWO EXTRA ITERATIONS TO INCREASE CHANCE OF CONVERGENCE
      NMAX=MIN0(NMAX,N1)
      IF(NMAX.GT.1) GO TO 10
      IER=-1
      RETURN
 10   ISIDE(1)=2
      DO 1 I=2,NMAX
      ISIDE(I)=2
  1   H(I)=.5*H(I-1)
      X(2)=XL
      N=2
  4   SUM=0.
      A(1,N)=FUN(X(N),H(N))
      A(2,N)=FUN(X(N)+H(N),H(N))
      SUM=A(1,N)+A(2,N)
      IF(ABS(SUM-A(ISIDE(N),N-1))/RELER.LT.ABS(SUM)+ABSER) GO TO 3
      IF(N.EQ.NMAX) GO TO 9
      N=N+1
      ISIDE(N)=1
      X(N)=X(N-1)
      GO TO 4
  3   A(ISIDE(N),N-1)=SUM
      IF(ISIDE(N).EQ.1) GO TO 5
  6   IF(N.EQ.2) GO TO 7
      N=N-1
      A(ISIDE(N),N-1)=A(1,N)+A(2,N)
      IF(ISIDE(N).EQ.2) GO TO 6
  5   ISIDE(N)=2
      X(N)=X(N-1)+H(N-1)
      GO TO 4
 9    IER=N-1
      XL=X(N)
      XU=X(N)+2.*H(N)
      RELER=SUM
      ABSER=A(ISIDE(N),N-1)
      RETURN
 7    IER=0
      ANSWR=A(2,1)
      RETURN
      END
$
```